

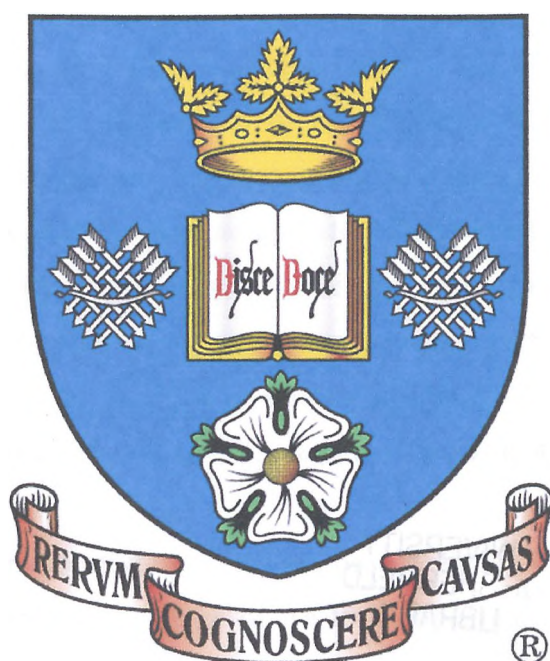
Characterisation and Interaction of Simulated High Level, Radioactive Waste (HLW) with Borosilicate Glass

By

Suzy Morgan

Thesis

Submitted for the degree of Doctor of Philosophy



Immobilisation Science Laboratory
Department of Engineering Materials
University of Sheffield

Sponsored by EPSRC and Nexia Solutions

October

2005

Abstract

Alkali borosilicate glasses have been widely used as an immobilisation network for high level, radioactive waste for the past 50 years. Increasing the waste loading would increase the efficiency of the process, but also increase the tendency of the waste towards devitrification in final storage. Devitrification could have a negative effect on the long term properties of the glass. “Yellow phase” is often observed within devitrified glass, and consists of many of the low solubility elements of the waste stream composition (Mo, Sr, Te, Cr and S). Yellow phase may also incorporate some of the more radioactive fission products such as ^{137}Cs and ^{90}Sr . The increased corrosion of the Inconel 601 melters in the early stages of melting time presents a problem, as decreased melter life means increased process inefficiency.

Simulated waste streams have undergone a range of heat treatments and it has been shown that elemental segregation of the calcine is inevitable. Scanning electron microscopy and transmission electron microscopy showed a characteristic segregation of the rare earths and actinide surrogates to a fluorite structured phase. Segregation of a yellow phase to the melt surface, containing loosely bonded and highly soluble (in aqueous solution) radionuclides was observed using X-ray powder diffraction. It was demonstrated that the calcination process currently in use is ineffective and the temperatures to which it currently operates are overestimated.

Simulated (non-radioactive) glasses have been melted in Inconel 601 crucibles using a variety of atmospheres, a range of waste loadings and waste streams which have undergone preliminary heat treatment. Some basic mechanisms for the dissolution of the waste into the glass have been proposed. The formation of a rare-earth enriched solute layer around the waste particles was shown using SEM, occurring concurrently with nucleation of yellow phase and segregation to the melt surface. The yellow phase, once incorporated into the body of the melt via convective mixing was seen to nucleate around bubbles within the viscous matrix. Fluorite-structured phases did not dissolve readily in the glass and were found to contain many rare-earths and actinide simulants.

Acknowledgements

Firstly, I would like to thank my supervisor, Dr. Russell Hand, whose advice and support has been invaluable over the last three years. I would also like to thank Mr. Charlie Scales, my industrial supervisor at Sellafield.

For help and technical support, I would like to extend my thanks in particular to Dean Padlock and Ian “Iceman” Watts (for all those ashtrays and paper weights!). I would also like to thank all the staff in Engineering Materials who have helped me at one time or another during my time here. Thanks also go to the EPSRC and Nexia Solutions (formerly BNFL) for funding.

On a personal note, I would like to acknowledge Peter Rose (Yoink!), for sitting next to me for three long years, for the Stutter Rap (and all the other downloads that endlessly slowed down our computer) and just generally for entertaining me- Peace out! To all my friends who have put up with me and fed me experimental pizzas (you know who you are!), and to my extremely tolerant housemates, Becky and Claire, for living with me, making me leave the house occasionally and explaining the intricacies of cement science. To my parents for their much needed financial and moral support, endless enthusiasm, proof-reading and for understanding science, DIY and sewing. Also, Lucy, for never tiring of talking to me online and off, and to Helena for the many hours of distraction and recipe advice- yes, I may have a proper job soon! Finally, I would like to thank Ric, for knowing what I was going through, for not letting me give up, and providing me with food whilst I was writing.

Note to Reader

The compact discs which are included with this work contain digital images of the GC-MS glass melts (**section 3.9**) and are best viewed in a digital media player. These discs also include still images of the same melts.

Publications and Conferences

Elements of the work described in this thesis have been presented as follows:

International Congress on Glass XX (ICG) Kyoto, Japan, 2004

-Oral presentation and paper entitled “Interactions of Simulant High Level, Waste with Borosilicate Glass Frit and Subsequent Batch Reactions” published in ICGXX Symp. Proc. 2004 S. Morgan, R.J.Hand and W.E. Lee.

SET for Britain, House of Commons, London, UK, 2003

-Poster presentation entitled “Disposal of Highly Active, Nuclear Waste in Glass” S. Morgan and R.J.Hand

Society of Glass Technology Crystallisation 2003 meeting, Sheffield, UK 2003

-Poster presentation entitled “Crystallisation of Molybdenum-containing Phases within a Simulated High Level Waste Borosilicate Glass” S. Morgan, R.J. Hand and W.E.Lee.

American Ceramics Society Nashville, USA, 2003

-Oral presentation (given by Prof. W.E. Lee); paper titled “The Characterisation and Dissolution of UK HLW with Borosilicate Glass” S. Morgan, P.B. Rose, R.J. Hand, N.C. Hyatt, W.E. Lee and C.R. Scales in Environmental Issues and Waste Management Technologies in the Ceramic and Nuclear Industries IX, *Cer. Trans* (2004), vol. 155 pp101-110

Materials Research Society Scientific Basis for Nuclear Waste Management XXVII Kalmar, Sweden, 2003

-Poster presentation; paper entitled “Interaction and Dissolution of Simulated, High Level Waste with Borosilicate Glass” S.Morgan, R.J.Hand, N.C.Hyatt and W.E.Lee published in Mat. Res. Soc. Symp. Proc. Vol. 807 (2004) pp. 151-156

Society of Glass Technology annual meeting, Birmingham, UK, 2003

-Oral presentation entitled “Crystallisation of problematic phases in the early stages of melting a high level, nuclear waste glass” S.Morgan and R.J.Hand

University Research Alliance meeting, BNFL Sellafield, UK 2003

-Poster presentation

“Molybdenum in Glasses containing Vitrified Nuclear waste” R.J.Hand, R.J.Short, S.Morgan, N.C.Hyatt, G.Möbus and W.E.Lee *Glass Tech.* vol. 46 (2) (2005) pp121-125

Contents

Abstract

Acknowledgements

Note to Reader

Published Work	Page No.
1. Introduction	1
2. Literature Survey	3
2.1 Review outline	3
2.2 Radioactivity	3
2.3 Nuclear Power Reactors	6
2.4 Reprocessing	10
2.5 Classification	11
2.6 Waste Immobilisation	13
2.7 Borosilicate Glasses	19
2.8 R7T7-A Comparison	25
2.9 Alternative Waste Forms	27
2.10 Glass Melting and Dissolution	28
2.11 Nitrate Decomposition	33
2.12 Durability of the Final Product	34
2.13 Summary	36
3. Overview of Experimental Techniques and Sample Preparation	38
3.1 Materials	38
3.2 Compositional Analysis	39
3.2.1 ICP-AES	39
3.2.2 XRF	41
3.2.3 Loss-on-Ignition	41

3.3 Glass Melting	42
3.4 Density Measurement	43
3.5 Thermal Analysis	43
3.6 X-ray Powder Diffraction	46
3.7 Fourier Transform Infra-red Spectroscopy	48
3.8 Electron Microscopy	49
3.8.1 Scanning Electron Microscopy	49
3.8.2 Transmission Electron Microscopy	52
3.9 Gas Chromatography and Mass Spectroscopy	54
3.10 Heat Treatment	59
3.11 Error calculation	59
3.10.2 Sample Designation List	61
4. Results	63
4.1 Compositional Analysis	63
4.2 Optical Observations	66
4.2.1 Simulant Waste	66
4.2.2 Waste Loaded Glasses	68
4.3 Density Measurements	70
4.4 Thermal analysis	70
4.4.1 Differential Thermal Analysis	70
4.4.2 Thermogravimetric Analysis	73
4.4.3 Differential Scanning Calorimetry	79
4.5 X-ray Powder Diffraction	85
4.6 Fourier Transform Infra-red Spectroscopy	96
4.7 GC-MS	106
4.8 Scanning Electron Microscopy	110
4.8.1 Simulant Waste	110
4.8.2 Waste Loaded Glasses	117
4.9 Transmission Electron Microscopy	135
5. Discussion	141
5.1 Simulant Waste	141
5.2 Waste Loaded Glasses	155

5.2.1 Yellow Phase	155
5.2.2 Waste Digestion	158
6. Conclusions and Further Work	170
6.1 Relevance to Real HLW Glass	170
6.2 Waste Characterisation	170
6.3 Waste Loaded Glass	171
6.4 Suggestions for Further work	172
References	174

Chapter 1: Introduction

*“Vitrification is the process of converting a material to a glassy form. The origin of the word (from the Latin **vitrum**, meaning glass) already suggests the fact that glassy materials and the art of glass-making have been known for thousands of years.”*
(Pegg, 2001)

Many long-lived fission products and actinides are generated in nuclear fuel during the operation of a reactor. These radionuclides will then go on to form a substantial fraction of high level waste (ref. **Figure 2.7.1**), which must be isolated from mankind for a suitably extended time period. Isolation requires the waste to be first converted into a form in which it can be safely transported and stored. In Britain today, vitrification is currently the only route commercially available for immobilising high level, radioactive waste (HLW) from various sources. This process is an integral part of the UK’s nuclear power programme, as it not only immobilises HLW, it deals with the wastes arising from the reprocessing of spent nuclear fuel. Vitrification of nuclear waste is a relatively recent development in the world of glass-making, with its beginnings found in the work of scientists of the 1950’s.

Vitrification as a quality-controlled process is extremely important. The quality of the glass produced by vitrification is a more accessible, and a more easily controlled component of the process than the retrieval of the solidified, stored waste, at least in the immediate future of the waste storage problem. Were this glass to be poorly manufactured, the effects of crystallisation, cracking and leaching all become much more pronounced. Glasses can be produced which are extremely resistant to aqueous corrosion, have a wide range of compositional variants and are still relatively simple to melt and produce (Ewing, 1988).

Crystallisation of the elements of the waste stream within the glass is just one problem facing those who wish to vitrify HLW. Tolerance of crystal phases in the waste is low due to their effect on the leaching of the radioactive elements into the environment, and also poor mechanical properties. Cracking of the final product in the canister may present a problem because of the now-increased surface area available for crystal growth and leaching.

The aforementioned inhomogeneities can be introduced at any stage of the glass manufacturing process. Therefore characterisation of the melting process is required in order that a quality control can be implemented on the end product. This can provide valuable information about heterogeneities and the source of such imperfections, and ultimately can lead to process improvement thereby reducing the problems created by imperfections. As is common to all glasses, the melting history will have a great effect on the final product. This includes changes in melt temperature, melting time, the atmosphere under which melting is conducted and the vessel in which it takes place. In particular, the HLW glass produces some distinctive phases upon melting, one of which is known as “yellow phase”. This yellow phase is detrimental to the process in several ways - firstly it increases the corrosion rate of the Inconel 601 melter, leading to an increase in cost and decrease in throughput of the melter. Secondly, the phase often contains water soluble alkali elements alongside highly radioactive isotopes, and should this phase come into contact with water, leaching of the radioactive isotopes could occur very quickly. Crystalline phases often associated with decreased product durability are not of concern within the melter system as they form only on subsequent pouring and cooling within the canister.

Other problem elements, such as the formation of refractory oxides within the melter (or prevention of such), and the dissolution of ^{137}Cs (a key yellow phase constituent) into the glassy matrix are also important in controlling the quality of the final glass. The dissolution of the waste stream as a whole is examined in this work, with particular emphasis placed on elements known to be problematic such as Cs and Mo. Examination of the waste stream and the interaction of the waste stream with the glass during the early melt stages is key to understanding the quality of the final product.

The current project therefore was designed to study the processes occurring during the vitrification of high level, nuclear waste. The work was carried out exclusively on inactive simulant material but nonetheless offers valuable insights into the vitrification of actual active waste.

Chapter 2: Literature Review

2.1 Outline of Review

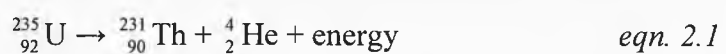
This review outlines the principles of radioactivity and how these principles are utilised for nuclear power generation purposes. The most common nuclear reactor types are discussed with the specific intention of looking at the types of fuel used and their lifetimes; and the classifications of wastes these fuels give rise to. The waste forms generated can then be immobilized in any number of ways, the most common of which are discussed in detail, and comparisons drawn with solidified wastes from other countries. Nitrate decomposition is discussed, followed by dissolution of batch elements in glasses because the waste streams are often nitrate-based liquids which are later solidified. Finally, a brief overview is given on the state of the art of long-term storage for solidified wastes. This review of literature will make clear the need for further work and outline the area on which this study concentrates, namely on the dissolution and early melting reactions of the stimulant HLW with the base glass used for immobilization.

2.2 Radioactivity

In 1896, in his Paris laboratory, Henri Becquerel accidentally discovered the effect now known as radioactivity by observing the effect of a packet of uranium salts on a photographic plate. Marie Curie went on to realise that certain rocks could emit this mysterious energy, and do so without diminishing in measurable mass or change in any observable way. This was the effect of conversion of mass to energy in an efficient way and the beginning of the nuclear age. The process of nuclear fission was first successfully described theoretically in 1904 by Ernest Rutherford, several years after the discovery of radioactive minerals. In 1934, Enrico Fermi showed experimentally that neutrons could split atoms to create elements lighter than the original. Nuclear fission itself was first observed in 1938 when two German scientists, Hahn and Strassman, attempted successfully to create a transuranic element, but the element was extremely unstable. The isotope, with its atomic mass higher than 92 began to decay as soon as it was bombarded by neutrons (Boorse *et al*, 1989; Hofmann, 2002). The scientists were successfully splitting the nucleus of the atom, giving two lighter elements and a neutron, in a process now known as “neutron induced fission” (Hofmann, 2002). Although it was not realized immediately, this

energy releasing process was self-sustaining. The splitting of the atom had been achieved, and with momentous results. This was a major breakthrough for the Allies during the Second World War, and many of the scientists who defected from Hitler's Germany began work on the world's first nuclear weapons in an undertaking known as "The Manhattan Project". The development of nuclear technology has since advanced at a fast pace, alongside the harnessing of this potential for power generation purposes. With increasing power generation from nuclear sources comes a new problem. How to deal with the nuclear waste arising from this process? Depending upon the process producing the waste and also the original fuel type, the resulting waste stream can differ significantly, requiring great care and thought to be taken during waste disposal. In addition there are wastes which have arisen from old military projects such as "The Manhattan Project" and early projects of a civilian and defence nature.

Radioactivity generated from nuclear sources, and waste in particular, can range from little more, in radioactivity terms, than background levels to a dose greater than that which is lethal to human life. This dosage depends on the quantity of the waste and the type of ionizing radiation which it emits - again dependent upon the source which generated the waste. Ionising radiation occurs in 3 main types in nuclear waste - α and β particles, or γ radiation. α particles are the most energetic of the three types of ionizing radiation, but despite their energy they can travel only a few centimetres in the air. A sheet of paper or contact with skin can prevent them from continuing their journey. Alpha decay is the emission of a ${}^4_2\text{He}$ nucleus, which often results from the decay of a material such as uranium.



The kinetic energy released in this process is proportional to the mass lost in the decay. Although alpha particles do not penetrate deeply, if alpha emitters are ingested into the body the damage to cells is extensive.

Beta particles are charged electrons (either β^- or β^+) emitted by the nucleus arising from the decay of a neutron into a proton. The mass of a nucleus which undergoes β^- decay is changed only a very small amount, whilst the mass number is unchanged. An

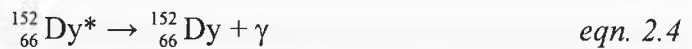
unseen neutral antineutrino, $\bar{\nu}_e$, accompanies each decay. For example, $^{14}_6\text{C}$ is unstable and emits a β particle, becoming the stable isotope $^{14}_7\text{N}$.



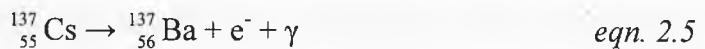
The neutrino has very little mass and is uncharged, and interacts only slightly with matter. β^+ decay occurs only for isotopes which have more neutrons than the stable form. For example:



where the neutrino is emitted together with an antiparticle, the positron (β^+). Although beta particles travel fast in air, they can only travel for a distance of around 3 metres. β radiation can penetrate the skin down to the germinal layer ($\sim 1\text{cm}$) where new skin cells are formed, but again much more damage will be caused if β emitters are ingested. β -decay is relatively fast in comparison to alpha decay and half lives are often long, for example as in the case of Cs^{137} , which has a half life of ~ 30 years. (Hofmann, 2002). Although beta particles can pass through a sheet of paper, they can be stopped by a thin sheet of aluminium foil, glass or appropriate clothing, and a β burn (dependent upon the dose level) can be similar to touching a hot surface, such as a cooker top. Fission fragments within the waste are often strong beta emitters. γ decay is a type of electromagnetic radiation that results from a redistribution of electric charge within a nucleus, and is by far the most penetrating type of ionizing radiation; a γ particle is a high energy photon, and the only thing which distinguishes γ radiation from the visible photons emitted is the wavelength, with γ “particles” having much shorter wavelengths. Gamma particles can be emitted when a complex nucleus undergoes a transformation from one configuration of neutrons and protons in its nucleus, to another, for example:



Isotopes such as ^{137}Cs and ^{99}Tc , and many of the α and β emitters produce gamma radiation in conjunction with the α or β emission process (Hesketh, 1996).



Heavy shielding is required to prevent interaction with gamma radiation, and often takes the form of a thick concrete wall or lead casing.

Nuclear wastes often generate all types of ionising radiation, although there is variation in the amount produced. The most dangerous threat to human life associated with waste is that which arises from the reactor core, commonly referred to as “High Level”. The term “high level” indicates that this waste contains a high percentage of the fissile elements from the process, and which also means that the waste is physically extremely hot due to radiogenic fission (British Medical Association, 1991).

2.3 Nuclear Power Reactors

Working reactors are generally one of three types; pressurised water cooled (PWR), advanced gas cooled (AGR) or fast breeder reactors. Water cooled and gas cooled reactors use the self sustaining reaction discovered by Fermi- neutrons split ^{235}U nuclei which creates 2 smaller nuclei and also releases energy as heat. This releases a number of free neutrons which then continue to split yet more U^{235} nuclei (**figure 2.1**).

However, if this reaction is allowed to continue in an uncontrolled manner with enough fuel, a state known as criticality is reached and causes a rapid energy release, i.e. an explosion. To prevent this, control rods are present which absorb the neutrons to reduce the energy emission of the reaction. To increase efficiency a moderator is also used to slow the neutrons down and moderate the neutron speed from fast to thermal - in the case of PWR reactors this is actually the light or heavy water in which the whole reactor is immersed. Boiling water reactors (BWR) are also used but make up only ~ 40% of the world’s commercial reactors. PWR reactors use a zircaloy cladding (slightly alloyed zirconium) around the fuel rods, through which pressurized water is pumped. This water serves as both moderator and heat transfer medium (Hesketh, 1996), allowing steam generators to power the electricity producing turbines (**figure 2.2**). A loss of cooling water can lead to core temperatures of ~2750°C, which is the fuel melting temperature, and so meltdown occurs (although no explosion) as in the case of Three Mile Island in Connecticut (USA) in 1979 (NRC Factsheet, 2004).

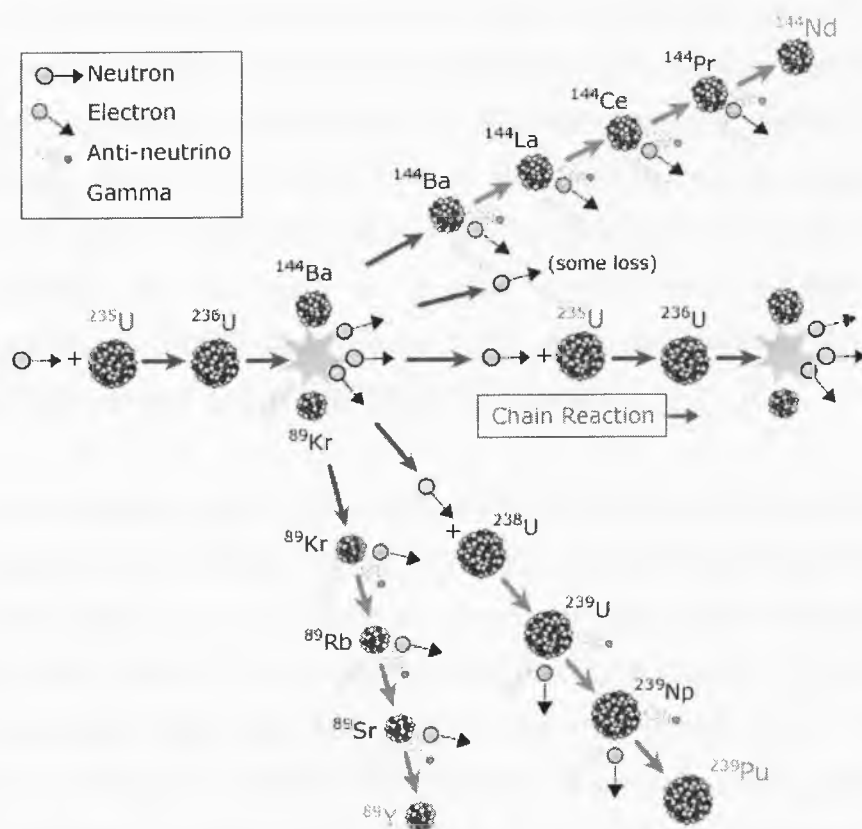


Figure 2.1: The fission process in a nuclear power reactor
 (<http://nobelprize.org/physics/educational/energy/fission>, 2004)

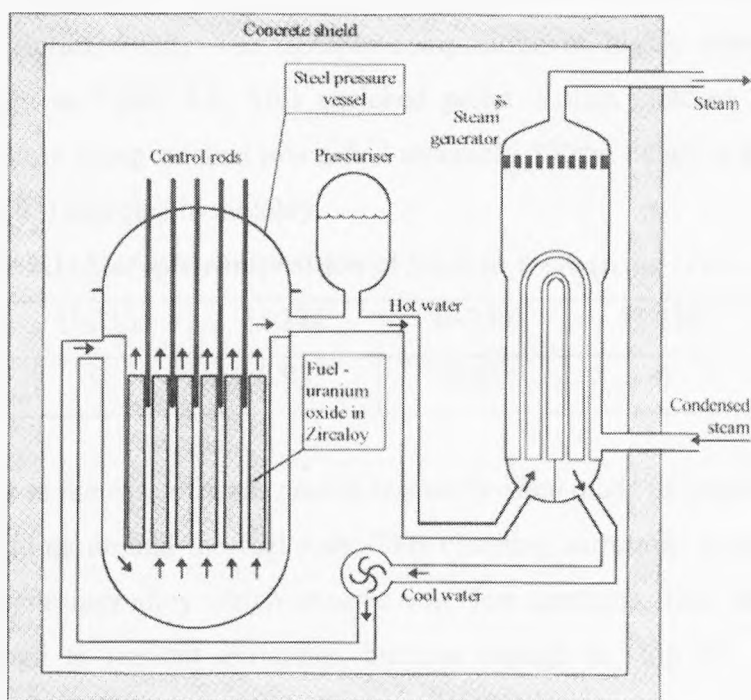


Figure 2.2: Schematic of a PWR (taken from Hesketh, 1996)

Modern PWR's typically consist of 157-241 fuel assemblies, each of which contains between 200-300 fuel rods. Inserted between these fuel rods are rods of Gd or B, placed to capture neutrons which will eventually destroy the neutron absorber. These are burnable (sacrificial) neutron poisons, as the capture process gradually destroys the absorber by forming an isotope which is inefficient in capturing neutrons. The isotopically enriched uranium dioxide fuel pellets used by PWR's are high melting point ceramics, and nowadays it is also possible to use mixed oxide, plutonium-enriched (MOX) fuels. These MOX fuels are beneficial as it allows recovered Pu from spent nuclear fuel (SNF) to be re-used.

Reactor fuels typically contain 3-5% enriched ^{235}U , which is found in its mineral form in pitchblende (U_3O_8), coffinite (USiO_4) and carnotite ($\text{K}_2[\text{UO}_2]_2[\text{NO}_4]_2 \cdot 3\text{H}_2\text{O}$). 1000 tonnes of ore yield around 2.5 tonne U. The ore is milled, then transported to a conversion plant, where it undergoes a chemical process to produce UF_6 . Enrichment of this product takes place to produce a UO_2 powder which is cold pressed into pellets around $0.75 \times 0.75\text{cm}$. Enrichment is often required as natural uranium contains 0.7% of the ^{235}U isotope. Magnox fuel, however, is not enriched. The remaining 99.3% is mostly ^{238}U , which does not contribute directly to the fission process, although it contributes indirectly by the formation of fissile isotopes of plutonium. Enrichment increases the percentage of ^{235}U , but accounts for approximately half the cost of the nuclear fuel (Heriot, 1988). The isotopic composition of highly enriched uranium (HEU) is given in **Table 2.1**. This enriched pellet is then sintered in a reducing atmosphere before being stacked into a fuel assembly 300cm height x 43cm diameter (King *et al*, 2003) and clad in zircaloy.

Table 2.1: Isotopic composition of LEU in wt% (King *et al*, 2003)

Isotope	U-233	U-234	U-235	U-236	U-238
Wt%	0	0.95	4.05	0	95

The moderator in the case of a gas cooled reactor is often made of graphite, taking the form of a cladding around the fuel rods. This cladding surrounds a natural uranium metal in a magnesium alloy which absorbs very few neutrons. This slows down the neutrons enough to prevent criticality, but not enough to stop the reaction from continuing. The cladding in a UK first generation reactor is known as Magnox;

magnesium alloy, no oxidation. The metal fuel used comprised an alloy of natural uranium (i.e. non-enriched) metal and Mg-based cladding alloy AL80. Early vitrified compositions (UK209 and Magnox Waste, or MW) are thus all characterised by high MgO and Al₂O₃ contents.

Boron rods are inserted in between the fuel rods to absorb any excess neutrons to prevent criticality. Pressurized gas (CO₂) is used as a coolant and is pumped around the reactor, absorbing heat, which is transferred to the water via a heat exchanger and subsequently used to produce steam to power turbines and produce electricity, as with the water in water cooled reactors (Hesketh, 1996). A typical fuel element in a Magnox reactor stays in the core between 3 and 5 years. A schematic of a Magnox reactor is seen in **figure 2.3**.

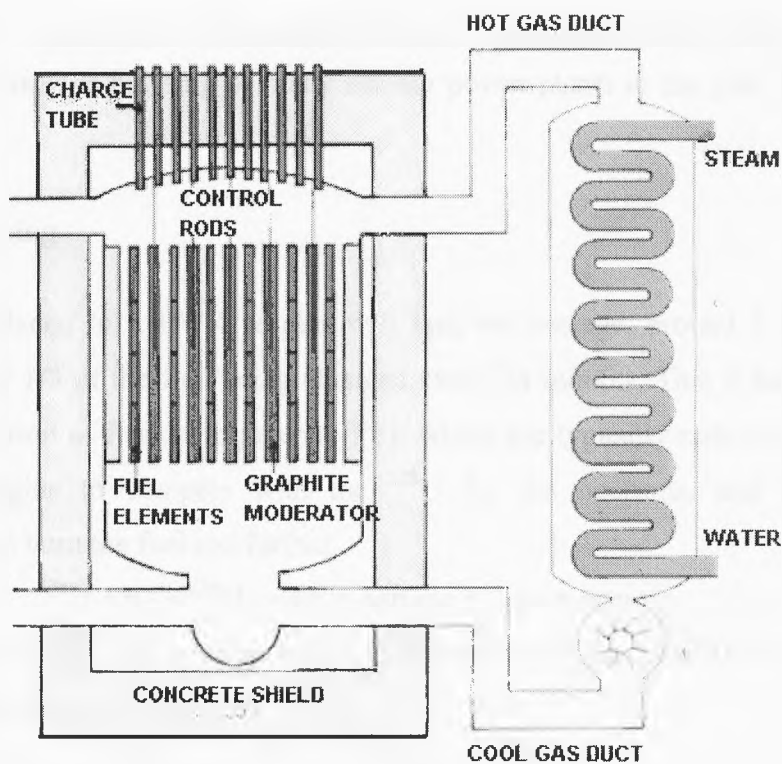


Figure 2.3: Magnox reactor schematic (taken from Hesketh, Ed. Wilson 1996)

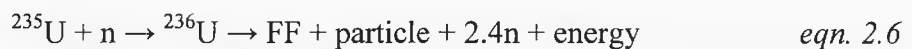
A fast breeder reactor works in a slightly different way to water and gas cooled reactors. It has a core of either ²³⁹Pu or ²³⁵U, which does not need to be moderated as a self sustaining reaction will occur with fast rather than thermal neutrons, and so the neutrons here are not slowed down. The core is surrounded by a layer of ²³⁸U that

absorbs neutrons created by the fission of the core material. This neutron absorption creates plutonium from the uranium cladding - a source of fuel for a new core. Cooling takes place by circulating a liquid metal (Na or K) around the core and again this coolant is used to produce steam for power generation (Hesketh, 1996). Production of ^{239}Pu , commonly known as “weapons grade” material, and used by the defence industry in the production of nuclear weapons makes the fast breeder reactor uncommon. However, an advantage of the system is its ability to use the same material as a fuel core and produce energy, allowing the reprocessing of much of the world’s supply of nuclear defence material, of which there is an excess (Bousquet and Brahler, 1997).

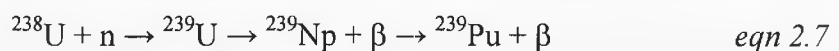
In terms of power output, the energy produced from a store of 3000 tonnes of fissile material can produce over 1 million MW power. When compared to a fossil fuel reactor, this is three orders of magnitude larger output per tonne of fuel and is the reasoning behind the building of many nuclear power plants in the past. (Bennett *et al*, 2001).

2.4 Reprocessing

A fuel rod placed in a PWR reactor will last, on average, around 3 years, with approximately 1/3 of the fuel being changed every 24 months. This is because, over time, the creation of fission fragments (FF), which are typically radioactive neutron absorbers, begins to compete with the ^{235}U for the neutrons, and it becomes uneconomic to burn the fuel rod further.



In addition to this, ^{239}Pu is often found in the spent nuclear fuel (SNF) when it is removed from the reactor core;



which, as a fissile element, again competes for the neutrons. However, as mentioned previously, it can also be used to create nuclear weapons.

Because of the neutron bombardment, these SNF rods are now high in radioactive fission fragments and very hot due to the continuing fission process, although the rate of fission is somewhat slowed. The rods are then moved into storage in a large

cooling pond until sufficiently cooled, usually after 6-12 months, to allow remote handling. The cooling pond contains 2000ppm B to act as a neutron absorber and to prevent criticality from being reached. The ponds used are large enough to contain 12yrs fuel and the rods in the pond have to be at least 23cm apart. A cooling system needs to be in place due to the continually generated heat, along with 2 back-up systems and a filter system, should any radioactive impurities leak from the rods. The filter system also helps maintain visibility in the pool, allowing the remote handling vehicles to operate effectively (Mesko, 1999). In countries where nuclear fuel is reprocessed (notably Britain and France) the rods are taken from the cooling pond at this stage and dissolved in highly concentrated nitric acid, after which the usable fissile uranium and plutonium are extracted. The extracted materials are used to create new fuel rods known as mixed oxide, or MOX fuel, which is the aim of the reprocessing cycle (Hesketh, 1996). Unfortunately, this process leaves behind a highly concentrated, radioactive solution, referred to as Highly Active Liquor (HAL). The HAL is generally stored in large, stainless steel tanks above ground. The HAL is subsequently calcined, mixed with borosilicate glass to give a high level waste (HLW), which is vitrified and moved to an above ground store. This is referred to as temporary storage, although the canisters may remain in storage for 50 years or more. The final step for storing this waste is intended to be permanent disposal in a repository (Larkin, 1986) although a site for a repository has yet to be identified in the UK.

2.5 Classification

Every user of radioactive substances operational in the UK today produces wastes which are broadly categorised into very low level, low, intermediate or high wastes. The classification depends upon the radioactive hazard they present. Very low level waste (VLLW) is non heat generating and the radioactivity levels are low enough to allow handling and disposal in general landfill. Low level waste (LLW) contains enough radiation to warrant special disposal but does not require shielding in handling or storage. Intermediate level waste (ILW) is highly radioactive, containing over 4000Bqg^{-1} of long-lived (over 30 year) alpha emitters and requires sophisticated handling and disposal. High level waste (HLW), in contrast to ILW, not only emits

long-lived alpha and beta particles and gamma radiation, but is also significantly heat generating (Desvaux *et al*, 1998).

Very low level waste is generated mainly from geological and medical sources. It can consist of such things as contaminated gloves and containers which have held radioactive isotopes of short half-lives, used for research or medical purposes. Very low level waste can be diluted and disposed of easily, and is often placed into general purpose landfill sites, or in a liquid form poured into the drainage system. Shielding required for handling is minimal, as radiation levels are little more than the background levels. UK classification states that very low level waste is “material which contains less than 400 kBq of beta/gamma activity per 0.1m³ or 40 kBq per single item” (DEFRA, 2001). The greatest volume of nuclear wastes are VLLW.

Low level wastes, such as clothing coming into contact with a radiation source, or perhaps a spatula with surface contamination are generally produced from the same sources as very low level waste. This is traditionally buried, a method known as “near-surface” disposal. In the UK, it is buried at Dounreay and Drigg sites, but can be buried at any licensed site. In the UK, a low level waste (LLW) material has an activity that exceeds very low level waste, but does not exceed 4 GBq per tonne of alpha or 12 GBq per tonne of beta/gamma activity (DEFRA, 2001).

Intermediate Level Waste (ILW), a classification which does not exist in the USA, is a non-heat generating radioactive type of waste, often arising from stages in the reprocessing of fuel, or from mill tailings from U mines. This waste is usually immobilized in a grout or cement and must be remotely handled. The storage times for these wastes (compared to VLLW and LLW) increases prior to encapsulation, to allow for safe handling. Classification states that such materials exceed LLW activity limits, but there is no radiogenic heating; hence cooling does not need to be considered when designing storage facilities (DEFRA, 2001). In the UK, Sellafield is the biggest producer of these wastes.

HLW arises from two main sources; reprocessing of spent nuclear fuel (SNF) to produce more fuel and the decommissioning of nuclear power plants and nuclear weapons. HLW is significantly heat generating, due to the presence of radiogenic fission products, e.g ¹³⁷Cs and ⁹⁰Sr, in the waste. This level of radioactivity and heat

generation **must** be taken into account when designing methods for storage and disposal for this waste.

2.6 Waste Immobilisation

Waste immobilisation techniques differ throughout the world. Immobilisation of LLW is usually achieved by packing the wastes into stainless steel containers and backfilling with grout. VLLW is sometimes also landfilled. ILW is often immobilised using a cement/grout combination and pouring into stainless steel containers. Whilst reprocessing of SNF is only carried out in the UK and France, immobilisation of HLW and SNF is a worldwide issue. Borosilicate glasses have been used as host matrices for immobilisation of HLW generated over the past 50 years. These wastes arise from such activities as atomic weapon decommissioning and reprocessing of spent nuclear fuel. In the United States, the majority of HLW comes from activities such as the Manhattan Project of the 1950's (Lutze, 1988; Roth and Weisenberger, 2000). This is partly due to the fact that fuel reprocessing has been disallowed in the US since the early 1980's, allowing the quantities of SNF to build up. Although HLW is commonly vitrified in a borosilicate glass, occasionally phosphate based glasses are used for HLW encapsulation within a ceramic melter - a method more commonly employed in Russia (USDoE, 2003). Phosphate glasses are known to have increased durability but poor mechanical stability. The borosilicate glass can vary in composition, and also the method of vitrification varies depending on the chosen method of the country of origin. France and Britain use very similar processes to immobilise the wastes produced from reprocessing, whilst the USA and Russia use different methods to immobilise their civilian and defence wastes.

The process applied in Tokai (Japan), PAMELA (Belgium) and Hanford (USA), uses a slurry fed ceramic melter, known as a Joule heated ceramic melter. This low temperature melter, which reaches 1150°C is heated internally using electrodes of Inconel 640, and the pre-mixed calcine and frit batches are added to the melter in careful proportions so as not to short out the electrodes due to any settling out on the bottom of the crucible of the noble metals. Electrodes placed within the melter produce an alternating current sufficient to dissipate the energy within the melt at a rate suitable to convert the feed into glass. (Chapman and McElroy, 1989). HLW

glass in the USA contains high concentrations of Ni, Cr and specifically Fe, which arise from the stainless steel cladding used for the fuel rods. Savannah River Waste, according to Matyas *et al*, (2002), contains 51.47% Fe (by oxide content) as compared to UK Blend waste of 4.21% Fe (by oxide content). One way to get around this problem of shorting out in a ceramic melter is to separate high activity waste from calcined, dissolved waste, thereby concentrating the radionuclides in the process. The highly active waste (HAW) then contains a large amount of P₂O₅ in solution from the additives used in the separation process. Borosilicate glass used to immobilise these wastes have an increased ZrO₂ and Al₂O₃ content which has been shown by Jantzen *et al*, (2000) to increase the durability of glasses with increased P₂O₅ content, arising from the separation process. Joule heated ceramic melting is, in general, a cold cap method, as the batch forms a cold cap on top of the melting batch, which creates reducing conditions in the melter but suppresses volatiles.

At BNFL Sellafield the types of waste are from historical (several decades old) sources and also modern reactors, and differ quite widely in composition. It is therefore better in this case to have a crucible melting system as, although the waste stream composition is well defined, the current waste stream being vitrified may not always be the only vitrified waste stream. This means that the crucible melter is more versatile due to the lack of electrodes within the glass melter and so electrode failure due to deposition of heavy metals at the bottom of the melter will not occur (Roth and Weisenberger, 2000). The historical waste streams within the UK waste immobilisation remit are not well characterised for use of the ceramic melter system.

The French developed a process for immobilising the HAL liquor which involves drying and denitration of the liquor in a tube furnace followed by vitrification in an induction heated melter with borosilicate glass frit. This process is known as the AVM/AVH process and a version of it is now used at Sellafield, in the UK (Quang *et al*, 2003). As noted previously HAL is produced when spent nuclear fuel (SNF) rods are sheared and dissolved in hot 6M HNO₃. The resultant HAL is then stored above ground in double walled stainless steel tanks, surrounded by several metres of concrete to prevent damage to the surrounding area from γ radiation. The tanks have internal cooling systems (**figure 2.4**) to prevent boiling due to overheating as the HAL still contains a large number of fission fragments which will continue to decay. From

these tanks, the liquor passes into a calciner (figure 2.5), which is a resistance heated, rotating furnace with a rabble bar inside.

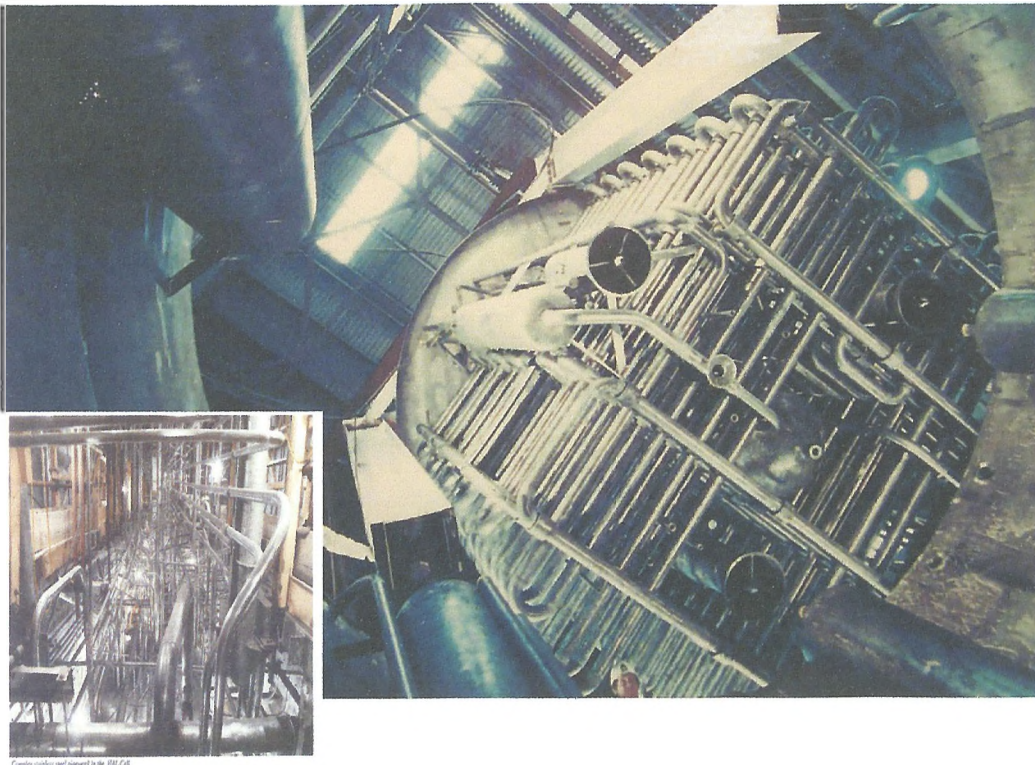


Figure 2.4: Internal cooling system of HAL tanks. Inset: pipework in the HAL cell surrounding the tanks (image courtesy of Nexia Solutions)

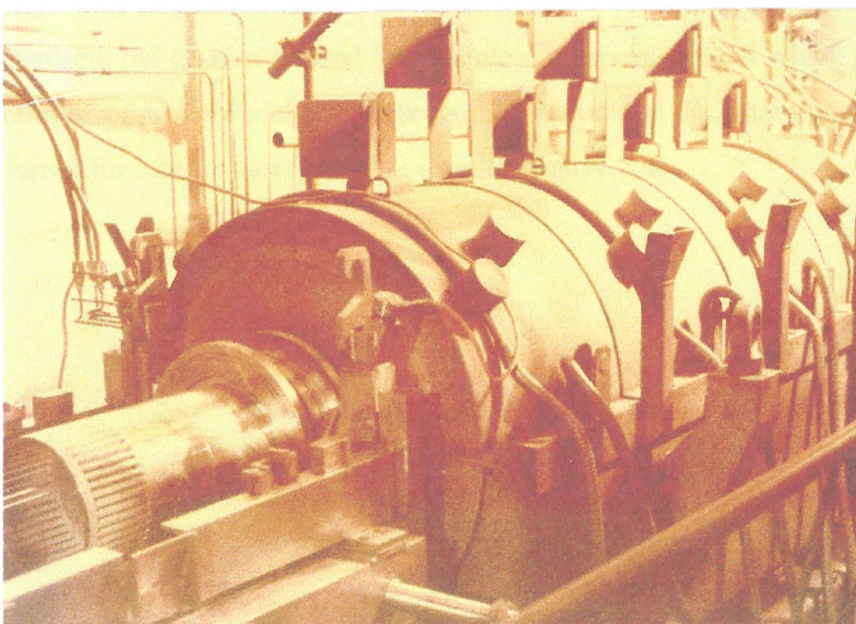


Figure 2.5: Rotary calciner at Sellafield (image courtesy of Nexia Solutions)

The calcination process is complicated by the volatilisation of Ru and the formation of refractory oxides which, because of their low solubility in glass, are difficult to incorporate in the subsequent glass melt. Therefore, prior to calcination, the raffinate is combined with a solution of lithium nitrate to produce complex Fe and Al species thus preventing the formation of refractory compounds of these metals (Larkin, 1986). Volatilisation of Ru is suppressed by adding sucrose to react with excess nitrate, thereby preventing the nitrate mediated oxidation of Ru to volatile RuO₄.

The calciner is angled 10° downwards, and the liquor is poured in at the top end of the furnace where it goes through several heated zones which should be at a temperature of around 300°C. Residence time in the calciner is <0.5hrs. Once partially denitrated and dehydrated, it forms a granular brown powder, in appearance much like instant coffee granules, and is poured into an inductively heated Inconel 601 pot melter along with a mixed alkali borosilicate glass. The borosilicate glass frit, manufactured to a fixed specification by James Kent, Stoke-on-Trent, is melted using a cold cap method in a furnace using molybdenum electrodes. The waste is added to give a 25wt% oxide waste loading. The calcine / glass batch (~250kg) is maintained at 1050°C for around 5 to 8 hours and sparged with compressed air (this sparge is Ar in the French Cap La Hague plant - Scales, 2001) to homogenise the melt prior to pouring. On pouring approximately 70kg of glass is left in the melter; this is known as the “heel”. Once fully homogenised, the glass is poured into stainless steel canisters at which point the canisters are allowed to cool and are subsequently sealed and decontaminated before being transferred for interim storage above ground (**figure 2.6**).

Three lines have been installed at Sellafield that are capable of vitrifying the HLW from 2500 MT of Magnox and oxide fuel per year and producing 600 canisters per year, each containing 150 litres of glass. The product canisters are 430mm in diameter by 1340 high and are fabricated of Type 309 stainless steel. Each canister contains 150 litres of borosilicate glass (20 wt% waste oxides) and weighs 470kg. The maximum heat output is 2.5 kW hr^{-1} (Larkin, 1986).

The whole process is a remote one, manipulated by remotely operated machines or MSM's (master slave manipulators), as the radiation would be deadly in too close contact. These "hot cells" as they are known, have thick concrete walls and lead shielding and cannot be entered. A breakdown in any equipment is costly and time consuming and so the process is carefully controlled so as minimise factors which lead to the damage/corrosion of any of the constituents of these hot cells.

The above ground, temporary storage in the UK for HLW is currently at Sellafield, where the reprocessing takes place. The storage facility is constructed of concrete, into which reinforced cavities are cast, and the canisters stacked above one another in the cavities (see figure 2.7).

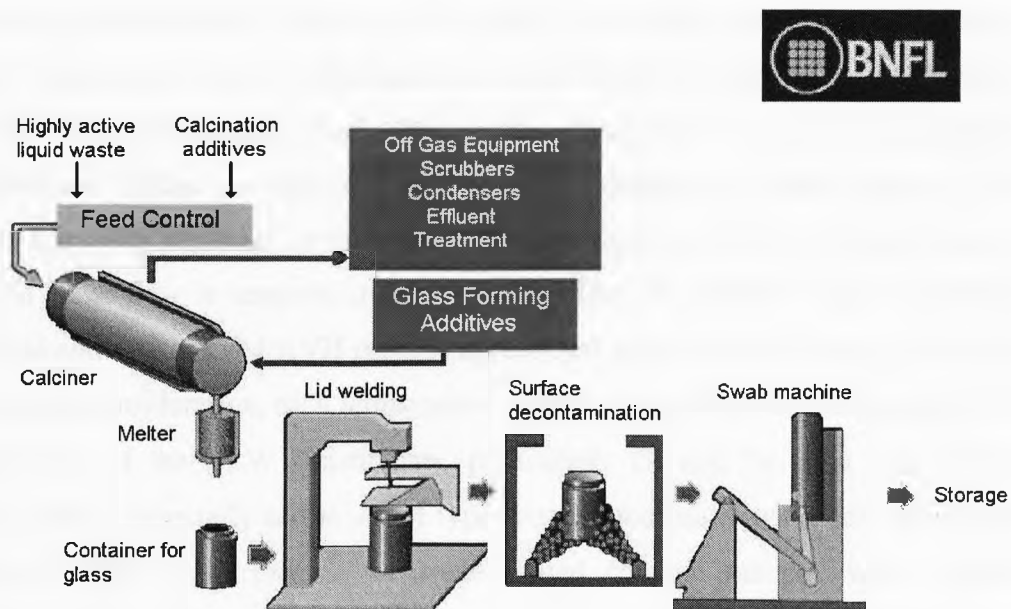


Figure 2.6: Continuous vitrification process (image courtesy of Nexia Solutions)



Figure 2.7: Interim storage facility at BNFL Sellafield. The coloured markers indicate which of the cavities contain canisters. (Image courtesy of Nexia Solutions)

The ability of borosilicate glasses to incorporate a wide range of elements found in a typical waste stream was the deciding factor in the choice of immobilisation matrix in the UK. Temperatures at which the glasses are melted are also an important consideration. Unlike an industrial process, glass melter in a radiologically “hot” process cannot be replaced or repaired easily so, to reduce melter corrosion, they are operated at as low a temperature as possible. Thus a standard melter at BNFL Sellafield and in the AVM/AVH process operates at about 1050°C (Scales, 2001). As a secondary consideration, melt temperatures should be kept low to reduce the risk of volatilisation of the HLW constituents, particularly Cs and Tc (Luo *et al*, 2001; Fardon, 1982), especially as the AVM type process does not have a cold cap. Some literature suggests that the use of Joule heated ceramic melter, which reduce volatilisation due to the effect of the cold cap, are preferable (Luo *et al*, 2001; Ewing, 1999).

2.7 Borosilicate glasses

When discussing the selection of a suitable composition for immobilisation matrices, Marples (1988) compared waste incorporation limits, ease of manufacture, viscosity of the glass frit and the durability of the final product. Marples concluded that, after hundreds of thousands of years, the radiation effects on the glasses will be minimal, with <1% changes in density. Borosilicate glasses have good long term durability, chemical durability, radiation stability and thermal stability. These properties, especially long term durability, are essential for the chosen material, as any matrix must be able to immobilise the very long lived actinides which have half lives of thousands or more years, and also contain the shorter lived fission products such as ^{137}Cs . ^{137}Cs is heat generating with a half life of 30 years. For the first few hundred years of the product lifetime, elements such as ^{137}Cs and ^{90}Sr will be one of the main sources of radioactivity and heat generation. The heat generation should not exceed the glass transition temperature of the host glass, which would then make the ions mobile within the glass, and borosilicate glass is suited to this (Marples, 1988; Bevilacqua *et al*, 1996). The long lived actinides also have great significance, as after the first 500 years of disposal actinides and their daughter products will account for more than half of the radiotoxicity of the glass product (**figure 2.8**). Thus the direct effects, such as radiation damage, leach resistance and residual radioactivity of long lived actinides such as ^{239}Pu and ^{237}Np should be taken into account when immobilising waste that contains any traces of these elements. The long term risk of a geological repository (in which all wastes will eventually be stored) is directly related to the quantity of these long lived actinides within the geosphere (Ewing, 1999).

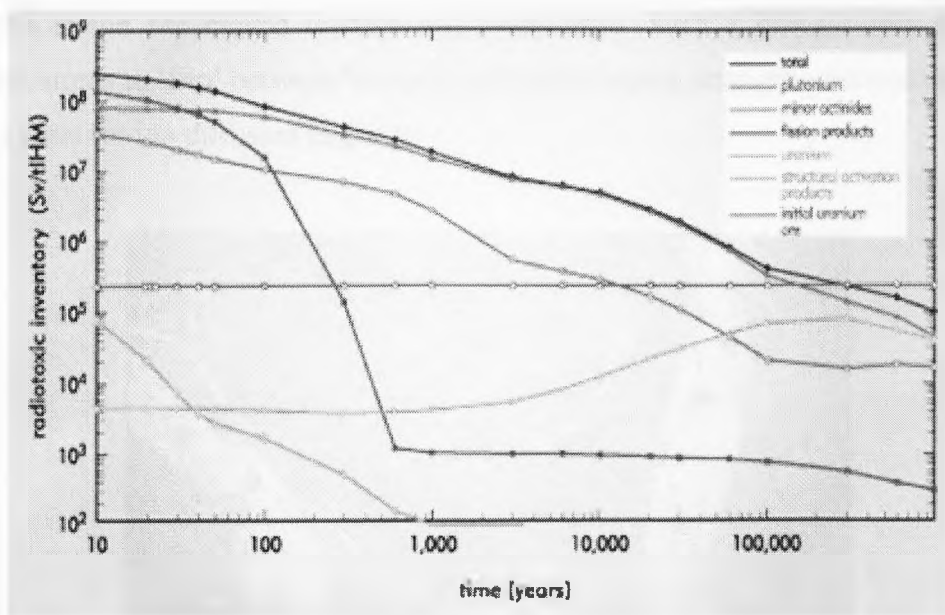


Figure 2.8: Radiotoxicity inventory against time- highlighted in green are the minor actinides, which account for more than half the radiotoxicity after 500 years (Matzke and Vernaz, 1993).

Other factors which may affect the long term durability of the glass and melter life time, are the formation of crystalline phases such as molybdates, refractory oxides within the glass and anything which is immiscible within the glass.

Greaves *et al*, (1991) also consider the effect of a mixed alkali network on the bonding structure of multicomponent glasses. This work proposes that the glass network of a multicomponent glass is not totally disordered but can be described in terms of a modified random network (MRN). In the MRN model cation environments are restricted to percolation channels threading randomly through the network rather than being dispersed randomly through bonds with silica tetrahedra. Layers of chains of corner-sharing SiO_4 units are cross-linked by ionically bonded alkali atoms (**figure 2.9**). The inter-network zones in silicate glasses are the basis for ionic diffusion, which ultimately undermines the stability of the structure. This ionic diffusion is the basis for glass corrosion and the method by which an alkali cation in a percolation channel (**figure 2.9**) can cross-over to an adjacent site. This occurs through the process of transferring the alkali cation non-bridging oxygen bond to the next silicate group along the edge of the percolation channel, and causing a local rearrangement of the oxygen bonding structure. This rearrangement occurs only in the silicate groups

that the cation has moved towards and away from. Such a process only requires oxygen atoms to ‘flip’ between bridging and non-bridging arrangements and could act as the basis for ion diffusion in glass.

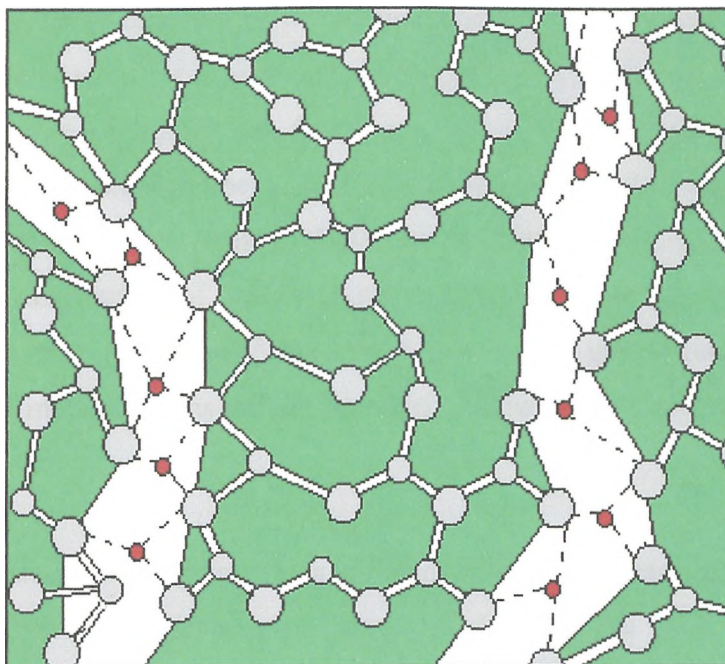


Figure 2.9: A schematic diagram of the MRN model of glass structure showing percolation channels formed by monovalent alkaline cations (in red) loosely bonded with oxygen atoms of surrounding silicate groups (in grey) (Greaves *et al*, 1991).

Ionic mobility in glasses is decreased when alkali cations of different sizes are present in the glass structure, particularly when they are present in equal amounts. The different ionic sizes cause interference in the percolation channels where local bond ordering energies are disturbed. This is known as the ‘mixed alkali effect’ and is responsible for greater long-term durability (Shelby, 1997), hence the choice of a mixed alkali borosilicate glass for immobilisation purposes. Work during the 1980’s at Harwell showed that mixed alkali glasses also have beneficial effects on the incorporation properties of the glass, in terms of molybdenum, transition elements and noble metals (Scales, 2001).

On cooling from the liquid phase, glass forming liquids do not undergo a sudden transformation at a defined temperature. Instead, a continuous change occurs from the

liquid form into a solid glass, and the structures in the melt remain almost intact throughout this process when the liquid becomes solid. At the glass transition temperature (T_g) glasses pass from exhibiting liquid-like properties to solid-like properties. This is called a gradual freezing process (Roth and Weisenberger, 2000; Taylor, 1985). The glassy state does not fit within the three classical states of matter because, although glasses possess the mechanical rigidity of crystals, they have the random or disordered structure of liquids. On freezing, waste is immobilised within the glass structure, with many elements being part of the glass matrix although some may not be fully incorporated. For example Calas *et al*, (2003) and Short (2004), when studying the incorporation of molybdenum in a nuclear waste glass using EXAFS found that molybdenum as MoO_4^{2-} does not bond with the glass structure, rather it is associated with mobile cations within the matrix, allowing easy removal (Short *et al*, 2005).

Molybdate phases are recognised as a problem in most nuclear waste glasses, and have been studied by researchers in France, the UK and the USA. Compositional analysis of these phases often highlights the presence of problem elements such as Cs, Tc and Sr, segregated within the phase, also known generically as “yellow phase” (Ewing, 1988). This phase is often yellow due to sulphate and chromate content, and may incorporate ^{137}Cs and ^{90}Sr ($t_{0.5}$ for both is ~ 30 yrs), two heat producing, highly radioactive problem elements for the first few hundred years of the waste lifetime. Schiewer *et al*, (1982) studied “yellow phase”, a blend of several highly radioactive elements including Mo, S and Cr, and found a reduction in the melter lifetime by about one third, due to the increased corrosion of the Inconel pot when yellow phase is present. Yellow phase and its formation was also studied by Owens (1981) and found to be, on average, 70% rare earth molybdates and 30% alkaline earth molybdates. These alkaline earth molybdates are believed to be the main problem (Camara *et al*, 1988), as they contain many of the elements which are highly radioactive, and are also water soluble.

Kawamoto *et al*, (1981) found that small molybdenum additions to a simple sodium borosilicate glass had a tendency to form MoO_2 (when Mo is present in +4 valence state). This phase has a reasonable durability but presents another problem - that of

thermal expansion mismatch between the glass and the MoO₂. This could lead to cracking on cooling and enhancement of the “heel” when pouring, leading to a shorter melter lifetime. Schiewer *et al*, (1982) suggests that prevention of the formation of molybdate phases is only obtained under reducing conditions, and that Mo³⁺ is more easily dissolved into the glass matrix than its oxidised counterpart, Mo⁶⁺. Contrary to this, Short (2004) found that melting under reducing conditions doesn’t work, as yellow phase constituents nucleated within the bulk of the glass whatever the melting conditions.

Crystalline phases in the final glass, possibly arising as a result of improper homogenisation of the melt in the presence of heel glass, can be tolerated in small amounts, but should not be present above a threshold value as discussed by Donald *et al*, (1997). For molybdenum, this threshold value is believed to be up to 3% waste loading in the glass, but is usually kept around 1%.

A particular type of calcined waste generated in the BNFL Sellafield process is known as a “blend” waste form and is the type with which this study will deal exclusively. This waste arises from mixing Magnox fuel and oxide fuel in a 25/75 blend. This waste solution contains dissolved fission products, impurities from cladding materials and traces of unseparated plutonium and uranium, plus several transuranic elements (Roth and Weisenberger 2000). A breakdown of the origin of elements contained in the waste is given in **table 2.2**, along with the origin of each of these elements (Larkin, 1986).

The Magnox fuel waste is added to the oxide fuel waste in order to increase the Al content of the waste glass, as the Magnox fuel has increased amounts of Mg and Al used in the Magnox fuel cladding. In controlled amounts Al can have beneficial effects on glass properties. Al can increase the stability of the borosilicate matrix and decrease the likelihood of amorphous and crystalline phase separation in the final product (Jantzen *et al*, 2000; Clark *et al*, 1982) and durability of the glass formed. Clark *et al*, (1982) demonstrated the increased durability of a high alumina waste glass used for US defence high level wastes, although the possibility of refractory oxides of Al forming within the glass increases. Unfortunately, adding Magnox waste increases the percentage of Mg in the glass, which is also likely to form refractory

oxides in the waste. However, Clark *et al*, found a layer of Mg(OH)₂ formed on the glass surface whilst leaching was found to decrease for glasses containing high Mg waste.

Table 2.2: Origin of elements in waste form (Larkin, 1986)

Fission Products				
Ge	As	Se	Rb	Y
Sr	Zr	Mo	Ru	Te
Nb	Ag	Cd	In	Sn
Cs	Ba	La	Ce	Pr
Sb	Dy	Nd	Sm	Eu
Gd	Tb			
Unextracted Actinides				
U	Pu			
Actinides				
Cm	Am	Np		
Corrosion products				
Fe	Cr	Ni		
Cladding				
Mg	Al			
Fuel Additives				
Fe	Al	Si	Mo	
Process Additives				
Na	Fe	SO ₄	PO ₄	
Neutron Poisons				
Gd				

Refractory oxides, such as spinels of Fe, Cr and Ni are highly insoluble and difficult to melt (Vienna *et al*, 1997). Elements with low solubility in the borosilicate glass matrix, such as sulphur, are also of concern. Hrma *et al*, (2001) noted that sulphur was immiscible within the melt and caused what is known as “gall” to form on the surface of the glass melt, a blanket layer over the top effectively giving reducing conditions within the melter. Sulphur also attacks the melter, reducing its lifetime, and as discussed previously this is not a desirable property (Roth and Weisenberger, 2000; Fardon, 1991). Glasses with low boron levels have lower tolerance for molybdenum phases and also, more importantly, lower tolerance for waste digestion (Larkin, 1986).

Additions thought to be beneficial to the final product must also be considered. Preceding and during the calcination process, there are two main additions made which are sucrose and lithium. Lithium is added to the calciner feed to condition the

waste, and forms a complex oxide when the metal nitrates are decomposed upon exposure to heat. Lithium complexes with, for example, Fe and Al which then have a higher reactivity than the corresponding amphoteric oxides. Sucrose is added to the calciner for two reasons, acting as a dispersant and a reducing agent. The sugar should react with the free nitrates in the system to prevent ruthenium oxidising and becoming volatile (Larkin, 1986; Owens *et al*, 1984). Ruthenium in solution is not a problem, but when heated it forms a solid precipitate which becomes highly volatile and leaves the system via the offgas. To prevent the formation of complex RuO_4 from the nitrosyl ruthenia, the sugar reacts with the free nitrates to reduce overall volatility. Ruthenium may also be problematic when it forms ruthenium dioxide, as these needle-like crystals can sediment to the bottom of the melter in a “raft” formation and pull other phases in the glass to the glass heel. This affects the properties of the glass heel, which will become highly viscous and likely to block the drain during a pour campaign (Fardon, 1991). The lithium is added to the HAL as LiNO_3 , which makes up half of the total lithia content of the waste glass. The other 2wt% is present in the frit, giving a mixed alkali glass. Lithia in the glass melt also increases fluidity, and therefore ease of pouring (Gribble, 2002)

2.8 R7T7- A comparison

The French reference glass for LWR fission product solutions is R7/T7, and has a non-radioactive version SON 681817, generally referred to as SON68. Factors determining loss of radioactive fission products (such as Cs but also Ru, Tc and Se) during glass melting in R7T7 have been studied, and characterisation of the solid glasses to determine their properties has also been undertaken. The final R7T7 glass is a black product, much like the UK blend and Magnox glasses (Larkin, 1986). **Table 2.3** gives a nominal R7T7 composition.

Table 2.3: R7T7 waste loaded glass, developed to reprocess PWR fuel (compiled from Matzke and Vernaz, 1993)

Oxide	R7T7	Oxide	R7T7
SiO ₂	45.48	AgO	0.03
Al ₂ O ₃	4.91	CdO	0.003
B ₂ O ₃	14.02	SnO	0.02
Na ₂ O	9.86	Sb ₂ O ₃	0.01
CaO	4.04	TeO ₂	0.23
MgO	1.84	BaO	0.60
TiO ₂	3.97	CeO ₂	0.93
Li ₂ O	1.98	Pr ₂ O ₃	0.44
Fe ₂ O ₃	2.91	Sm ₂ O ₃	0.31
P ₂ O ₅	0.28	Gd ₂ O ₃	0.03
ZrO ₂	2.65	Nd ₂ O ₃	1.59
NiO	0.42	Rb ₂ O	0.13
Cr ₂ O ₃	0.51	Cs ₂ O	1.29
SrO	0.33	RuO ₂	0.46
Y ₂ O ₃	0.20	Rh ₂ O ₃	0.12
MoO ₃	1.70	PdO	0.33
MnO	0.25	ThO ₂	0.33
		UO ₂	0.52

Some precipitates and second phases are encountered as heterogeneities, which include platinoids inclusions, Mo inclusions, and other elements of low solubility. RuO₂ inclusions are a problem for both R7T7 and UK blend glass, and Ni and Cr impurities due to corrosion of the Inconel melter are also common to both glasses. Platinoids in the form of rods were observed by Pacaud *et al*, (1991), alongside spherical, metallic platinoids and chromite crystals. Heterogeneous distribution of the platinoid particles was observed throughout the glasses, with settling towards the bottom of the as-cast block. The chemical durability of the glass, however, was found not to be affected by the presence of platinoids, leading Pacaud *et al*, to conclude that the platinoids were detrimental to melter lifetime due to settling out, but not detrimental to overall durability.

The “Yellow phase”- i.e., alkali or alkaline earth molybdates is also a problem, although somewhat less in an R7T7 glass as the waste stream contains less Mo than the UK stream. Powellite type molybdates are observed as being more highly developed in the presence of platinoids. However, it is claimed that these problematic phases constitute less than ~1% of the glass, giving excellent homogeneity within the final product (Matzke and Vernaz, 1993). R7T7 glass was designed to hold a

maximum of 18.5% radioactive waste oxides (Quang *et al*, 2003), in comparison to WRW13 (the commercial BNFL glass designed for the blended waste stream) which was designed to contain 25% oxides. The product glass has a high activity content overall, mainly ^{137}Cs and ^{90}Sr . Durability studies using PCT-1 tests revealed results up to 1/10 of the accepted suitability criteria (Gong *et al*, 1999).

Given the similarity of the two waste forms, it can therefore be concluded that the UK glass, loaded with a blend waste, may act in a similar way under long term storage conditions and be equally as durable, although given the problematic phases within the melting system these assumptions are questionable.

2.9 Alternative Waste Forms

Other waste forms have been considered for HLW immobilisation including Synroc, and other ceramics, but for large volumes these have been disregarded in favour of borosilicate glasses. A good overview of these waste forms is given by Donald *et al* (1997) and the reader is referred to this. Of these alternative wastefoms, Synroc is briefly described as some of the problems experienced within HLW glasses in relation to Mo are also common in Synroc.

The main minerals in Synroc-C are hollandite ($\text{BaAl}_2\text{Ti}_6\text{O}_{16}$), zirconolite ($\text{CaZrTi}_2\text{O}_7$) and perovskite (CaTiO_3). Rutile (TiO_2) acts as a buffer phase. Zirconolite and perovskite are the major hosts for long-lived actinides such as Pu, although perovskite is principally a host for Sr and Ba. Hollandite immobilises the larger ions such as Cs, K, Rb and Ba (Bennett *et al*, 2001). These ceramic wastefoms are usually made in a reducing environment so as to reduce elements of the waste to metallic and alloy form, which are then encapsulated in the ceramic. The minerals used for Synroc fabrication also occur in nature, where they have demonstrated their capacity to survive for many millions of years in a wide range of geological environments. The Synroc-C wastefom can hold up to 30% HLW by weight. Different forms of Synroc have been developed to deal with military radioactive wastes, including Pu as well as other applications related to partitioning and transmutation of wastes. HLW can be partitioned into separate components, some of which can be transmuted into different forms (less radioactive or shorter-lived). This occurs usually by neutron bombardment in a reactor or accelerator. Those components which are not suitable for transmutation

can then be immobilised in Synroc. Initial leach rates of Mo (0.4- Synroc; 2.6- borosilicate) and Cs (0.02- Synroc; 2.4- borosilicate) in Synroc are almost one third of those experienced in a borosilicate glass with a similar waste loading.

The waste form is the key component of the immobilization process, as it determines both waste loading which directly impacts cost, and chemical durability, which determines environmental risk. To achieve maximum savings and optimum performance the Synroc waste forms are tailored to suit the particular characteristics of the nuclear waste to be immobilised, rather than adopting a single waste form for all waste streams (Ringwood, 1985).

Another variant, Synroc-F, was developed which was rich in pyrochlores - $(Ca, Gd, U, Pu, Hf)_2Ti_2O_7$, and was developed for the disposal of unreprocessed spent fuel from light water reactors and further developed for plutonium immobilisation. This pyrochlore-rich ceramic was found to be more efficient for immobilising uranium contained in the chosen waste stream without the loss of rare-earth neutron absorbers from the crystalline structure (which tended to be displaced by U). A pyrochlore-rich titanate ceramic with an increased loading of natural U and neutron absorbers (Gd, Sm, Hf), which are needed for nuclear criticality control was fabricated by the US DoE (Department of Energy). Pyrochlore is similar to zirconolite and can incorporate up to 50% by mass of PuO_2 and/or UO_2 . There is twice as much U as Pu (23% : 11.5% by mass) so that high ^{238}U levels will ensure additional criticality control as ^{239}Pu decays to ^{235}U . There is as much Hf and Gd (each) as Pu. The baseline wastefrom is 95% pyrochlore and 5% rutile (TiO_2) with Hf replacing one tenth of the Ti. However, there are large variations according to feedstock composition and impurities (Jostsons, 2002). The sensitivity to feedstock variations is one of the reasons why borosilicate glass rather than Synroc is used for HLW immobilisation.

2.10 Glass Melting and Dissolution

Dissolution of batch components in glassy or silicate melts is a complex and not yet fully understood topic. Dissolution studies often concentrate on one batch component, or the corrosion of an electrode, such as Mo, in the glass batch leading to unwanted contamination such as colouring. Chandra (2002) studied the effects of silica dissolution within a simple soda lime silica batch, concluding that raw material

segregation occurred as a result of compositional changes and affected the dissolution of batch components. The time taken to obtain complete homogeneity of the glass increased when feldspar (sand substitute) was added to a commercial glass melt.

Park *et al*, (1999) investigated the corrosion mechanisms of molybdenum disilicide in borosilicate glass for direct comparison to alumina-zirconia-chrome-silica (AZCS) refractories used in glass melting. The kinetics and mechanisms of corrosion of MoSi_2 varied according to the position of the sample within the melt. Above the glass line a semi-protective SiO_2 layer formed which has good oxidation resistance. Below the glass line, a protective Mo-rich layer composed of various molybdenum silicates forms, with corrosion resistance comparable to AZCS refractory blocks. At the glass line however, simultaneous dissolution of SiO_2 and vaporization of MoO_3 leads to comparatively rapid contamination and corrosion, giving the so-called glass line cut.

Inhomogeneity in glass melting may be caused by segregation of the raw materials, melt segregation, volatilisation of oxides from the melt surface and refractory contamination (Hartley, 1963). The melt corrosion of oxide refractories by slag in a hot furnace can be likened to the corrosion or dissolution of the nuclear waste calcine particles in the glassy melt. Refractories typically consist of a large aggregate held together with a finer, more porous matrix, which is more reactive than the larger grain. Attack and corrosion of refractories by liquid slags can be both a chemical (corrosive) wear and a physical/mechanical wear, such as erosion. Lee and Zhang (1999) state that open pores and microcracks are the main channels of initial slag penetration into refractories. Although theoretical models can be provided for the attack of refractories dependent upon capillary radius, pressure, slag viscosity and penetration depth, what is not currently included in the calculation is the textured microstructure of the grain. Viscosity of the slag once it has penetrated the grain also determines the rate of mass transport within the liquid. According to the Stokes-Einstein relation, the ionic diffusivity in the slag is inversely proportional to viscosity changes, so when the composition changes because of dissolution in the slag, viscosity is reduced preventing further penetration. The predominant degradation mechanism becomes mass transport which is enhanced as viscosity increases (Wiederhorn *et al*, 1988). Reaction products from these processes can consequently remain attached to the solid, become fugitive in the form of fluid liquid or gas, or be a

combination of both. In certain cases, passive corrosion occurs, whereby the solid reaction product attaches itself to the surface of the refractory and decreases the rate of corrosion. This often includes MgO and Al₂O₃ containing refractories.

According to McCallum *et al* (1952), dissolution of refractories into slag is controlled by one of two mechanisms, either; a chemical reaction at the interface (reaction controlled dissolution); or transport of a reacting species through the liquid (diffusion controlled dissolution). Raw material segregation and corrosion of a glass melt can be a result of inadequate mixing, which can result in an overlap of reactions in the melting sequence and release of gases at different times, so the extent to which the glass is reacted or which mechanism is dominant can be difficult to predict (Tooley and Tiede, 1945). The segregation of sulphate and phosphate salts on nuclear waste melts has been studied by Li and Langowski (1996). Through this work and other related studies (Li *et al*, 2000) it was observed that sulphate segregation was a kinetic process which occurred during batch to glass conversion and that batch materials appeared to have a strong impact on the tendency of the melt to segregate. It was also noted that molten salts accumulated on the batch surface, and an increase in Al₂O₃ enhanced the phase segregation. The waste will be dissolved first by chemical reaction and the solute layer will be removed by transport controlled dissolution, into the liquid which surrounds it, whilst the segregated layer should undergo dissolution at increased temperatures.

This theory is supported by the work of Wilburn and Tomasson, (1965) and Hong *et al*, (1993), who studied glass melting sequences using differential thermal analysis (DTA) and thermogravimetric analysis (TGA) methods. Their work showed that slow solid state reactions between batch components were followed by faster reactions. These faster reactions took place between solid SiO₂ and a low melting eutectic liquid, followed by complete dissolution of the remaining SiO₂.

A simplified static description of the steps going on within the multicomponent frit/calcine system is given in **Figure 2.10** taken from Roth and Weisenberger, (2000). The first reactions between the calcine and the glass frit begin at the phase boundary between the frit and calcine, at temperatures in the region of the frit softening point, generally around 600°C. Dehydration, volatilisation and denitration can also take place from around 250°C according to published data (CRC, 1997). Liquid is absent at

this stage allowing removal of chemically bound water and solid state reactions to proceed. A second stage sees the melting of inorganic salts and the dissolution of crystalline compounds by the glassy melt. At the end of this second stage, the crucible contains a mixture of glass melt, refractory particles and gas bubbles. The third and final melting stage then causes complete dissolution of the HLW at temperatures up to 1050°C by dissolution of refractory phases and bubble removal (Hrma, 1988). Processes which are not taken into account in the static diagram are those of convection within the melter, and also the process known as “sparging”- bubbling of a gas through the glass melt to encourage homogeneous mixing. These processes help to homogenise the final glass product, and if the sparging does not take place there can be as much as 35wt% waste loading at the top of the melt, whilst there is only 25wt% waste loading at the bottom (Scales, 1990).

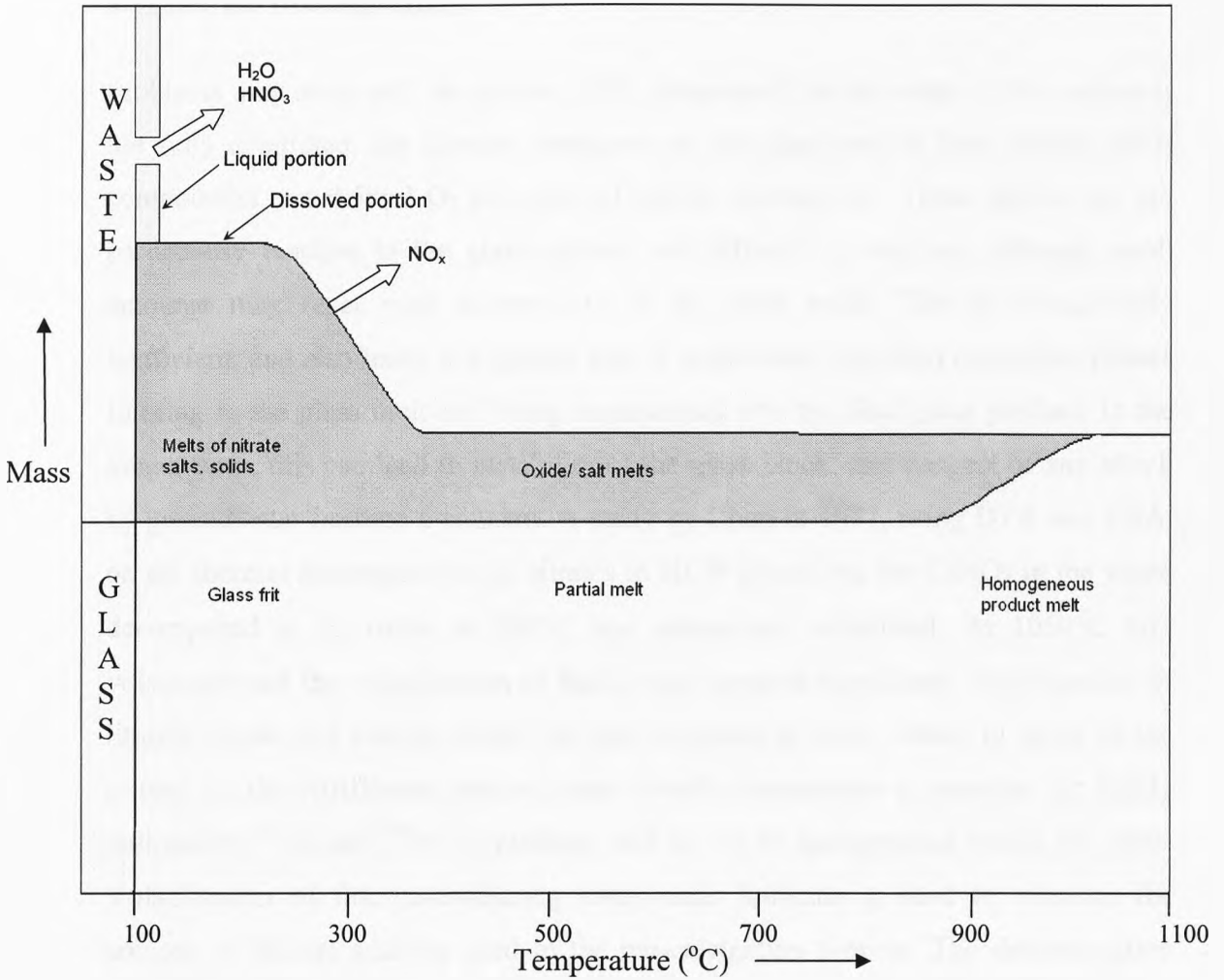


Figure 2.10: Static process description of frit/calcine system (taken from Roth and Weisenberger, 2000)

The partitioning of trace elements within minerals can be compared to the dissolution process of a crystalline/amorphous waste form within a glassy matrix. Goldschmidt (1937) laid the theoretical foundation for partitioning of trace elements between crystals and melts. Recognising that specific element ions enter specific lattice sites, Goldschmidt proposed that the key variables controlling partitioning are the charge and size of the trace ion relative to the charge and size of the lattice site. There is an energy penalty for size and charge mismatch that is reflected in the lower partition coefficients (likelihood of partitioning) for ions that do not fit well onto lattice sites, compared to ions that do.

2.11 Nitrate Decomposition

Problems may arise with the nitrates (NO_3 compounds) in the waste. If the calcine is not fully denitrated, the nitrates decompose in the glass melt to form nitrites (NO_2 compounds) and 0.5mol O_2 per mole of nitrate decomposed. These nitrites are not particularly reactive in the glass system, and difficult to dissolve, although small amounts may react with components of the glass batch. This is energetically inefficient, and also leads to a greater risk of undesirable (durable) crystalline phases forming in the glass melt and being incorporated into the final glass product. In the longer term, this can lead to instability of the glass block, and dangers of any attack by groundwater become a concern. A study by Chun in 1977, using DTA and TGA, on the thermal decomposition of nitrates in HLW found that the CsNO_3 in the waste decomposed to its oxide at 900°C and completely volatilised. At 1050°C SrO volatilised and the volatilisation of RuO_4 also becomes significant. Volatilisation of lithium nitrate and lithium nitrite had also occurred to some extent. In terms of the impact on the vitrification system, these results demonstrate a potential for highly radioactive ^{137}Cs and ^{90}Sr to volatilise, and so not be incorporated within the glass. Volatilisation of lithium-containing compounds indicates a need to examine the amount of lithium additive used in the pre-calcination process. The decomposition products of the nitrates often found in the HAL are often also volatile. Strydom *et al*, (1987) show that the decomposition reaction of a rare earth nitrate such as $\text{Ce}(\text{NO}_3)_3$ is a single irreversible reaction, and that $\text{Nd}(\text{NO}_3)_3$ decomposes to oxynitrate accompanied by two reversible processes. Lanthanum nitrate (Gobichon *et al*, 1996) also behaves in a similar way to the neodymium nitrate, and as the ionic radii decrease in size, the temperature at which decomposition begins also decreases. The increased activation energy needed for decomposing those nitrates of increased radii increases the inefficiency of the vitrification process.

Smith *et al*, (1995) investigated the effects of nitrate additions upon a glass wasteform with a high Fe content and found that the $\text{Fe}^{2+}/\text{Fe}^{3+}$ redox ratio of the nitrated samples was identical to that of an untreated glass. This does not however agree with much of the work undertaken in the area of nitration. Feng *et al*, (1989) found that the oxidation state of a glass with an excess of network formers (such as Al) was insensitive to a reducing atmosphere, whereas glasses with deficits of these network

formers are sensitive to very small atmospheric changes. The nitrates present in the HAL upon addition to the calciner, and the sucrose (a well-known reducing agent) added during the process of calcinations are added to a melter which is sparged with compressed air. Glasses with a deficit of network formers, sensitive to changes in redox conditions must be carefully monitored when they are being fabricated. The topic of nitration is an important consideration for the overall quality of the glass.

2.12 Durability of the final product

Eventually, after reprocessing, classification and immobilisation, the question of long term storage and associated durability questions arise.

It is generally agreed that any proposed repository should have a multi-barrier method of protection in place, to prevent migration of waste elements of the waste toward the water table. Several multi-barrier methods have been proposed, but few have been proven to a satisfactory level to allow further investigation. In European repositories (a design such as that currently being tested at Sweden's Åspo site adjacent to Oskarshamn); the waste will be stored in saturated rock below ground using a deep disposal concept. Sweden's proposed repository (**Figure 2.11**) site at either Östhammar or Oskarshamn will be used for the SNF generated by their 11 nuclear power reactors.

All Swedish spent nuclear fuel is currently stored in Clab, a central interim storage facility. Here the water cools the fuel and provides radiation shielding. Since spent nuclear fuel has an elevated level of activity for a very long period – on the order of 100,000 years - the long term storage method needs to be changed. The deep repository for Sweden would consist of a number of parallel tunnels at a depth of about 500m, connected by a central tunnel for transportation and communication. Vertical holes with room for 1 canister in each are to be drilled from the floor of the tunnels. It is engineered of materials that occur naturally in the earth's crust, with a view to the repository imitating nature as closely as possible. Multiple barriers will be used to prevent the radionuclides in the fuel from escaping into the environment. Nearest the fuel is the copper canister with a cast iron insert. Its function is to isolate the fuel from the environment. The canister is surrounded by a layer of bentonite clay called a buffer, since it is intended to protect the canister against small movements in

the fuel from the environment. The canister is surrounded by a layer of bentonite clay called a buffer, since it is intended to protect the canister against small movements in the rock and to keep the canister in place. The buffer swells when it comes into contact with water, and the clay acts as a filter in the unlikely event that any radionuclides should escape from a canister. The rock also retards the transport of the radionuclides, but its primary purpose is to protect the canister and the buffer from mechanical damage and to offer a stable chemical environment (www.skb.se).

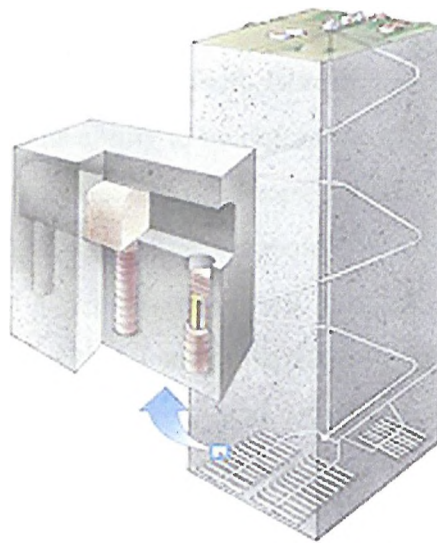


Figure 2.11: Proposed deep repository in Sweden for SNF (taken from www.skb.se¹)

A permanent repository is not yet available in Britain and will not be available for the foreseeable future, as the siting of such a repository is both politically and environmentally a sensitive issue. The site must remain geologically stable for extended periods, ideally several million years and be remotely situated. Quality of the final immobilised SNF or HLW product is an important part in helping this concept become an acceptable option.

¹ SKB are the 4 nuclear utilities in Sweden and have set up the jointly-owned Swedish Nuclear Fuel and Waste Management Company currently responsible for engineering and building the Swedish deep repository

possible, thereby preventing the release of radioactive elements. Crystallisation and cracking can affect the glass durability; for example, some crystal phases will probably have a reduced durability compared to the original glass. These phases would be much more soluble when in contact with water and dissolve from the glass easily. Cracking decreases the mechanical strength of the glass, and more importantly, increases the surface area which would contact any leachant, and thus an increase of devitrification products on that surface.

2.13 Summary

Since HLW immobilisation has become a concern, many types of possible matrices have been investigated for use in this field. Borosilicate glass has stood out as the most popular choice, due to its ability to incorporate a wide range of elements present in a typical HLW stream. Optimisation of process control has been a key concern and numerous studies have led us to the technology currently in operation today. Alongside this, modelling and predictive work looking at long term stability and durability of the glass, compositional and devitrification effects, radiation damage and storage solutions, has been significant and extensive, in an effort to maintain maximum waste loadings at minimal temperatures.

However, as the wasteform has a complex and often varying composition, there is still much work to be done in the field of immobilisation, particularly with reference to problematic phases such as yellow phase, and batch melting reactions. Previous studies have shown that batch materials have a great effect on batch segregation, and that batches are often sensitive to redox conditions. Segregation within the melter is of key concern, and previous studies have shown compositional effects on these segregated layers, and found drivers for segregation within the waste stream.

The French R7T7 is glass the most suitable comparison to the UK WRW13 glass, as the AVM/AVH process and the immobilisation process used at BNFL Sellafield are similar in nature. Experience at Marcoule with waste glass tells us that although platinoids are an issue when it comes to melter lifetime, they do not have an extensive effect on the batch melting, as they simply sink to the bottom of the melter. This also makes R7T7 a suitable comparison as the waste stream used to carry out this study contains no Ru.

Nitration and sucrose additions to the melter feed have long been accepted ways of suppressing certain elements of the feed, or for oxidation/reduction purposes. Previous work has shown the effect of these nitrate additions to be beneficial to a HLW melter if carefully controlled, although nitrate compounds such as the rare earths are found increasingly difficult to decompose as ionic radii increases.

Understanding of the product contained within these HLW canisters is currently completely dependent upon simulant, non-radioactive full scale glasses, as the level of radioactivity in the real glasses is simply too high to allow observation of the final product or any testing of it. Simulated glasses are melted under a continuous vitrification process as with the real HLW, but non-radioactive isotopes of elements present in the real waste are used as substitutes for the radioactive elements. These may be non-radioactive isotopes of the same element if available, or in the case of elements such as U, an appropriate rare earth species.

Chapter 3: Overview of Experimental Techniques and Sample Preparation

3.1 Materials

All samples used in this study to fabricate waste loaded glasses or in the study of the simulant calcine originated from industrial processes. The calcine is a full scale simulant manufactured during inactive commissioning of the third vitrification line at BNFL Sellafield. The simulant calcine was made up from a nitrate based liquor and passed through a rotary calciner. Suitable substitutions were made for the radioactive elements of the waste and Ru and other platinoids were omitted due to cost.

The base glass comes from James Kent Ltd in Stoke-on-Trent and is a random sample of a batch on site at BNFL Sellafield. The base glass is identical to that used to immobilise real radioactive waste and was taken from a larger batch later to be used for vitrification of active wastes. At the time this work was conducted, James Kent Ltd were supplying all the frit used in vitrification by BNFL.

Standard analyses of the manufactured frit and using XRF are supplied by CeramResearch in Stoke-on-Trent to James Kent Ltd. The nominal composition for the frit is tabulated in **Table 3.1.1**. The simulated calcine material composition is given in **Table 3.1.2**.

Table 3.1.1: Nominal composition of frit used at BNFL Sellafield (glass supplied to this analysis)

Component	Wt%
SiO ₂	62.9 ± 1.0
B ₂ O ₃	23.0 ± 0.8
Na ₂ O	11.4 ± 0.5
Li ₂ O	2.7 ± 0.4

Table 3.1.2: Nominal composition (by XRF) of simulant blend waste stream provided by BNFL

Oxide	Nominal composition (wt%)	Oxide	Nominal composition (wt%)
Al ₂ O ₃	5.6	HfO ₂	0.15
B ₂ O ₃	0.07	K ₂ O	0.01
BaO	1.06	La ₂ O ₃	3.52
CaO	0.01	Li ₂ O	8.28
CeO ₂	7.44	MgO	6.02
SrO	2.4	MoO ₃	8.98
Cr ₂ O ₃	0.91	Na ₂ O	0.15
Cs ₂ O	7.28	Nd ₂ O ₃	11.38
ZrO ₂	11.2	NiO	0.6
Fe ₂ O ₃	4.21	P ₂ O ₅	0.4
Gd ₂ O ₃	12.2	Pr ₆ O ₁₁	3.52
RuO ₂	0	TeO ₂	1.29
SiO ₂	0.09	TiO ₂	0.01
Sm ₂ O ₃	1.89	Y ₂ O ₃	1.47
		Total	100.15

3.2 Compositional Analysis

The nominal compositions were checked using ICP-AES and XRF. As these techniques were not available in Sheffield, the samples were sent away for analysis.

3.2.1 Inductively Coupled Plasma Atomic Emission Spectroscopy (ICP-AES)

Inductively Coupled Plasma Atomic Emission Spectroscopy (ICP-AES) is a widely used technique for analysing trace elements in materials. In this technique, the element is not excited, but merely dissociated from its chemical bonds and placed into an unexcited, un-ionised ground state. This atom is then capable of absorbing radiation at a discrete wavelength over a narrow bandwidth. A number of ways are available for dissociating elements of interest from their bonds, and the energy required can be generated in a number of ways. However, currently only plasma devices, burners and furnaces are used commonly. For the purpose of this investigation, only one method, that of dissolution for use with a flame technique, will be discussed. Ceramics are, by their nature, difficult to dissolve, and so two methods have been developed; dissolution by fusion decomposition and dissolution by acid

attack decomposition. Decomposition by fusion commonly uses a lithium metaborate flux, followed by leaching using a mineral acid. The advantage of this method of dissolution is the formation of a low melting eutectic mixture. Volatile elements can be analysed using this method. Acid attack does not use a flux, so reducing the amount of dissolved solid content. HF is commonly used at temperatures up to 100°C (Walsh and Alkemonde, 1955). Error occurs with volatilisation in ICP-AES, and also normalising for oxide as opposed to nitrate content. More oxygen is associated with an oxide so elemental % will be slightly increased for a nitrate than for the oxide values given in analysis.

ICP-AES was carried out at the Savannah River Laboratory (SRS), SC, USA. The analysis was run by D. Peeler of SRS Labs. Some ICP-AES was also carried out by P. Rose and F. Gong at the Vitreous State Laboratory (VSL), Washington D.C, USA.

3.2.1.1 Sample Preparation

Simulant Calcine

The composition of the simulant calcine using ICP-AES was determined at SRS. In this case sample preparation consisted of milling to $<75\mu\text{m}$ and using LiBO_2 and $\text{Na}_2\text{O}_2/\text{NaOH}$ fusions. Some analysis of the simulant waste was also undertaken using ICP-AES at VSL. In this case the samples were ground into a powder and sieved through a $75\mu\text{m}$ sieve. The powders were subjected to microwave dissolution beforehand in a HF and HNO_3 solution. Li and B contents in the samples were examined.

Waste loaded glasses

Material compositions of the base glass and fully waste loaded glasses were determined using Inductively Coupled Plasma- Atomic Emission Spectroscopy (ICP-AES) at the Savannah River Laboratory in South Carolina, USA. Sample preparation consisted of milling to $<75\mu\text{m}$ and using LiBO_2 and $\text{Na}_2\text{O}_2/\text{NaOH}$ fusions.

3.2.2: X-Ray Fluorescence (XRF)

Wavelength-dispersive x-ray fluorescence spectrometry -XRF- is a non-destructive analytical technique used to identify and determine the concentrations of the elements present in solids, powders and liquids. XRF is capable of measuring all elements from ^4Be to ^{92}U . When a specimen is irradiated using a beam of sufficiently short wavelength x-ray radiation, a characteristic x-ray spectrum can be observed from the excited sample. Utilising high intensity x-ray tubes, detectors and x-ray optics, XRF is a quantitative analytical method. It may be noted that the detection limit is dependent on the peak to background ratio of the spectral lines but the method has a detection limit for most elements of approximately 5ppm.

3.2.2.1 Sample Preparation

Samples of simulant waste, borosilicate frit and yellow phase were prepared by grinding in an agate pestle and mortar, then sieving to a particle size $<75\mu\text{m}$. I acknowledge D. Peeler of SRS Laboratories and R. Cecil and P.B. Rose at VSL for performing this work.

3.2.3: Loss on Ignition

25wt% waste loaded batches were prepared having first determined the average loss-on ignition value for the waste stream. This was done by inserting 6 batches of weighed, calcined material in alumina crucibles into a furnace and heating at 1000°C for 14 hours. The samples were then weighed and the weight loss calculated as a percentage. On average, LOI was found to be $31.4 \pm 7\%$. This LOI figure was then taken into account when calculating batch sizes, in the following calculations;

$$\frac{\text{oxide waste loading}}{0.686} = \text{calcine in batch (\%)}$$

and

$$100\% - \text{oxide waste loading\%} = \text{Glass frit \%}$$

3.3 Glass melting

Batch components were glass frit (**Table 3.1.1**), supplied by James Kent Ltd, in a particulate form, (1-5mm) and a simulant waste stream (**Table 3.1.2**) supplied by BNFL. The simulant waste stream was granular in appearance, ranging from powder fines to large particles of up to 5mm in length. Batch particle size was irregular, and only controlled by separating out particles as fines; <75 μ m, <150 μ m, <250 μ m, <1000 μ m and above. An equal amount of each of these particulate sizes was added to each batch prepared to simulate the heterogeneity of the batch in the real process. The suppliers of the chemicals originally used to make these materials is not known. It should be noted that Ru had been omitted from the waste stream due to cost reasons. Many of the radioactive species which would be present in the real waste stream have been replaced by non-radioactive isotopes of the same element or by an oxide with similar chemistry. Many of the rare earth elements have been removed, and simulated by increasing the amount of Nd present. Gd was also present not only to simulate fission products but also to represent the fact that it is added to the real waste as a neutron poison. Mg and Al are present in high percentages due to the fact that the waste simulates a blended stream of Magnox:oxide waste in a 25:75 ratio, and as noted in **chapter 2** Magnox fuel is characteristically high in these elements. The omission of Ru was believed not to have a great impact in this study as, although Ru is a problematic element, it does not appear to have an impact on the formation of molybdate containing phases within the melt, and rather settles to the bottom of the melter (see **p. 36**). It does however increase corrosion of the melter and thus releases Ni and Cr into the glass, an effect which has not been simulated in this study.

Glasses for investigation were melted using an electric furnace with Kanthal SiC elements. The temperature of the furnace was regulated by a Eurotherm controller, and calibrated regularly using a K-Type thermocouple supplied by Sigma. All melts for microscopy/XRD/thermal analysis examinations were performed in 75ml Inconel 601 crucibles supplied by Alpha-Aesar at 1050°C for varying times. Once melted for the desired amount of time, batches were not poured but quenched in the crucibles in water. This was to maintain the integrity of the body of the melt. Water was not allowed to come into contact with the glass during the quenching process.

3.4 Density Measurement

The Archimedes method was used to measure density of a powder or bulk sample. The sample was placed in a vessel in air and weighed, and subsequently suspended in a liquid of known density at temperature, T, and weighed again. The density of the sample is given by:

$$\rho_{TRUE} = \frac{W_A}{W_A - W_W} \times \rho_W \quad \text{Eqn. 3.4.1}$$

where ρ_{TRUE} is true density, W_A is weight in air, W_W is weight in liquid and ρ_W is density of liquid at the measured temperature. The liquid used is usually distilled water, although the technique is perfectly applicable to other liquids if the sample is soluble in water. Density was calculated by weighing powder samples first in air and then in approximately 25ml of liquid. In the current work kerosene was used as the fluid to avoid hydration effects. Samples were ground to $<75\mu\text{m}$. The temperature of the kerosene was measured and noted for each measurement. Samples were weighed using an electronic balance accurate to $\pm 0.1\text{mg}$. Density bottles were used for this work.

3.5 Thermal Analysis

Thermal analysis takes advantage of the effect of the enthalpy change during a first order phase transition. A sample is allowed to heat or cool and its temperature is monitored. At a first order transition, heat is evolved and the heating or cooling cycle stops until the transition is complete. This work is usually done with a reference sample so as to compare ΔT of the sample with ΔT of the reference to give the results in a more quantitative and usable format.

In the small samples used for DTA, TGA and DSC, ambient atmosphere dilutes gaseous reaction products, accelerating decomposition reactions and shifting the gas producing reactions to lower temperatures, which may affect the reaction sequence. Therefore, additional tests on larger samples are necessary to confirm thermal analysis data.

3.5.1 Sample preparation

Simulant calcine and waste loaded glass samples were prepared for analysis in the same way.

Differential Thermal Analysis (DTA)

Differential thermal analysis (DTA) was performed using a Perkin Elmer DTA 7, which was calibrated using aluminium (amu 26.98, m.pt 660°C) and gold (amu 196.97, m.pt 1063°C) standards in air and Perkin Elmer thermal analysis suite Pyris V.6. The analysis was conducted on a powdered sample, ground to $<75\mu\text{m}$ using an agate pestle and mortar. Around 50mg of the sample was weighed and recorded to within $\pm 0.0001\text{g}$, using an electronic microbalance. The standard consisted of an equivalent amount of finely divided alumina powder which was weighed to an accuracy of $\pm 0.0005\text{g}$ and placed in an alumina crucible. The sample was placed in an identical crucible in the furnace, and both sample and reference heated to 1050°C at 4°C/min. This rate of temperature increase was selected after first performing DTA on samples heated to 1050°C at a rate of 1, 4 and 10°C/min. Temperature and ΔT measurements were taken every 0.1secs. Cooling curves were not recorded for these samples as it was not necessary for the events being examined. Glass transition (T_g), nitrate decomposition and phase formation temperatures were indicated by endo/exothermic dips on the resulting trace. These temperatures were then used to determine the temperatures at which subsequent heat treatments would be undertaken. Alumina crucibles were used due to the possibility of damage to a Pt crucible as the waste stream was thought to be corrosive to Pt. Atmospheric changes were achieved by feeding a chosen gas through the sample chamber at a constant rate of 50ml/min. An oxidising atmosphere was created using compressed air or O_2 , an inert one using He and a reducing atmosphere was obtained using 2.84% H_2 balanced with Ar.

Simultaneous DTA/TGA with GC-MS

DTA/TGA combined analysis was performed using a TA Instruments SDT 2960 Simultaneous DTA-TGA. Samples weighing 50mg ($\pm 0.0005\text{g}$) were batched separately in a Pt crucible, using a standard consisting of an empty, dried Pt crucible. The sample was heated at a rate of 4°C/min to 1050°C and held for 1 hour. This was carried out in different atmospheres of air, 2.84% H_2 balanced with Ar, O_2 and He.

These atmospheres flowed at a constant optimum rate for the apparatus of 50ml min^{-1} through the furnace chamber. The same method of sample preparation was applied when the thermal analysis equipment was used in conjunction with a GC-MS. A He carrier gas flowed through the furnace chamber at a constant 50ml min^{-1} . GC-MS will be explained in detail in **section 3.10**.

Thermogravimetric Analysis (TGA)

Thermogravimetric Analysis (TGA) was performed using a Perkin Elmer Pyris 1 TGA. The analysis was conducted on a powdered sample, ground to $<75\mu\text{m}$ using an agate pestle and mortar. Around 50mg of the sample was weighed and recorded to within $\pm 0.0001\text{g}$, using an electronic microbalance. The standard consisted of an equivalent amount of finely divided alumina powder weighed to an accuracy of $\pm 0.0005\text{g}$ and placed in an alumina crucible. The sample was placed in an identical crucible in the furnace, and both were heated to 1050°C at $4^\circ\text{C}/\text{min}$. Temperature and $\Delta W(\text{mg})$ measurements were taken every 0.1secs.

Differential Scanning Calorimetry (DSC)

Temperature compensated DSC works by recording the differences between the enthalpy changes occurring in the sample and a reference heated at the same temperature rate (dT/dt). The system involves two control loops: on the one hand, the sample and reference temperatures may increase at a chosen rate; on the other, when a temperature difference occurs between the sample and the reference concurrent with an exothermic or endothermic reaction in the sample, the second control loop adjusts the thermal power to the sample in order to reduce this difference to zero. A signal proportional to the difference between the energies provided per unit time to the sample and the reference (dH/dt) is then recorded versus the temperature (T). The baseline characteristic of the calorimeter is first stored during a precalibration experiment without the sample and then subtracted from the calorimetric signal with the sample. Two distinct calibrations are performed for enthalpy or heat capacity measurements.

High temperature DSC (quantitative DTA) was performed using a Netzsch Instruments DSC 404C, calibrated with In, Zn, Ag, Au and Sn in alumina. A carrier

gas of He was used, and the furnace used Ar flowing at a constant rate of 20ml min⁻¹. A flowing air atmosphere (50ml min⁻¹) was used in the sample chamber for all experiments. As with the other thermal analysis measurements alumina crucibles were used (as there was the possibility of some damage to Pt crucibles). The apparatus was used in conjunction with Netzsch TA4 Proteus analysis software to calibrate, measure, and analyse the data. The sample was ground using an agate pestle and mortar to <75µm and 20mg (±0.0001g) weighed out using an electronic microbalance. An empty reference pan, identical to the one that contained the sample, was placed in the furnace chamber. Measurements were taken using a heating rate of 4°C/min in a flowing air atmosphere.

3.6 X-Ray Powder Diffraction (XRD)

X-Ray Diffraction (XRD) may be used to determine the crystalline compounds present in a system. Bragg's Law states that

$$n\lambda = 2d \sin \theta \quad \text{eqn. 3.6.1}$$

where n is an integer, λ is a wavelength, d is the difference between two lattice planes and θ is incident angle. The sample is placed in the path of X-rays of known λ (commonly Co or Cu is used as a source of radiation) and this beam is diffracted a certain angle θ depending upon the lattice plane d . This is shown in **Figure 3.6.1**.

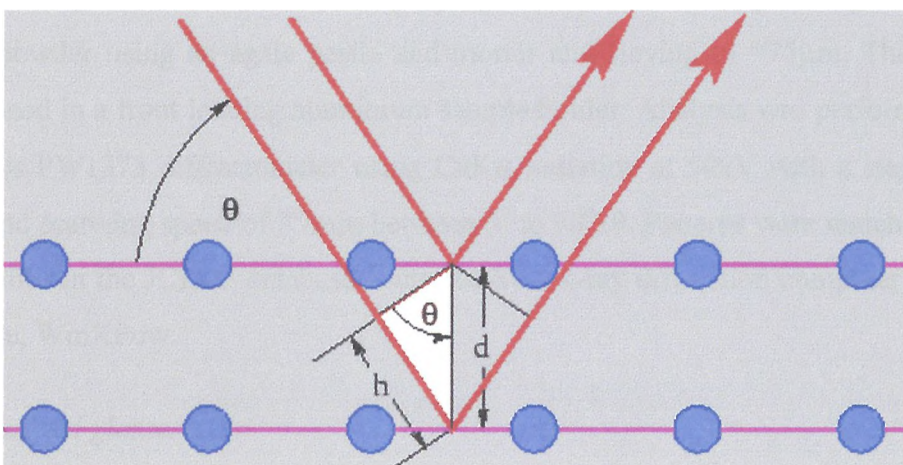


Figure 3.6.1: X-ray diffraction

For the purpose of this investigation, one type of XRD machine was used, in which the x-ray source remains still whilst the sample is rotated around an axis. The detector then moves around the sample and the same axis point to maintain equality between angles of incidence and diffraction. The counts are then measured due to the diffraction of the x-ray beam. The distance between the x-ray beam and source remains equal to keep the beam focussed and prevent error, such as peak broadening. Patterns produced by glasses or glass ceramics characteristically have an amorphous hump, caused by the scattering of x-rays by the amorphous material, and in the latter case also peaks which are due to the presence of one or more crystalline phases. The samples are ground prior to examination so as to obtain a randomly oriented crystal distribution. However, using front loading sample holders available for this work means that the distribution may not be entirely random, and increased orientation gives different intensities of the peaks, although the phases should still be identifiable, as the peak positions will not shift. Shifts in peak positions commonly occur either when a sample contains a solid solution which causes movement of the peaks along the 2θ axis, showing an increasing shift as the angle increases or when a zero error is present so that all peaks are shifted by the same amount.

3.6.1 Sample preparation

Simulant Calcine

Powder X-ray diffraction (XRD) sample preparation consisted of grinding a sample to a fine powder using an agate pestle and mortar and sieving to $<75\mu\text{m}$. The sample was placed in a front loading aluminium sample holder. Analysis was performed with a Philips PW1373 diffractometer using $\text{CuK}\alpha$ radiation at 50kV with a step size of 0.05° and scanning speed of $2^\circ/\text{min}$ between 5° to $90^\circ 2\theta$. Patterns were matched to the ICDD files in the JCPDF database using the Stoe x-ray diffraction computer analysis software, WinXPow.

Waste loaded glasses

Glasses for analysis using XRD were first coarsely crushed using a cleaned percussion mortar. The glasses were then ground using an agate pestle and mortar and sieved to $<75\mu\text{m}$. The powders were placed in a front loaded sample holder. The same

diffractometer and experimental conditions were as described above. The only difference was that in this case a multi-sample changer holding 25 samples was used. The sample changer was loaded with samples in groups of three and an empty sample disc to allow observation of any error with the sample changer and also to eliminate any Al peaks from the sample holders from resulting patterns.

3.7 Fourier Transform Infra- Red Spectroscopy (FTIR)

Infra-red spectroscopy is a widely used form of vibrational spectroscopy. A continuous infra-red light source passes through a thin sample to a monochromator. The technique utilises the vibrations which arise when a molecule changes state. In a simple diatomic molecule, such as carbon monoxide, two atoms are held together by the overlap of a number of orbitals. At a certain internuclear distance, a balance occurs between the attractive bonding forces and the repulsive interactions between the electrons of the two atoms. This equilibrium bond distance can be changed by the application of energy, and a system such as this will vibrate at a particular frequency. The vibrational bond frequency depends on the mass of the two atoms at either end of the bond and the strength of the bond (force constant) holding them together. On this basis, it is expected that heavy atoms held by weak bonds will vibrate at lower frequencies than lighter atoms held by multiple bonds. **Table 3.7.1** shows the positions of some characteristic group vibrational absorptions.

Table 3.7.1: Characteristic vibrations associated with some common molecules (compiled from Clark and Hester, 1987)

Group	Characteristic vibration (cm ⁻¹)
O-H	3000-3800
N=O	1350-1600
N-O	900-1300
M-NO ₂	N-O 1300-1500
M-ONO	N=O 1400-1600 N-O 1000-1200
M=O	800-1000

Fourier transforms are used as a way of allowing the data for a complete sample spectrum to be recorded in one scan, as opposed to multiple scans. In this way, several scans can be recorded of the whole spectrum thereby decreasing the signal to noise ratio, so increasing the accuracy of the technique (Clark and Hester, 1987).

3.7.1 Sample preparation

Samples of simulant waste and waste loaded glasses were prepared in the same way. FTIR spectroscopy was performed on pellets fabricated from a well ground mixture of sample material and KBr. The sample (~2mg), approximately 1wt% of the total disc weight, was weighed and the weight noted to ± 0.5 mg. Around 200mg of IR transparent KBr was then combined with the sample in an agate pestle and mortar and ground for approximately 2mins. A Perkin Elmer Spectrum 2000 FT-IR in transmission mode (range $4000\text{--}600\text{cm}^{-1}$) was used with the pellets mounted in a plastic sample holder. Pellets were pressed in a stainless steel die using pressures of 10tonnes. The die was cleaned using acetone after each pellet had been removed so as not to contaminate the next pellet.

3.8 Electron Microscopy

3.8.1 Scanning Electron Microscopy and Energy Dispersive X-ray Spectroscopy (SEM/EDX)

Scanning Electron Microscopy (SEM) uses a beam of electrons directed at the sample to gain information about the surface or near surface of the specimen. **Figure 3.8.1** shows a schematic of the main components of an SEM system.

The electron source is usually a tungsten filament thermionic type (as with the machine used for these experiments). The electrons are accelerated to an energy between 1 and 30keV - usually around 15keV for powders and 20keV for bulk samples. Between 2 and 3 condenser lenses demagnify the beam before it hits the specimen until it may have a diameter of only 10nm, dependent upon the capability of the microscope.

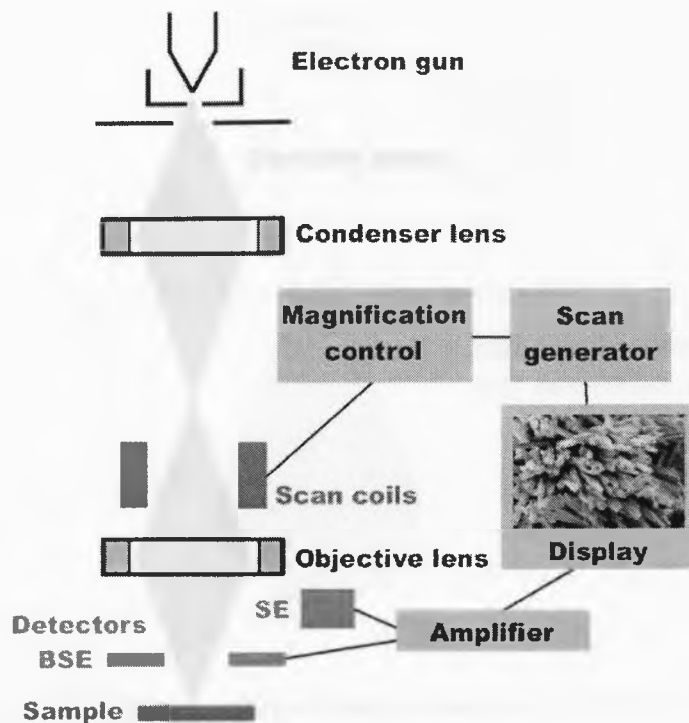


Figure 3.8.1: SEM Schematic (Goodhew, 1997)

SEM also has the ability to detect backscattered electrons from the sample, as well as secondary electrons. Secondary electrons is a term used to describe those electrons which escape from the specimen with low energies (<50eV). These electrons are likely to be electrons to which a small amount of energy has been transferred near the sample surface via the electron beam. These electrons are abundant and the intensities are therefore commonly used in imaging. Backscattered electrons are not as numerous as secondary electrons, but are high energy, primary electrons that have left the surface of the sample before all the energy has been transferred, and still have high incident energy. These electrons are used for imaging and analysis as it is possible to see atomic number differences using this technique e.g a heavier element such as Cs will appear much brighter than a lighter element such as Na (see **Figure 3.8.2**).

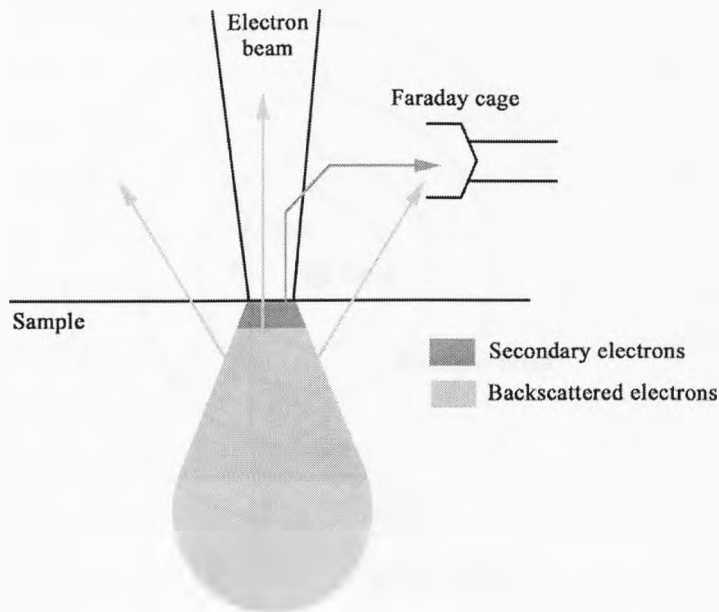


Figure 3.8.2: Backscattered electron source (Goodhew, 1997)

Energy Dispersive X-ray Spectroscopy (EDX) is a technique commonly available within a SEM (**Figure 3.8.3**). It arises from a secondary effect, and happens when an atom is in a highly excited state and the empty electron state is filled. A single outer electron jumps into the inner shell vacancy and an X-ray is emitted. The X-ray has a characteristic energy which is the difference between the energies of the two excited states and so, by measuring this wavelength, which is characteristic for each atomic species then it is possible to determine the species present in the specimen. Each of these techniques in an SEM has what is known as a different interaction depth. This is the region into which the electrons penetrate the sample and is a common area of error in the technique. EDX can be used to scan a single area of the sample, a spot scan, or can be used over an entire area in a technique known as ‘element mapping’. Element mapping involves scanning an area of the sample to determine what elements are present, and then rescanning this area slowly, for a fixed number of scans. Each scan yields new information, and every time an element, for example, Cs, is detected, image analysis software will add a white pixel to the sample image for that element, so creating a ‘map’ of all the elements and their positioning within the sample. This is extremely useful when cross-referenced with a secondary or backscattered image from the same area.

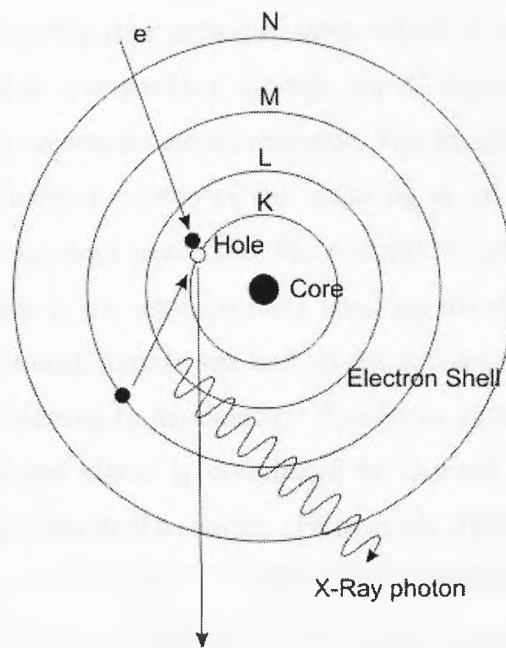


Figure 3.8.3: X-rays generated by sample, allowing EDX imaging (Goodhew, 1997)

3.8.2 Transmission Electron Microscopy (TEM)

Transmission electron microscopy uses principles very similar to those of SEM. However, TEM samples are very much thinner than SEM samples, allowing the electrons to pass through the sample. The electrons that pass successfully through the sample and do not get scattered over large angles are used for imaging. A scanning transmission microscope may, however, collect electrons that have been scattered through relatively large angles, thus achieving an effect called ‘Z-contrast’ imaging. The inelastic scattering power of an atom is proportional to the square of its atomic number Z , which means that atoms with a higher atomic number appear brighter. This gives some compositional indication of the structure that is being examined. Z contrast imaging is a direct imaging method, providing an instant view of atomic composition.

Z-contrast imaging can be undertaken using a scanning transmission electron microscope (STEM), which forms a highly focused probe of high energy electrons, which is scanned across a thin sample. Most of the beam is diffracted through small angles, but some electrons will be scattered through much larger angles, and it is this component that is collected by an annular detector and used to form the Z-contrast

image. Rutherford scattering (the principle upon which Z-contrast works) intensity depends very strongly on composition through the Z^2 dependence of the scattering cross section, where Z represents atomic number. The image can be thought of as a map revealing the scattering power of the material at an atomic resolution. The relative phases of the incident beam and the scattered beams reaching the annular detector are unimportant as the total intensity reaching the detector depends only on the incident intensity at each atomic site and on the species present, which scatters a small fraction of that intensity to the detector. The inner detector angle is sufficiently large so that the collected signal is dominated by thermal diffuse scattering. This signal is generated very close to the sample. (Pennycook, 1992).

Diffraction patterns are the way in which the crystallographic information is interpreted from a TEM. In this study, the TEM is used purely to gain information on a nanoscale relevant to the microstructure of the samples, so diffraction patterns were not used other than to prove the amorphous/crystalline nature of a sample.

3.8.3 Sample preparation

Simulant Calcine - Scanning Electron Microscopy and Energy Dispersive X-ray Spectroscopy (SEM/EDX)

Powder samples for this technique (used in conjunction with EDX and BEI) were prepared by placing a small amount of the sample (~2mg) on a sticky carbon pad secured to an aluminium stub. The sample was not ground before placing it onto the carbon pad. Once secured, the sample was carbon coated using a carbon coater. A JEOL JSM 6400 SEM was used in both secondary electron and backscattered imaging modes. The samples were analysed using an accelerating voltage of 15keV with a spot size of 9. EDX maps and spot analysis used an accelerating voltage of 20keV and spot size 9. All analysis was conducted using a Be window in the microscope which restricted analysis of the lighter elements. Link ISIS software was used to evaluate the data from the EDX detector and to conduct line and area scans of the sample. For EDX mapping, samples were mounted in epoxy resin and allowed to set under vacuum. These samples were then ground and polished in oil to 6, 3 and 1 μ m using diamond paste. These samples were also carbon coated before being put into the microscope.

Transmission Electron Microscopy (TEM)

Simulant calcine samples for examination using the Phillips EM 420J transmission electron microscope (TEM) were prepared by grinding in an agate pestle and mortar and sieving to $<50\mu\text{m}$. The sample was then dispersed in acetone and, using a uPVC pipette was dropped onto a copper grid. The acetone was allowed to dry and the sample was then carbon coated. The sample was analysed using the EDX analysis available and also the mass difference (z) function on the microscope, known as Z-contrast imaging. Data was once again interpreted using Link ISIS software.

Waste loaded glasses- Scanning Electron Microscopy and Energy Dispersive Spectroscopy (SEM/EDX)

Samples were prepared by sectioning the glass using a diamond cutting wheel and an oil based lubricant. The bulk sample was mounted in cold setting epoxy resin and left under vacuum for 15 minutes to reduce the bubbles in the resin. The sample was then removed and once set was progressively ground in oil using 120, 240, 400, 600, and 1200 SiC grit wheels, and polished using 6, 3, and 1 micron diamond pastes. The sample was carbon coated prior to examination using a CCU1 carbon coater. A JEOL JSM 6400 SEM was used in both secondary electron and backscattered imaging modes. For bulk samples an accelerating voltage of 20keV with a spot size of 9 was used. EDX mapping and spot analysis used an accelerating voltage of 15keV and spot size 9. All analysis was conducted using a Be window in the microscope which restricted analysis of the lighter elements. Link ISIS software was used for image analysis and to evaluate the data from the EDX detector used for line and area scans and element mapping.

3.9 Gas Chromatography and Mass Spectroscopy (GC-MS)

Gas chromatography is a technique used to separate gases into separate components for analysis. The sample gas flows into the chamber together with a carrier gas kept at a constant flow rate, where it moves through an inlet tube (passing through several pressure regulators) into a capillary column. The capillary column is housed within a heated furnace chamber. The optimum chamber temperature is determined by passing a series of gases through the capillary in order to identify the temperature at

which gases will flow and still separate. The capillary column facilitates the separation of the gases or eluents. The column may be packed or hollow, but due to the fact that an unpacked column was used in the investigations later described, the unpacked column system is concentrated on here. The capillary is 6 metres in length and housed in the chamber, wound in a coil hung from the chamber ceiling. The column is usually made from a gas-impermeable polymer. The gas molecules within the capillary separate out due to their differing sizes. Once released from the column and analysed, the retention time determines sample composition when matched with calibration standards.

Mass spectroscopy is employed in order to make the technique quantitative. GC-MS allows the separated gas to pass from the capillary column, which acts as a flow restrictor, through an inlet into the mass spectrometer. A schematic of the GC-MS is shown in **Figure 3.9.1** and of the mass spectrometer in **Figure 3.9.2**.

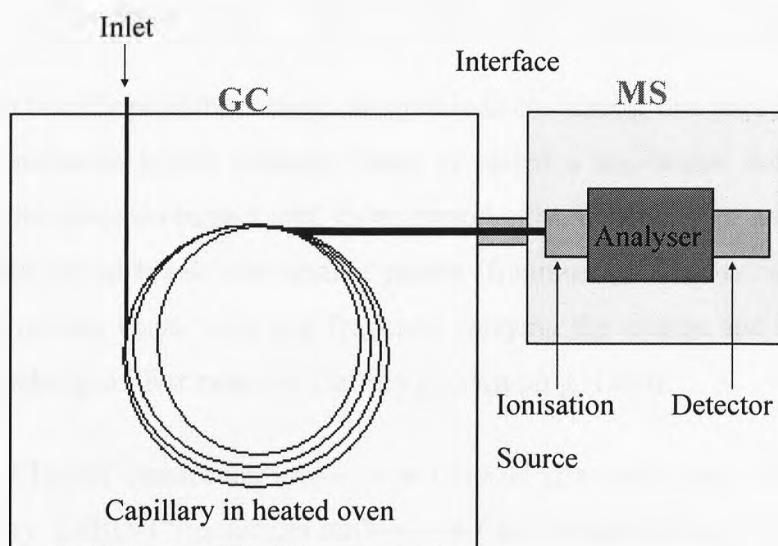


Figure 3.9.1: Schematic of GC-MS system

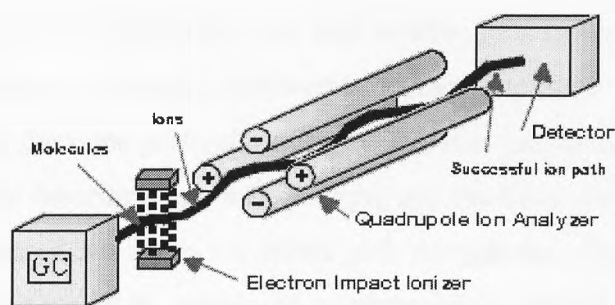


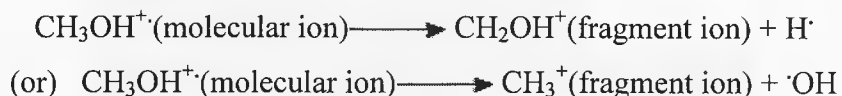
Figure 3.9.2: Schematic of a mass spectrometer

The charged particles (ions) required for mass analysis are formed by Electron Impact (EI) Ionization. The gas molecules exiting the GC are bombarded by a high-energy electron beam (70 eV). An electron which strikes a molecule may impart enough energy to remove another electron from that molecule. Methanol, for example, would undergo the following reaction in the ionising region:



(note: the symbols $^{\cdot+}$ indicate that a radical cation was formed)

EI Ionization usually produces singly charged ions containing one unpaired electron. A charged molecule which remains intact is called a molecular ion. The energy imparted by the electron impact and, more importantly, instability in a molecular ion can cause that ion to break into smaller pieces (fragments). The methanol ion may fragment in various ways, with one fragment carrying the charge and one fragment remaining uncharged. For example (Jeffrey and Kipping, 1964):



Molecular ions and fragment ions are accelerated by manipulation of the charged particles through the mass spectrometer. Uncharged molecules and fragments are pumped away. The quadrupole mass analyzer uses positive (+) and negative (-) voltages to control the path of the ions. Ions travel down the path based on their mass to charge ratio (m/z). EI ionization produces singly charged particles, so the charge (z) is one. Therefore an ion's path will depend on its mass. The angle of deflection

varies, being larger for a lightweight ion, and smaller for a heavier, slower ion. If the (+) and (-) rods shown in the mass spectrometer schematic were ‘fixed’ at a particular rf/dc voltage ratio, then one particular m/z would travel the successful path shown by the solid line to the detector. However, voltages are not fixed, but are scanned so that ever increasing masses can find a successful path through the rods to the detector. The detector in this case works by producing an electronic signal when struck by an ion. Timing mechanisms which integrate those signals with the scanning voltages allow the instrument to report which m/z has struck the detector at a given time. The mass analyzer sorts the ions according to m/z and the detector records the abundance of each m/z . Regular calibration of the m/z scale is necessary to maintain accuracy in the instrument. Calibration is performed by introducing a well known compound into the instrument so that the compound's molecular ion and fragment ions are reported accurately.

The sample is not only analysed in terms of mass, but also can be verified by using the retention times within the capillary column. This means that molecules with the same molecular weights such as CO_2 and N_2O can be separately identified. **Table 3.9.1** shows an example of several molecules, their formula and where the typical peaks occur. If the retention times of two peaks which could be from different eluents match, then these peaks arise from the same molecule, as opposed to two different ones (Jeffrey and Kipping, 1964; Duckworth *et al*, 1986). **Figures 3.9.3-4** shows the crucible/MS/GC arrangement as it was used in the laboratory.

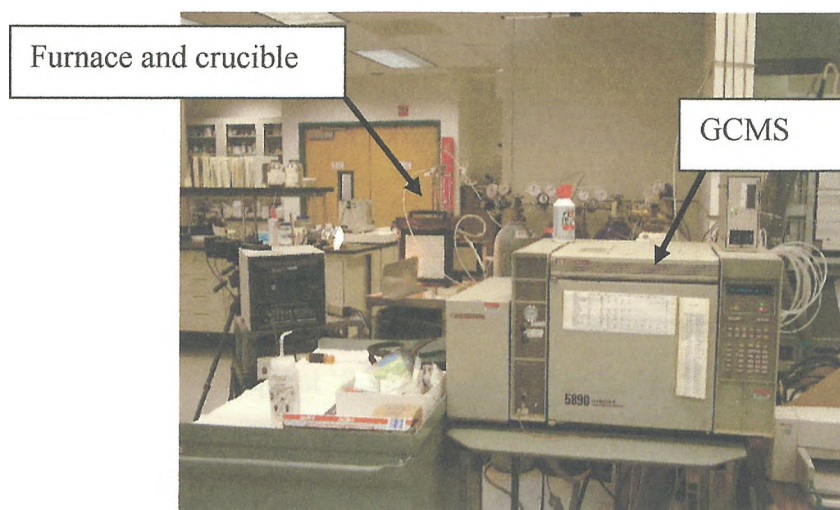


Figure 3.9.3: Crucible/GCMS arrangement

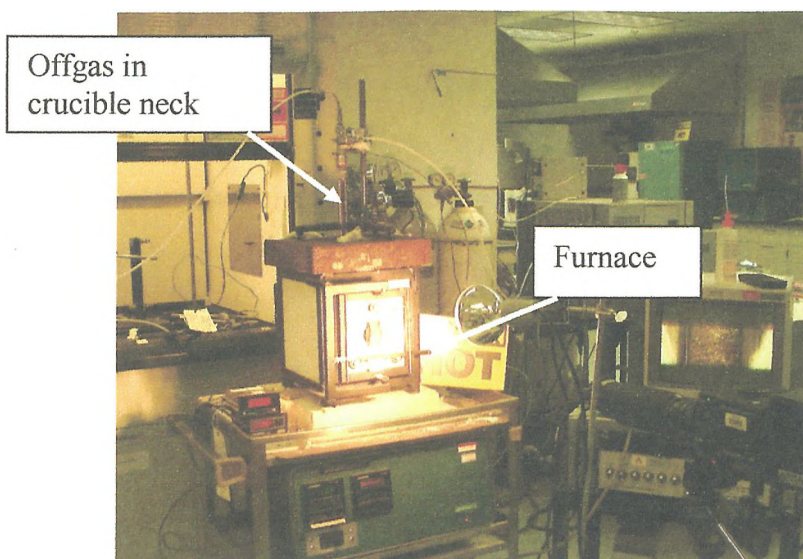


Figure 3.9.3: Crucible in furnace, connected to GCMS system. Offgas can be clearly seen in neck of crucible

Table 3.9.1: Peak placements for GC-MS for several common molecules

Molecule	Formula	Peak 1 (amu)	Peak 2 (amu)	Peak 3 (amu)	Peak 4 (amu)
Carbon dioxide	CO ₂	44	28	16	22
Helium	He	4	-	-	-
Nitric oxide	NO	30	14	15	-
Nitrogen	N ₂	28	14	-	-
Nitrogen dioxide	NO ₂	30	46	16	-
Nitrous oxide	N ₂ O	44	30	14	28
Oxygen	O ₂	32	16	-	-
Water	H ₂ O	18	17	16	-

The data may be quantified by passing a known amount of a gas through the system to obtain a calibration factor, and normalising the results from the original experiment. The flow rate is kept constant throughout the experiments, as over bombardment of the detector and subsequent ‘flooding’ gives broad, large error data peaks.

3.9.1 Sample preparation

GC-MS samples were fabricated in two ways, depending on the placement of the sample being analysed. Samples were placed either in a 7cm diameter silica crucible

inside a furnace or in a TA Instruments SDT 2960 Simultaneous DTA-TGA. Sample preparation for DTA/TGA was identical to the method used previously for DTA/TGA analysis alone (see **section 3.5**). A Hewlett Packard 5890 GC-MS was connected via a stainless steel inlet tube to the machine and the data was analysed using Hewlett Packard 5890 analysis software package. Larger samples of around 10g were analysed using the silica crucible and furnace. These samples were mixed in their as-received form to give a 25wt% waste loading and placed in the silica crucible. The silica crucible was cleaned prior to use with water and acetone, and heated to remove any residue. The crucible mouth was sealed using a rubber 'O' ring and sealant. The inlet for the GC-MS was placed adjacent to the crucible mouth and the two were connected using stainless steel connectors. The carrier gas was run through the machine at a constant rate. It should be noted that the furnace in which the samples were placed also allowed for observation of the glass melt due to a silica window in the front of the furnace, which was subsequently recorded using a video camera with a light filter attached.

3.10: Heat treatment

Heat treatment of the calcine was performed at certain points according to previous analysis. Samples were heated in an electric furnace with Kanthal SiC elements at a rate of 4°C/min. The temperature of the furnace was regulated by a Eurotherm controller, and calibrated regularly using a K-Type thermocouple supplied by Sigma. Samples were allowed to dwell at a chosen temperature for 15 minutes to equilibrate.

Table 3.10.2 lists sample abbreviations for purpose of identification in the following chapters.

3.11 Experimental Errors

Experimental error was estimated taking into account random error (from machine/system operating parameters and calibrations) and systematic error. The method of determining error was such as that used for a set of repeated measurements y_i (of the same quantity) in different experimental systems, all with different

uncertainties σ_i . The procedure was to minimize the sum of squares of the deviations divided by weighting factors (taken to be the uncertainties of the individual measurements). The standard deviation was then calculated from the square root of the variance. The standard deviation will be larger than the one calculated assuming all data points have the same uncertainty, but is a better representation of the data.

Table 3.10.2: Key to sample names

Sample Name	Sample description
5M25	25wt% (as-rec'd) waste loaded glass, melted for 5 minutes at 1050°C, water quenched in Inconel crucible.
10M25	25wt% (as-rec'd) waste loaded glass, melted for 10 minutes at 1050°C, water quenched in Inconel crucible.
15M25	25wt% (as-rec'd) waste loaded glass, melted for 15 minutes at 1050°C, water quenched in Inconel crucible.
HT200G	25wt% waste loaded glass, loaded with calcine heated to 200°C/22hrs, melted at 1050°C (performed both as a furnace and DSC experiment)
HT400G	25wt% waste loaded glass, loaded with calcine heated to 400°C/22hrs, melted at 1050°C (performed both as a furnace and DSC experiment)
HT700G	25wt% waste loaded glass, loaded with calcine heated to 700°C/22hrs, melted at 1050°C (performed both as a furnace and DSC experiment)
HT1000G	25wt% waste loaded glass, loaded with calcine heated to 700°C/22hrs, melted at 1050°C (performed both as a furnace and DSC experiment)
AR-G	25wt% waste loaded glass, loaded with as-received calcine, melted at 1050°C (performed both as a furnace and DSC experiment)
PNL25RED	25wt% waste loaded 10g batch melted under reducing conditions- R.T to 1050°C at 4°C/min, hold 1hr- in a closed, pure silica crucible for offgas analysis.
PNL25IN	25wt% waste loaded 10g batch melted under inert conditions- R.T to 1050°C at 4°C/min, hold 1hr- in a closed, pure

	silica crucible for offgas analysis.
PNL25IN/T	25wt% waste loaded 50mg batch melted under inert conditions- R.T to 1050°C at 4°C/min, hold 1hr in TGA/DTA
PNL25RED/T	25wt% waste loaded 50mg batch melted under inert conditions- R.T to 1050°C at 4°C/min, hold 1hr in TGA/DTA
PNL25OX/T	25wt% waste loaded 50mg batch melted under inert conditions- R.T to 1050°C at 4°C/min, hold 1hr in TGA/DTA
Ar-calc	As-received calcine, no heat treatment
C100- C1050 (intervals at 100)	calcine, heat treated: R.T to (xT/°C) at 4°C/min, air quench
HT200	calcine, heat treated: R.T to 200°C/ hold 22hrs, air quench
HT400	calcine, heat treated: R.T to 400°C/ hold 22hrs, air quench
HT700	calcine, heat treated: R.T to 700°C/ hold 22hrs, air quench
HT1000	calcine, heat treated: R.T to 1000°C/ hold 22hrs, air quench

Chapter 4: Results

This chapter is intended to display all results and characterisations related to the simulant waste form and the waste loaded glasses. Some initial discussion is also given. More detailed discussion and the conclusions drawn are given in **chapter 5**.

4.1 Composition analysis using ICP-AES and X-ray Fluorescence Spectroscopy (XRF)

The composition of the calcine, analysed using ICP-AES at SRS is shown in **Figure 4.1.1**. Note that analysis data for Cs is not given as this technique is unsuitable for Cs detection. The oxide wt% totals 60% due to ~40% of the calcine being non-oxide (i.e. nitrate and water containing) material. Gd, Nd, Mo and Zr contributions are high as these are waste stream elements expected to be major constituents due to fission reactions and fuel cladding. An independent ICP analysis carried out at VSL was also undertaken on the as-received calcine and on a loss-on-ignition sample. These results have been tabulated in **Table 4.1.1** and show some corroboration with results from the SRS. Compositional analysis by XRF of the as-received calcine was supplied courtesy of BNFL. XRF analysis of the as-received calcine and base glass frit was also conducted at VSL (frit analysis is not shown as the analysis supplied with the batch was found to be specific and correct when compared to VSL analysis). **Table 4.1.1** shows combined results from XRF and ICP data. The difference between the independent analysis and the supplied composition is significant in terms of the Mg and Al thought to be present in the simulant blended waste. This has repercussions when looking for Mg and Al containing phases in the XRD analyses, as a smaller percentage of oxide present in the waste means a more dilute solution when in the glass melt. All the analysis figures are normalised (due to a high percentage nitrates in the waste). It can be seen that the analyses differ from the nominal composition of the BNFL supplied waste composition. The areas of greatest disagreement are the Mg, Al, Gd, Mo, Nd, Sr and Zr oxides. Al and Mg content are both decreased according to the VSL analysis by the same magnitude which suggests batch inhomogeneity. Some rare earths, Zr and Mo are increased, suggesting an area particularly rich in one phase was sampled (see **section 4.5** and corresponding X-ray diffraction results). Samples of

a “yellow phase” found in a V26 glass were also analysed using XRF at VSL, and resultant figures are shown in a normalised form in **Table 4.1.2**.

Table 4.1.1- Compositional analysis of as-received simulant calcine (combined XRF and ICP-AES results)

Oxide	BNFL supplied Calcine Comp. Oxide Basis	VSL	SRL
Al ₂ O ₃	5.6	1.83	5.173
B ₂ O ₃	0.07	0.05	0.0378
BaO	1.06	1.06	0.9534
CaO	0.01	0.02	0.0378
CeO ₂	7.44	6.96	6.37
Co ₃ O ₄	0	0.01	0
Cr ₂ O ₃	0.91	0.84	0.8288
Cs ₂ O	7.28	7.84	N.A
Eu ₂ O ₃	0	0.07	0
Fe ₂ O ₃	4.21	3.99	3.64
Gd ₂ O ₃	12.2	12.61	10.794
HfO ₂	0.15	0.21	1.008
K ₂ O	0.01	0	0
La ₂ O ₃	3.52	3.31	3.038
Li ₂ O	8.28	9.76	7.56
MgO	6.02	1.88	5.11
MoO ₃	8.98	12.36	7.714
Na ₂ O	0.15	0	1.1536
Nd ₂ O ₃	11.38	11.22	9.772
NiO	0.6	0.57	0.49
P ₂ O ₅	0.4	0.17	0
Pr ₆ O ₁₁	3.52	3.47	3.08
RuO ₂	0	0	0
SiO ₂	0.09	0.12	0
Sm ₂ O ₃	1.89	1.87	1.624
SrO	2.4	2.86	2.352
TeO ₂	1.29	1.49	1.148
TiO ₂	0.01	0	0
Y ₂ O ₃	1.47	1.86	0
ZrO ₂	11.2	13.57	9.366
Total	100.15	100	81.30*

* N.B: The oxide% does not equal 100% due to the inability of the technique used to analyse for Cs, seen from previous analyses to be ~7-9%. It is also possible that, due to the way in which the samples were prepared, errors were incurred in the analysis of lithia content.

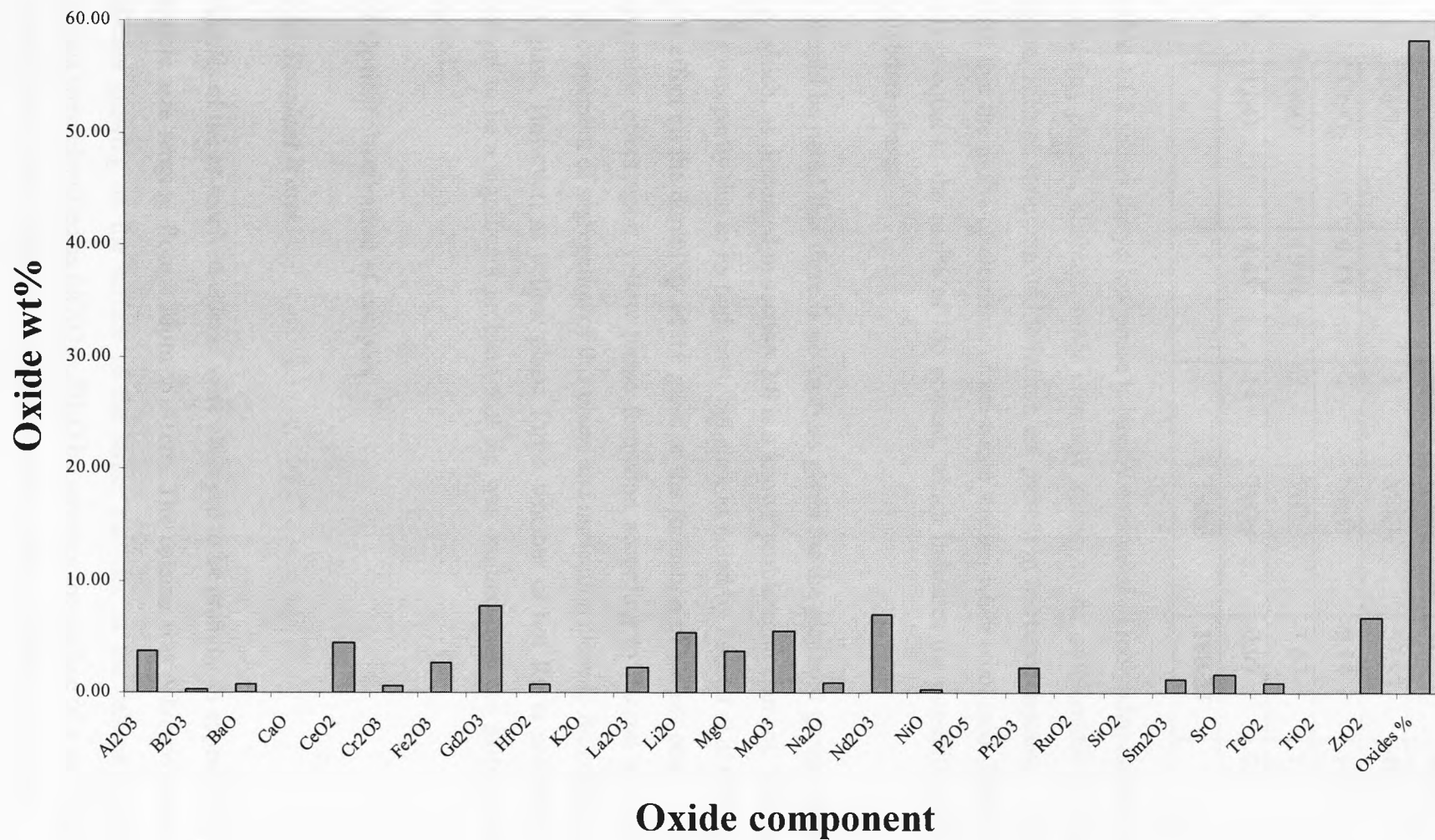


Figure 4.1.1: Oxide components of simulant calcine as determined by ICP-AES.

Table 4.1.2 – “Yellow phase” compositional analysis by XRF and ICP

Compound	Wt %	mol%	Compound	Wt %	mol%
BaO	2.2	1	MoO ₃	57.93	40.2
Cr ₂ O ₃	4.11	2	Na ₂ O	9.14	14.7
Cs ₂ O	19.86	7	SrO	1.67	1
Li ₂ O	4.45	14	TeO ₂	0.97	0.6
			Total	100.33	

Table 4.1.2 shows the yellow phase is largely composed of molybdenum and caesium containing phases, although other elements known to be problematic in the waste stream, such as strontium and tellurium are present in increased amounts. It should be noted that the mol% of elements of the waste stream, when combined (but excluding Mo) is equal to the mol% of Mo present, which indicates the possibility of several molybdate phases.

It should be noted that there is no analysis given for the platinumoid group, particularly Ru, which, as discussed in **section 2.8** is a known problematic element. The omission of Ru was partly due to its high cost, but also, as noted by Pacaud *et al* (1995), it has little effect on the durability of the glass or the formation of yellow phase. The most noticeable effect upon yellow phase formation according to Pacaud *et al* was the encouragement of segregation of this phase and nucleation close to Ru colloids within the glass. However, as yellow phase forms whether or not Ru is present it is not thought to be a significant problem that Ru was omitted from the particular calcine studied.

4.2 Optical observation of samples

4.2.1 Simulant Waste

Samples of the as-received calcine were observed to be granular in appearance, with a particle size ranging from <50µm to <1cm. The calcine was a brown colour, with crystals growing on the surface of the larger particles as the calcine aged. These crystals were identified as Li(NO₃)₃.3H₂O by scraping the surface of a calcine particle to collect the visible (<400µm) crystals from the surface and then using X-ray powder

diffraction. Subsequent heat treatment of the calcine samples revealed a change in colouration of the calcine, due to a change in oxidation state of some of the material constituents (**Figure 4.2.1**). Elements likely to give such a change in colour are numerous in the calcine, and include Fe, Mo, Nd, Cr, Gd. The most noticeable colour change occurred between 513°C and 600°C. The temperatures were nominally chosen according to results obtained using thermal analysis (see **section 4.4.1.1-2**) and samples removed at those furnace temperatures.

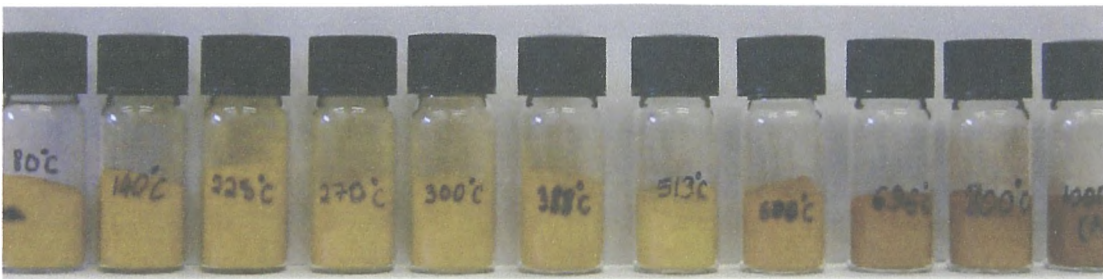


Figure 4.2.1: Colour change observed as calcine is heat treated

The calcined material became darker upon heat treatment, although the number of elements within the sample possible made pin-pointing the cause of the colour change difficult. Upon heating of as-received calcine samples to attempt to form a glass, a lower melting point, seemingly less dense phase formed on the surface of the calcine powder within the crucible. This liquid, upon splat quenching was a bright yellow/green in colour (**Fig 4.2.2**).



Fig 4.2.2: Low melting point phase formed on the surface of the calcine at high temperatures.

The quenched phase appeared to be of a porous nature indicating the degassing which would take place as the melt progresses.

4.2.2 Waste loaded glasses

Upon water quenching of a fully waste loaded glass after 5 minutes at 1050°C, it was noted that within the Inconel crucible, a surface layer had formed on top of the glassy melt. This surface layer was observed to cover the entire melt surface and was a vibrant yellow/green in colour. Further melting and quenching at 10 and 15 minute intervals revealed the gradual disappearance of the surface layer, although after 10 minutes melting around 80% of the surface was still covered. After 15 minutes only ~10% of the yellow/ green surface layer (**figure 4.2.3**) remained[†]. A scraping of this surface layer was also taken for analysis using X-ray diffraction. **Figure 4.2.3** shows the melt progression and the gradual disappearance of the surface layer from above the crucibles.

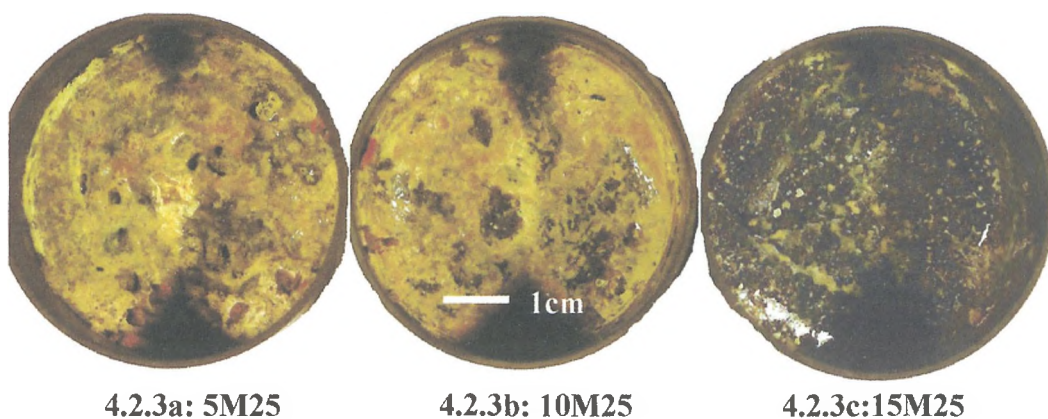


Figure 4.2.3: Surfaces of fully waste loaded samples water quenched within Inconel crucibles at 5, 10 and 15 minutes (key to sample names found in Table 3.10.2).

The crucibles were backfilled with resin and cross sectioned. This showed that particles of calcine, of <1mm, were still visible to the naked eye at 10 minutes of melting. There was also an obvious reaction zone around these particles, as the surrounding glassy matrix was coloured green (**Figure 4.2.4**) and the colouration was much stronger in the areas surrounding the calcine particles.

[†] The surface layer may appear yellow/brown in **Figure 4.2.3** but it should be noted this is due to colour reproduction and the actual colour of the surface was yellow/green.



Figure 4.2.4: Cross sections of crucibles quenched after 5, 10 and 15 minutes.

Yellow deposits were also noted on the crucible walls (**Figure 4.2.6**) and assumed to be the volatiles condensing on the walls. Due to gas evolution of the glass batch during melting and the batch decreasing in height as it melts, some of the yellow phase had been deposited in increased amounts on the crucible walls.

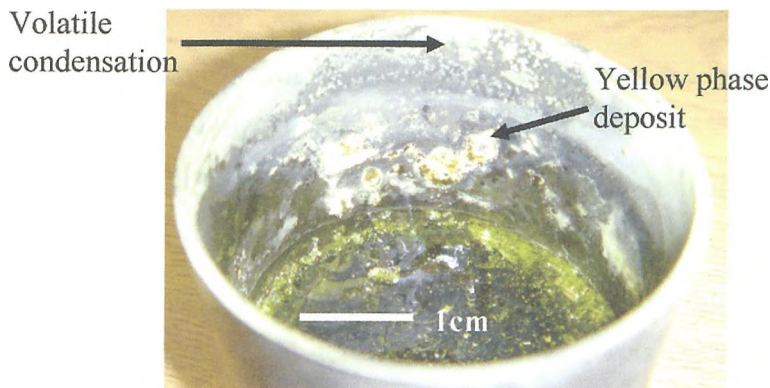


Figure 4.2.6: Surface of 15M25 showing “yellow phase” deposits on crucible walls

For comparison, samples of V26 simulant (Magnox) glass taken from BNFL stores were studied visually and examples of yellow phase were seen within the bulk of the glass upon breaking it open (**Fig 4.2.5**), and in the bulk samples of other glasses containing both WRW13 (blend) and WRW5 (Magnox) waste.

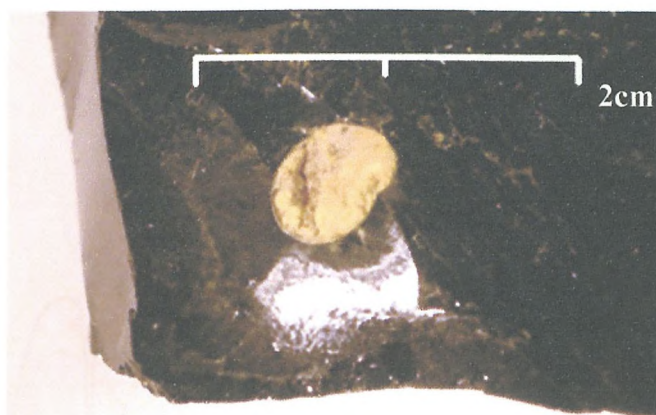


Figure 4.2.5: “Peanut” of yellow phase in bulk of Magnox glass (photograph taken from *Short, 2004*)

4.3 Density measurements

The densities of ground ($<50\mu\text{m}$) as-received calcine and a sample of synthesised CsLiMoO_4 were measured. The density of the calcine was 3485.4 kg m^{-3} . The density of the CsLiMoO_4 was 3465.6 kg m^{-3} . The density of the borosilicate frit was 2412.1 kg m^{-3} . No values were found in the literature for the CsLiMoO_4 and calcine densities, but the borosilicate glass density was found to be consistent with published data (Weast, 1981). The theoretical density of CsLiMoO_4 was calculated from structural information, and found to be 3465 kg m^{-3} .

4.4 Thermal Analysis

4.4.1 Differential Thermal Analysis

Differential thermal analysis was performed on several samples of the as received calcine due to its heterogeneous appearance. Several endothermic and exothermic events were noted (**Figure 4.4.1**).

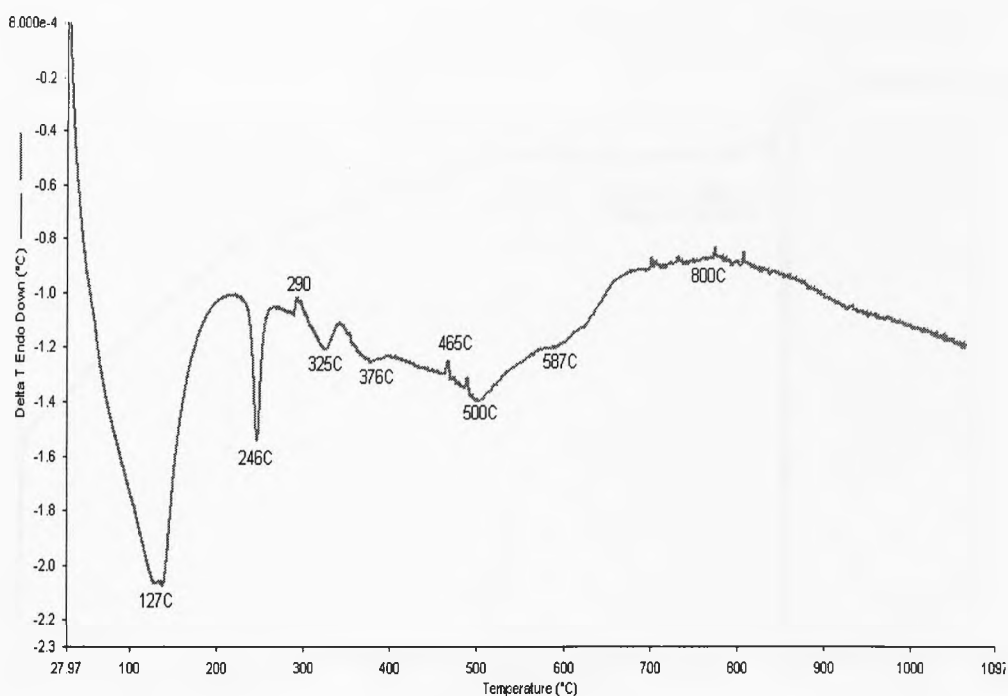


Figure 4.4.1: DTA data from as-received simulant calcine

The intense endotherm between room temperature and 125°C can be attributed to dehydration. Between 125 – 400°C several endothermic events were can be observed. The sharp intense endotherm at 246°C is attributed to the melting of a waste component, identified as LiNO_3 (see **section 4.5**). The weak endotherms observed at 325°C and 376°C may be associated with the loss of chemically bound water molecules (“water of hydration”).

A sample of synthesised CsLiMoO_4 was also analysed (**Figure 4.4.2**) to determine the melting point of the phase, given the identification of this phase with the use of XRD (see **section 4.5**). The melting point was determined to be $\sim 772^\circ\text{C}$ by onset due to the large endotherm at this point.

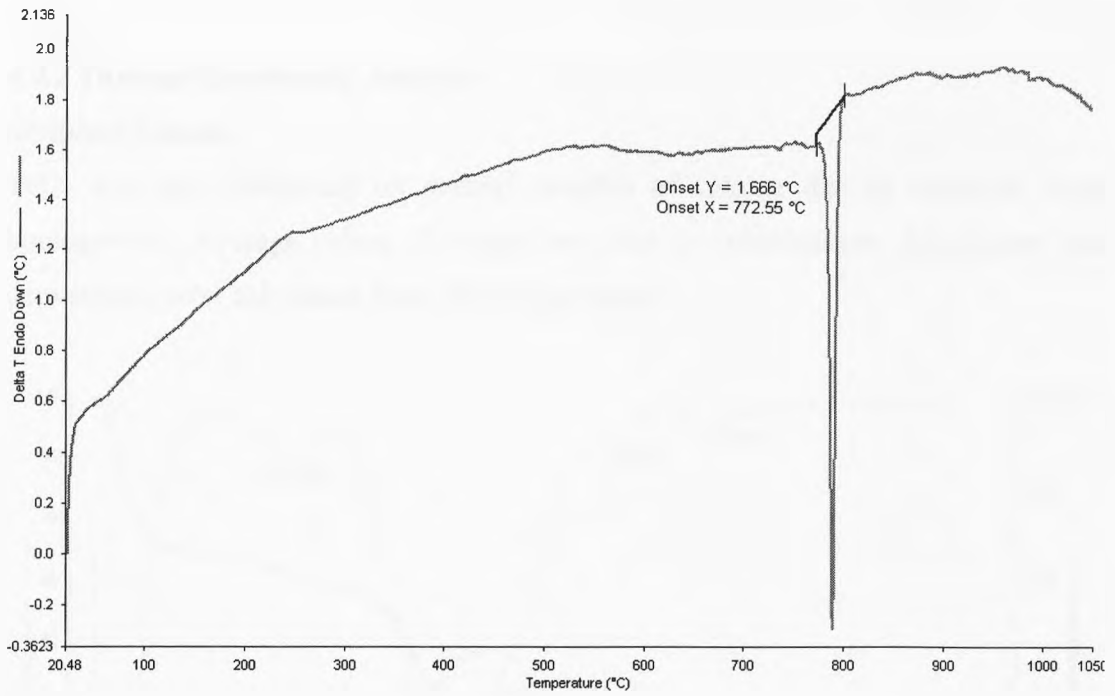


Figure 4.4.2: DTA of synthesised CsLiMoO₄

A sample of the frit supplied by James Kent Ltd was subjected to DTA (**Figure 4.4.3**) and two endothermic events could be observed, with the glass transition temperature seen at ~520°C. No obvious melting was observed as the sample was already glassy before the analysis began. T_g (~520°C) was calculated using the onset method.

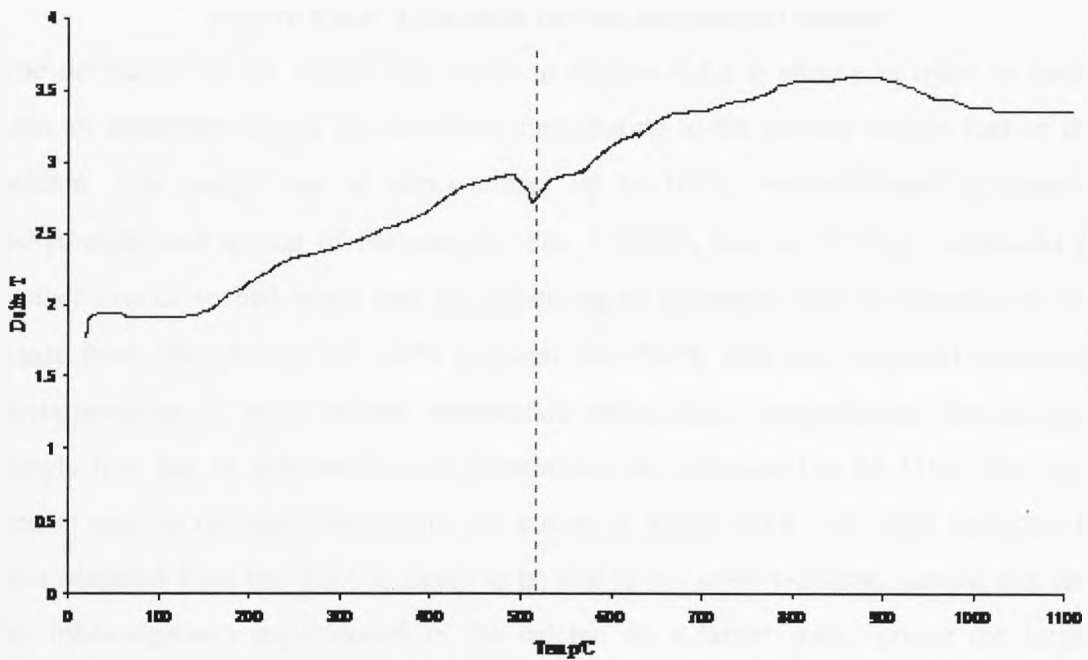


Figure 4.4.3: DTA analysis of as-received frit (T_g)

4.4.2 Thermal Gravimetric Analysis

Simulant Calcine

TGA was also conducted on several samples of calcine due to concerns about homogeneity. Average values of weight loss (due to volatilisation, dehydration and denitration) were calculated from these experiments.

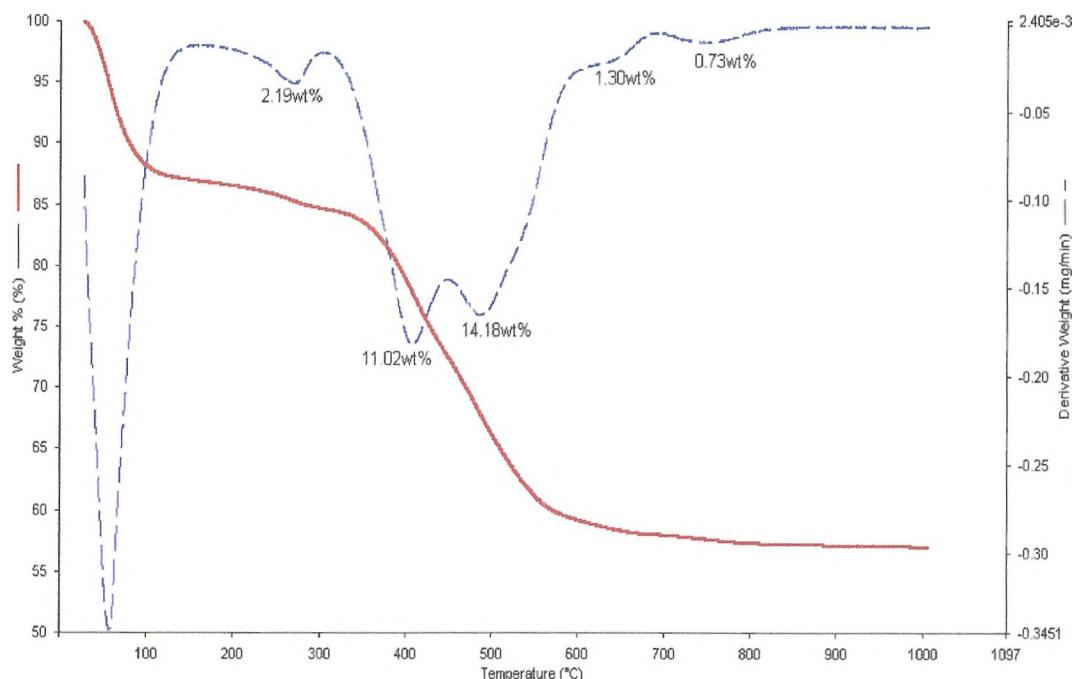


Figure 4.4.4: TGA data for the as-received calcine

The derivative of the weight loss curve in **Figure 4.4.4** is shown in order to better gain an understanding of the reactions contributing to the overall weight loss of the calcine. The weight loss at temperatures up to 100°C was attributed to general dehydration and drying of the sample. The 2.19wt% loss at 300°C is attributed to further loss of sorbed water and the beginning of decomposition of elements of the waste form. Weight loss of ~30% between 400-700°C was also observed indicating decomposition of the of nitrate compounds within these temperatures. On average, weight loss due to dehydration and denitration was calculated to be 31%. The TGA results used to calculate this figure are shown in **Table 4.4.1**. The large variation in data obtained from the TGA is likely to be due to the small (<50mg) sample size and the inhomogeneity experienced in the calcine on a larger scale, giving the larger samples (<10g) from the furnace experiments an advantage in terms of overall sample representation.

Table 4.4.1: Av. weight loss % for L.O.I calculation (* indicates furnace detailed in section 3.3)

Method	TGA	TGA	TGA	TGA	Furnace*	Furnace*	Av.
%Wt loss	29.42	14.4	50.2	29.38	31.4	33.6	31.4%

TGA was also conducted on simulant waste samples under different atmospheres using oxidising, reducing, and inert gases (Figure 4.4.5).

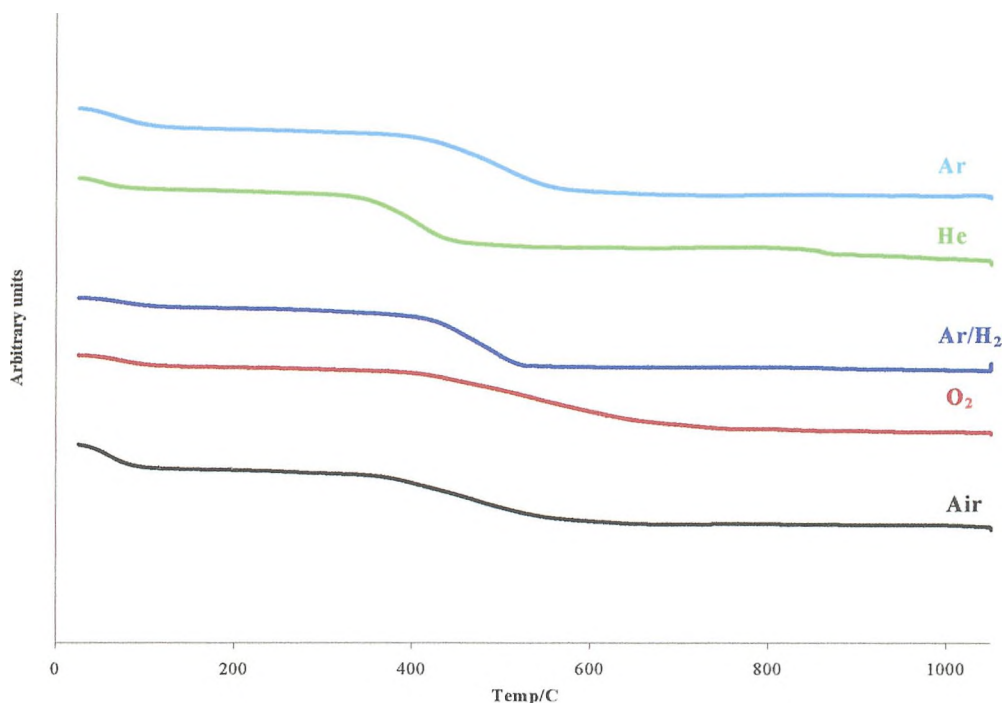


Figure 4.4.5: TGA of simulant waste samples under different atmospheres

The rate of denitration appeared to change when atmospheric changes were introduced to the melting process, with the pure O₂ atmosphere giving the slowest rate of denitration of the sample and the reducing atmosphere appearing to increase the rate of denitration more than when heated in other conditions.

Waste Loaded Glasses

Simultaneous TGA/DTA was conducted on several fully loaded waste samples under different atmospheres (Figures 4.4.6-9) illustrating the fact that final incorporation of the waste into the glass does not take place until 1000°C. The endothermic event which begins at 900°C and which is complete by the time the material reaches 1000°C is attributed to the digestion of the waste by the glass melt.

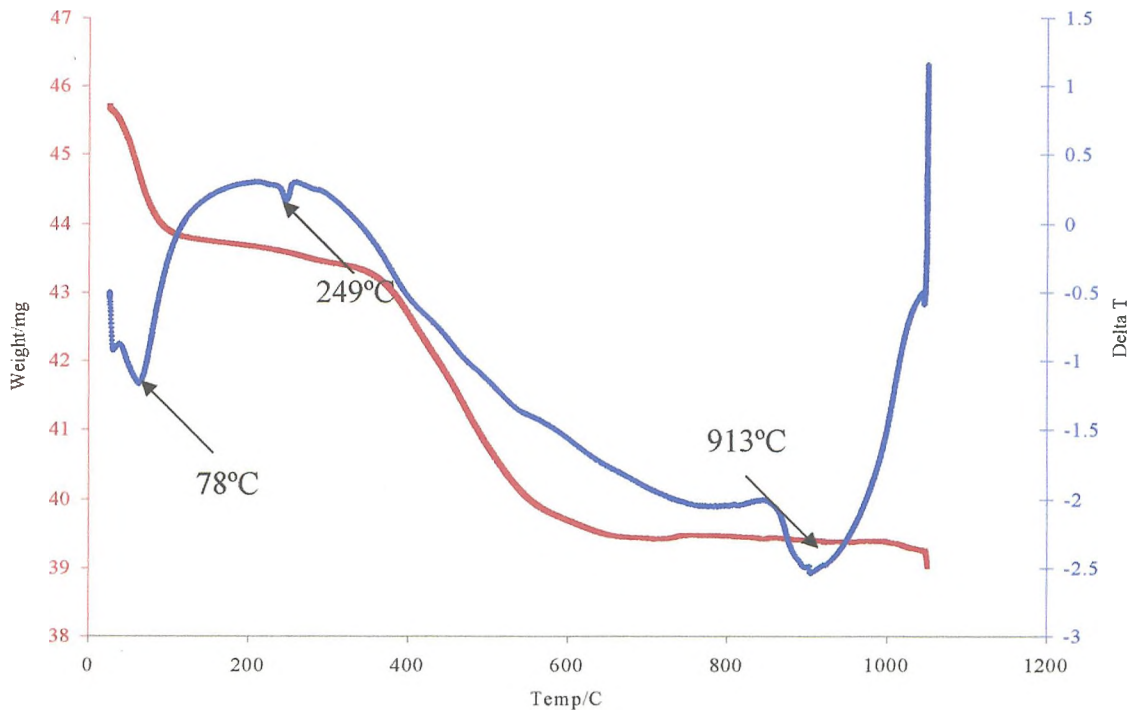


Figure 4.4.6: TGA/DTA for 25wt% waste in air $4^{\circ}\text{C min}^{-1}$

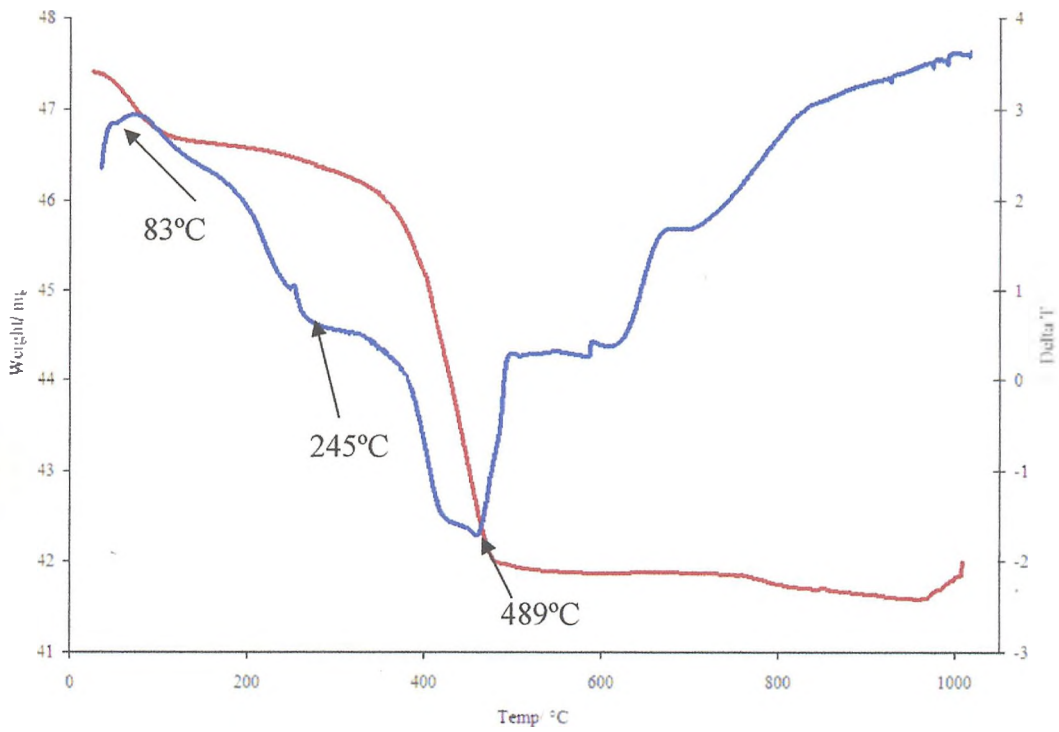


Figure 4.4.7: TGA/DTA for 25wt% waste in Ar/H_2 $4^{\circ}\text{C min}^{-1}$

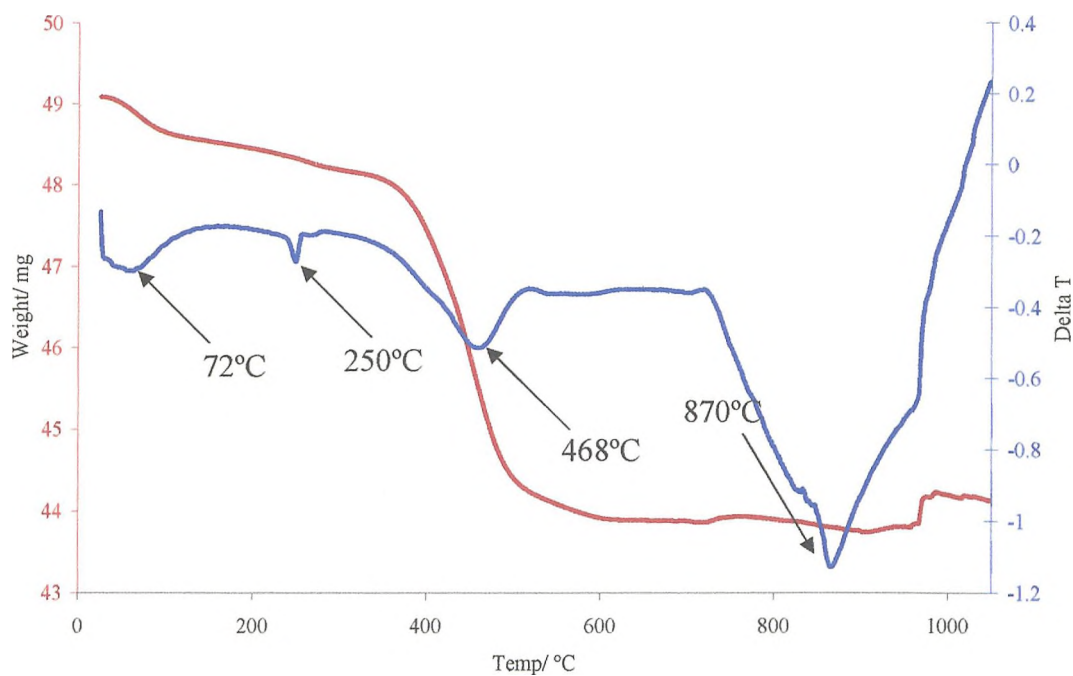


Figure 4.4.8: TGA/DTA for 25wt% waste in He $4^{\circ}\text{C min}^{-1}$

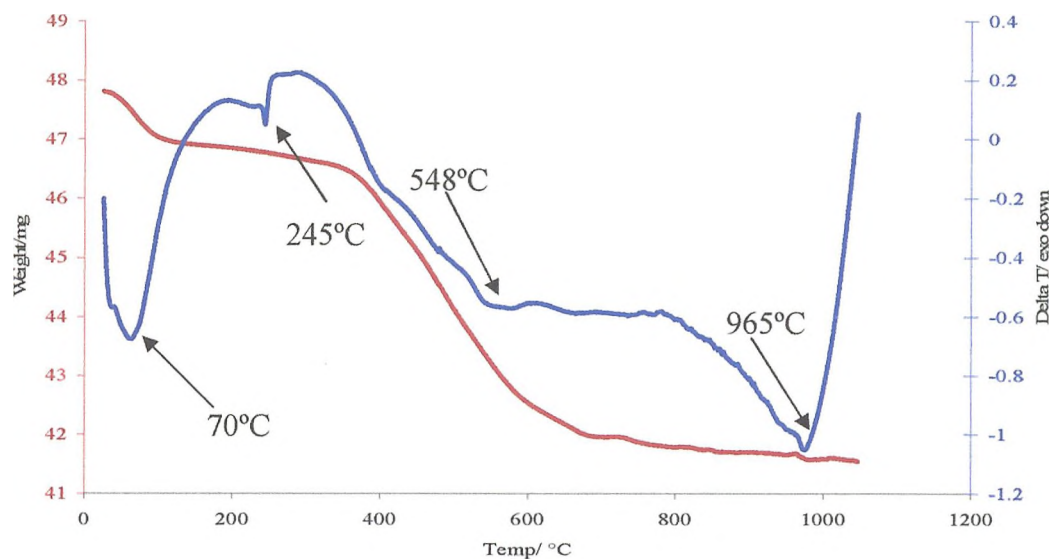


Figure 4.4.9: TGA/DTA for 25wt% waste in O_2 $4^{\circ}\text{C min}^{-1}$

The broad endothermic events 70°C to 100°C are attributed to the dehydration of the sample. At $\sim 200^{\circ}\text{C}$ the peaks are attributed to the melting of LiNO_3 , $\text{Sr}(\text{NO}_3)_2$ at ~ 550 - 650°C , general nitrate decomposition from 245 - 665°C and the incorporation of the waste and formation of CsLiMoO_4 above 870°C . This peak is not present in the reducing atmosphere due to the formation of an apparently metallic Mo deposit.

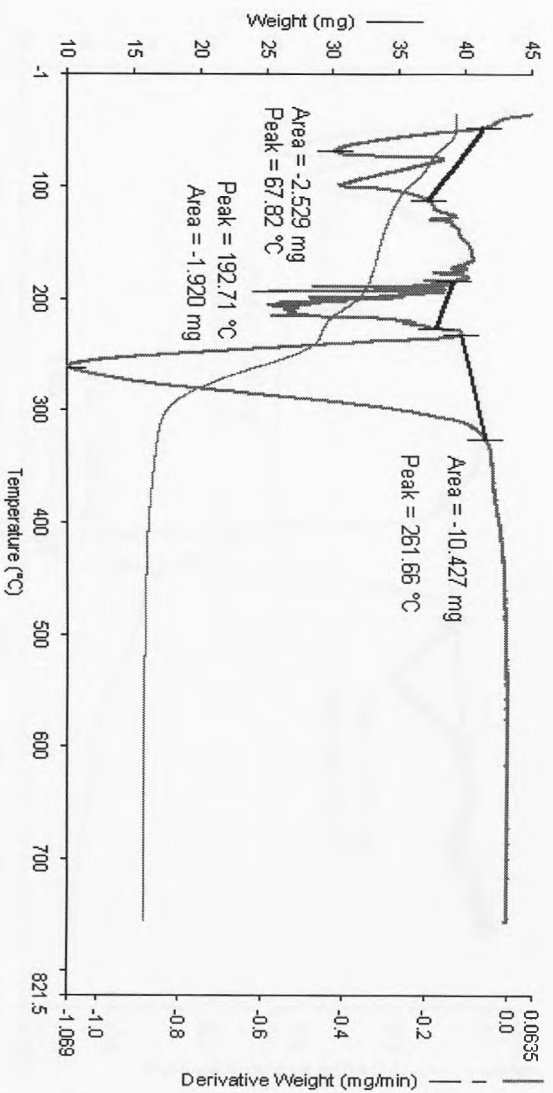


Figure 4.4.10: TGA for $\text{Ce}(\text{NO}_3)_2 \cdot 4\text{H}_2\text{O}$

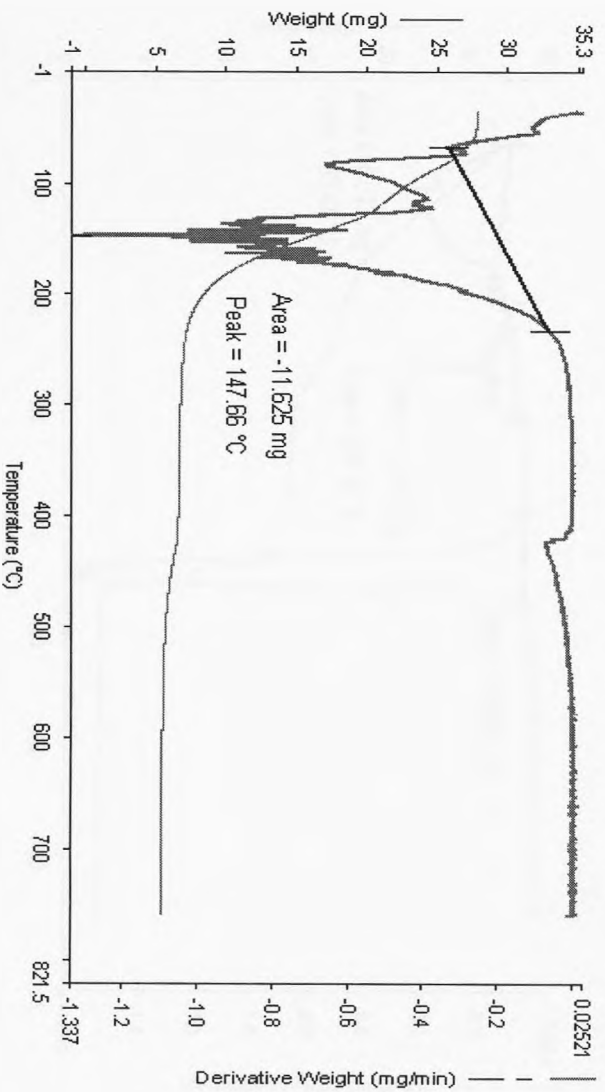


Figure 4.4.11: TGA for $\text{Cr}(\text{NO}_3)_3 \cdot 6\text{H}_2\text{O}$

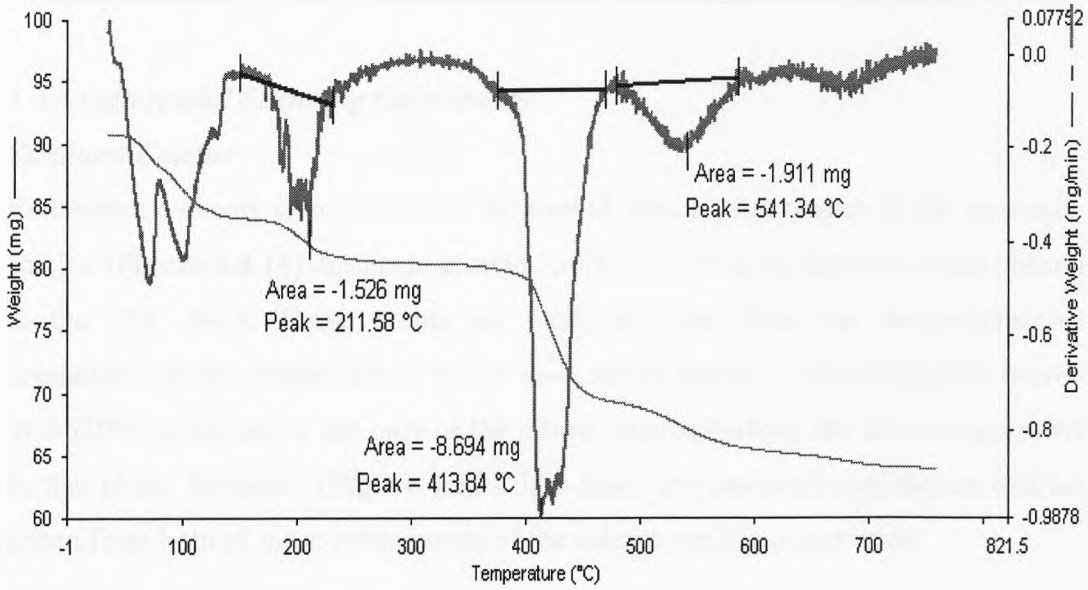


Figure 4.4.12: TGA for $\text{LaNO}_3 \cdot 3\text{H}_2\text{O}$

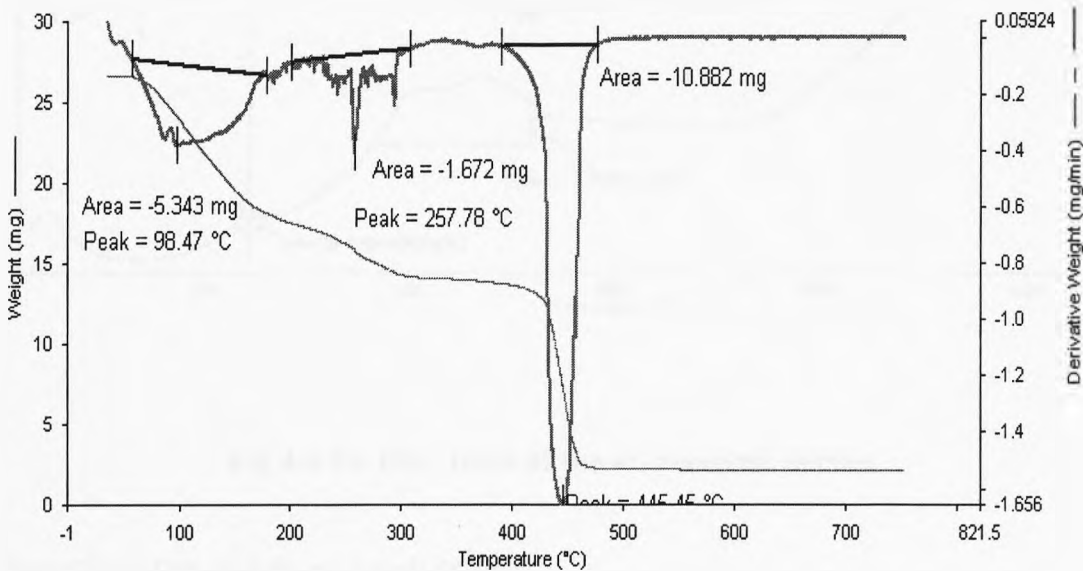


Figure 4.4.13: TGA for $\text{MgNO}_3 \cdot 6\text{H}_2\text{O}$

The TGA curves and derivatives are shown for several hydrated nitrates (Figures 4.4. 10-13). These nitrates were chosen as being representative due to the increased percentage of these compounds within the waste stream. In each case, decomposition of the nitrate is complete by $\sim 600^\circ\text{C}$ or before. The events occurring in each sample at

~210°C, 163°C, 227°C and 271°C are attributed to the sorbed water present in each compound, as the evaporation of water of hydration is clear on each graph at ~100°C.

4.4.3 Differential Scanning Calorimetry

Simulant Calcine

Endothermic events which could be associated with crystal phases in the as-received calcine (**Figure 4.4.14**) disappear around 550°C, as shown by the two events observed in the DSC trace. These events are likely to arise from the decomposition of crystalline nitrate phases found in the as-received calcine. The endotherm between 380-520°C is indicative not only of the nitrate decomposition, but also coincides with further phase formation (**Figure 4.5.2**). It is likely the observed endotherms will have arisen from both of these components of the calcine melt in conjunction.

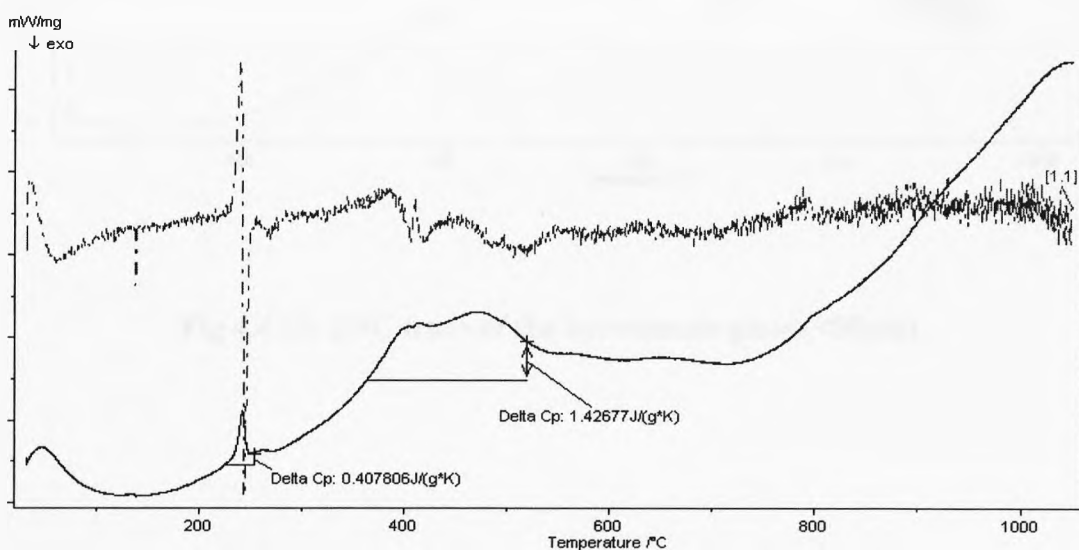


Fig 4.4.14: DSC trace of the as- received calcine

Base Glass Frit and Waste Loaded Glass

The curves obtained for many of the glass/calcine mixtures (**Figures 4.4.16-18**) using DSC had no apparent base line. The lack of baseline is also possibly due to the calibration methods used for the instrument. It should be noted that baseline curves on DSC traces are usually “flat” in appearance, as opposed to having a constant upwards slope. However, another reason for the lack of baseline could be because the mixtures were already glassy due to the presence of the base glass frit, and so there is no

obvious peak for the expected liquid. There appears to be a break in the curve around 520°C where the liquidus should be, and a gradual slope, indicating a slow transition from a solid to a 'free-flowing' liquid.

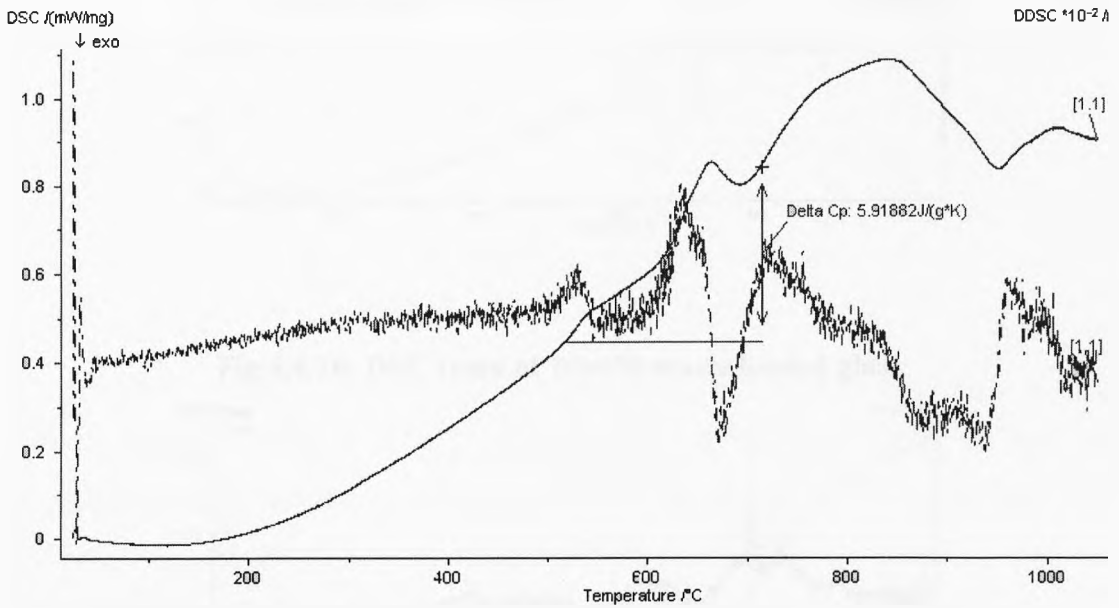


Fig 4.4.15: DSC trace of the borosilicate glass (<50µm)

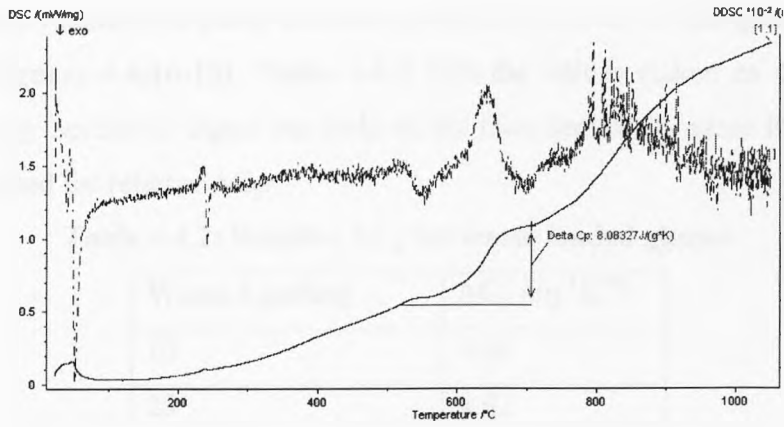


Fig 4.4.16: DSC trace of 10wt% waste loaded glass

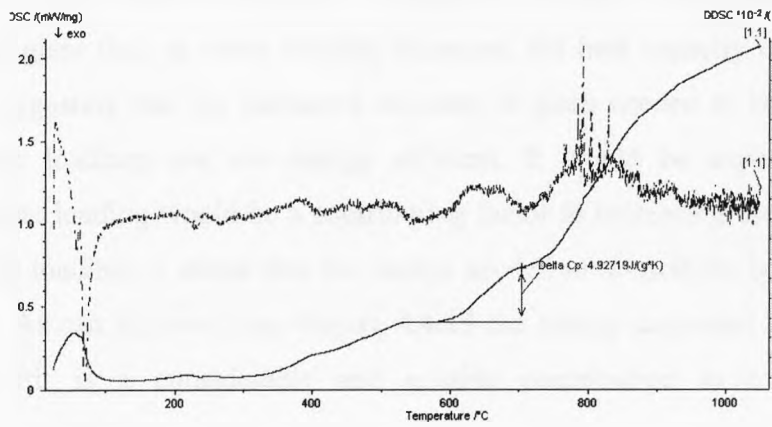


Fig 4.4.17: DSC trace of 25wt% waste loaded glass

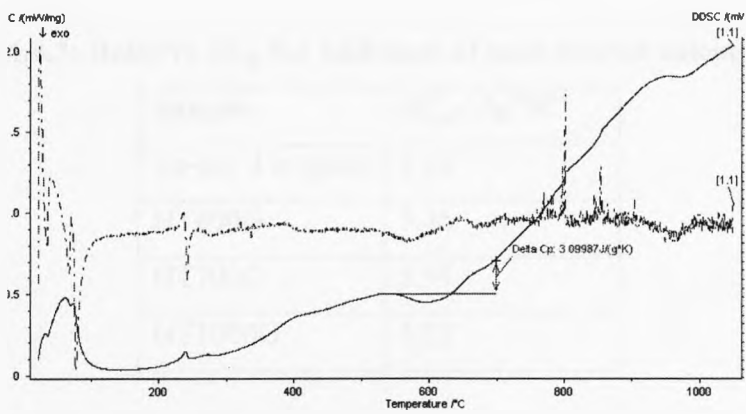


Fig 4.4.18: DSC trace of 35wt% waste loaded glass

No apparent crystallisation peaks are seen on the DSC curves for the glass and calcine mixtures (**Figures 4.4.16-18**). **Table 4.4.2** lists the values (taken as a measure of relative energy needed to digest the body of the then denitrated waste from 611°C to 703°C) obtained for relative ΔC_p .

Table 4.4.2: Relative ΔC_p for waste loaded glasses

Waste Loading	$\Delta C_p / \text{Jg}^{-1}\text{K}^{-1}$
10	8.08
25	4.92
35	3.09

It can be observed from the difference in relative calculated heat capacities of each waste loaded glass that, as waste loading increases, the heat capacity of the mixture decreases, suggesting that the increased amounts of glass needed to be melted with smaller waste loadings are not energy efficient. It would be expected that the increased waste loading would be a contributing factor to increasing the ΔC_p but that at these waste loadings it seems that the energy needed to re-melt the borosilicate frit is dominant. As can be seen from **Figure 4.4.15** the energy expended to re-melt the borosilicate frit is a considerable and notable contribution to overall energy expenditure.

Table 4.4.3 lists the values obtained for the relative heat capacities of the heat treated calcine when added to the glass batch in 25wt% waste loading.

Table 4.4.3: Relative ΔC_p for additions of heat treated calcine to frit

Sample	$\Delta C_p / \text{Jg}^{-1}\text{K}^{-1}$
As-rec'd in glass	4.92
HT400G	3.46
HT700G	8.91
HT1000G	5.27

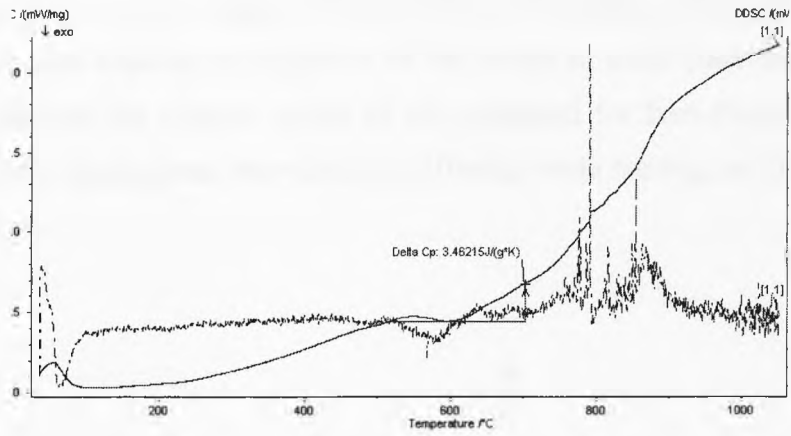


Fig 4.4.19: HT400 in glass (25wt%)

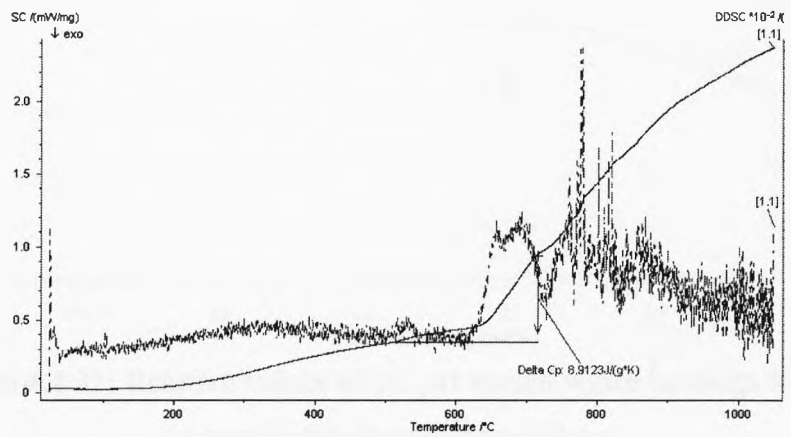


Fig 4.4.20: HT700 in glass (25wt%)

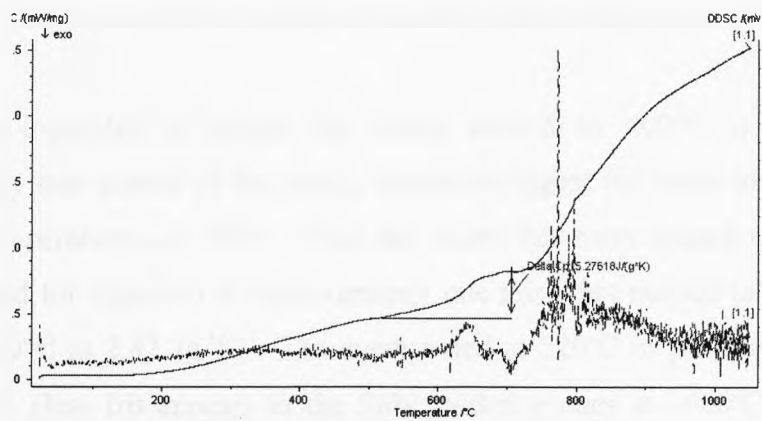


Fig 4.4.21: HT1000 in glass (25wt%)

Upon addition of the heat treated waste stream to the glass, it is observed that the relative total heat capacity of digestion of the waste in each glass differs. **Figure 4.4.22** summarises the relative values of ΔC_p obtained for heat treated samples in glass (at 25wt% loading) and the values for differing waste loadings of the as-received sample in glass.

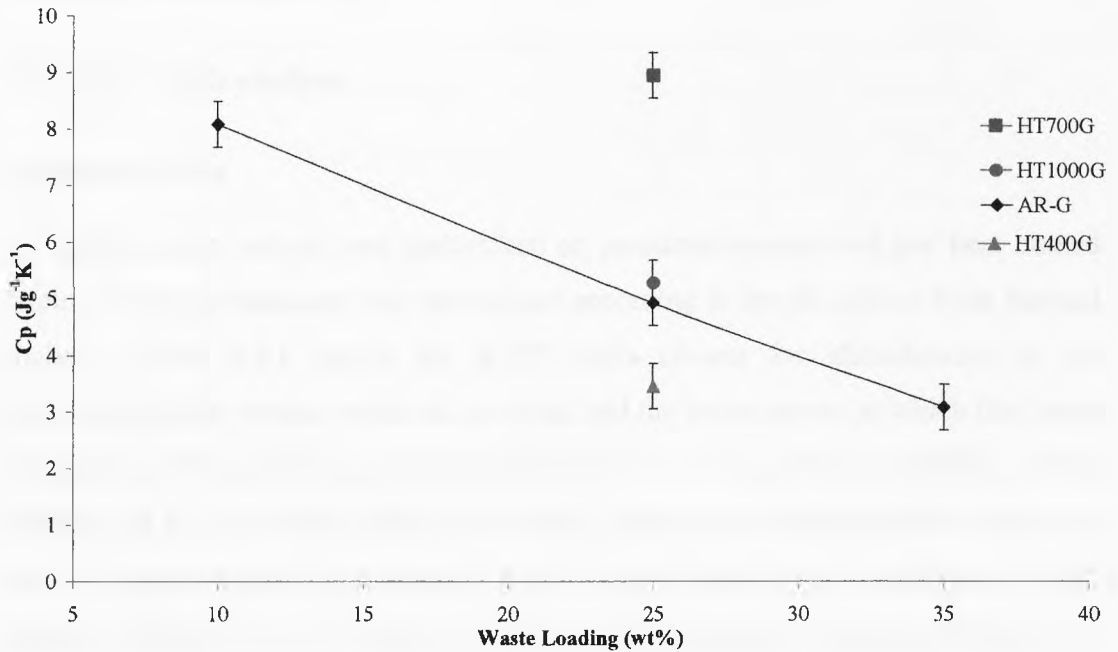


Figure 4.4.22: Relative values of ΔC_p at varied waste loadings and heat treatment of calcine samples.

Figure 4.4.22 illustrates clearly the difficulty of incorporating low waste loadings and nitrate containing calcine. It also highlights the increased energy input needed to incorporating the waste once it has been heated to temperatures above 400°C.

The energy expended to digest the waste treated to 400°C is 3.46 $Jg^{-1}K^{-1}$, approximately one quarter of the energy needed to digest the waste after it has been heated to temperatures of 700°C. Once the waste has been treated to 1000°C, the energy needed for digestion is approximately one third that needed to process waste heated to 700°C at 2.87 $Jg^{-1}K^{-1}$. The event noted at 520°C in previous experiments involving the glass frit appears in the fully loaded glasses at ~600°C. It should be noted that errors are expected in this technique, so quantitative data is referred to simply to get a comparative value for each sample, rather than an exact measure of heat capacity. For instance, in the HT400 sample, the weight loading will be slightly

inaccurate as the weight loading was originally calculated for a fully nitrated waste, and then adjusted for a weight loss of ~5wt% (calculated from **Figure 4.4.4**) to account for partial denitration and dehydration. The oxide waste loading was subsequently adjusted for the HT700 and HT1000 samples, using an estimated weight loss of 31.4wt% for both, to account for the complete denitration and dehydration as observed in DTA and TGA.

4.5 Powder XRD analysis

Simulant Calcine

X-ray diffraction analysis was undertaken on powdered as-received and heat treated calcine. The heat treatment was determined according to results gained from thermal analysis. **Table 4.5.1** details the ICDD cards chosen for identification of the crystalline phases present within the material and the temperatures at which they were observed. Although the as-received material was of a poorly crystalline nature (**Figure 4.5.1**), strontium nitrate and lithium nitrate were detected both in the as-received material, and in the samples which had been heated to temperatures of 550°C **Figure 4.5.2** illustrates the phase evolution in the simulant waste upon further heat treatment.

Table 4.5.1: JCPDF cards chosen for the phases identified

Phase	JCPDF no.	Phase	JCPDF no.
Nd ₆ MoO ₁₂	35-246	Na ₅ La(MoO ₄) ₄	72-2158
BaFe ₂ O ₄	44-0897	CsLiMoO ₄	72-2479
Sr ₂ (MoO ₄)	45-080	Nd _{0.20} Ce _{0.80} O _{1.90}	75-153
SrZrO ₃	70-694	Sr(NO ₃) ₂	76-1375
MgO	71-1176	LiNO ₃	80-203

A rare earth, fluorite-structured oxide phase (LnO_{2-x}) characterised by broad reflections was identified in the as-received calcine, indicating the phase to have been poorly crystalline and possibly a solid solution. The fluorite-type phase detected within the calcine was identified as possibly being Nd_{0.2}Ce_{0.8}O_{1.9}. Although many fluorite based phases were possibilities, this one was chosen because of the quantity

(~10wt%) of both Nd and Ce in the calcined material. Fluorite structures easily accommodate a wide range of ions within their structure and the characteristic peaks were broad, indicating in the first instance a poorly crystalline, largely amorphous structure. Upon heating, the broad peaks remained, probably reflecting the presence of several rare earth cations (La, Nd, Ce, Gd) with a range of ionic radii (1.18 – 1.08Å, for 8-fold co-ordination; Shannon and Prewitt, 1974) incorporated within the fluorite structure. In addition, the failure to identify Zr and Al containing crystalline phases may suggest that these elements may have been incorporated into the rare earth oxide phase and thus were subsequently unidentifiable using XRD. As heating continued and the decompositions of lithium nitrate (~600°C) and strontium nitrate (~700°C) were observed, other crystalline peaks began to emerge. **Table 4.5.2** illustrates at what temperatures phases began to be identified using X-ray diffraction. Dependent upon the calcine samples being analysed (as previously mentioned, the calcine was heterogeneous on both a micro and macro scale) molybdates and oxides formed at higher heat treatment temperatures[‡]. **Table 4.5.3** shows the melting and decomposition points of nitrates that were identified as being present in the waste stream.

The x-ray diffraction patterns compiled in **Figure 4.5.2** are separated and the phases identified in the following **Figures 4.5.3-11**. **Figure 4.5.1** shows the presence of the identified crystalline nitrate phases.

Sr(MoO₄), Nd₃MoO₇, and CsLiMoO₄ (Figures 4.5.3-5) were identified as forming at temperatures above ~600°C. Presumably, the Sr released by the decomposition of strontium nitrate contributed to the formation of the molybdate. It should be noted that there was probably some amorphous, unidentifiable material present which may also have contributed to the formation of these phases. Since no crystalline Mo containing phases were detected within the sample below 550°C, it was assumed that the molybdenum was also present in an amorphous form, possibly as a nitrate, based on the large percentage of the material found to be nitrate based using thermal analysis.

[‡] General decomposition temperatures of nitrates which were possibly present in the calcine were determined using data obtained from the 61st edition of the CRC Handbook. More accurate experimental confirmation was later undertaken with the use of GC-MS and FT-IR techniques.

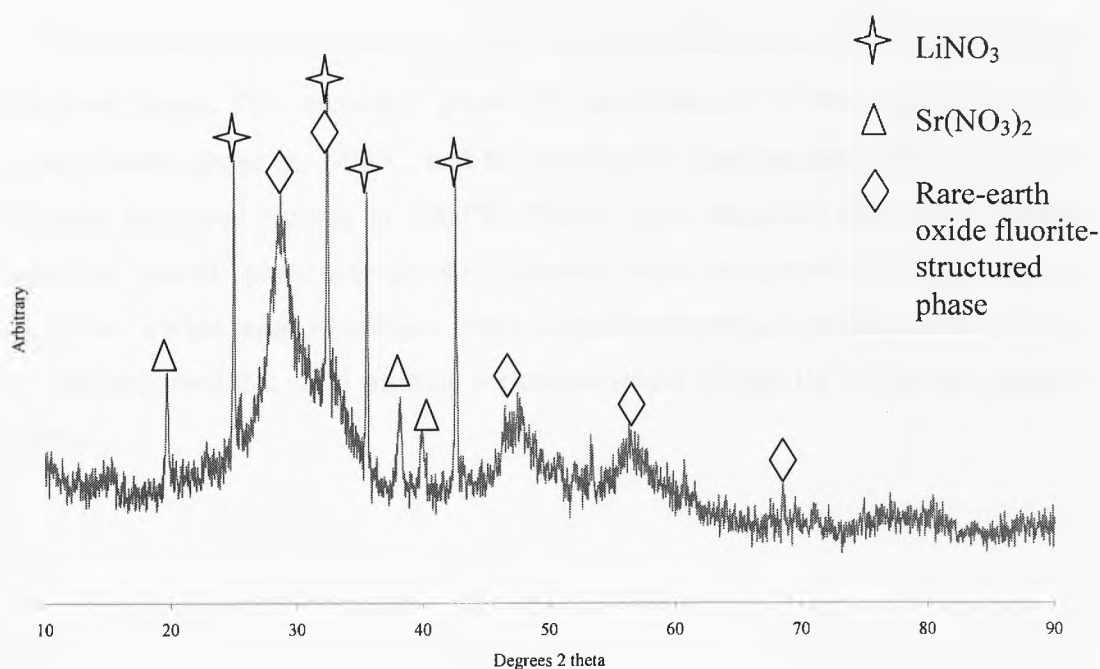


Figure 4.5.1: XRD analysis of as-received simulant calcine

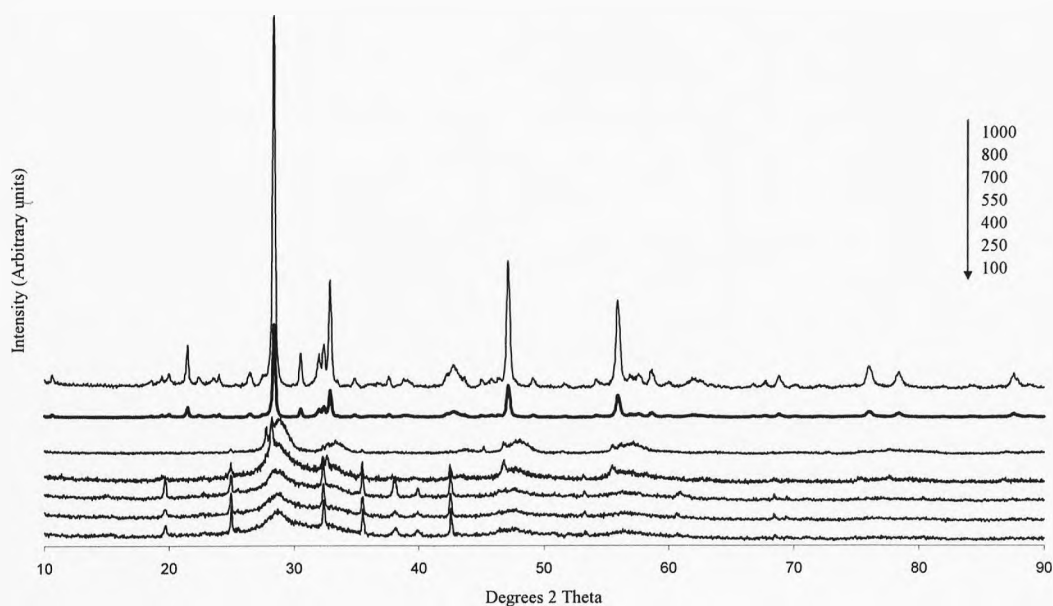


Figure 4.5.2: Phase evolution of the simulant waste upon heat treatment

It was also observed that, above temperatures of 700°C , a secondary fluorite-structured, rare-earth oxide phase formed at a lower 2θ angle as a 'shoulder' on the peaks already present. The d-spacing of its most intense peaks were at 3.17\AA and

1.94Å, contrasting with 3.10Å and 1.89Å of the original rare earth oxide, fluorite structured phase. This secondary phase was accompanied by the development of a ternary fluorite phase at ~900°C, and the subsequent disappearance of all except the originally identified fluorite at 1000°C. Phases were identified in the heat treated calcine as “parent” phases, or crystal structures which are known for their ability to incorporate a wide range of cations. Exact d-spacings were not matched for all phases, as it was expected that solid solution formation would change the diffraction patterns slightly.

Table 4.5.2: Phases identified in calcine material

T/Phase	$\text{Nd}_{0.2}\text{Ce}_{0.8}\text{O}_{1.9}$	$\text{Sr}(\text{NO}_3)_2$	LiNO_3	$\text{Sr}_2(\text{MoO}_4)$	CsLiMoO_4	BaFe_2O_4	SrZrO_3	MgO	$\text{Na}_5\text{La}(\text{MoO}_4)_4$
200	✓	✓	✓	-	-	-	-	-	-
300	✓	✓	✓	-	-	-	-	-	-
400	✓	✓	✓	-	-	-	-	-	-
500	✓	✓	✓	-	-	-	-	-	-
550	✓	✓		-	-	-	-	-	-
600	✓	✓		✓	-	-	-	-	-
700	✓	-	-	✓	✓	-	-	-	-
800	✓	-	-	✓	✓	-	-	-	-
900	✓	-	-	✓	✓	✓	-	✓	-
1050	✓	-	-	✓	✓	✓	✓	✓	✓

✓ = Phase definitely present ✓ = Phase depletion

Table 4.5.3: Nitrate compounds and their thermal data (Figures compiled from CRC handbook)

Compound	M. pt (°C)	decomposition pt (°C)
CsNO ₃	414	414
FeNO ₃	40	126
LiNO ₃	264	600
MgNO ₃	129	-
Al(NO ₃) ₃	73.5	150
Sr(NO ₃) ₂	570	-

The CsLiMoO₄ (Figure 4.5.3) identified within the calcine was of a cubic structure, and all reflections easily identified using the ICDD database indicating a single crystalline phase. In contrast to the fluorite phase, the peaks for CsLiMoO₄ were very narrow and sharp.

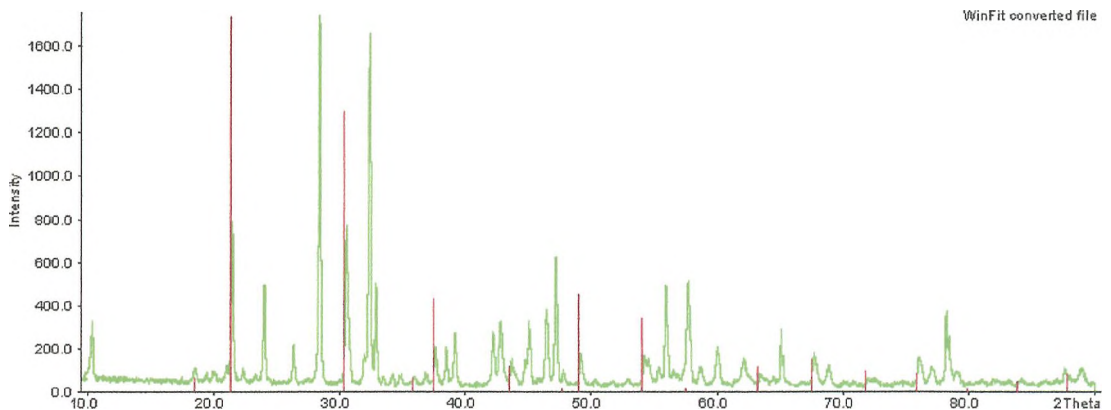


Figure 4.5.3: Identified CsLiMoO₄ phase within immiscible yellow surface layer (identifying peaks indicated with red markers)

MgO (Figure 4.5.4) was also identified as forming at higher temperatures. This slightly refractory oxide was only observed above 1000°C, but may not have contained all the Mg present in the waste form due to the ease of incorporation of Mg into the rare earth oxide phase.

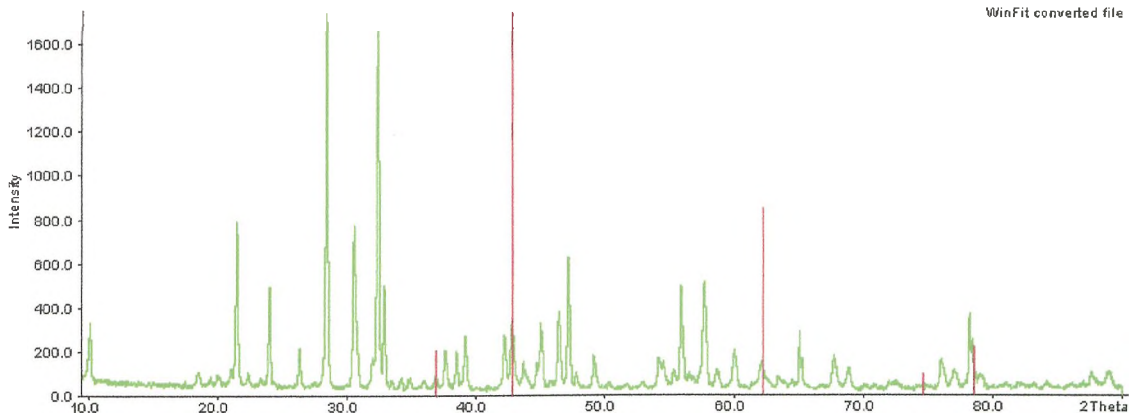


Figure 4.5.4: MgO phase identified within the heat treated calcine at 1000°C

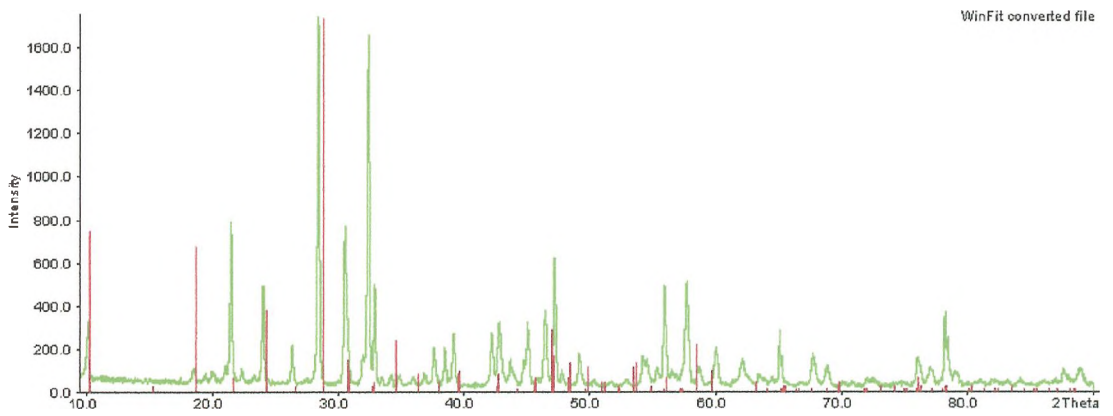


Figure 4.5.6: Na₅La(MoO₄)₄ phase identified within the heat treated calcine at 1000°C

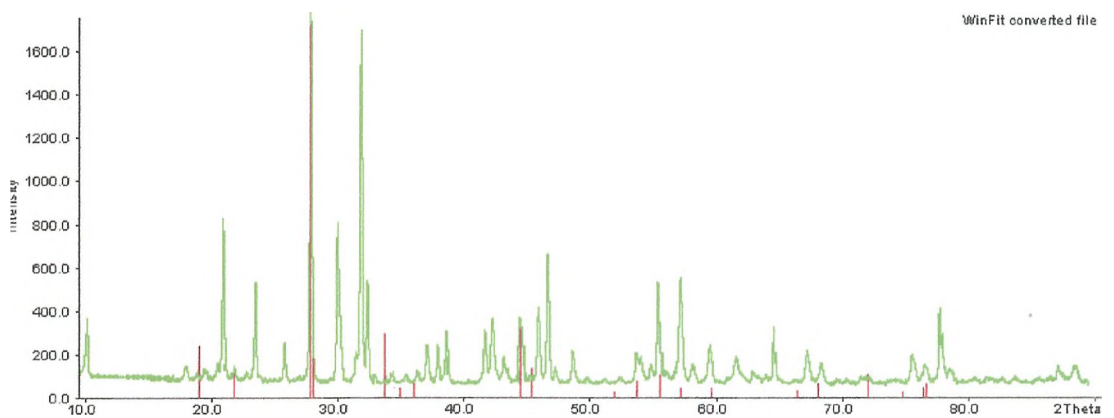


Figure 4.5.7: BaFe₂O₄ phase identified within the heat treated calcine at 1000°C

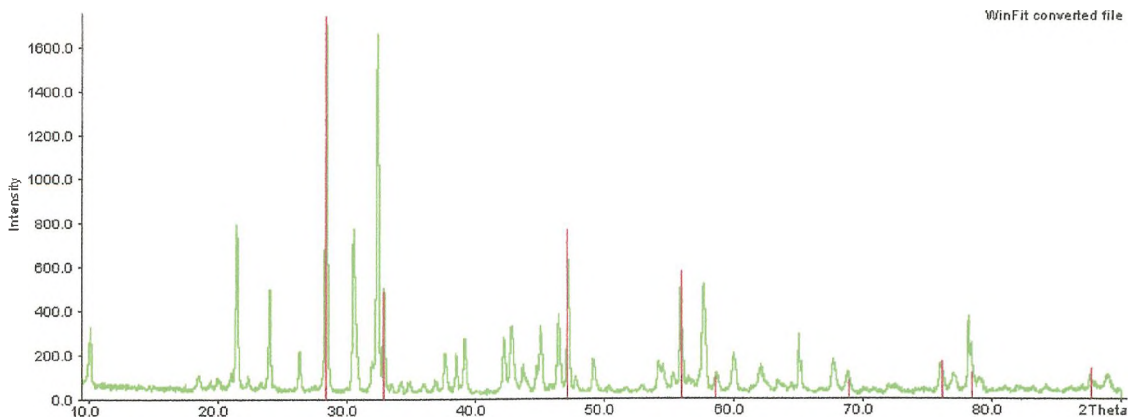


Figure 4.5.8: $\text{Nd}_{0.2}\text{Ce}_{0.8}\text{O}_{1.90}$ phase identified within the heat treated calcine at 1000°C

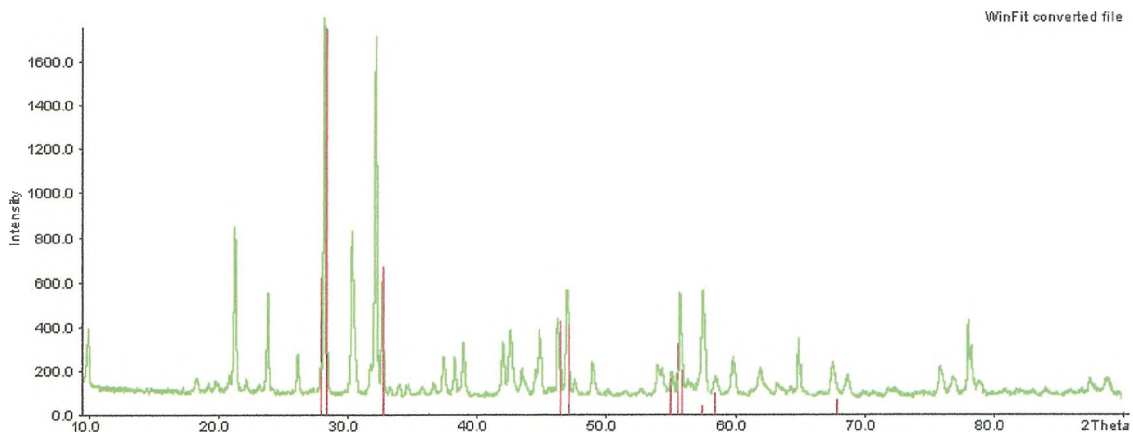


Figure 4.5.9: $\text{Nd}_6\text{MoO}_{12}$ phase identified within the heat treated calcine at 1000°C

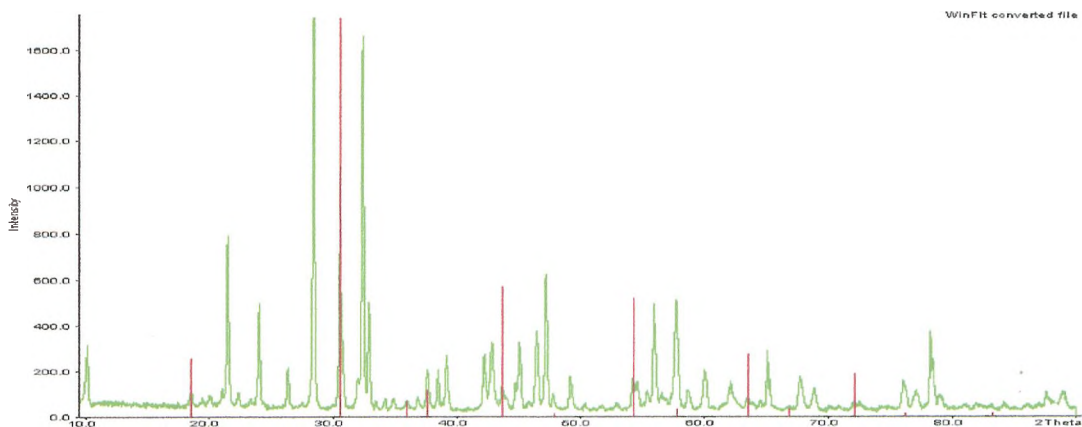


Figure 4.5.10: $\text{Sr}_2(\text{MoO}_4)$ phase identified within the heat treated calcine at 1000°C

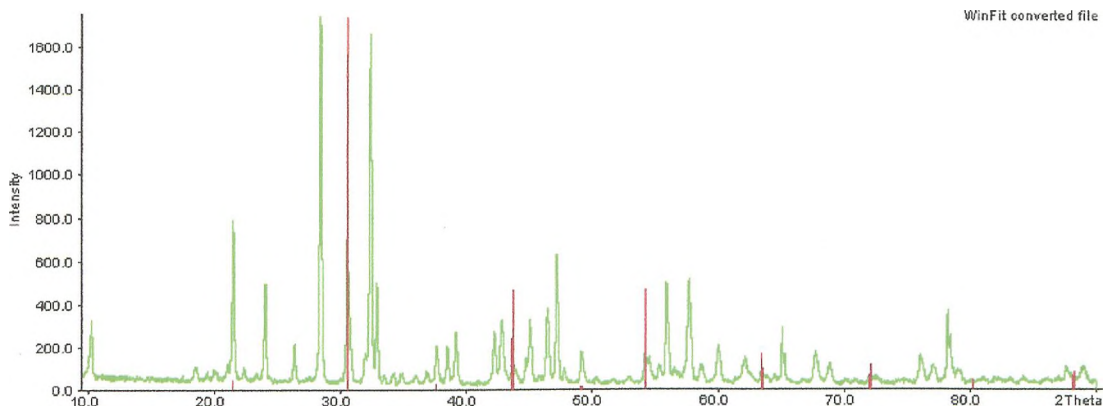


Figure 4.5.11: SrZrO₃ phase identified within the heat treated calcine at 1000°C

Waste Loaded Glasses

Waste loaded glasses were also analysed using XRD. The presence of the glassy melt however, made analysis more complex due to the amorphous hump present in the XRD data.

A series of samples were analysed after being air quenched at temperatures up to 1050°C. These glasses revealed the development of similar phases to those found in the calcine, although the possibility of detection of some phases was lowered due to a decreased concentration of elements within the overall melt and the presence of the amorphous material. For ease of comparison the separate traces have been compiled into one (**Figure 4.5.12**). Phases identified within the waste glass are not shown in **Figure 4.5.12** as they can be directly related to phases identified within the waste form.

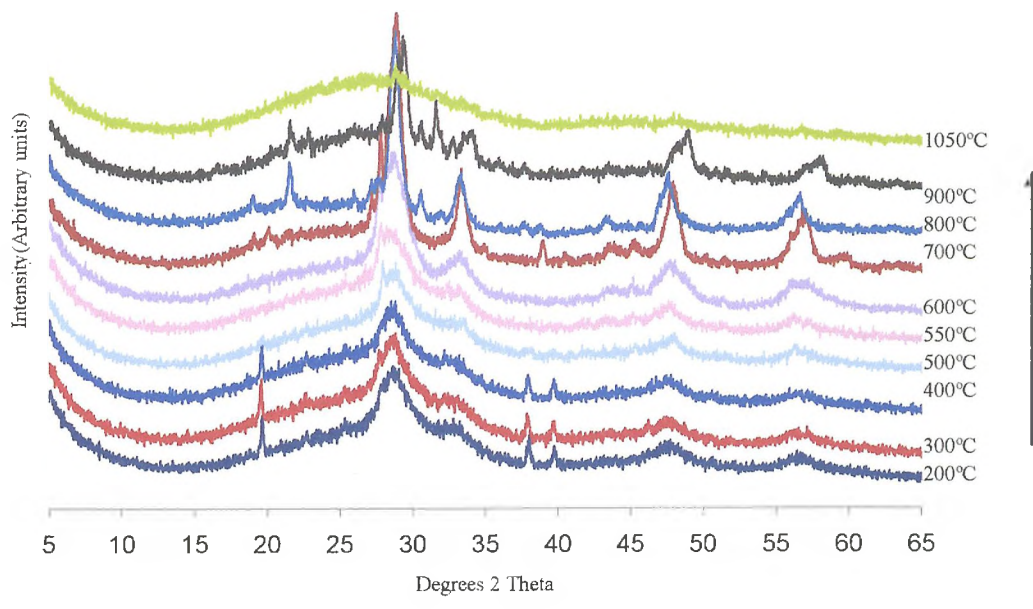


Figure 4.5.12: Heat treated 25wt% waste loaded glass phase evolution

Table 4.5.4: Phases identified in the waste loaded glasses

T/Phase	$\text{Nd}_{0.2}\text{Ce}_{0.8}\text{O}_{1.9}$	$\text{Sr}(\text{NO}_3)_2$	LiNO_3	CsLiMoO_4	BaFe_2O_4	SrZrO_3	MgO
200	✓	✓	✓	-	-	-	-
300	✓	✓	✓	-	-	-	-
400	✓	✓	✓	-	-	-	-
500	✓	✓	✓	-	-	-	-
550	✓	✓	-	-	-	✓	-
600	✓	✓	-	-	-	✓	-
700	✓	-	-	✓	✓	✓	✓
800	✓	-	-	✓	✓	✓	✓
900	✓	-	-	✓	✓	-	✓
1050	-	-	-	✓	-	-	-

✓ = High phase intensity ✓ = Phase depletion

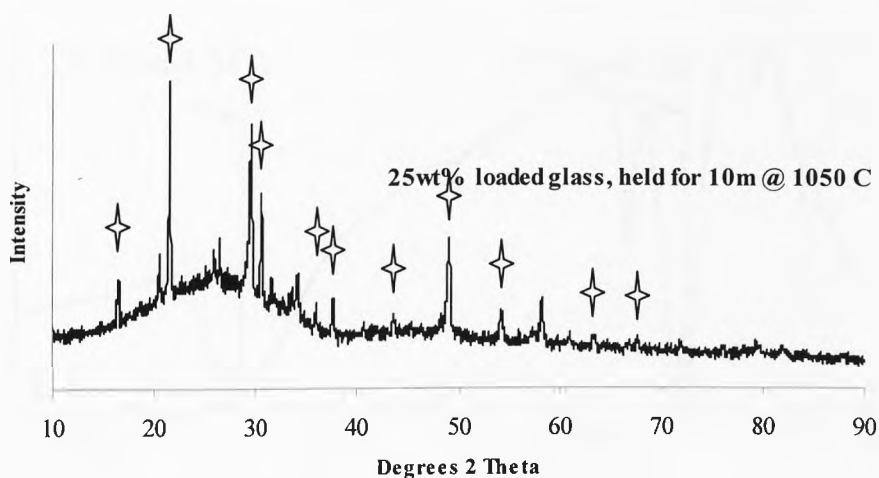


Figure 4.5.13: Surface analysis of 10M25  = CsLiMoO₄

Data for the analysis of the surface of 10M25 is seen in **Figure 4.5.13**. Similar analysis was undertaken on 5M25 and 15M25, producing almost identical results. CsLiMo₄ was the only identifiable phase on the XRD diffraction pattern, although there were some reflections at low angles which could not be matched with any patterns within the ICDD database, and so it was thought that another phase was present, but as yet unidentifiable.

4.6 Phase evolution using FTIR

Simulant Calcine

The infra-red spectrum of the as-received material has some interesting features and strong absorption bands. An example of spectra obtained for the as-received material is shown in **Figure 4.6.1**. Strong absorption bands at $\sim 3430\text{cm}^{-1}$ and 1387cm^{-1} can be seen. Several other absorption bands can be seen, although they are less dominant than those at $\sim 3430\text{cm}^{-1}$ and $\sim 1387\text{cm}^{-1}$. It is expected due to the flexible nature of the nitrate group bonds that there will be several peaks in different positions indicating the various stretches of the group.

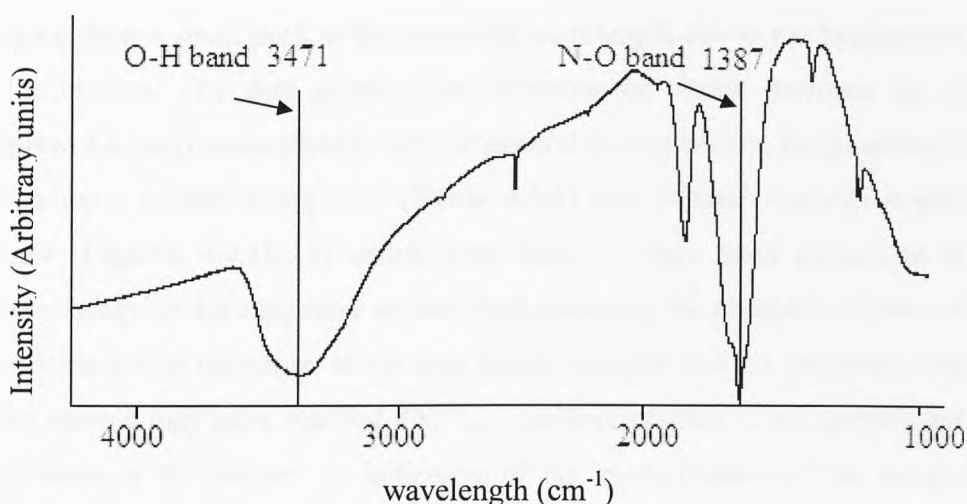


Figure 4.6.1: FTIR As-received calcine

Figure 4.6.2a-l illustrates the FTIR series spectra in full, including as-received samples ranging to samples heat treated to 1000°C.

The bands at 3430cm^{-1} and 1387cm^{-1} were attributed, respectively, to the O-H and N-O stretches of H_2O molecules and the NO_3^{2-} oxyanion, and confirmed a high water and nitrate content (Liu *et al*, 2005). FT-IR analysis of a sample heated to 140°C revealed a decrease in the intensity of the absorption band associated with O-H stretch of water at 3430cm^{-1} . A further reduction in the intensity of the O-H absorption band in the infra-red spectra of the samples which had been heated to 375°C was associated with the loss of chemically bound water (“water of hydration”) previously observed using thermal analysis. A decrease in the intensity of the absorption band associated with the N-O stretch of the NO_3^{2-} species occurred in the samples which had been heated from $400\text{-}700^\circ\text{C}$. In addition, this absorption band is resolved into two components as the temperature at which the calcine has been heat treated is increased; a broad band (at $1550\text{-}1250\text{cm}^{-1}$) and a sharp band at 1385cm^{-1} . The broad band is observed to decrease in intensity above 400°C , whereas the sharp band remains essentially unchanged. The band at 1045cm^{-1} is attributed to the symmetric stretch of the NO_3^- oxyanion, whilst the band present at 1370cm^{-1} is believed to be the asymmetric stretch and the band at 830cm^{-1} represents the symmetric bending of the NO_3^- anion (Liu *et al*, 2005).

The dehydration of the sample upon heating is apparent using FTIR, although all samples show a small peak at the attributed wavelength due to the hygroscopic nature of the calcine. The data shows some evidence of nitrate presence up to 800°C (**Figures 4.6.2a-j**), coincidental with the general decomposition temperatures obtained for common nitrate compounds (**Table 4.5.3**) and thermal analysis conducted on nitrates (**Figures 4.4.10-13**) which were likely to have been present in the HAL system. Irregularities may have arisen when assessing the complete nitrate content of the calcine due to the nature of the heat treated samples and the possibility that not all of the sample may have reached 800 °C. The development of an unattributed, broad band between 807-846cm⁻¹ is indicative of the crystallisation of the sample at this point and the formation of new phases from the decomposed nitrate phases.

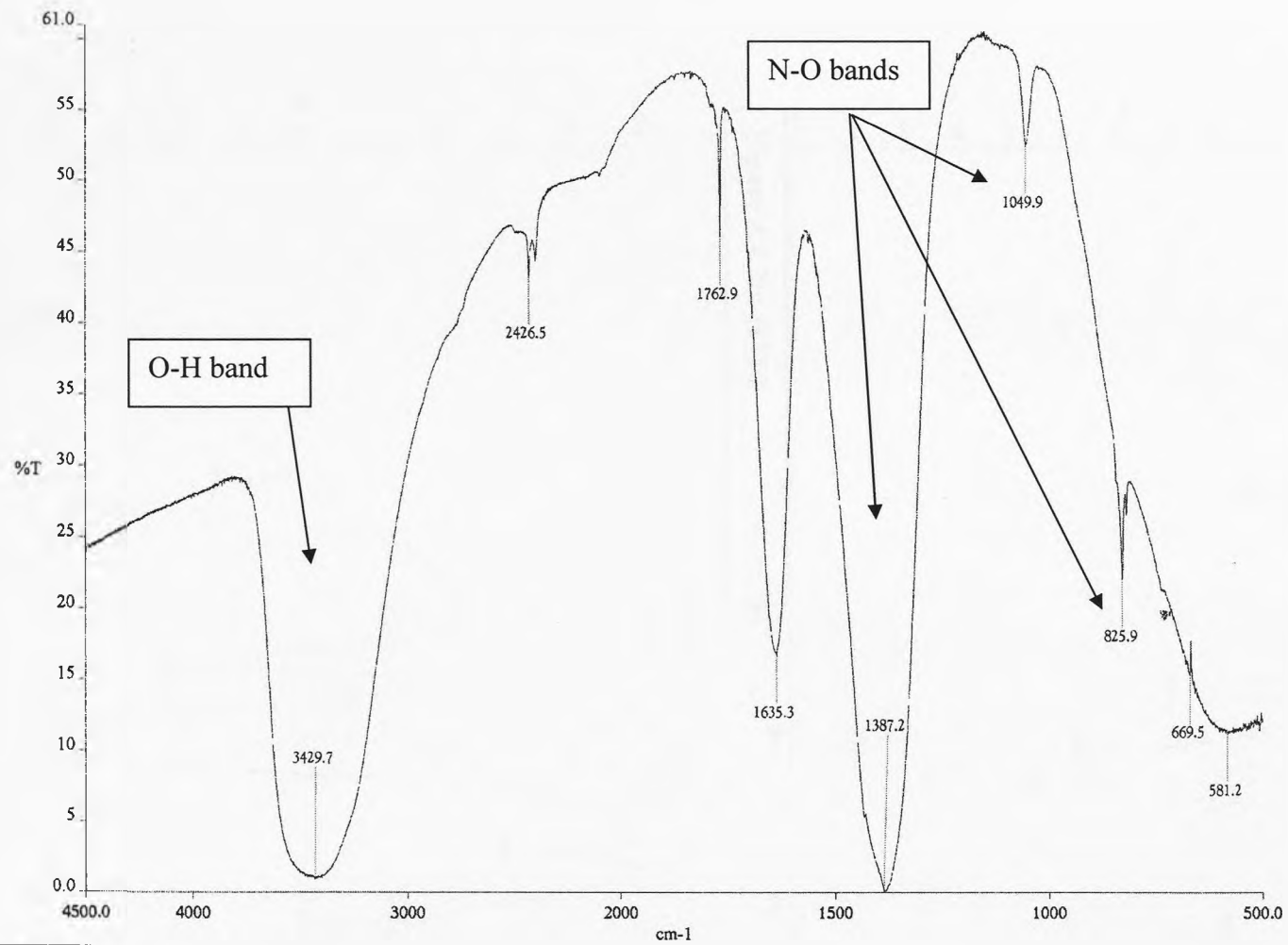


Figure 4.6.2a: As-received calcine

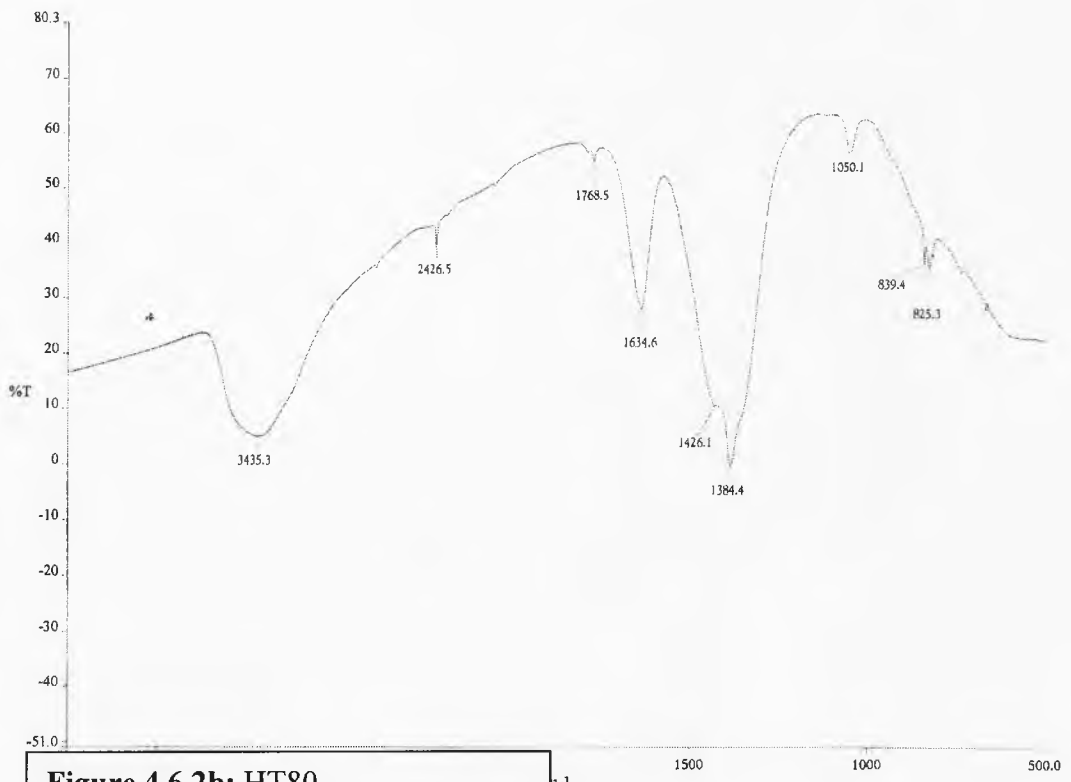


Figure 4.6.2b: HT80

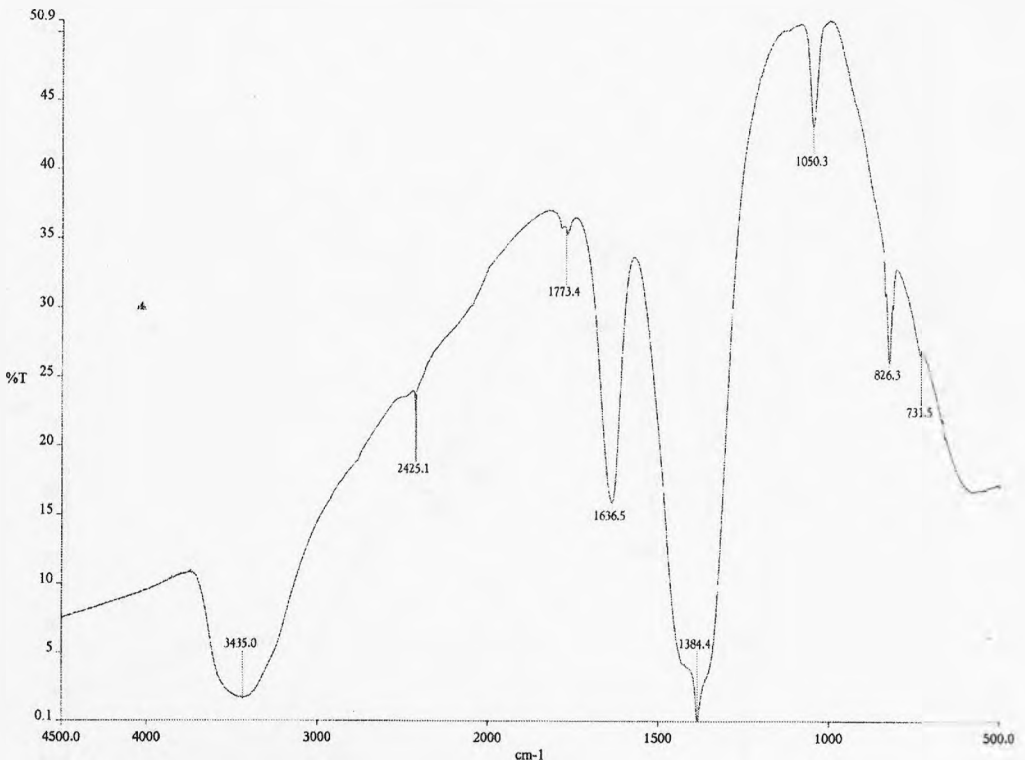


Figure 4.6.2c: HT150

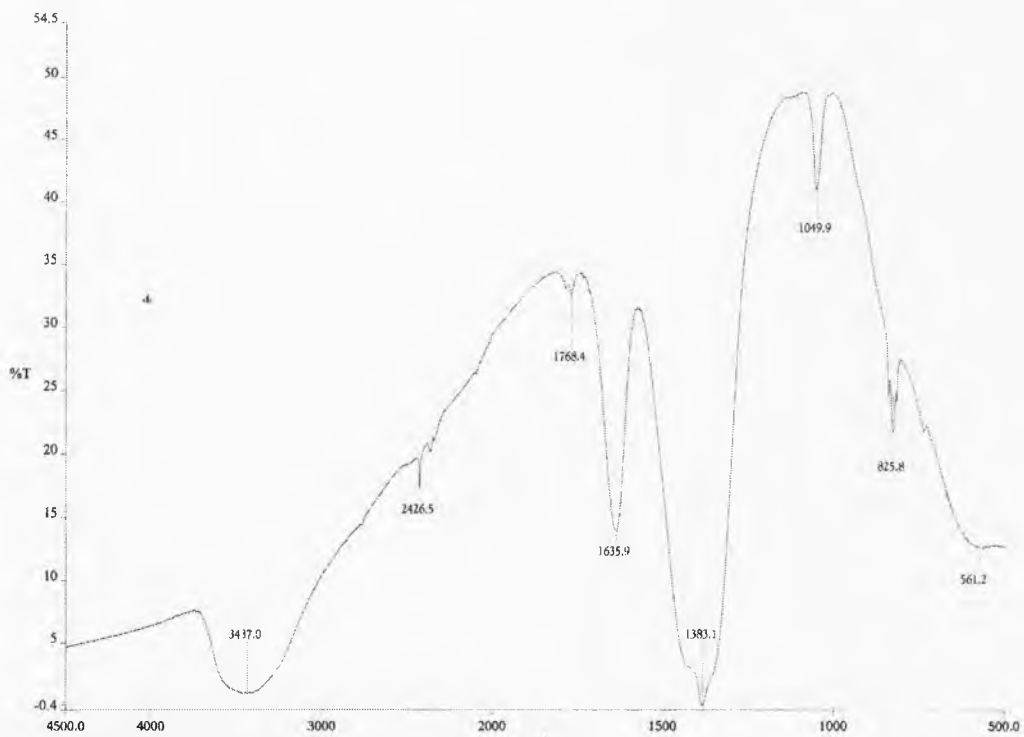


Figure 4.6.2d: HT200

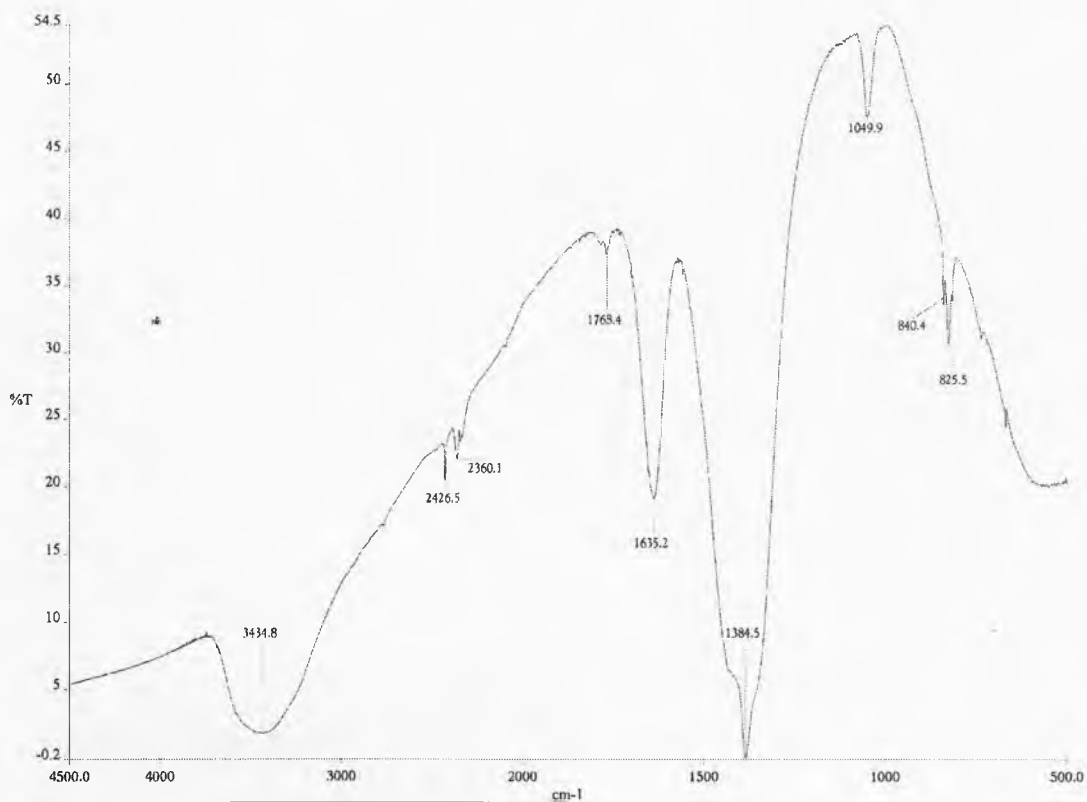


Figure 4.6.2e: HT250

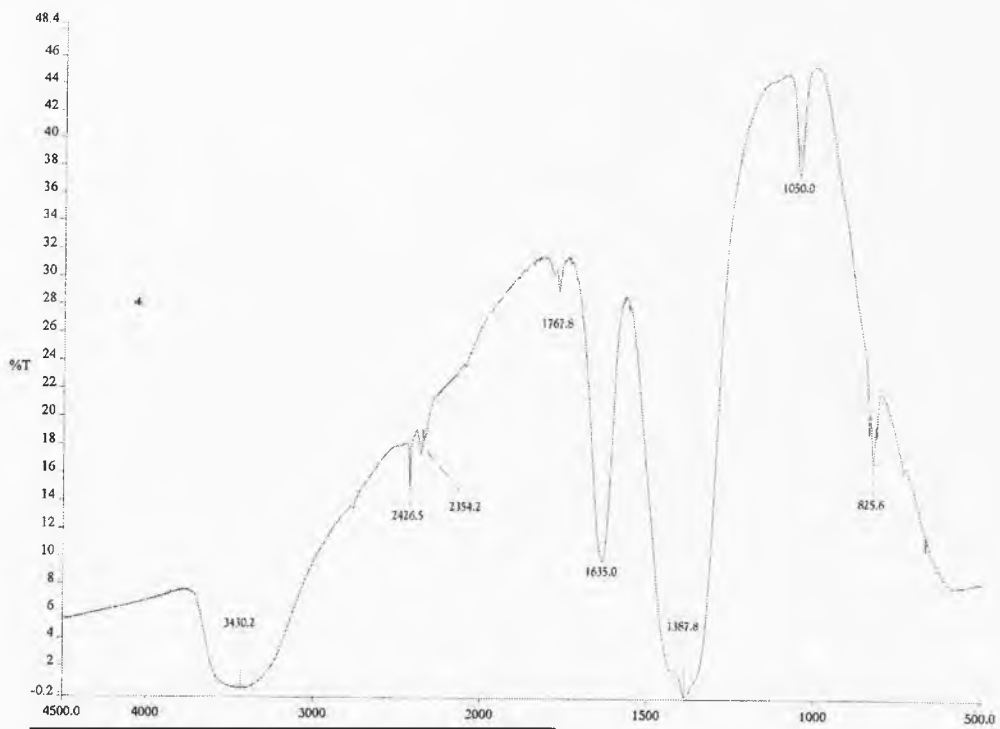


Figure 4.6.2f: HT300

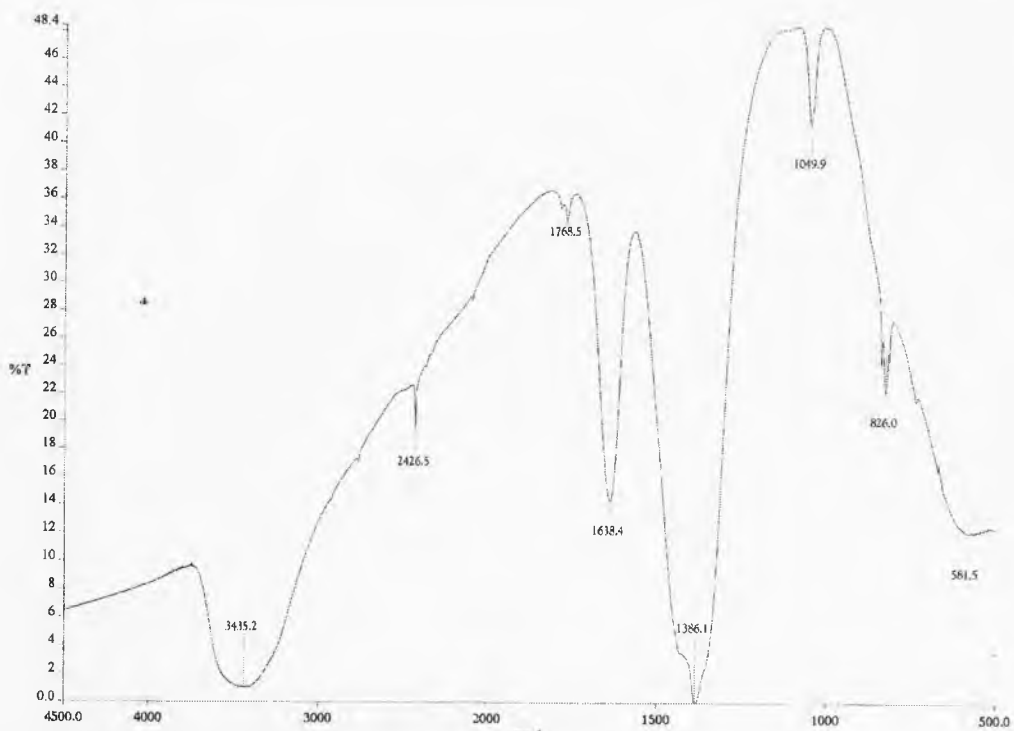


Figure 4.6.2g: HT400

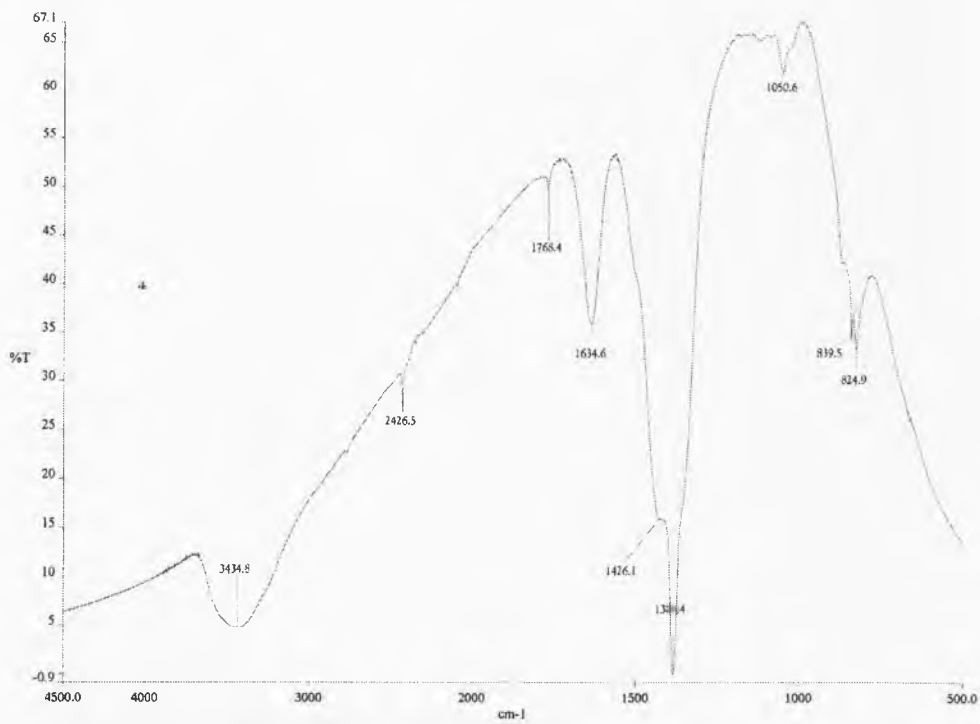


Figure 4.6.2h: HT500

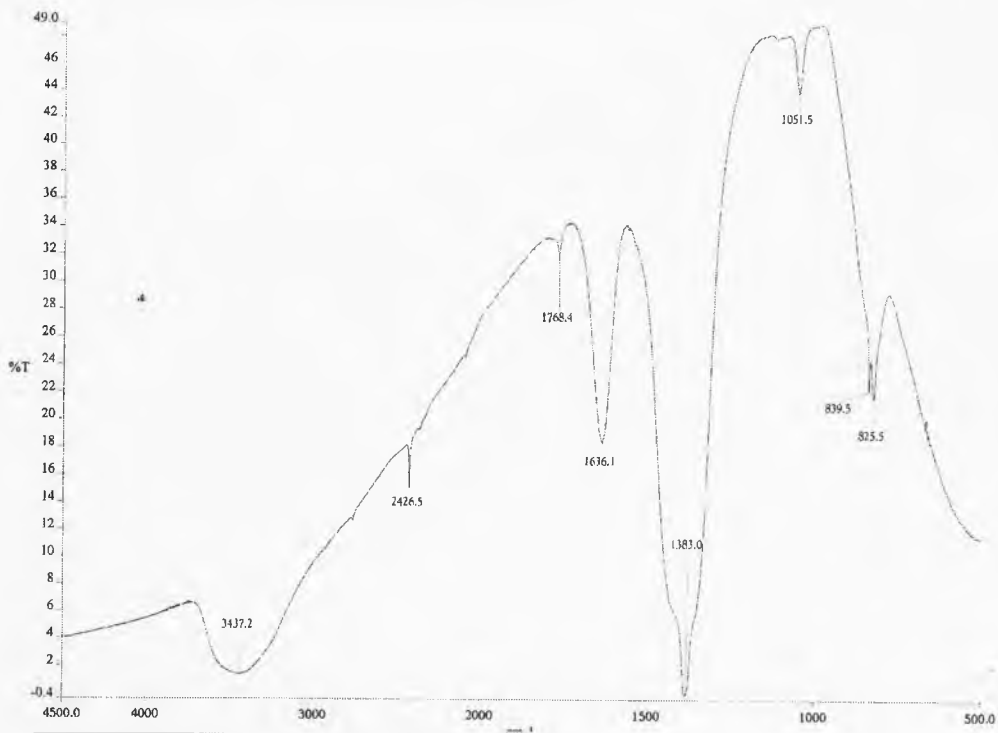


Figure 4.6.2i: HT600

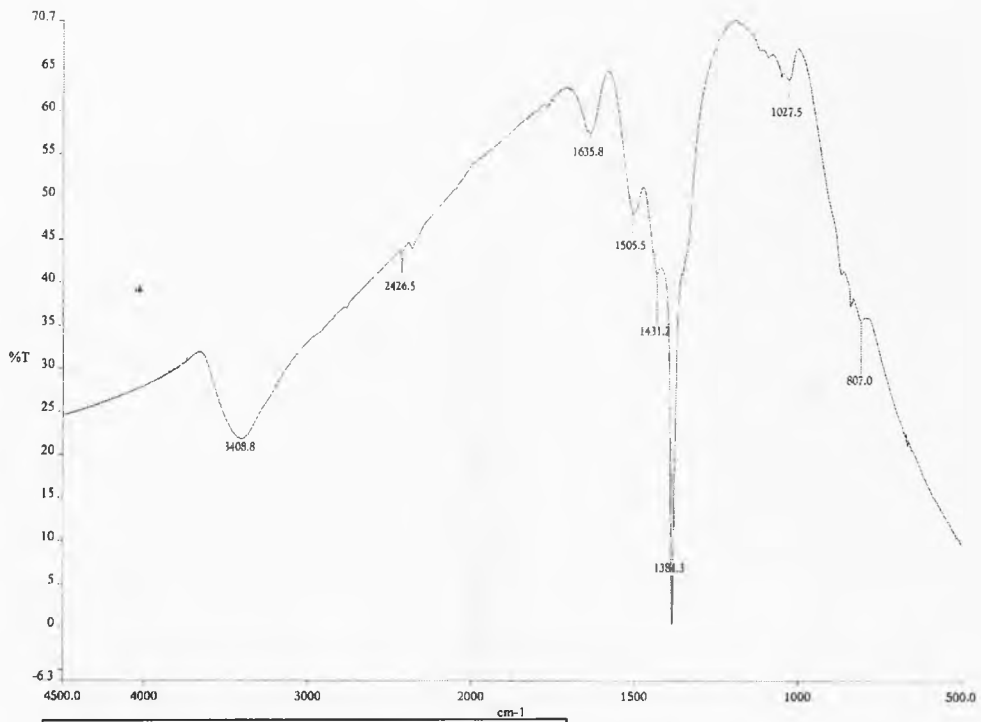


Figure 4.6.2j: HT700

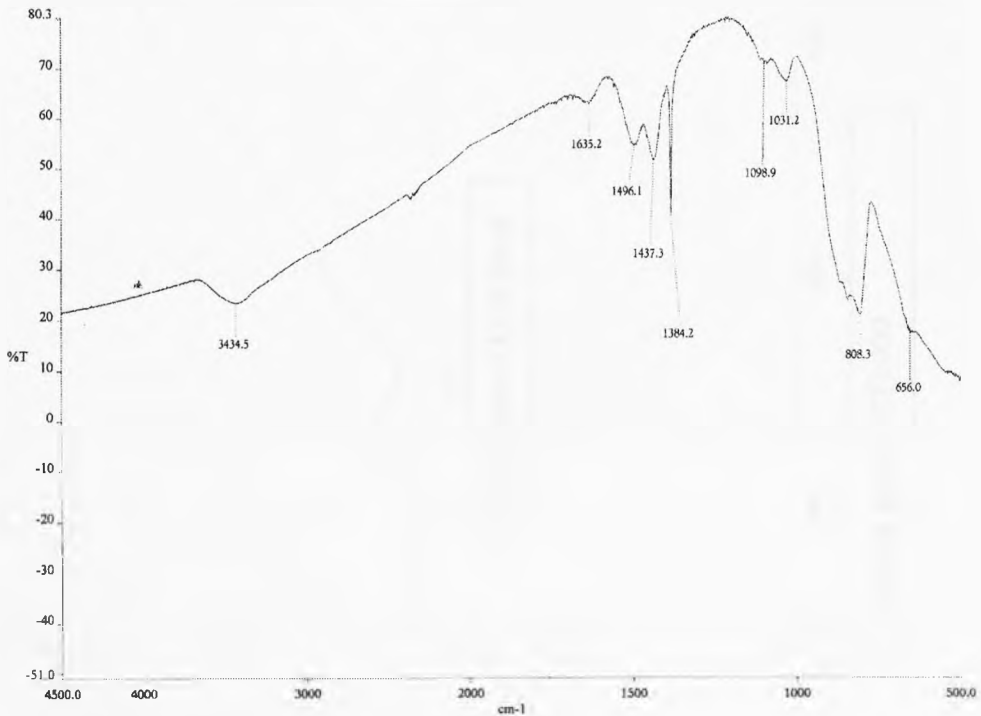


Figure 4.6.2k: HT800

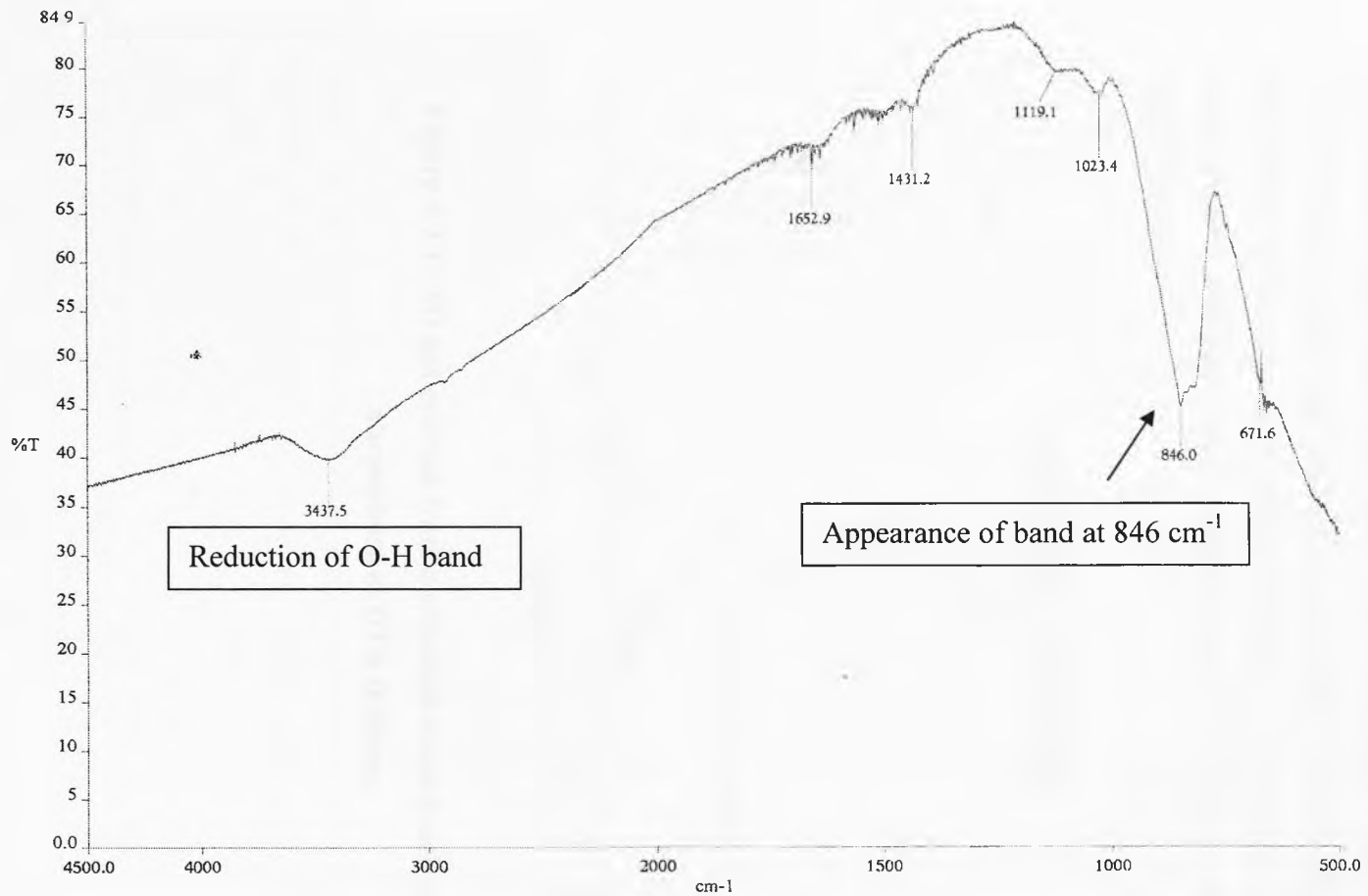


Figure 4.6.2l: HT1000

4.7 Gas Chromatography-Mass Spectroscopy

4.7.1 GC-MS with TA methods

Gas chromatography- mass spectrometry was undertaken on fully loaded waste glass samples simultaneously undergoing thermal analysis. The GC-MS revealed an offgas which consisted mainly of nitrate derived gases, and which corresponded to the temperatures at which the main weight losses took place as determined by TGA (Figure 4.7.1.).

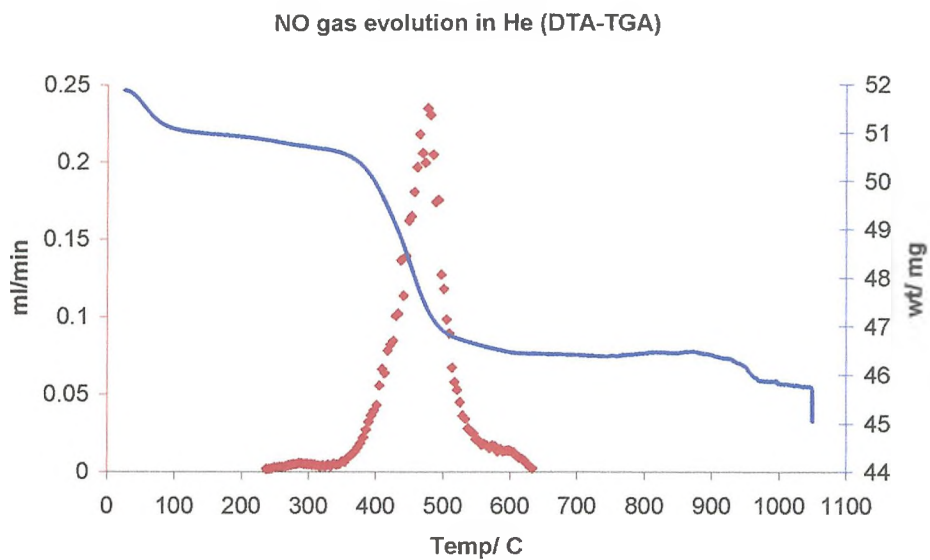


Figure 4.7.1: NO gas evolved from a simulant waste batch melted in an He atmosphere in DTA furnace.

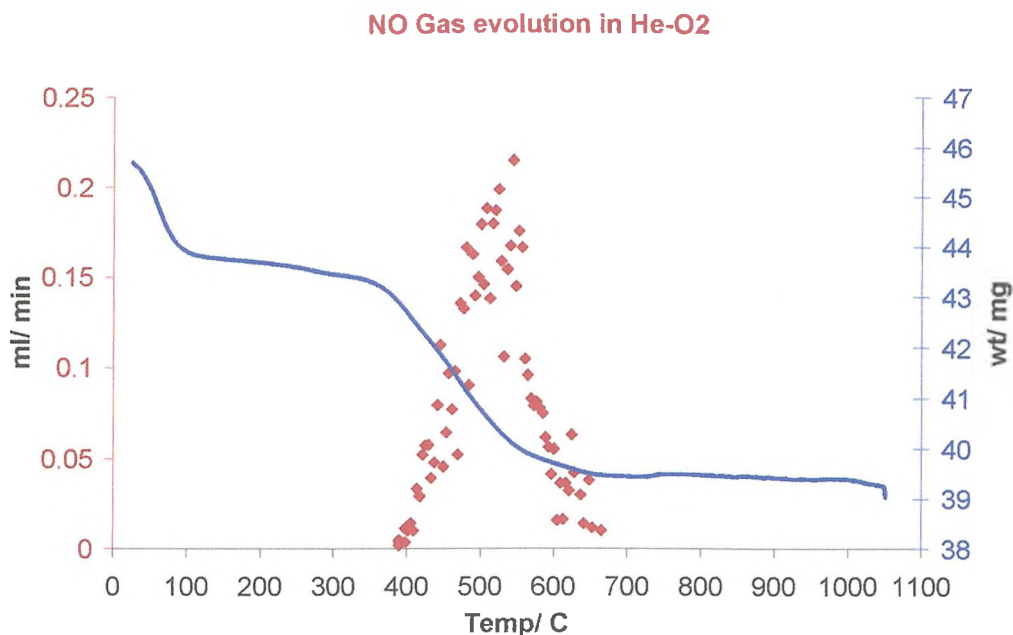


Figure 4.7.2: NO gas evolved from simulant waste batch melted in an He-O₂ atmosphere in DTA furnace.

Initial analysis of a waste sample using GC-MS in conjunction with DT-TGA showed that the evolved gas was almost completely NO under both inert and oxidising atmospheres (**Figure 4.7.1-2**), as would be expected because of the residual nitrates present in the calcine. The total amount of NO evolved whilst in He-O₂ atmosphere was 2.60×10^{-2} g (8.6×10^{-4} moles) from a 50mg batch, and in a pure He atmosphere the total NO evolution was 2.42×10^{-2} g (8.06×10^{-4} moles). These results were significantly within the operational error ($\pm 10\%$) of the GC-MS to indicate that in reality the amount of gas evolved was the same in each experiment. This gas evolution corresponded with the main weight loss peak of the TGA curve (**Figure 4.7.1-2**)

4.7.2 GC-MS on larger scale melting

During larger scale melting of a 10g batch in a dynamic He atmosphere, NO was again evolved, but N₂O and CO₂ were also detected. CO₂ is likely to be a product of corrosion of the stainless steel tube used as the crucible inlet, due to the fact that the calcine material used was produced from nitrates, not carbonates, and the visual appearance of the inlet tube blackened as the experiment continued. The evolution of

the two NO_x gases took place at different times during the melting process with most of the N_2O evolved in the early stages of the melt, from around 300°C to 380°C . The NO detected by the GC-MS began to evolve at 320°C , and finished around 700°C . In total, 0.687g of NO were evolved (0.0229 moles), 0.171g of O_2 (0.0053 moles), and 0.046g of N_2O (0.0010 moles) when the melt was conducted under inert[§] conditions (**Figure 4.7.3**). The gas evolution begins at around 300°C and continues until 700°C as the nitrates within the calcine decompose. This corresponds with the melting point of LiNO_3 being 253°C , and $\text{Sr}(\text{NO}_3)_2$ at 570°C when factoring in likelihood of time difference due to the batch reaching temperature at a later stage than the furnace.

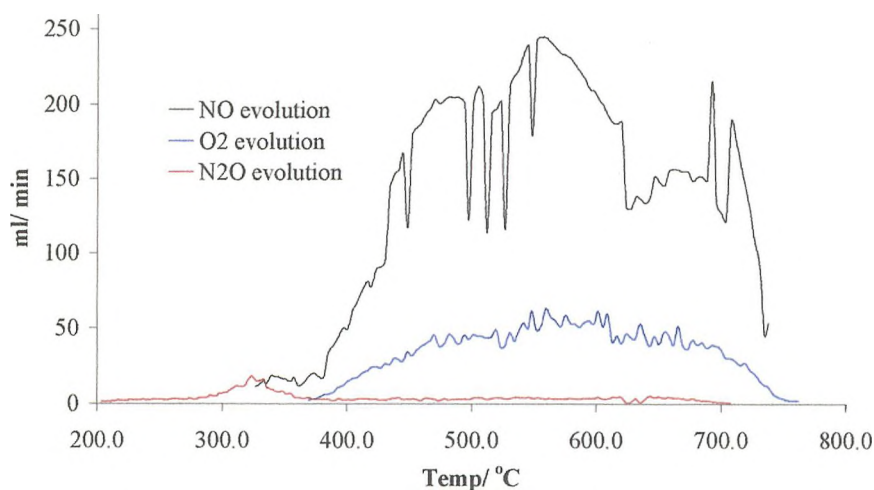


Figure 4.7.3: NO , N_2O and O_2 evolution from a fully loaded glass in He atmosphere.

The NO/O_2 ratio observed from experiment shows that there is 4 times as much O_2 as would be expected from the decomposition of the most common gas, NO . This ratio may be due to recombination of the O_2 within the glass melt to form oxides. During GC-MS analysis of a large scale batch, the melt was observed through a silica window inserted in the furnace. Still images are shown in **Figure 4.7.4**, and the compact disc provided with this work has digitised film clips of the glass melt. What is possible to note from the images is the gradual sagging of the batch and the fusion

[§] N.B: Other experiments were conducted under reducing and oxidising conditions also, but the data was unusable due to the nature of the detector in the MS. Larger ions “flooded” the detector plate and made subsequent analysis impossible.

of the glass beginning around 800°C. Movement of both gas bubbles and particles within the melt can be observed.

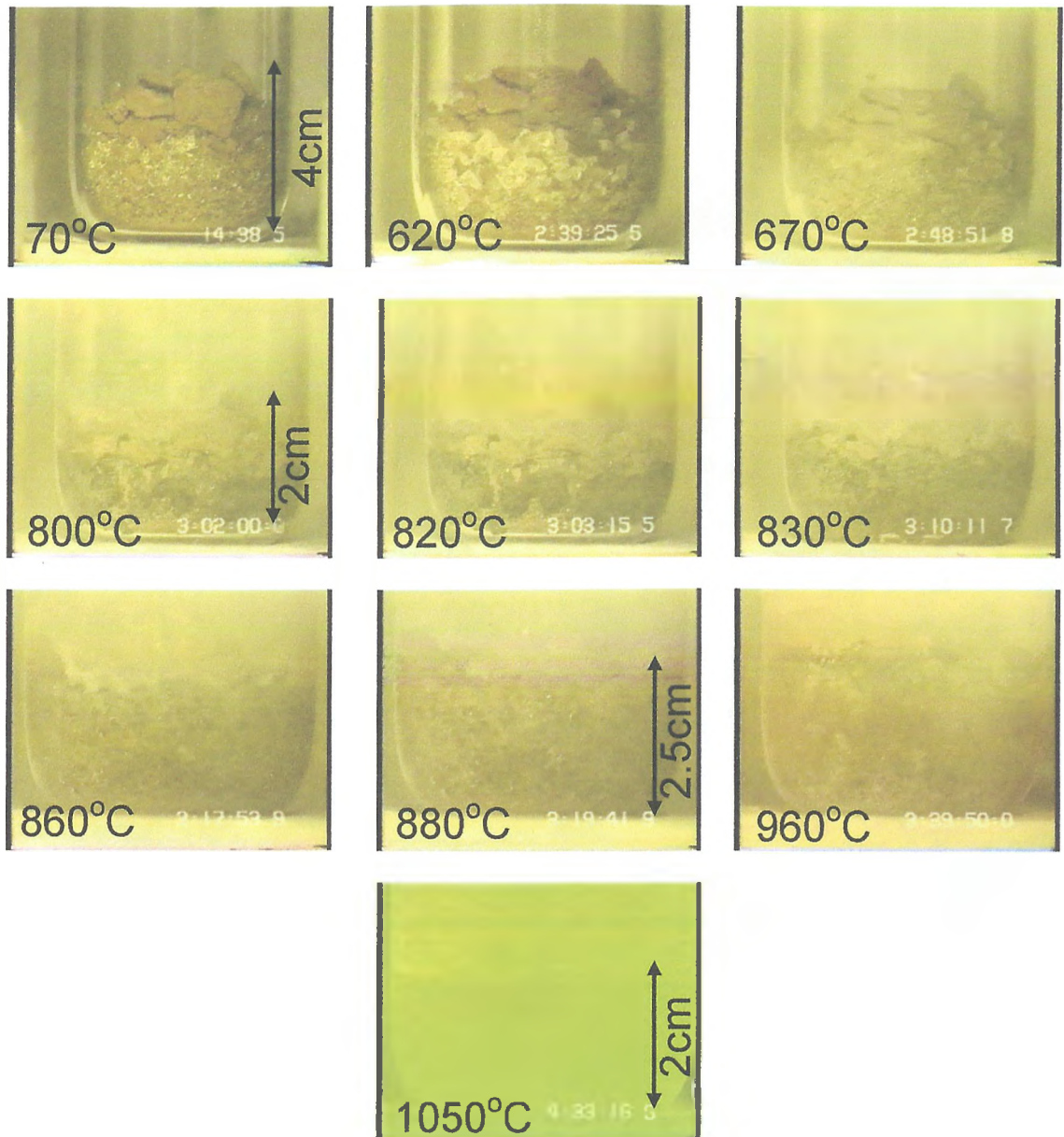


Figure 4.7.4: Melt progression of a 25wt% waste loaded batch under He atmosphere, illustrating batch sagging and glass fusion at around 800°C. (Note increase in batch size, due to gas evolution). Images taken during continuous melting process.

4.8 Scanning Electron Microscopy

4.8.1 Simulant Waste

Figure 4.8.1 shows a BEI image of simulant, as-received waste. More detailed elemental mapping of this sample was also undertaken.

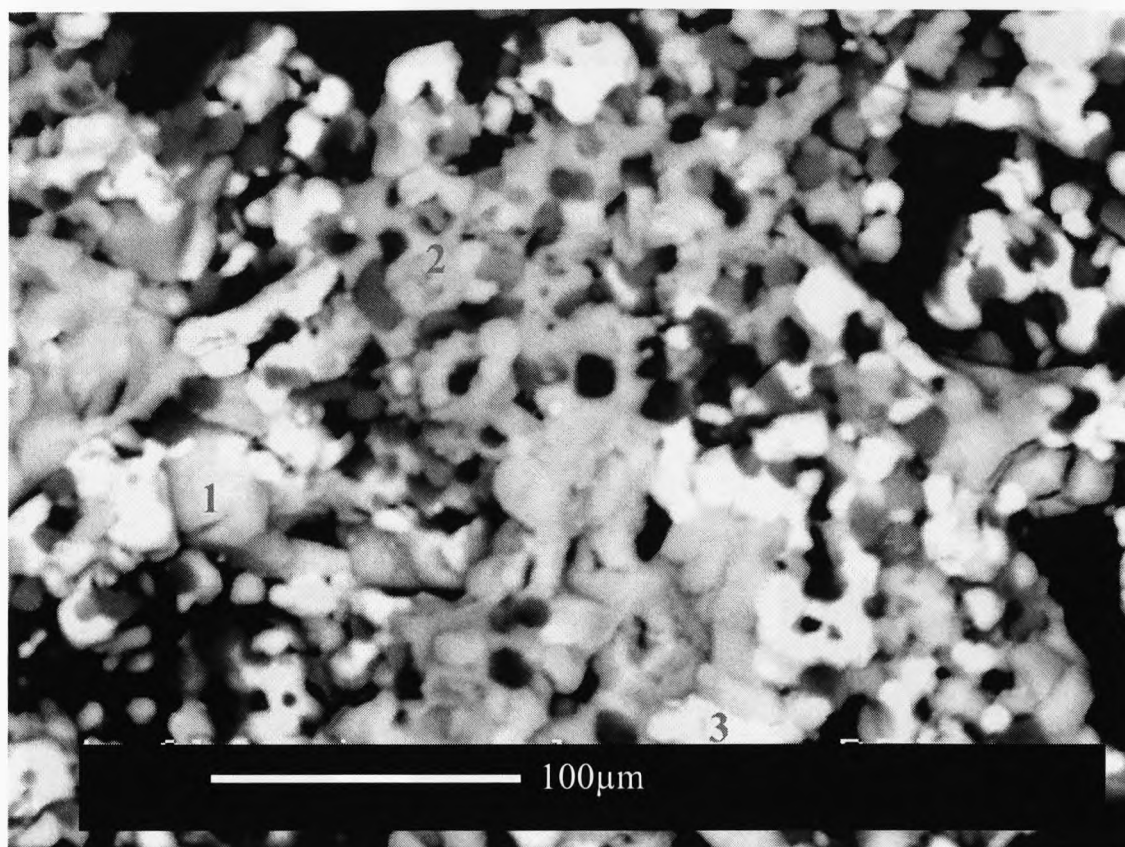


Figure 4.8.1: BEI of resin mounted, as-received calcine

The backscattered image shows light (1) and dark (2) grey phases. A bright white phase (3) consisting of the heavier elements and a very dark grey phase (4) are also seen. An EDX of an area containing all phases revealed the presence of many of the major elements of the waste stream, including Mo, Cs, rare earths, Al, Sr, Fe and Zr. EDX maps of a chosen area are shown in **Figure 4.8.2**, using the spectrum previously collected from the area scan. The segregation of elements in the waste indicated a multiphase system. EDX revealed the white phase (as viewed by BEI) contained the rare-earth elements, Nd and Gd, the black phase was rich in Fe and Al, the dark grey phase contained some of the Sr, Te and Zr and the lighter grey phase contained the rest of

the Sr and Ba, Mo and Cs. On average, within the as-received sample, the phase grains were ~ 10-20 μ m in size, whilst the granules of calcine ranged from 50 μ m to <1cm.

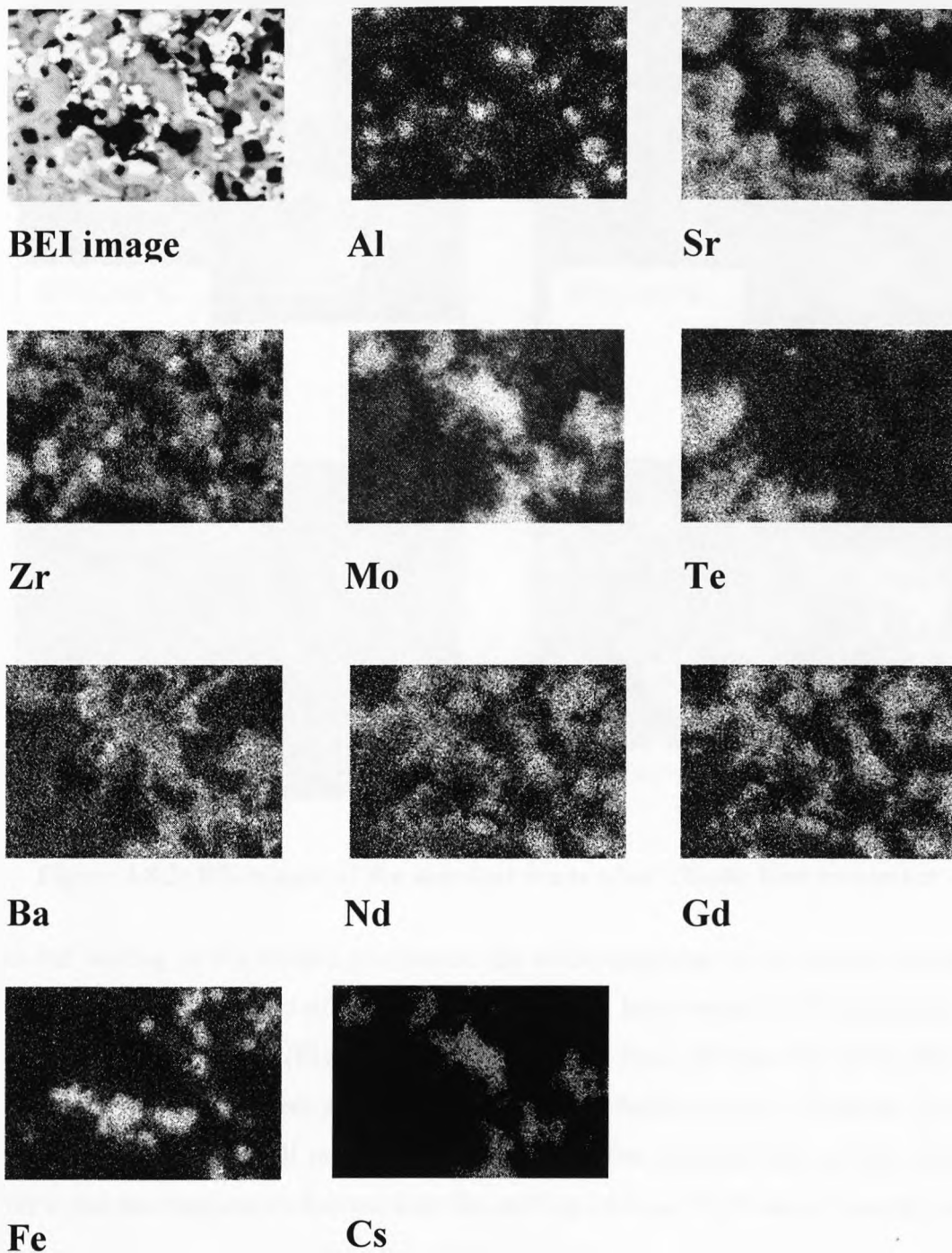


Figure 4.8.2: EDX element maps of as-received calcine.

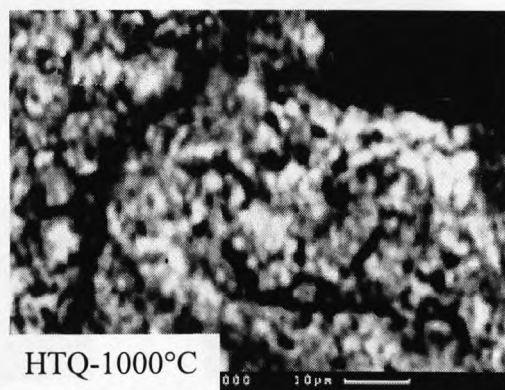
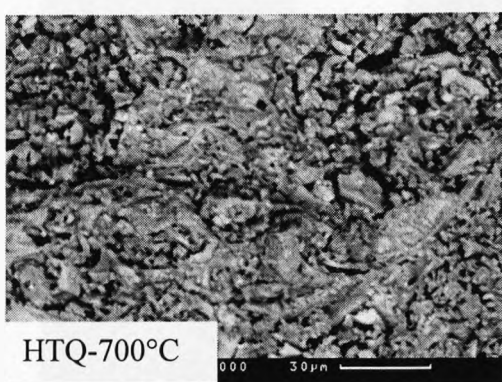
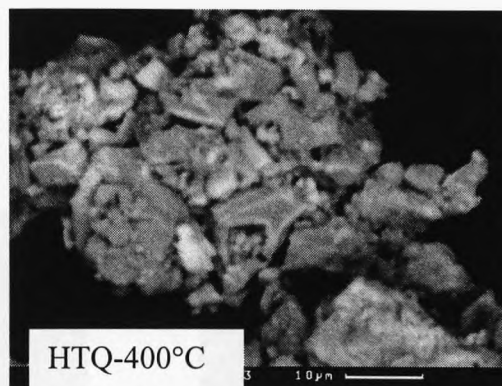
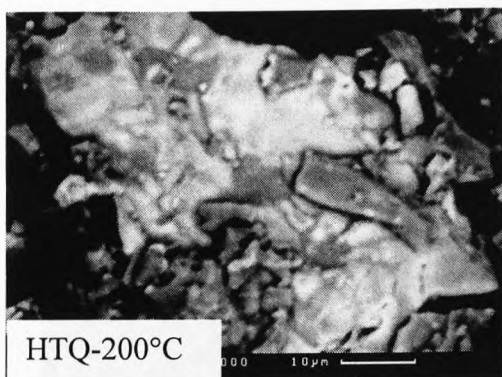


Figure 4.8.3: BE images of the simulant waste after 22hour heat treatment

As the heating of the calcine progresses, the microstructures of the phases become finer, indicating that more of the material is likely to have melted or decomposed as temperature is increased (**Figure 4.8.3**). The particle sizes decrease by ~20% due to shrinkage and densification, and the phase grain sizes decrease from ~10 μm to $\leq 3\mu\text{m}$. LiNO_3 and $\text{Sr}(\text{NO}_3)_2$ will no longer be present in the material heat treated above 700°C and the compounds formed from the melting of these waste stream constituents have reacted to form this finer, polycrystalline structure.

X-ray maps for elements identified using the EDX technique are shown in **Figure 4.8.4**. Samples heat treated to an intermediate temperature of 200°C were difficult to

map due to the heating effects of the beam and the unreacted nature of some of the material contained within the calcine, and therefore no analysis data is given.

HTQ400

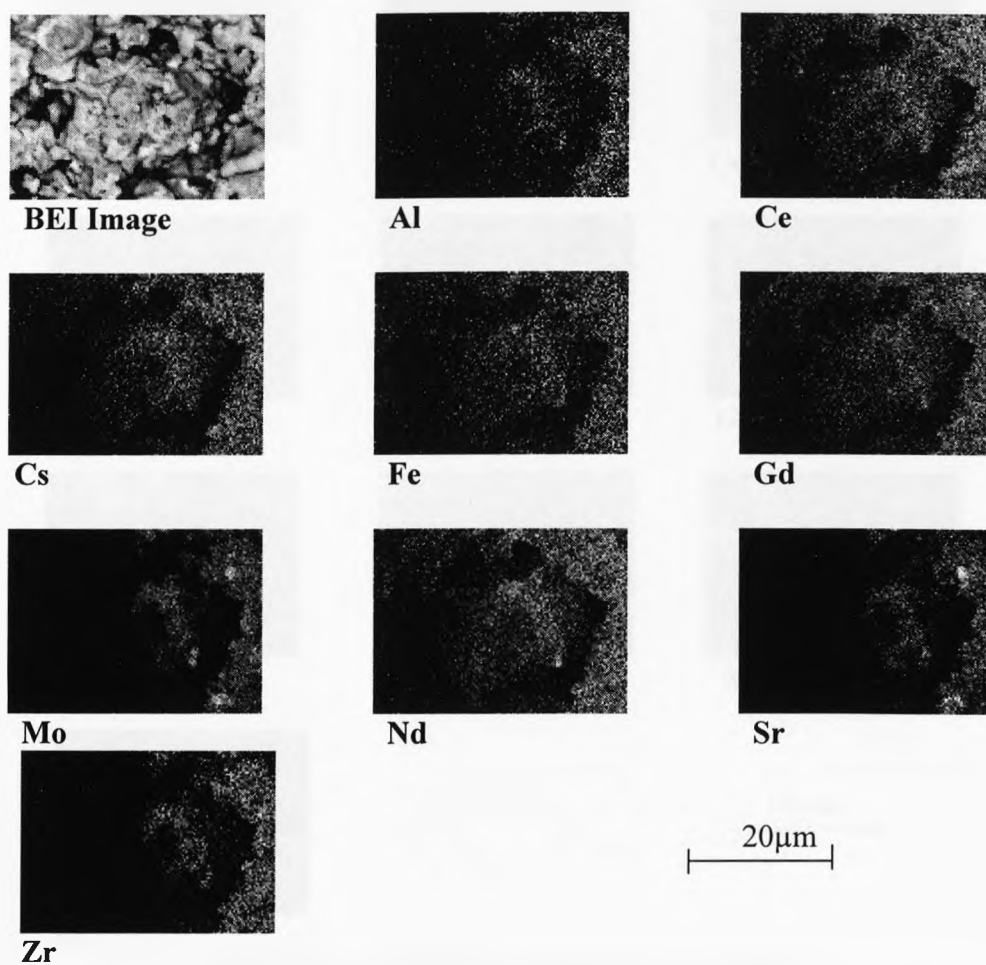


Figure 4.8.4: Element mapping for HTQ400

HTQ400 exhibited phase segregation (as viewed in BEI) and a light grey phase containing Cs, Mo, Nd and Zr, a bright white phase containing Cs, Mo and Sr and a darker grey phase containing Ce and Gd, and traces of Al and Fe.

HTQ700

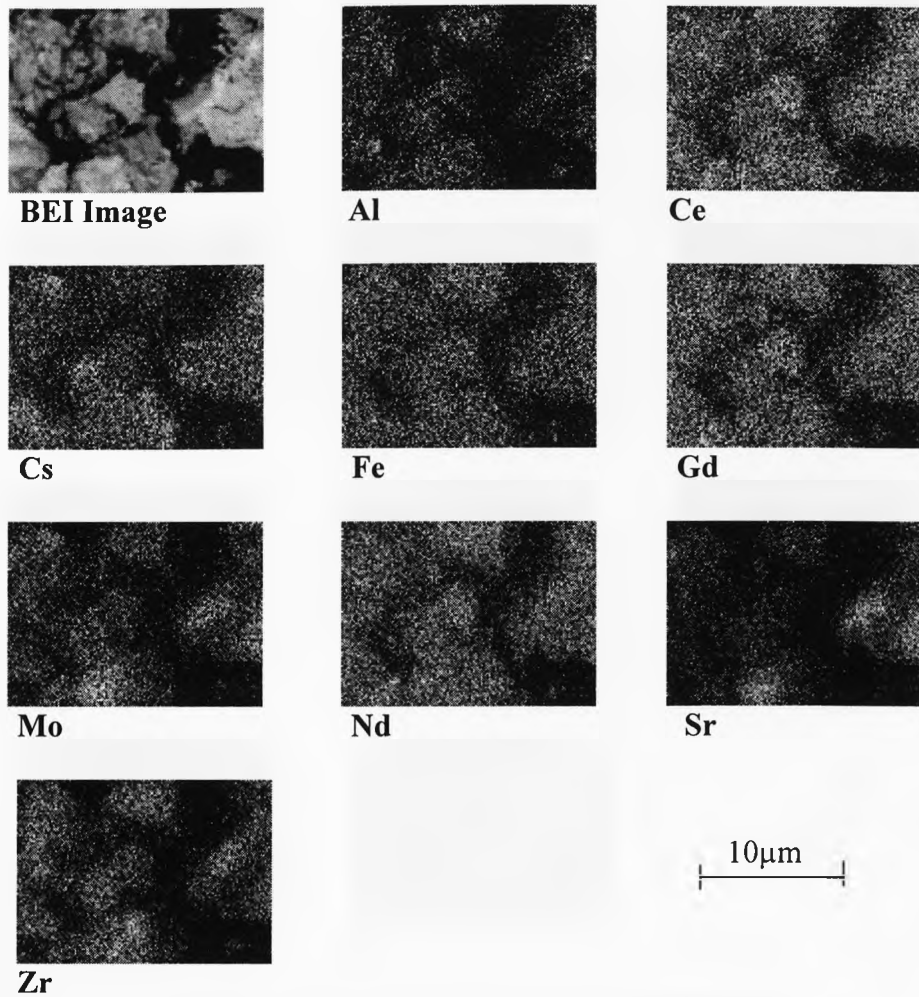


Figure 4.8.5: Element mapping for HTQ700

HTQ700 exhibited phase segregation and a light grey phase containing Cs, Sr, Mo and Zr. A bright white phase containing Cs, Mo and Nd was also observed alongside a darker grey phase containing Ce, Gd, Nd, Fe and traces of Al.

HTQ1000

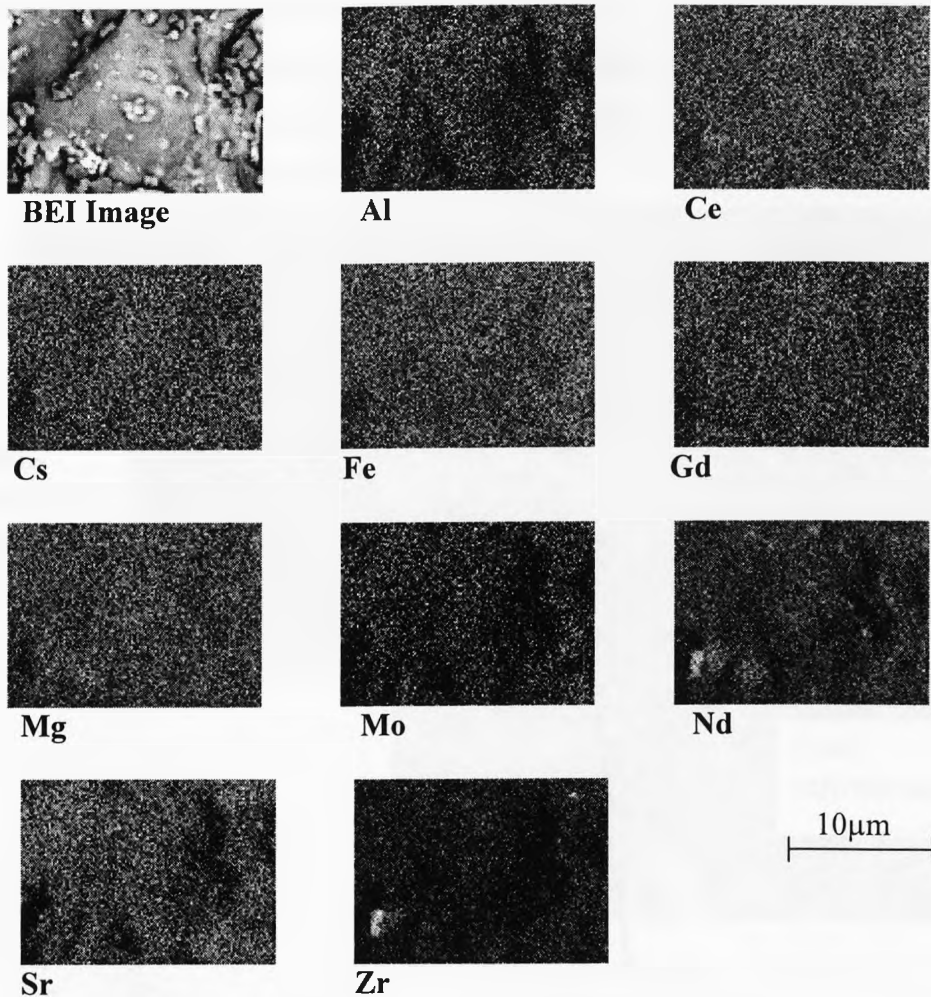


Figure 4.8.6: Element mapping for HTQ1000

HTQ1000 also exhibited phase segregation (**Figure 4.8.6**). A light grey phase containing Sr, Mo, Cs was seen, and a bright white phase containing Zr, Nd and traces of Ce alongside a darker grey phase containing Al, Ce, Fe and Mg.

HTQ1000 was much more uniform compared to the other heat treated samples. Some segregation was detected with the formation of a Zr and Nd containing phase, but elements were much more homogeneously spread throughout the bulk of the material.

Figure 4.8.7 shows a BEI of the “yellow phase” on the surface of sintered and quenched calcine. EDX of this, and other sections of the yellow, low melting point layer forming on the calcine/glass surface above 1000°C indicated the presence of Cs and Mo in the majority of samples, and Sr, Te and Cr (Figure 4.8.7 inset) in others. The EDX analysis highlights the presence of Mo and Cs in the same phase, and also the presence of minor elements such as Sr, Te and Cr. When examined at higher magnification (Figure 4.8.8), the yellow phase is seen to consist of two different microstructures, one of a much finer nature and a more porous matrix surrounding grains ranging from ~4-10µm in size.

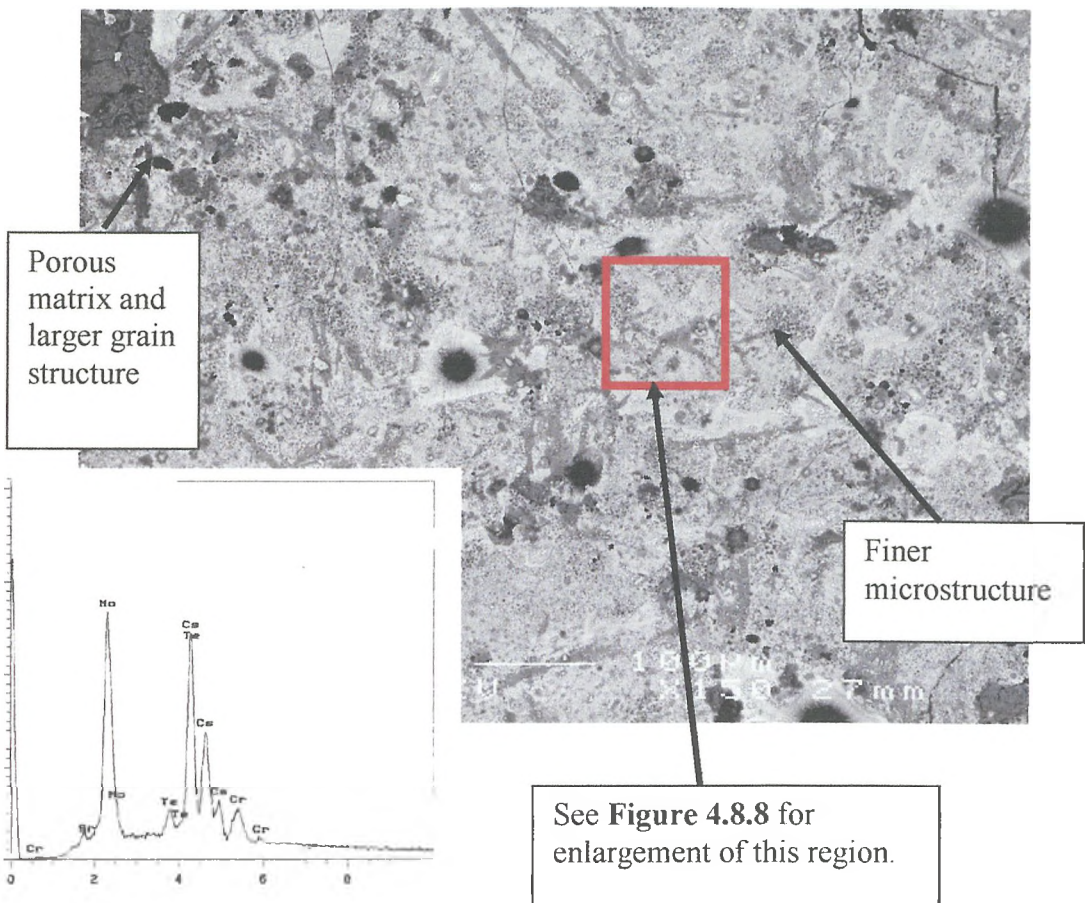


Figure 4.8.7: BEI of microstructure of low melting yellow phase from calcine surface (inset: EDX of the entire area shown in BEI).

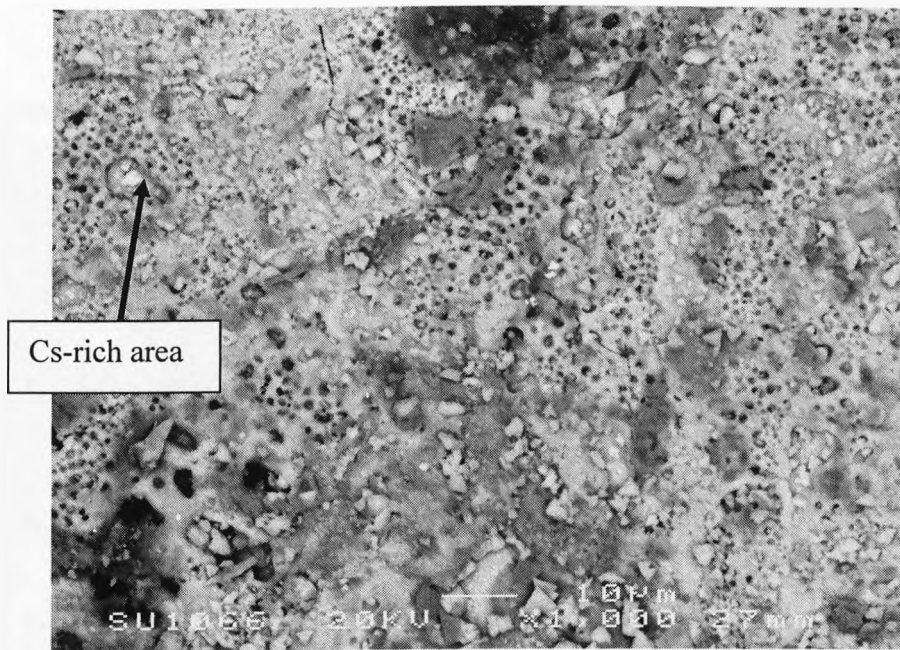


Figure 4.8.8: Backscattered electron image of yellow phase fine structure (enlargement of area marked on Figure 4.8.1.7)

Figure 4.8.8 is an enlarged view of the porous microstructure. The small areas of seemingly brighter particulates are rich in Cs whilst the overall matrix is Mo and Sr rich.

4.8.2 Waste Loaded Glasses

Sample 5M25 analysis

As discussed previously sample 5M25 was quenched after 5 minutes of melting in a 75ml capacity Inconel 601 crucible. Cross sectioning and subsequent analysis under the SEM revealed the effect that the convection currents within the glassy melt had started to have on the composition of the glass matrix. **Figure 4.8.9** shows a cross section through the melt and EDX element maps of the same area, with the dark area at the top being the resin used to mount the sample.

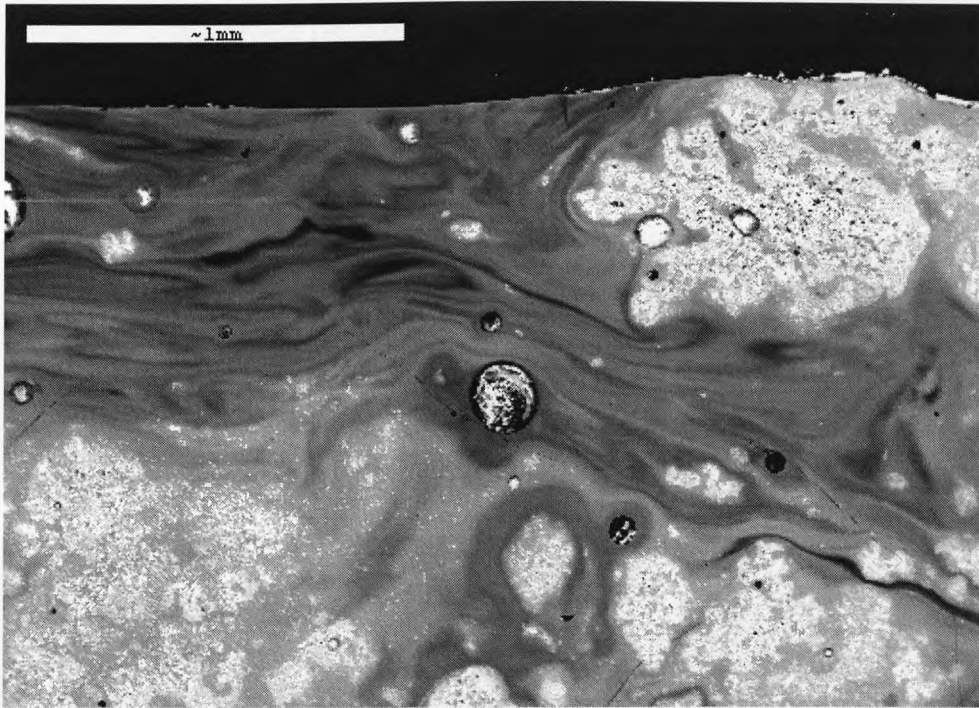


Figure 4.8.9: BEI of 5M25 in cross-section (top of melt aligned with top of image)

Elemental x-ray maps of the area show the segregation of Cs, Mo and La to the same phase, whilst Zr, Al, Fe, Mg, Ce, Gd and Nd did not appear to dissolve into the surrounding matrix, although Mg appears to be distributed more widely than other elements of the waste stream. The presence of Cs and Mo is not observed anywhere in the melt or calcine particle, with the exception of the surface layer (**Figure 4.8.10**).

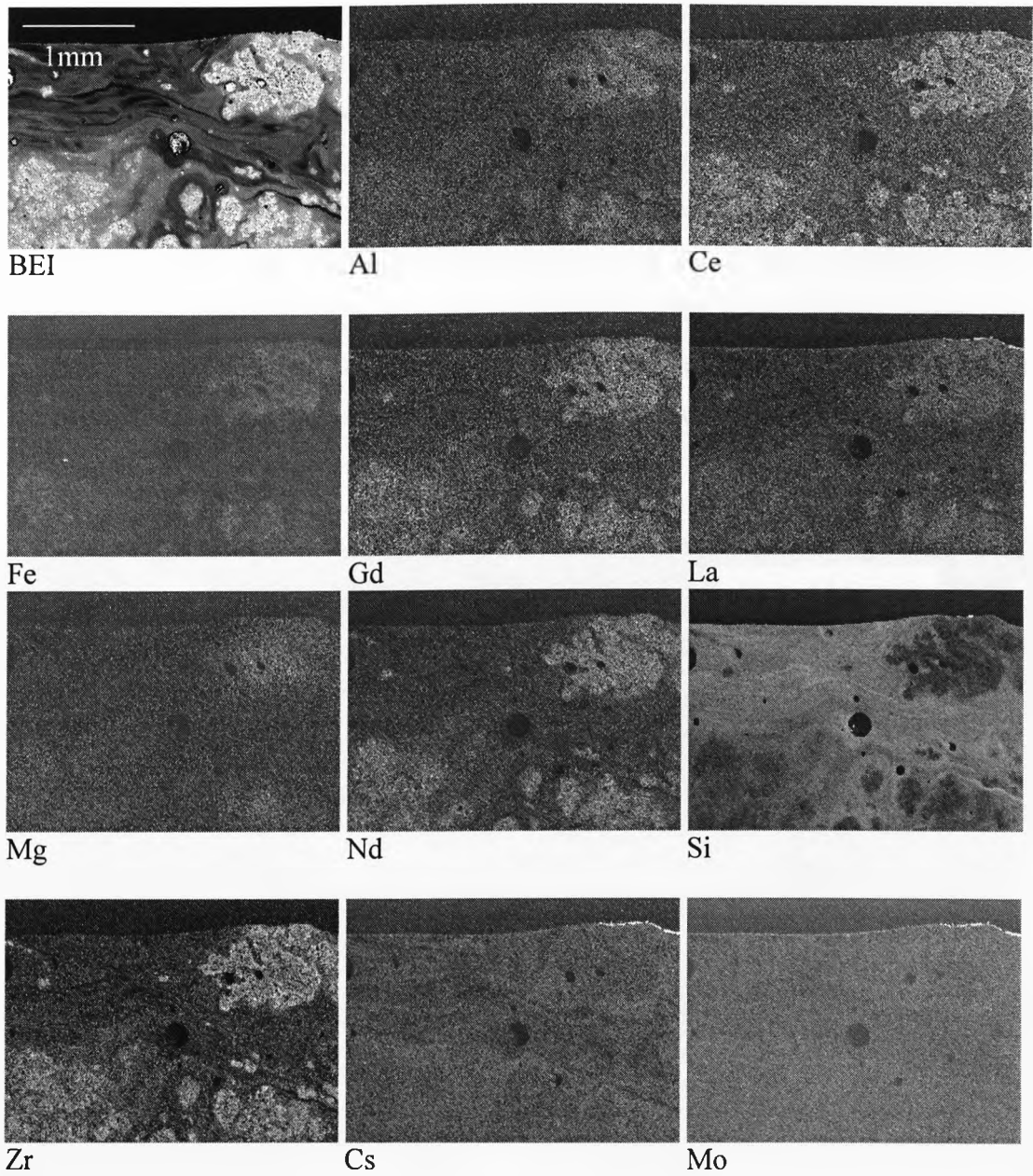


Figure 4.8.10: Backscattered image of sample 5M25 in cross section, and electron maps of the area (top of image denotes top of melt).

Sample 10M25 analysis

Sample 10M25 was sectioned after 10 minutes of melting in an Inconel 601 crucible. **Figure 4.8.11** shows the further dissolution of the calcine particles within the glassy melt and the presence of a non-continuous surface layer, determined by EDX to be rich in Cs and Mo. The presence of a Cs and Mo rich particulate (see **Figure 4.8.12** element maps) can also be seen ~ 1.3mm from the surface of the melt, along with some of the phase collecting in and close to bubbles in the process of rising to the surface of the melt. Also visible is a crack which has occurred due to the rapid cooling of the sample.

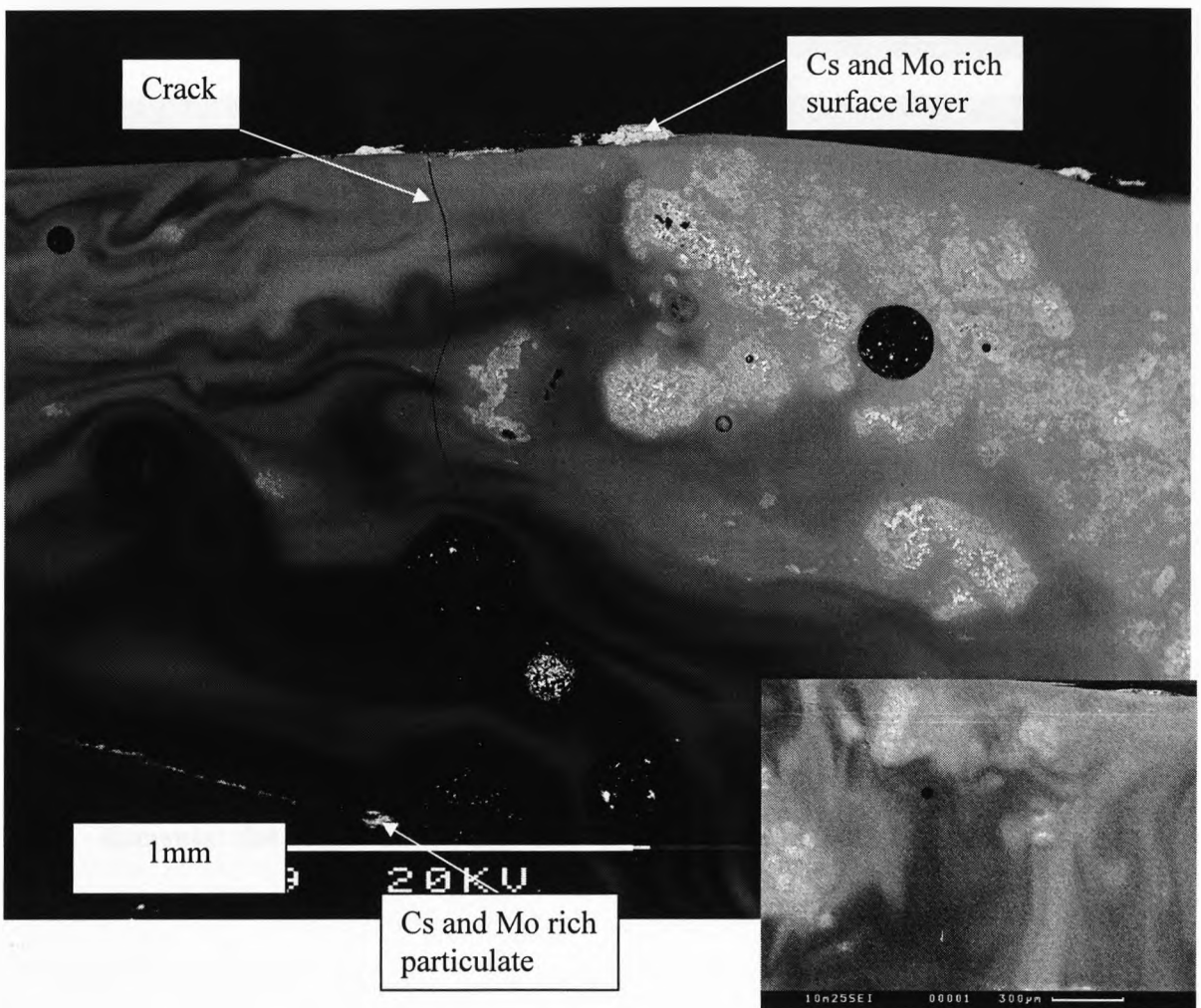


Figure 4.8.11: Backscattered electron image of 10M25 in cross section, where top of image denotes top surface of sample (inset: evidence of convection currents within the glassy melt).

Elemental dot maps of the area (**Figure 4.8.12**) show the segregation of Cs and Mo to the same phase, whilst Zr, Fe, Mg, Ce, and Nd appeared less soluble in the surrounding matrix, although they are more widely distributed than in sample 10M25. Cs and Mo are observed elsewhere in the melt in the form of the surface layer and also the “nugget” of this phase (indicated by “N” in **Figure 4.8.12**) within the body of the melt, close to a bubble.

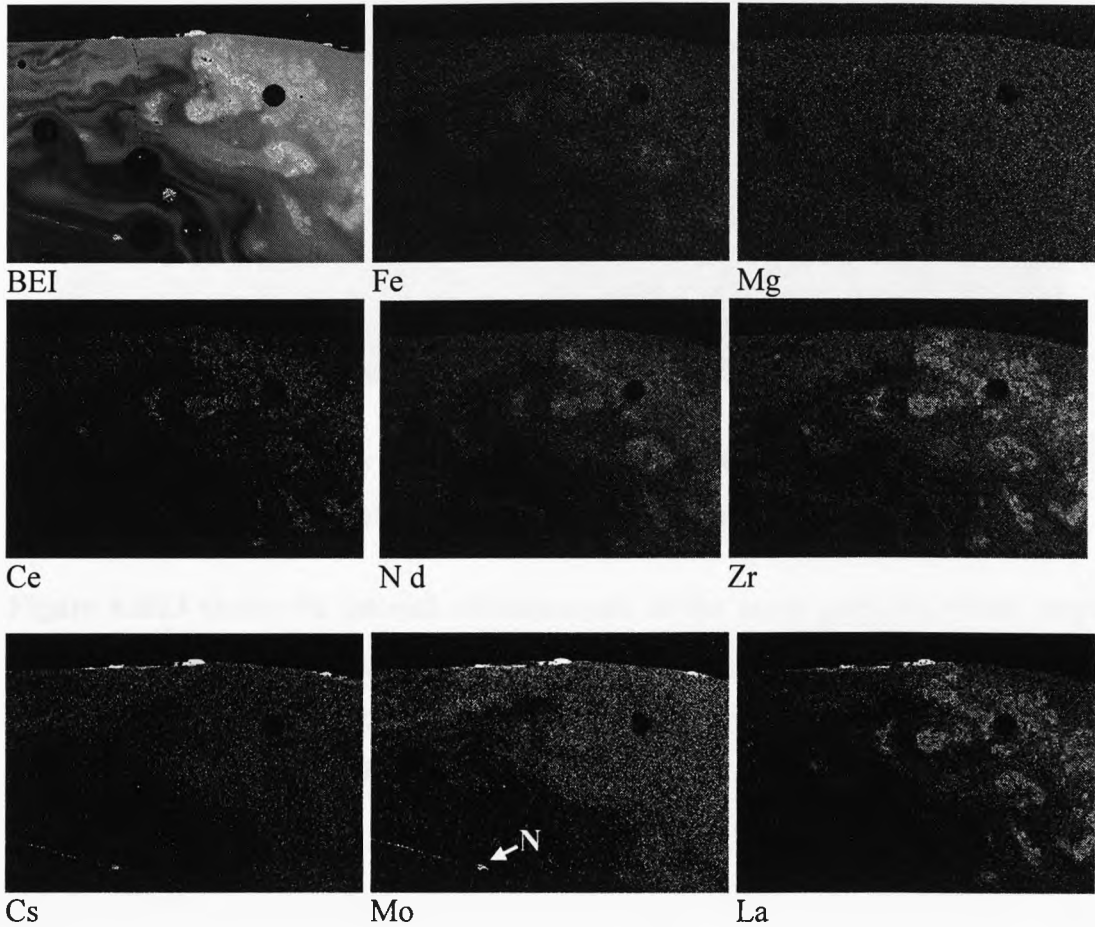


Figure 4.8.12: Backscattered image of sample 10M25 in cross section, with elemental dot maps of the same area (top of image denotes top of melt).

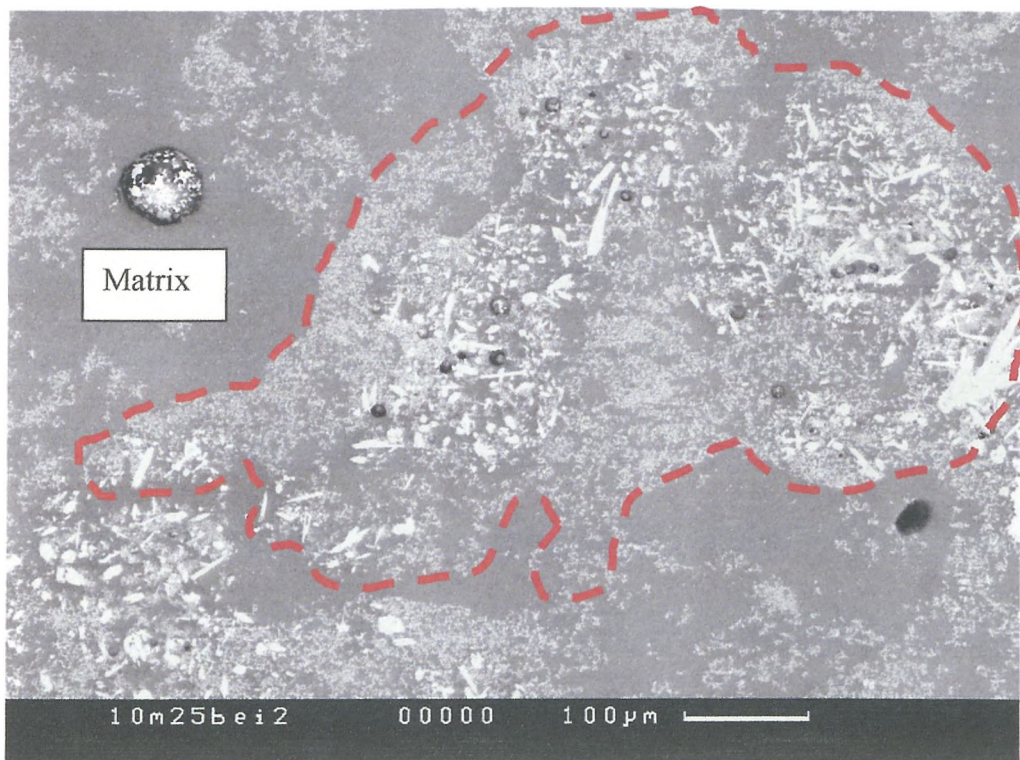


Figure 4.8.13: Cross section of a calcine particle in glassy matrix of sample 10M25, showing the internal microstructure of the waste form.

Figure 4.8.13 shows the internal microstructure of the waste particles, where larger needles of higher atomic number material, measuring $\sim 50\text{-}100\mu\text{m}$ are surrounded by a finer matrix of lighter elements. Segregation of the La to the Cs and Mo containing phase is also apparent (see **figure 4.8.12**).

Sample 15M25 analysis

Sample 15M25 was sectioned after 15 minutes of melting in an Inconel 601 crucible. **Figure 4.8.14** shows the further dissolution of the calcine particles within the glassy melt and evidence of the convection currents in the melt on the dissolution of the calcine particles. The presence of a Cs- and Mo-phase is now obvious within the body of the melt, but it is not seen toward the melt surface. The mixing of the melt by convection and degassing is thought to have broken up the Cs/Mo-rich surface layer and dispersed the phase, into the melt. These two elements remain associated with each other.

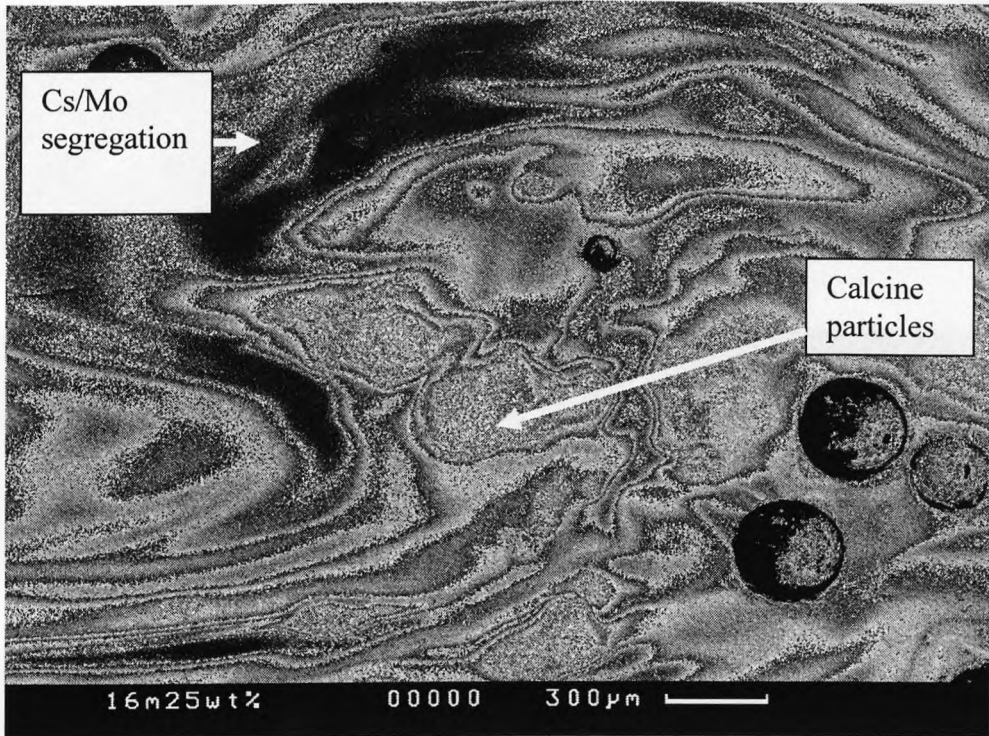


Figure 4.8.14: BEI of sample 15M25 in cross section, with top of image depicting top surface of sample.

Elemental x-ray (Figure 4.8.15) maps shows some segregation of Cs and Mo to the same phase within the body of the melt (indicated by arrows), surrounding a particle of still undissolved calcine. Zr and Ce are still highly concentrated within the body of the calcine particles although Al and Mg are uniformly distributed within the glassy matrix.

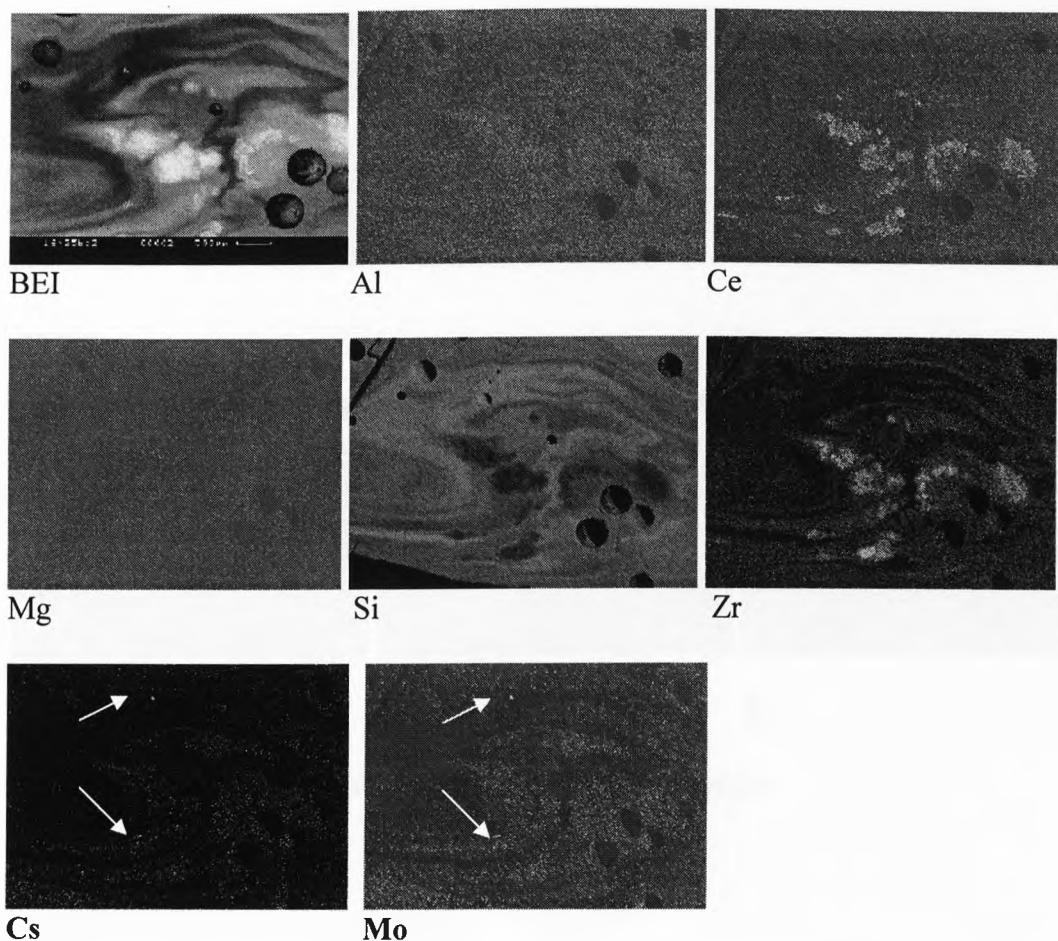


Figure 4.8.15: Backscattered image of sample 15M25 in cross section, with electron maps of the same area (top of image denotes top of melt).

Sample HT200G analysis

The top surface of sample HT200G (**Figure 4.8.16**) reveals a Cs- and Mo- rich region. There is some evidence of Cr enrichment within this region. Zr appears to be evenly distributed across the entire surface of the melt.

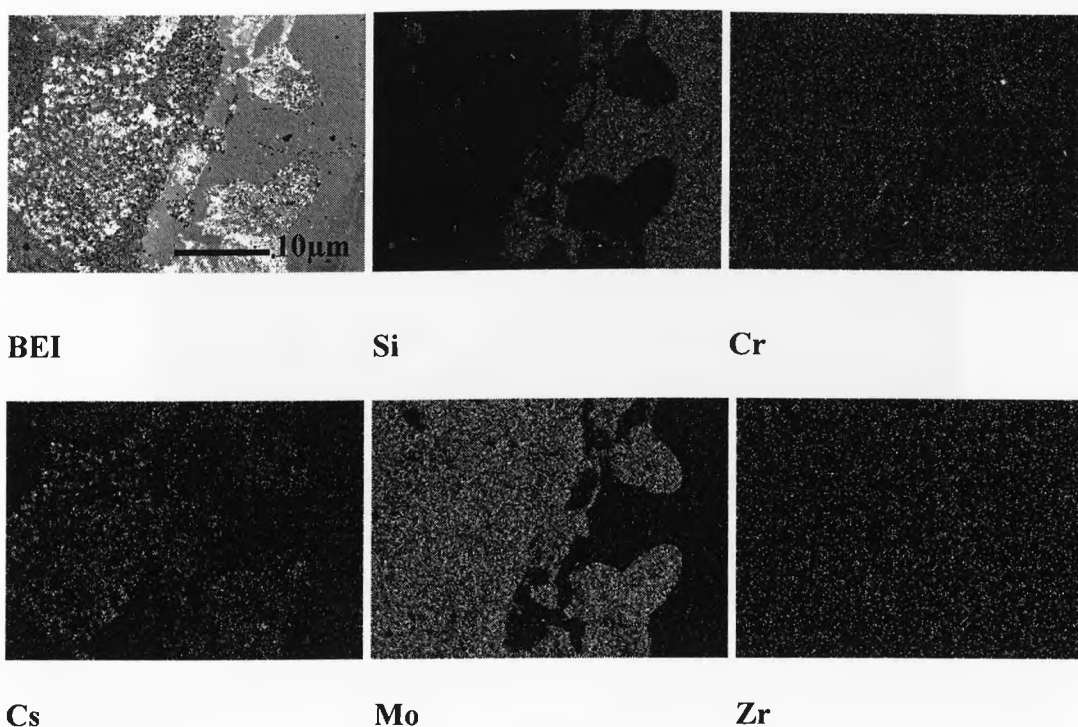


Figure 4.8.16: HT200G surface

Sample HT400G analysis

The surface of sample HT400G can be seen in **Figure 4.8.17**. In this case 2 phases can be seen, a Mo-rich phase (phase 1) with regions enriched in Cs within it (phase 2).

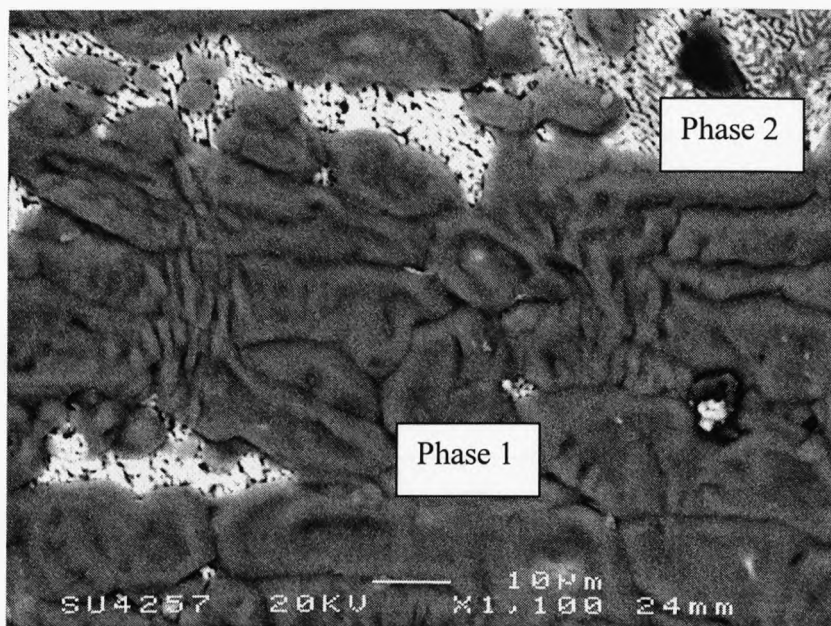
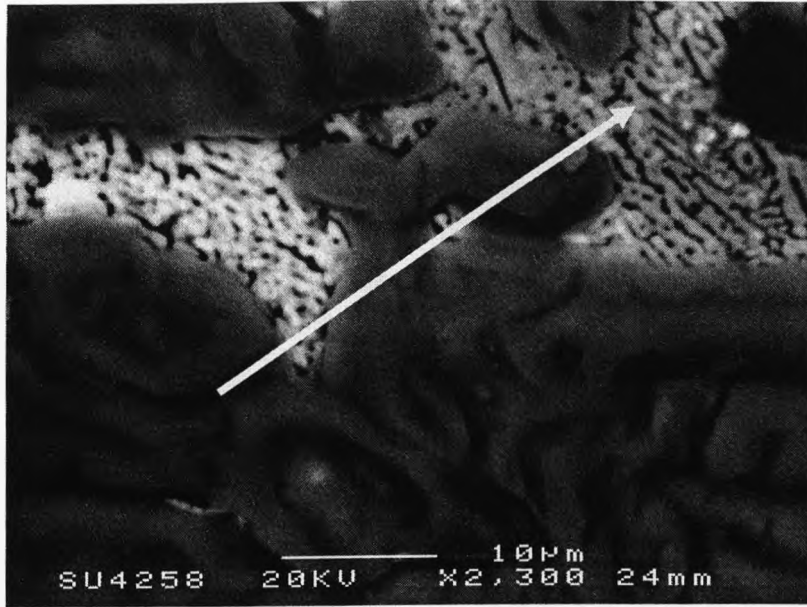
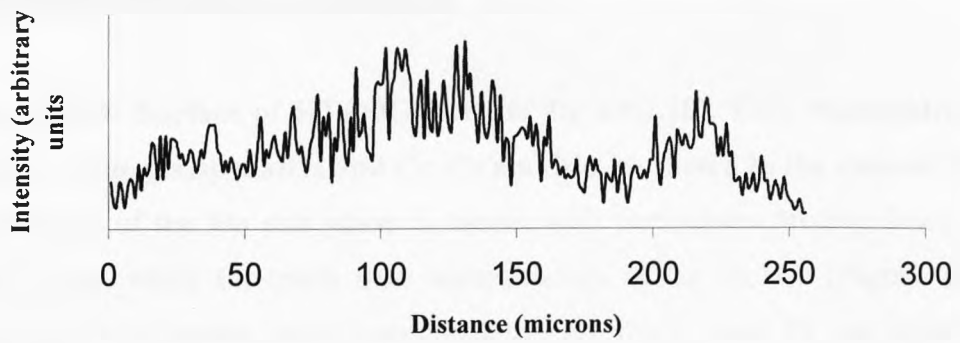


Figure 4.8.17: HT400G sample surface showing 2 distinct phases



Cs



Mo

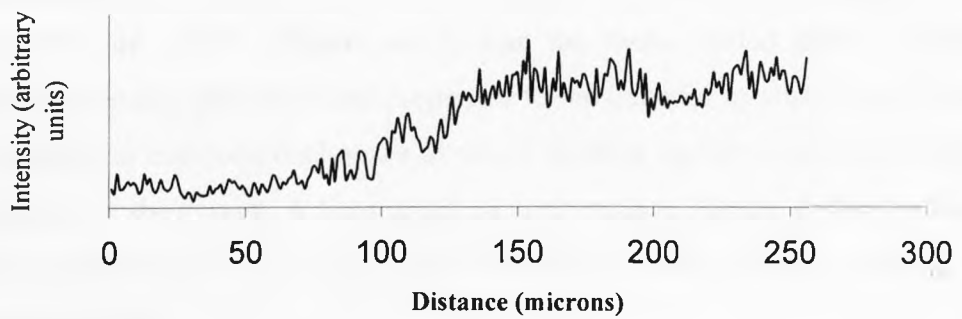


Figure 4.8.18: Linescan of HT400G surface, indicating concentration of Cs and Mo. Markers indicate where linescan was performed.

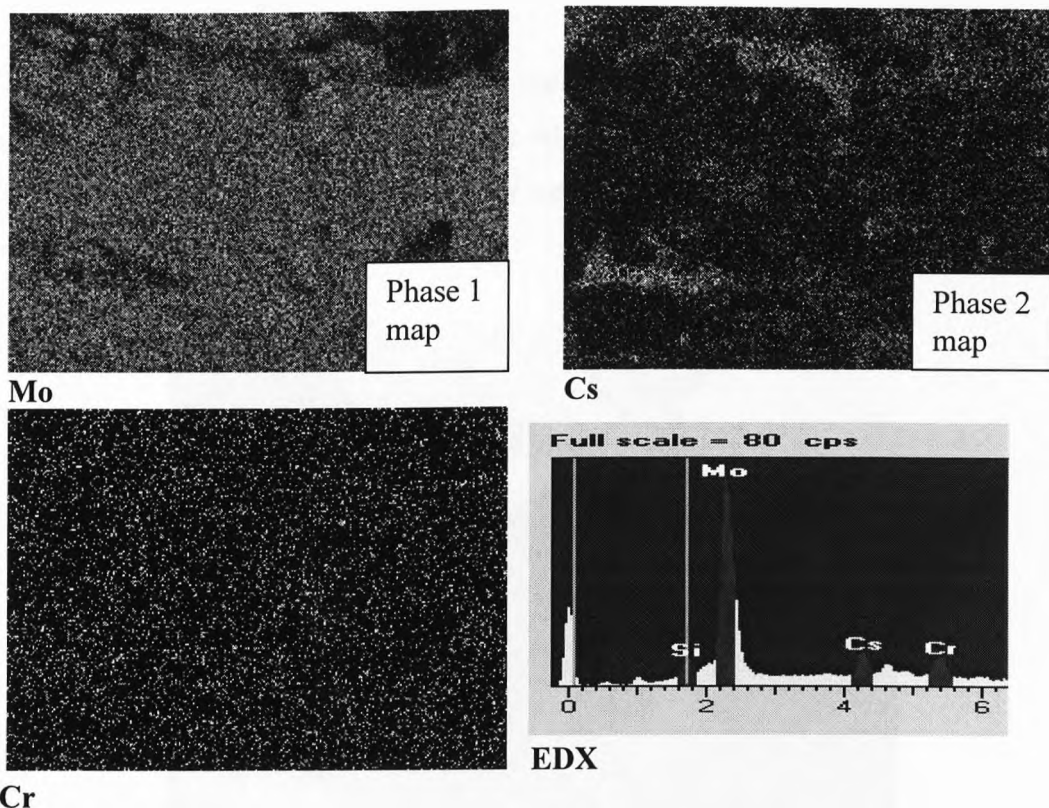


Figure 4.8.19: Surface of HT400G (seen in fig 4.8.2.10). EDX highlighting the presence of the glassy matrix and Cr, Cs and Mo, as shown in the element maps. The structure of the Mo rich phase is coarse, with particulates ranging from $\sim 10 - 30\mu\text{m}$ in size, whilst the much finer microstructure of the Cs rich (**Figure 4.8.17**) phase appears to involve layers approximately $1\mu\text{m}$ thick. Some Cr was detected in conjunction with this surface layer, but appeared diffuse (**Figure 4.8.19**). The structure of the Cs-rich phase 2 appears to be that of a eutectic phase. This is in agreement with the propensity for the yellow surface phase to form and melt at lower temperatures of $\sim 700^\circ\text{C}$ (**Figure 4.4.2**) than the waste loaded glass ($\sim 1050^\circ\text{C}$). Eutectics generally give enhanced properties to the material in which they form and are the point in compositional space at which there is equilibrium between the two components of the system. A linescan of the melt surface (**Figure 4.8.18**) for the Mo and Cs confirmed the Cs-enriched area was indeed depleted in Mo, although there was some overlap.

Sample HT700G analysis

The surface of sample HT700G can be seen in **Figure 4.8.20**. A Cs- and Mo-rich surface layer can be observed, this time with Cr-rich areas within this layer. Cr is associated with certain areas of the melt only, and is not rich in areas where Cs is present (**Figure 4.8.21**).

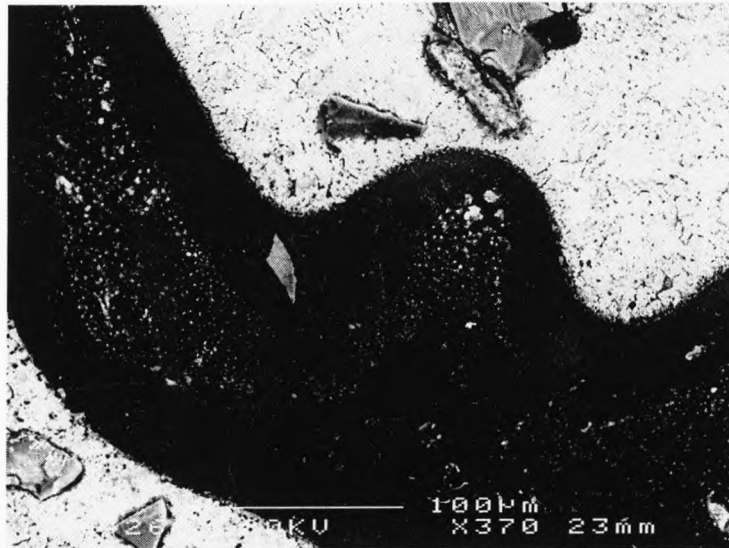


Figure 4.8.20: Backscattered image of HT700G melt surface.

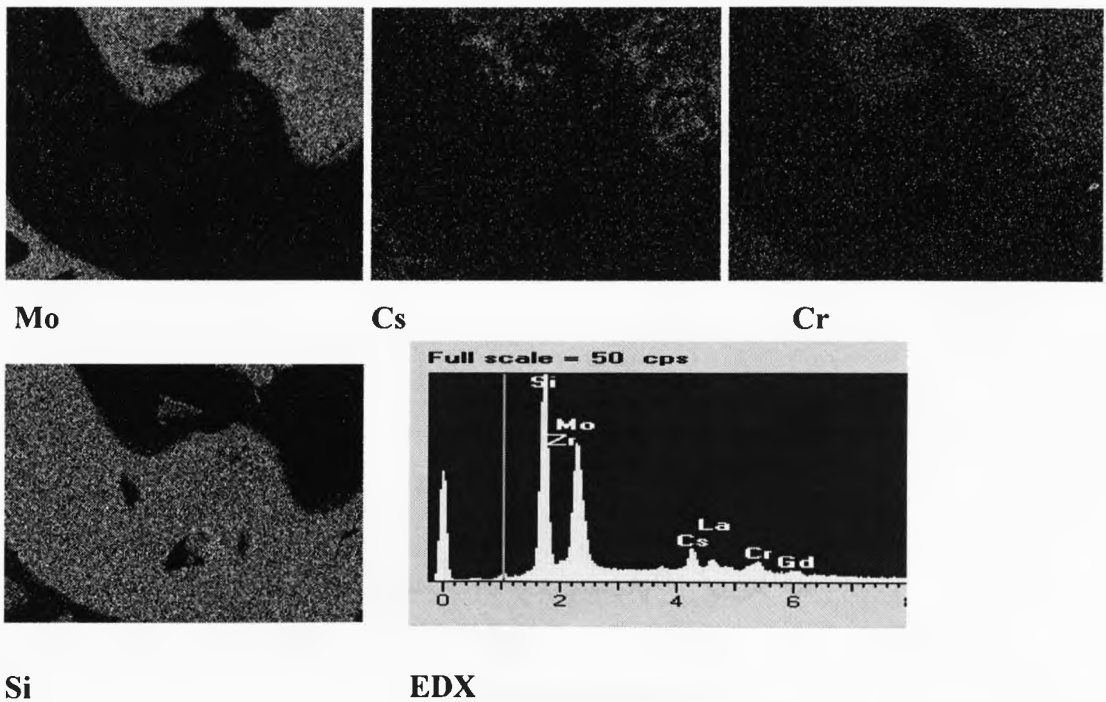


Figure 4.8.21: Element dot maps of HT700G surface (see fig. 4.8.2.12)

Linescans of the area (Figure 4.8.22) indicate the presence of Mo and Cs in the same area, but also the presence of a Mo-rich phase with some Cs-depletion indicating phase separation within the yellow phase, in agreement with the apparent eutectic component formed within HT400G.

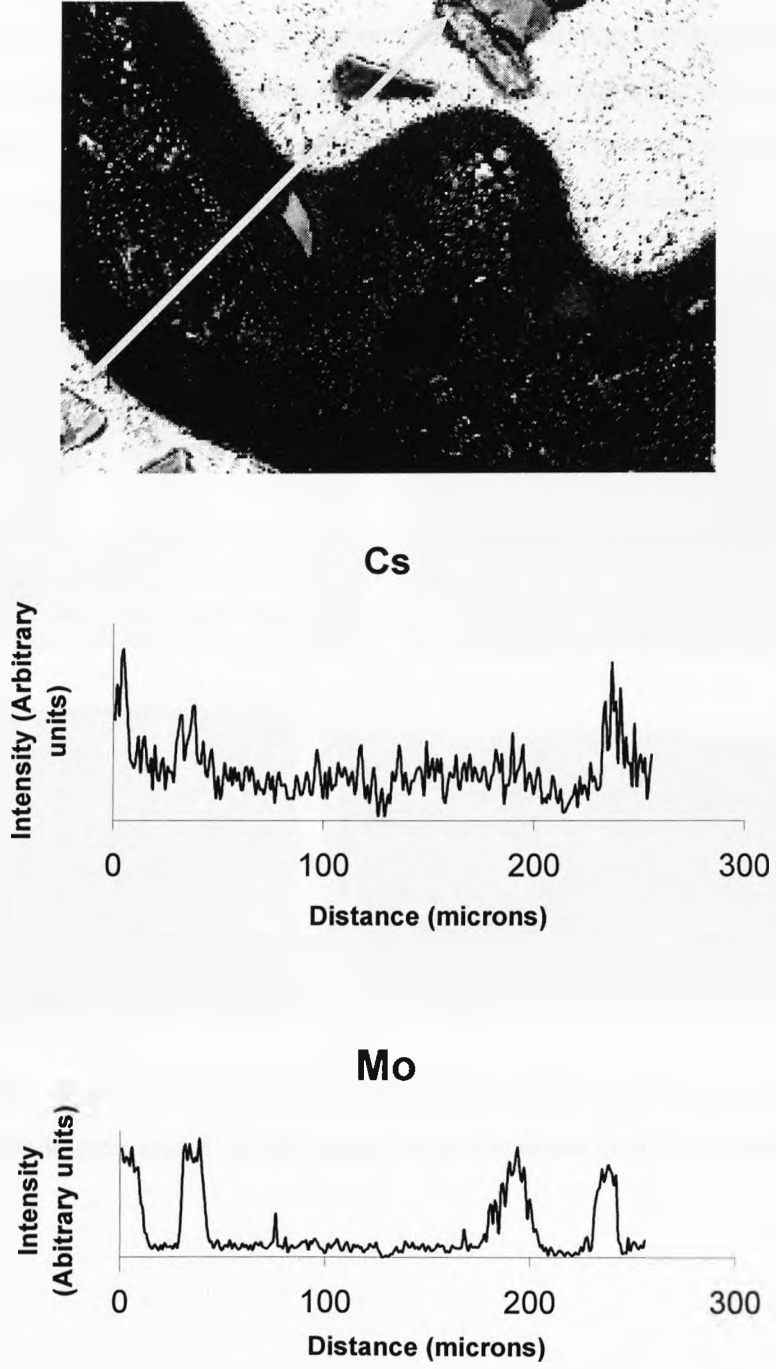


Figure 4.8.22: Linescan of HT700G surface for Cs and Mo

Sample PNL25RED analysis

As well as looking at cross sections of the melt, the melting vessels were examined for evidence of any reactions occurring above the melt. The crucible walls and neck of sample PNL25RED are shown in **Figure 4.8.23**. Some whitening can be seen above the melt line, but appeared as Si under EDX, consistent with the same effect on the quartz crucibles and windows in other melts indicating SiO₂ deposition upon heating. The neck of the crucible, shown in **Figure 4.8.23b** is darkened with sticky deposits of nitrate. BEI-EDX analysis (**Figure 4.8.23c-d**) and elemental x-ray maps of the nitrate deposit (**Figure 4.8.24**) indicated needle-like Mo rich crystals on the walls, with points of the needles being rich in Te, and a general background deposit of Cs.

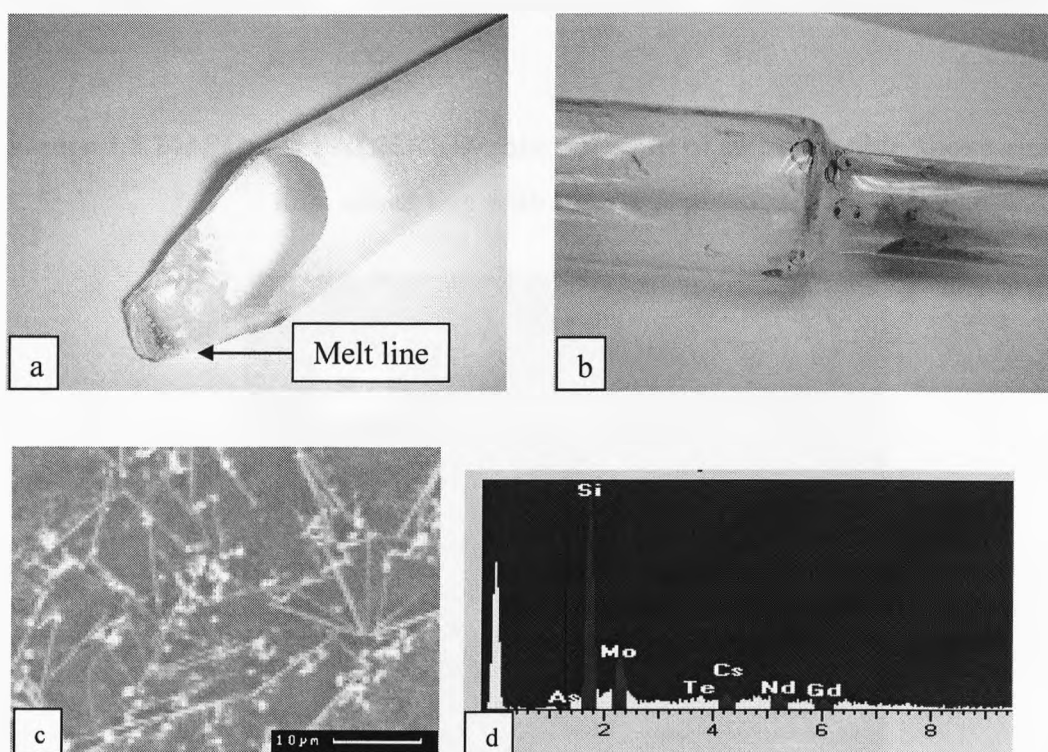


Figure 4.8.23: a) Base of crucible and melt line b) nitrate deposits on neck c) BEI of neck area and d) EDX taken from the same area as the BEI.

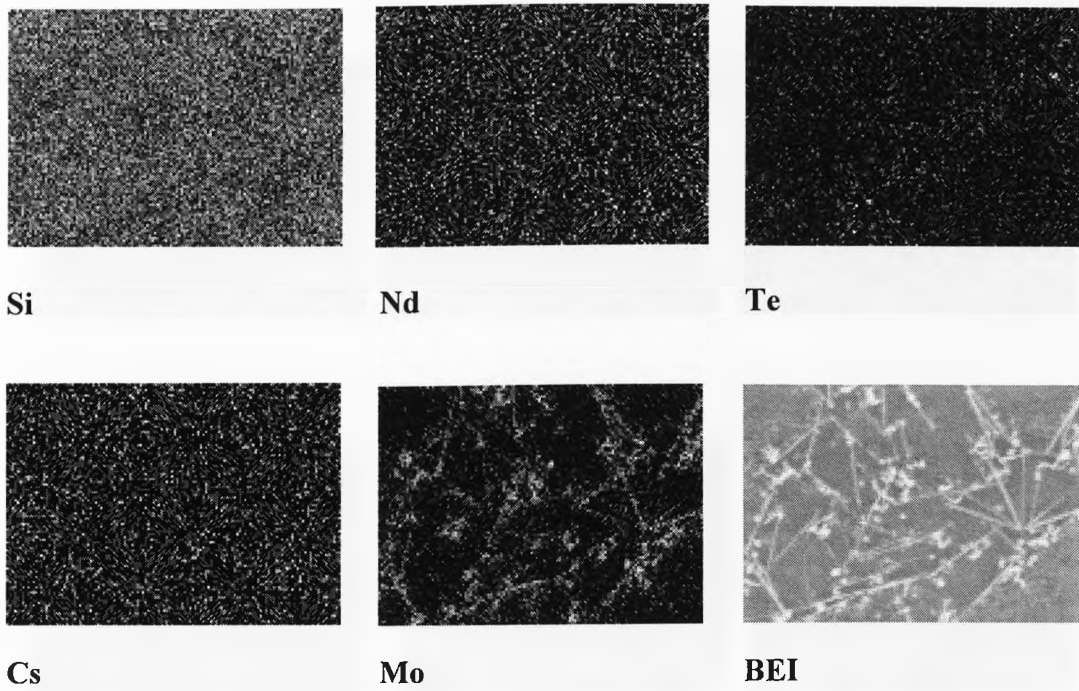


Figure 4.8.24: Sample PNL25RED- internal walls of silica crucible above melt line, coinciding with nitrate deposition

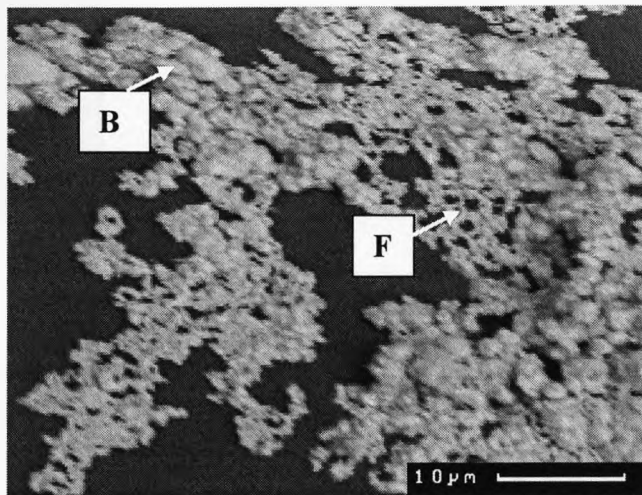


Figure 4.8.25: Surface of sample PNL25RED, showing a bulbous deposit (B) interconnected by a finer lattice (F).

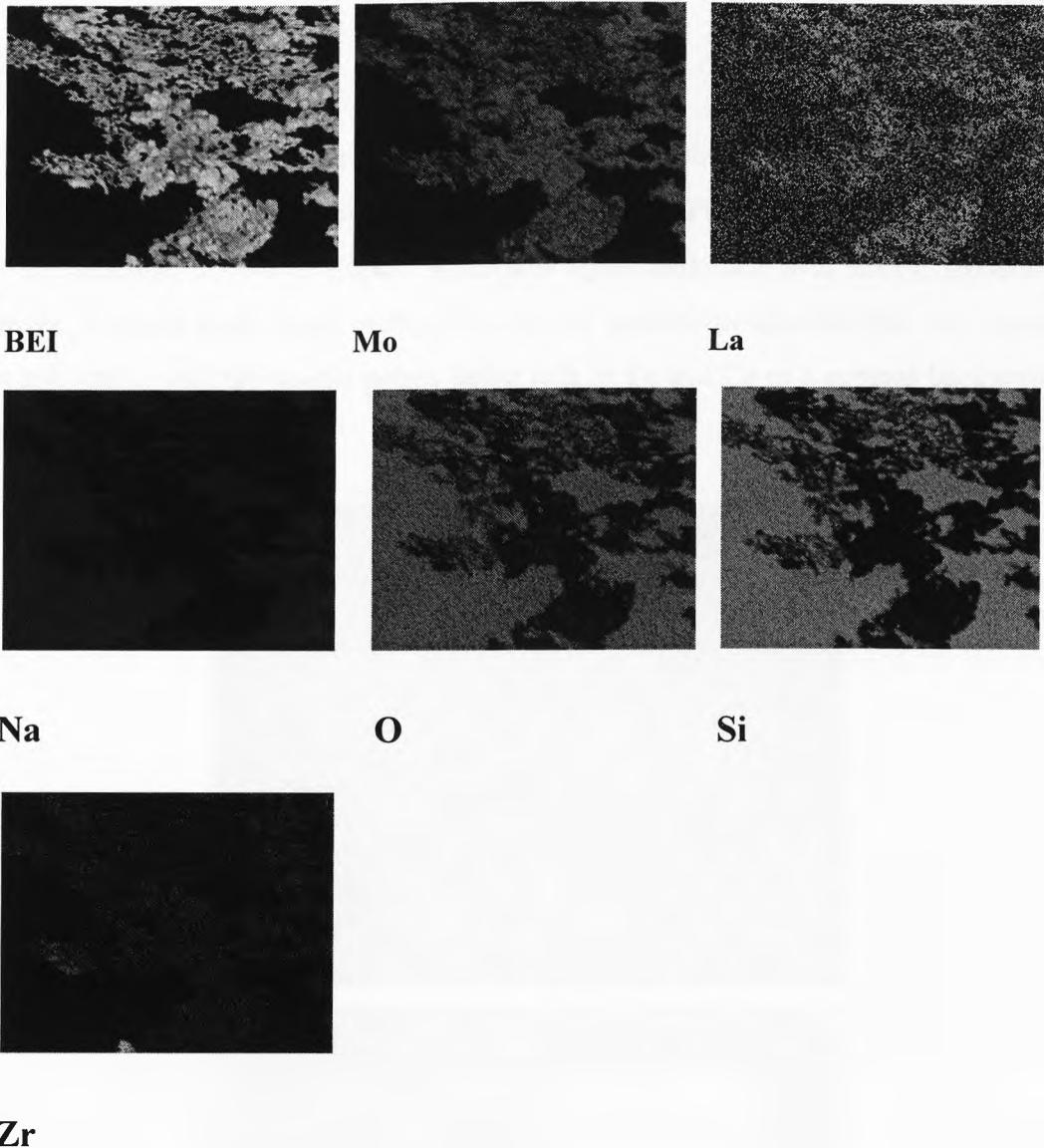


Figure 4.8.26: Electron maps of metallic deposit on surface of sample PNL25RED glass

Under reducing conditions, a shiny region was observed on the surface (**Figure 4.8.25**) of the waste loaded glass suggesting a metallic deposit, likely to be Mo (**Figure 4.8.26**). The shiny region had a bulbous structure, interconnected by a finer lattice network (**Figure 4.8.26**). The bulbous structure was rich in Mo, whilst the lattice phase was rich in La but with minor Zr. This metallic region is consistent with what would be expected under reducing conditions (Short, 2004), and reducing conditions have previously been used by Carter *et al* (2002) when adding wastes to Synroc to prevent the formation of Cs and Mo rich phases.

Sample PNL25IN analysis

The crucible walls and neck of sample PNL25IN are shown in **Figure 4.8.27**. Some whitening can be seen above the melt line as with the PNL25RED sample. The neck of the crucible, shown in **Figure 4.8.27a** is again darkened with sticky deposits of nitrate. Element x-ray maps of the NO_x deposit indicate needle-like Mo rich crystals on the walls, with the needle points being rich in Te and Cs in a general background of Fe (**Figure 4.8.28**).

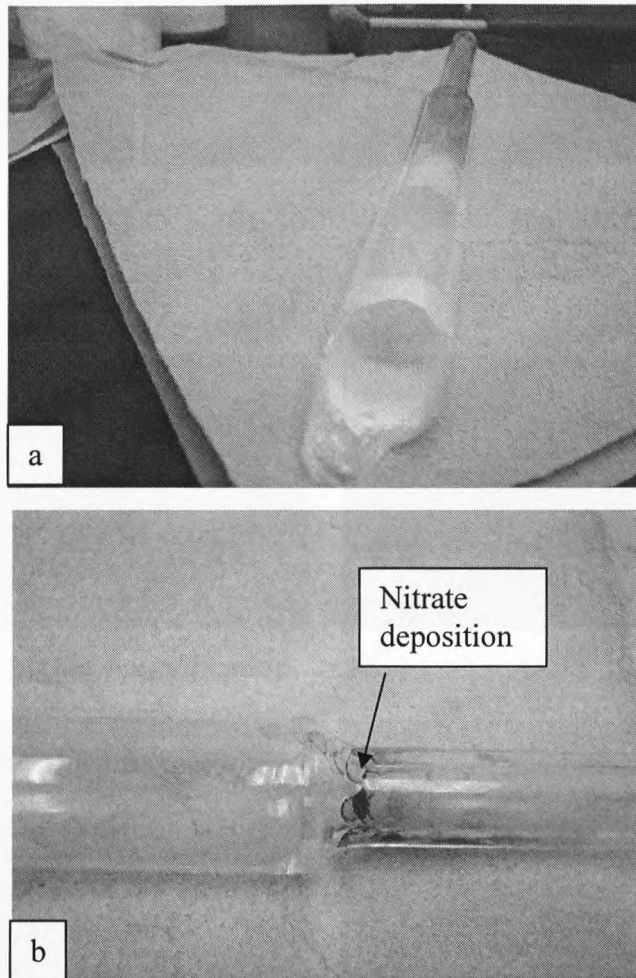
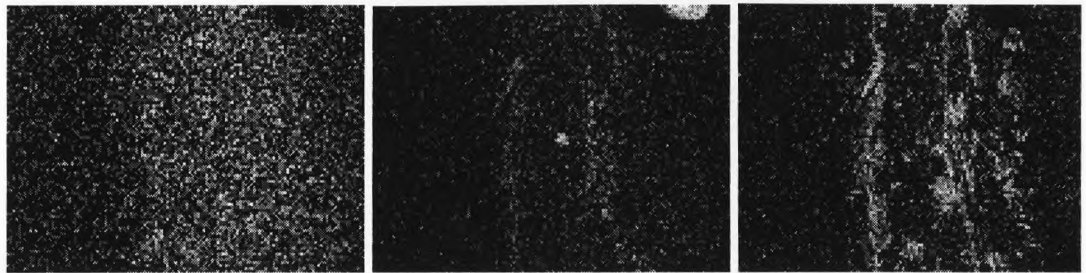
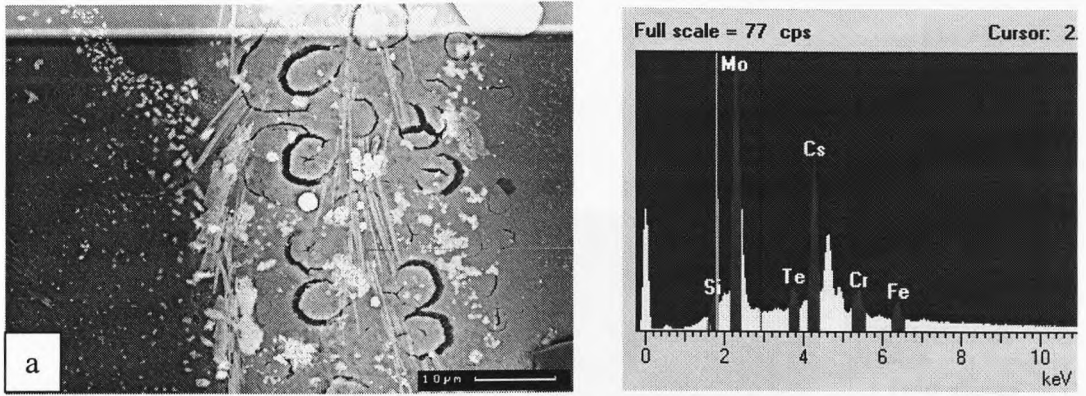


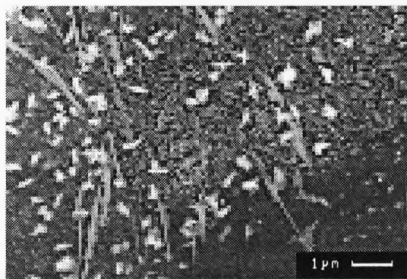
Figure 4.8.27: a) PNL25IN crucible b) neck of crucible and NO_x deposits.



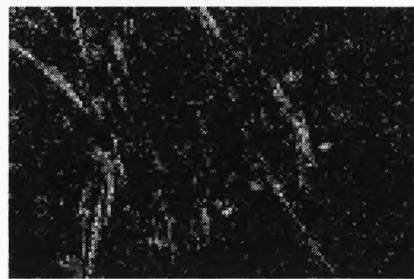
Fe

Cs

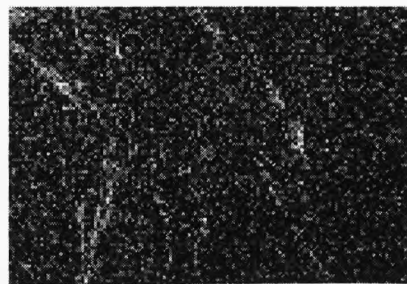
Mo



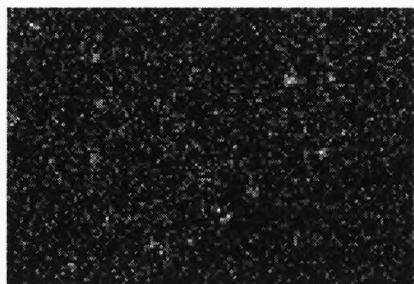
BEI at higher magnification



Mo



Cs



Te

Figure 4.8.28: BEI-EDX of PNL25IN crucible walls coinciding with areas of NO_x deposition, showing the presence of Te alongside the Cs & Mo deposition.

4.9 Transmission Electron Microscopy

As-received sample analysis

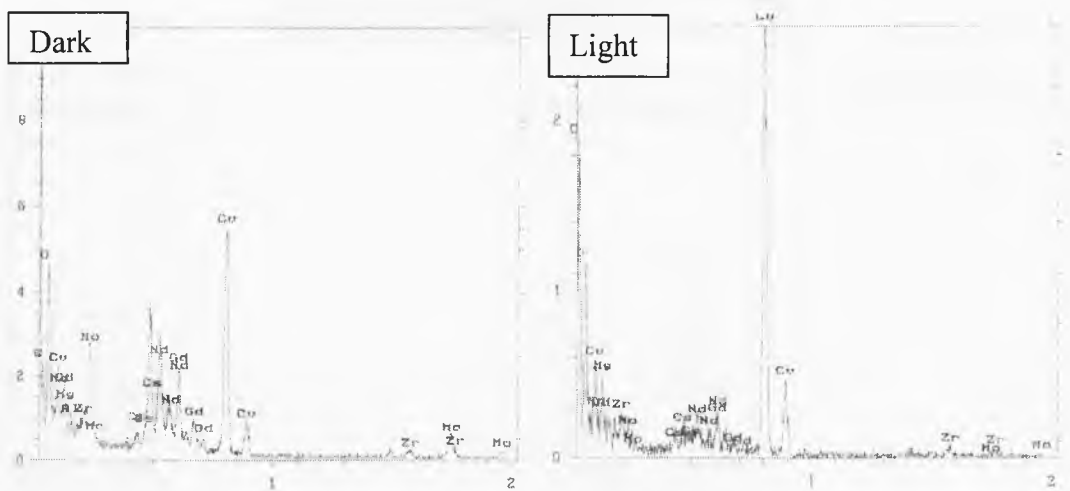
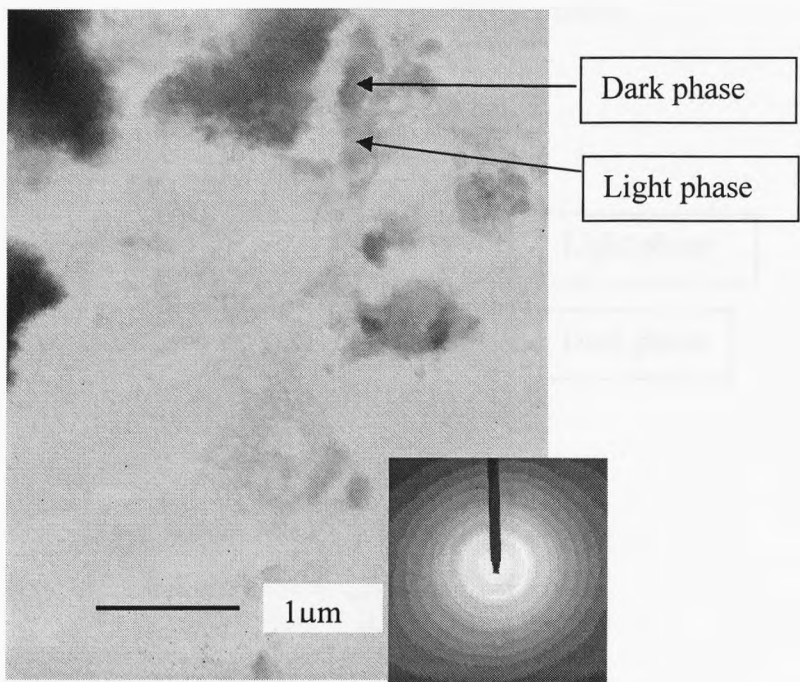


Figure 4.9.1: Z-contrast image of as-received calcine, illustrating the presence of dark and light phases and EDX of same phases (inset: diffraction pattern highlights amorphous nature of material)

Dark and light phases (due to Z-contrast) can be observed in the as-received calcine. The darker phase is rich in rare earths and Mo and Cs, whilst the light phase (**Figure**

4.9.1) contains Mg. Some overlap is expected in EDX analysis due to the small size of the sample and beam interaction with areas surrounding the analysis spot. The increased intensity of the Cu peak due to the interaction of the beam with the sample grid is in evidence in the EDX (Figure 4.9.1) and makes the intensity of the surrounding peaks resulting from the sample correspondingly smaller.

Sample HT200 analysis

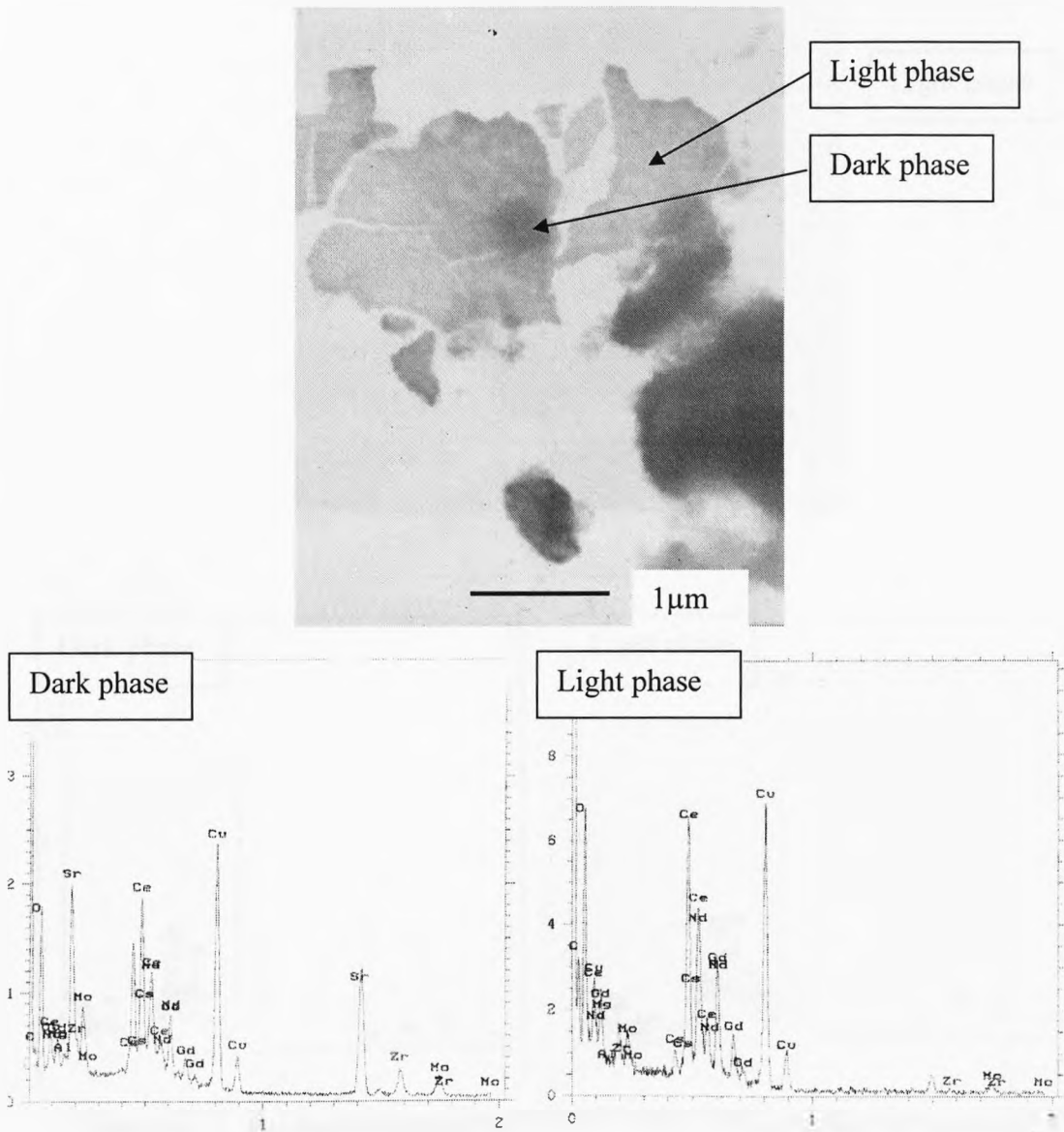


Figure 4.9.2: Z-contrast image of HT200 calcine, illustrating the presence of dark and light phases and EDX of same phases

Using Z-contrast dark and light phases can again be observed in the HT200 calcine (Figure 4.9.2). The darker phase is rich in rare earths, Mo, Cs and most obviously Sr.

The lighter phase is Sr deficient, but contains more rare earths and Mg than the darker phase.

Sample HT400 analysis

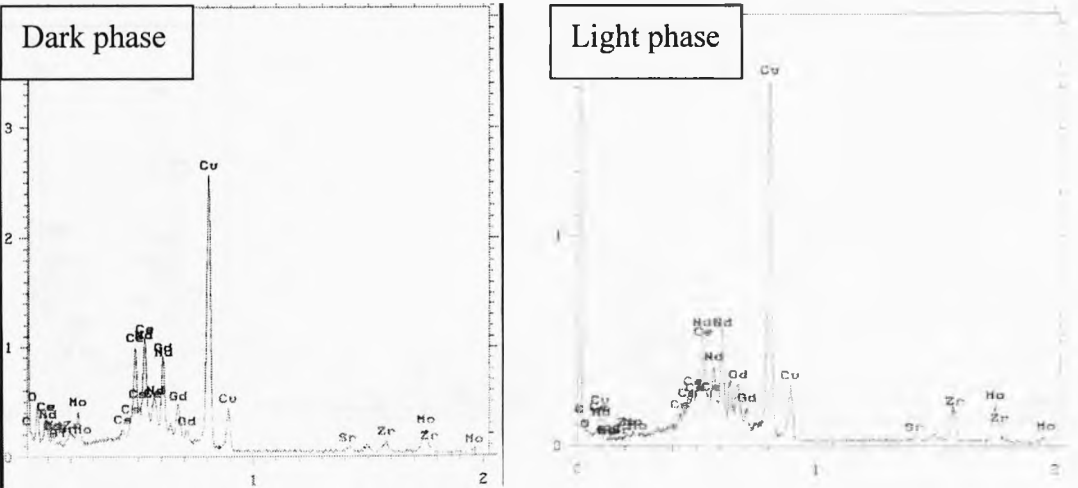
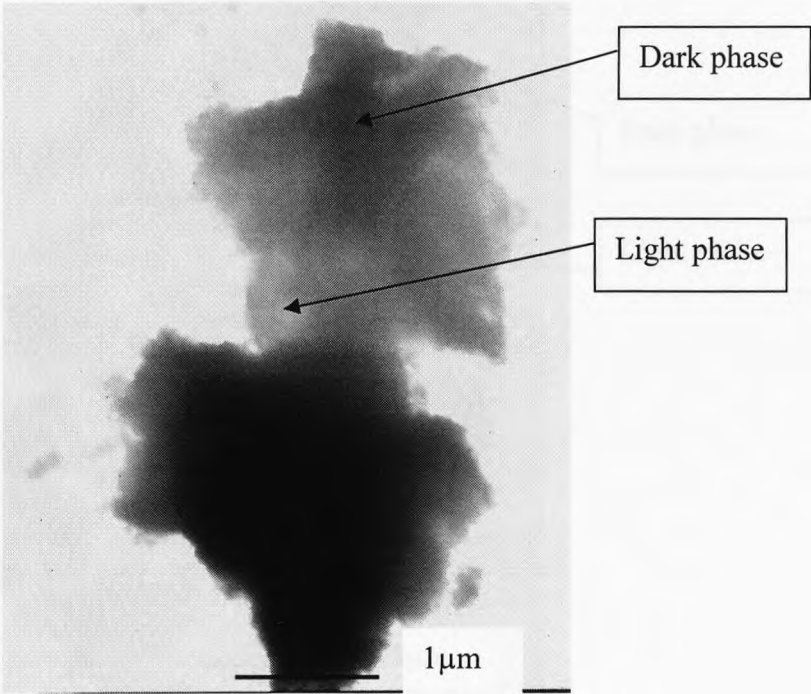


Figure 4.9.3: Z- contrast image of HT400 calcine, illustrating the presence of dark and light phases and EDX of same phases

Dark and light phases are again present in the HT400 sample (Figure 4.9.3). The darker phase appeared richer in rare earths and Mo and Cs from analysis of the

relative intensities of the EDX. However, the dark and light phases throughout the sample were in close conjunction and so differentiation by EDX became difficult.

Sample HT700 analysis

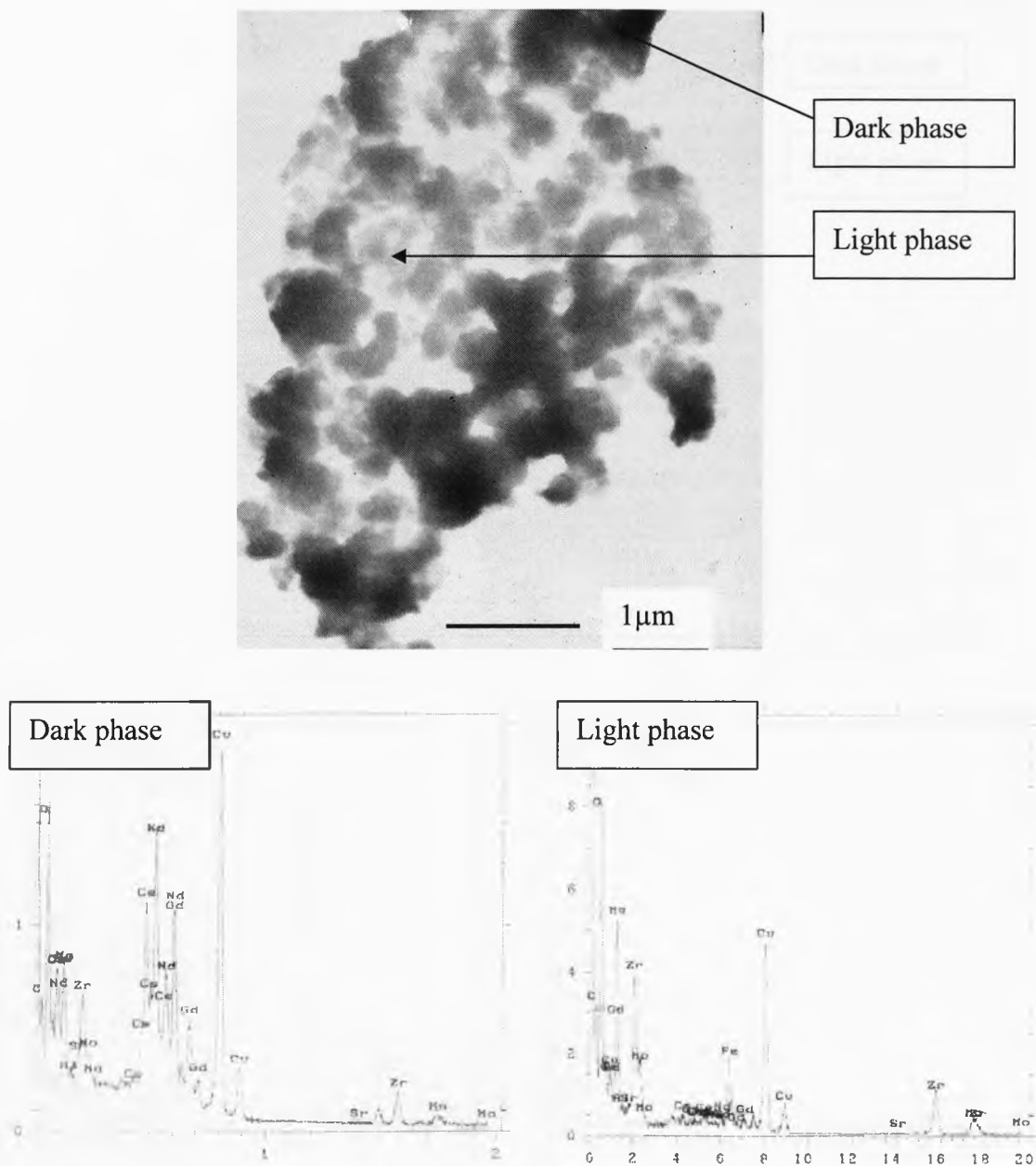


Figure 4.9.4: Z- contrast image of HT700 calcine, illustrating the presence of dark and light phases and EDX of same phases

In the HT700 sample, a change in microstructure is obvious, as the sample becomes much finer grained, consistent with the XRD (Figure 4.5.2) and SEM (Figure 4.8.3) data for this heat treatment temperature. The darker phase is rich in rare earths and

Mo and Cs, whilst the light phase contains increased amounts of Mg, Zr and Fe in compared to the darker phase.

Sample HT1000 analysis

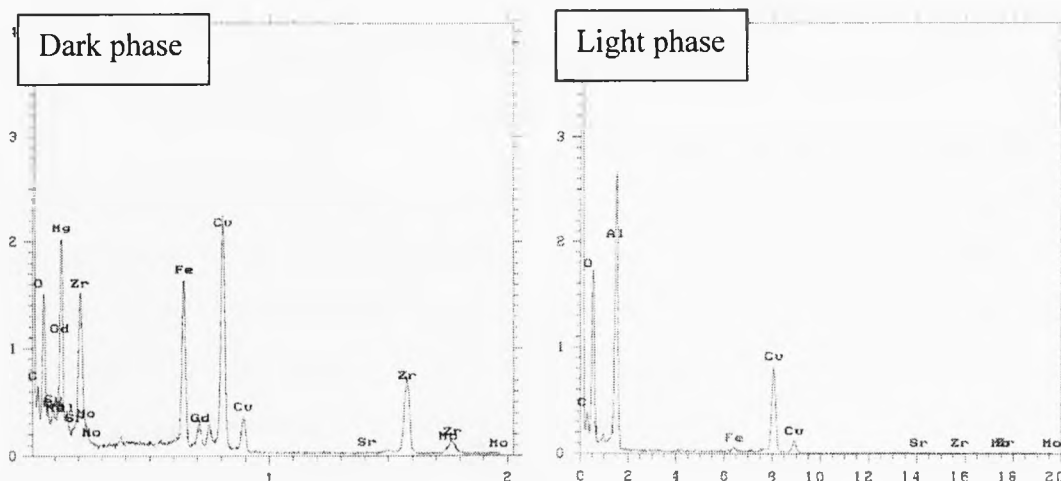
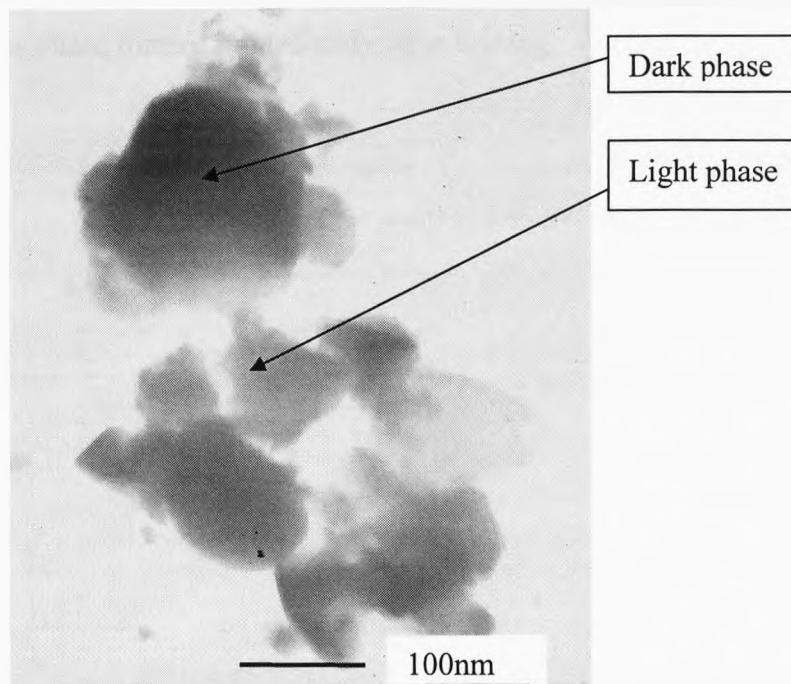


Figure 4.9.5: Z- contrast image of HT1000 calcine, illustrating the presence of dark and light phases and EDX of same phases

The darker phase (**Figure 4.9.5**) is rich in Fe, Zr and Mg, whilst the light phase would appear to contain only Al and some Fe. No amorphous patterns were obtained from this sample, concurring with the XRD data (**Figure 4.5.2**) showing it to be crystalline.

In summary, the characterisation of the HLW simulant reveals an inhomogeneous nature and a high (between 15-50wt%) nitrate content.

The characterisation of the simulant waste interaction with the glass frit indicates that the calcine is of low solubility within the glass melt, and that there is a low density, low melting, yellow phase formed immediately upon heating.

Chapter 5: Discussion

This chapter collates all the evidence from previous chapters and brings it together in a cohesive discussion. Vitrification of a high level waste glass, in this case where the waste stream consists of a Magnox: oxide blend, is discussed with relation to the raw material properties of that waste and the dissolution of that waste in a mixed alkali borosilicate glass during the early stages of the melting process. The implications of the effects of the waste material properties on the glass melt are then discussed with a view to developing some understanding of the processes occurring during vitrification of this complex system. For that reason, this chapter is split into two parts, the first of which deals with raw material characterisation and the second with the digestion of the waste by the glassy matrix and the stages observed in this dissolution.

5.1 Simulant Waste

The calcine is a heterogeneous material. Compositional analysis of the calcine (**section 4.1**) varies between the analyses obtained at SRL, VSL and BNFL. The VSL analysis is believed to be the most representative of the average composition, as several samples were analysed and the results averaged. However, the differences in composition arise from batch heterogeneity on a large scale. The oxide wt% totals 60% ($\pm 10\%$) due to $\sim 40\%$ ($\pm 10\%$) of the calcine being non-oxide (i.e nitrate and water containing) material. The oxide wt% averages the many samples taken and tested for L.O.I. by TGA and simple weight loss measurements. This is supported by the sensitivity of the melt to atmospheric changes indicating a network former deficit as seen in the VSL composition and discussed by Feng *et al* (1989). Gd, Nd, Mo and Zr contributions are high as these are waste stream elements expected to be major constituents due to fission reactions and fuel cladding.

The results presented in chapter 4 are summarised in **Table 5.1.1** and demonstrate that the calcine is sensitive to heating and ageing effects (**Figures 4.5.2 and 4.4.4**), as would be expected in a sample with high nitrate content, as nitrates are often hygroscopic (Cotton *et al*, 1999). The colour change (**Figure 4.2.1**) cannot be attributed to one specific element of the waste stream due to the large numbers of ions

present which would affect such a change upon heating. The denitration of the sample is also believed to have an effect upon this colour change.

A large number of nitrates, as discussed by Chun (1977) and detailed in other published data (CRC handbook) are brown in colour, and NO_x gases are often dark brown and produce a tacky condensate. The differing particle sizes of the as-received calcine are indicative of a calcination process which produces sticky particulates, consistent with the nitrate-containing solids. Thermal analysis revealed several events taking place as the raw waste material was heated. The dehydration of the material, occurring at 125°C , (**Figures 4.4.4**) was followed by what was thought to be the loss of sorbed water at 325°C and 375°C . Sorbed water was assumed to be part of the system due to the similar behaviour (when undergoing thermal analysis) of other nitrates containing sorbed water (**Figures 4.4.10-13**). An endothermic event was observed in the as-received material at similar temperatures to those of the nitrates containing sorbed water.

This dehydration coincided with other chemical reactions starting at $\sim 270^\circ\text{C}$, characterised by an intense endotherm and some weight loss until 400°C . At around 400°C , and continuing until 700°C a dramatic drop in weight was observed, averaging 31 wt% of the sample. Since it was known that the sample had been fabricated from a solution simulant waste in highly concentrated HNO_3 along with additives of LiNO_3 , the above temperatures were taken to be the temperatures at which the major nitrate components decomposed (Chun, 1977). Data compiled from Weast (1981) (see **Table 4.5.3**) shows that this is indeed the case and the nitrates should have decomposed by the time the material reaches 700°C . Since LiNO_3 was a known additive to the original solution, the intense endotherm present on the DTA at 254°C (**Figure 4.4.1**) was attributed to the melting of LiNO_3 as published data shows the melting point is at 264°C . Weight loss from nitrate decomposition varied up to 50%, with some contribution from dehydration of the sample. The dehydration was not counted as a major contribution to the industrial processing of the calcine, due to the fact that the samples will absorb water in the laboratory atmosphere prior to experiment although some contribution had to be taken into account as the differential thermal analysis highlighted the presence of a “water of hydration” in the samples.

Table 5.1.1: Summary of Waste Characterisation

Analysis Technique	Observations made												
Optical	<ul style="list-style-type: none"> • Colour change upon heating 												
DTA	<ul style="list-style-type: none"> • 125°C Dehydration • 246°C LiNO₃ melts • 400°C Denitration • 570°C Sr(NO₃)₂ melts } Phases identified using XRD • 800°C Formation of CsLiMoO₄ } Phases identified using XRD 												
TGA	<ul style="list-style-type: none"> • 400-700°C denitration and weight loss av. 31% • Atmospheric contribution- slowest rate of denitration in oxidising atmosphere - fastest denitration in reducing atmosphere 												
DSC	<ul style="list-style-type: none"> • Thermal decomposition of a crystalline phase at 250°C, 400°C-600°C 												
XRD	<ul style="list-style-type: none"> • R.E oxide present in as-received, poorly crystalline material. Secondary/tertiary R.E phases developed at 700°C (decomposing at 900°C) • LiNO₃ & Sr(NO₃)₂ present in as-received material, decomposition by 500°C and 600°C respectively • Molybdate formation from 700°C • MgO formation at 1000°C, other trace phases crystallising 												
FT-IR	<ul style="list-style-type: none"> • O-H, N-O stretch of OH⁻ and NO₃²⁻ anion detected in samples up to 400°C and 700°C respectively • At 700°C band at 1426 cm⁻¹ splits into 2 components - at 700°C-800°C band at 1385cm⁻¹ decreases dramatically 												
GC-MS/TA	<table border="1"> <thead> <tr> <th>Evolved Gas (50mg batch)</th> <th>Gas</th> <th>He</th> <th>O₂-He</th> </tr> </thead> <tbody> <tr> <td></td> <td>NO</td> <td>2.42 x 10⁻³g</td> <td>2.6 x 10⁻³g</td> </tr> <tr> <td></td> <td>Temp/°C</td> <td>300-570</td> <td>400-650</td> </tr> </tbody> </table>	Evolved Gas (50mg batch)	Gas	He	O ₂ -He		NO	2.42 x 10 ⁻³ g	2.6 x 10 ⁻³ g		Temp/°C	300-570	400-650
Evolved Gas (50mg batch)	Gas	He	O ₂ -He										
	NO	2.42 x 10 ⁻³ g	2.6 x 10 ⁻³ g										
	Temp/°C	300-570	400-650										

GC-MS	Evolved Gas (10g batch)	Gas	He	Temp/°C
		NO	0.687g	320-700
		N ₂ O	0.0464g	300-380
		O ₂	0.171g	320-700
Optical camera	<ul style="list-style-type: none"> • 620°C batch softening • 800°C batch sagging • 900° melt 			
SEM	<ul style="list-style-type: none"> • As-rec'd : 4 phases - R.E oxide/Fe & Al/ Sr, Te & Zr/ Cs, Mo & Sr, Ba • HT400 : 4 phases - R.E oxide/ Fe & Al/ Cs, Mo, Nd & Zr/ Cs, Mo & Sr; • HT700 : 4 phases - R.E oxide/ Fe & Al/ Cs, Mo, Sr & Zr/ Cs, Mo & Nd • HT1000 : 4 phases - R.E oxide/ Zr & Al /Ce & Mg/ Cs, Mo & Sr; • Yellow phase: Sr, Mo, Cs, Te, Cr – Cs rich particulates in Mo matrix 			
TEM	<ul style="list-style-type: none"> • As-rec'd : 2 phases - R.E, Mo& Cs/ Mg • HT200 : 2 phases - R.E, Mo & Cs & Sr/ Mg & Sr • HT400 : 1 phase - R.E, Mo & Cs (more homogeneous) • HT700 : 2 phases - R.E, Mo & Cs/ Mg, Zr & Fe • HT1000 : 2 phases – Al/ Mg, Zr & Fe 			

Thermal analysis of simulant waste samples under different atmospheres, using oxidising, reducing, and inert gases showed the change of rate at which the major weight loss component occurred, i.e the rate of denitration. A highly oxidising atmosphere appeared to give the slowest yield of nitrate gases, whilst under reducing conditions the rate of denitration was comparatively fast. This may be explained by the fact that NO_3^- oxyanions have an oxidising effect on the glass melt, and the increased amounts of oxygen present in the atmosphere also react with the batch components. The weight loss under these circumstances is inhibited as the oxygen from the nitrate components is consumed more slowly than if the batch were melted in a reducing atmosphere where the oxygen from the nitrates would combine rapidly with the batch components.

As-received powdered and heat treated calcine was subjected to X-ray diffraction analysis, the results of which were given in **Figures 4.5.2**. The as-received material was of a poorly crystalline nature, and appeared to be mostly amorphous. Crystalline strontium nitrate and lithium nitrate were detected in all as-received samples. As noted previously, the LiNO_3 arises from additions made to the HAL tanks at an earlier stage of the waste treatment process (Larkin, 1986). $\text{Sr}(\text{NO}_3)_2$ has a low enthalpy of formation of -52.069kJ/mol . Both crystal phases were observed in the heat treated material in decreasing amounts until a temperature of 550°C , consistent with published data (CRC Handbook) for the decomposition of these compounds and the thermal analysis data as discussed in **section 5.1.1** (see **section 4.4** and **Table 4.5.3**).

A rare earth, fluorite-structured oxide phase characterised by broad reflections was identified in the as-received calcine. This was a strong indication of a poorly crystalline, solid solution phase. The rare earth phase, $\text{Nd}_{0.2}\text{Ce}_{0.8}\text{O}_{1.9}$, incorporates many elements within its structure, being loosely based on that of disordered pyrochlore (Müller and Roy, 1974). Studied by Kutty *et al* (2005), Ewing (2005) and Boccaccini *et al* (2003), pyrochlores are currently being researched for use as stand-alone immobilisation matrices for fission products and actinides, and particularly Pu. Pyrochlores, and their antecedents have been found in Synroc, and as a devitrification product in a HLW glass, all of which demonstrates a willingness of the fluorite-type

structure to incorporate a wide range of elements within its matrix. The fluorite (CaF_2) structure upon which the rare-earth oxide is based, is shown in **Figure 5.1.1**.

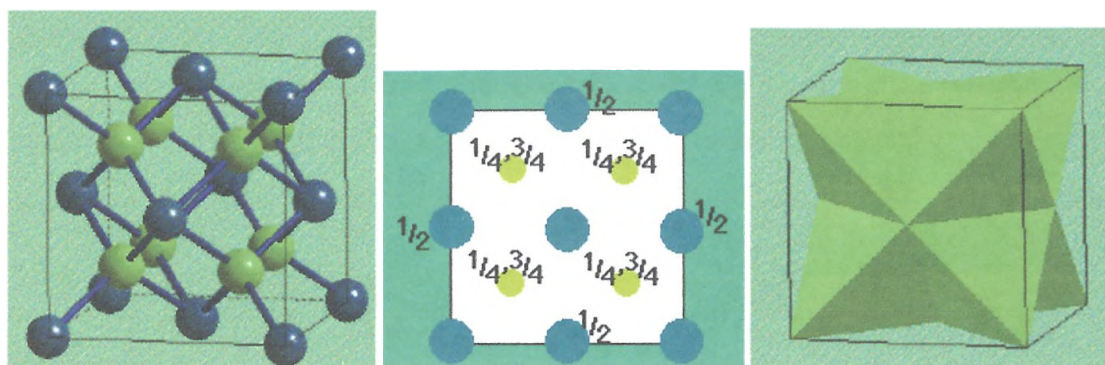


Figure 5.1.1: Fluorite cell shown as (right to left) “ball and stick” model, plan view showing atom positioning within the unit cell, and tetrahedra placement (Heyes, 1999).

Upon heating, the broad XRD peaks remain, indicating the probable presence of several rare earth cations (La, Nd, Ce, Sm, Gd) with a range of ionic radii (1.18 – 1.08Å, for 8-fold co-ordination) (Shannon and Prewitt, 1974) within the fluorite structure. In addition no separate phases containing these rare earths or the actinide substitutes were detected. The fluorite structured rare-earth oxides are present from the calcination stage and onwards. The minor actinides would account for more than half the radiotoxicity of the long-term product, meaning that incorporation within a stable phase is desirable. Actinide surrogates in glass increase in solubility in glass when melted in reducing conditions or at increased (>1200°C) temperatures (Lopez *et al*, 2003). Lopez *et al* (2003) concluded that the Ce solubility (an actinide surrogate) was <0.5mol% for borosilicate glasses at 1350°C, indicating a low solubility of the actinide surrogates within the UK waste glass, supported by the SEM characterisation of the 5-15M25 (**Figures 4.8.9-15**) waste glasses. The rate of denitration within the calcine was increased when calcination took place in a reducing atmosphere (**Figure 4.4.5**). Therefore, this is suggestive that if the calcine was to be in a reduced state before being combined with the glass melt, it would increase actinide solubility and the supply of energy to the glass melter could possibly be decreased.

Evaluation of the as-received calcine sample using SEM and elemental mapping (see **Figures 4.8.1-2**), revealed the segregation of elements in the waste stream to four

different phases. A phase containing the rare-earths, (appearing as white using BE imaging) corresponds to the rare-earth fluorite phase seen using XRD. As noted by Gobichon *et al* (1997) increasing the ionic radius of a rare earth nitrate also means an increase in the temperature at which decomposition takes place. Phases containing these larger rare earths are numerous, and it can be assumed that they are partially amorphous nitrates, as detection is minimal using XRD. **Table 5.1.2** gives ionic radii for the rare earths identified in the compositional analysis of the simulant waste as a means of examining the likely impact on the activation energy needed for decomposition.

Table 5.1.2: Ionic radii of rare earth cations (*Shannon and Prewitt, 1974)

Rare Earth Cation	Ionic radii (Å)*
Gd	1.078
Nd	1.123
Ce	1.15
La	1.185

According to the conclusions of Gobichon *et al*, (1997), La and Nd nitrates would need increased activation energy for decomposition, and Nd is abundant within the waste, at 11.22 oxide wt% (**Table 4.1.1**). The detected rare-earth oxide phase, although easily incorporating cations with a range of ionic radii within its structure, cannot account for the 31 oxide wt% of rare-earths present within the waste stream. It must therefore be considered that the rare earth nitrates contribute considerably to increasing the overall activation energy needed to decompose the nitrate phases which, according to compositional analysis, constitute a large percentage of the waste.

A phase rich in Fe and Al (**Figure 4.8.2**) in the as-received calcine demonstrates the segregation of these refractory forming elements to one phase, which suggests the addition of LiNO₃ to prevent the formation of refractory oxides has been successful. The third phase, which contained some of the Sr, Te and Zr was noted alongside the fourth phase partitioning the rest of the Sr and including Ba, Mo and Cs (**Figure 4.8.2**).

Elemental segregation such as that described above is generally observed specifically in one place in HLW simulants, a phase known as 'yellow phase'. The yellow phase of this study (see **Figure 4.1.3**) contains Mo, Cs, Li, Ba, Sr, Te, Na and Cr. The presence of Sr and Te in one separate phase within the as-received calcine (see **Figure 4.8.2**) and Sr, Mo, Ba and Cs in another phase indicates that a precursor to yellow phase may exist within the raw material. Camara *et al* (1988) discussed the formation of yellow phase in oxidising conditions within a glass, and stated that, if a glass were to be melted under reducing conditions, the valence state of the molybdenum is such that its solubility increases and production of yellow phase decreases. The as-received calcine is produced under oxidising conditions and in the presence of an oxidising agent, which will decrease the solubility of Mo and increase the likelihood of phase segregation, such as that seen in Synroc (Carter *et al*, 1996), discussed earlier. It should be noted however, that Short (2004) does not concur with this, stating that reduction within a glass melt simply allows yellow phase to nucleate and crystallise upon the reduced elements of the melt.

The formation of other crystalline phases from temperatures of 550°C and upwards, suggests that the nitrates, consistent with the thermal analysis data obtained and discussed in **section 5.1.1 (Figures 4.4.1-4)**, have decomposition temperatures below 700°C. The strongly amorphous nature of the material in its as-received form suggests that other, amorphous, nitrates are also present, as it is highly unlikely that LiNO₃ and Sr(NO₃)₂ make up the majority of nitrate based compounds present within this material. Referring to the compositional analysis discussed in **section 5.1.1 (tables 4.1.1)**, the Li₂O accounts for 8wt% of the waste stream, whilst SrO₂ accounts for 2.5wt% of the waste stream.

As seen from the thermal analysis, the amount of nitrate based material is approximately 31wt%. Sr₂(MoO₄), Nd₆MoO₁₂ and CsLiMoO₄ (**Figure 4.5.3,6 and 9**) were identified as forming at temperatures above 750°C. The Sr released from the nitrate contributed to the formation of the molybdate, whilst there was probably some amorphous, unidentifiable material present which would also contribute to the formation of the phase. Since no crystalline Mo containing phases were detected within the sample below 550°C, it was assumed that the molybdenum was also

present in an amorphous form, possibly as a nitrate, again based on the large percentage of the material found to be nitrate based.

$\text{Nd}_6\text{MoO}_{12}$ began to form at higher temperatures, after the rare-earth oxide phase reflections became narrower, indicative of a more crystalline phase. The CsLiMoO_4 identified within the calcine had a cubic structure, and all reflections were easily identified using the ICDD database indicating a single crystalline phase. In contrast to the rare-earth fluorite-structured phase, the peaks for CsLiMoO_4 were very narrow and well defined. The sudden formation of this phase between 750°C - 800°C showed that it had comparatively low formation (and melting) temperatures in comparison with the other calcine constituents, as confirmed by thermal analysis data when a synthesised CsLiMoO_4 produced an intense endotherm at 750°C (**Figure 4.4.2**).

As no crystalline Cs containing phases were detected by X-ray diffraction in the as-received material, it was deemed possible that, as well as CsNO_3 being present in an amorphous form, the Cs may have been associated with molybdenum as there is a known propensity for the two elements of the waste stream to form a separate phase. This is supported by the observation of Cs-and Mo-rich regions with reacting calcine particles (see **Figure 4.8.2**). This has been noted by Carter *et al* (1996) when studying Synroc, who it was found that caesium molybdates are problematic phases that may form if conditions within the melter are not suitably reducing. DSC (**Figures 4.4.14-21**) shows thermal events associated with a possible crystal phase in the as-received calcine which “melt out” at the higher temperatures, leaving only 2 obvious peaks to be identified. These peaks may arise either from the denitration and recrystallisation processes occurring simultaneously. Reactions at ~ 380 - 600°C are attributed to a combination of the two processes of denitration and phase recrystallisation. The reaction occurring at $\sim 230^\circ\text{C}$ is thought to be due to melting of LiNO_3 .

Above temperatures of 700°C , a secondary rare-earth oxide phase formed at a lower 2θ angle as a ‘shoulder’ on the fluorite peaks already present. This secondary phase was accompanied by the development of a tertiary phase at $\sim 900^\circ\text{C}$, and the subsequent disappearance of all except the originally identified phase at 1000°C . As explained previously, due to the nature of fluorite, and the number of elements within the waste stream, the specific secondary and tertiary phases which form at 700°C and

above cannot be identified. MgO was also identified as forming at higher temperatures. This refractory oxide was only observed above 1000°C, but may not have contained all the Mg present in the waste form due to the ease of incorporation of Mg into the fluorite phase and the fact that MgO formed only after the decomposition of the secondary and tertiary fluorite phases. MgO is known to be a problematic phase within glass melts if it is present in increased amounts. However, in small amounts Mg will stabilise the glass melt, which in turn increases chemical durability, as discussed by Donald *et al* (1997).

The infra-red spectrum of the as-received material (**Figure 4.6.2a**) has some interesting features and strong absorption bands. The most dominant feature of the calcine subjected to FTIR were the absorption bands at $\sim 3430\text{cm}^{-1}$ and $\sim 1387\text{cm}^{-1}$, attributed to the O-H and N-O vibrational bonds of H₂O molecules and the NO₃²⁻ oxyanion, which confirmed the high water and nitrates content first identified using DTA/TGA (**Figure 4.4.2-4**). The subsequent decrease of the intensity of the band (**Figure 4.6.2d**) attributed to the H₂O molecule was therefore fully expected, as was the decreasing intensity of the N-O band in samples heated between 400-600°C. The absorption band which resolves into two components as heat treatment progresses (**Figure 4.6.2j**); a broad band (at 1550-1250 cm^{-1}) and a sharp band at 1385 cm^{-1} ; is associated with a vibrational effect directly connected with the evolution of the nitrate phases as they decompose. The bands and their associated movements with the NO₃ group are listed in **Table 5.1.3** (Liu *et al*, 2005). These bands, which disappear at 800°C, coincide with the decomposition of all nitrates within the system, and the subsequent formation of other crystalline phases due to the release of cations from the amorphous nitrates. It is likely therefore, that as this band is no longer present in the system at 800°C, it is a vibrational component of the both the amorphous and crystalline nitrate phases believed to be present in the system, as discussed earlier in reference to XRD (**Figures 4.5.2**).

Table 5.1.3: Wave numbers and assigned groups (compiled from Liu et al, 2005)

Assignment	IR (cm ⁻¹)
O-H	3420 (C ₁)
NO ₃ ⁻ (asym. str)	1370
NO ₃ ⁻ (sym. str)	1045
NO ₃ ⁻ (sym. bend)	830

The band which remains unchanged from 400-700°C in the NO₃⁻ group can be attributed to the presence of nitrate groups which decompose at higher temperatures, in particular Sr(NO₃)₂. The broad band is consistent with the N=O stretch of an M-ONO group, possibly amorphous rare earth nitrites.

Other vibrational bands, related to the Mo-O stretch of SrMoO₄ and the MoO₄²⁻ group (**Figures 4.6.2k**) are present in all samples, further confirming that amorphous molybdates are present. These bands exist at 808-846cm⁻¹ and concur with the data obtained by Nazri and Julien (1995) and NIST. Between 700°C and 1000°C these bands become increasingly intense, and XRD reveals the presence of molybdates (**Table 4.5.3**). SrMoO₄ is not observed using XRD at higher temperatures. However, CsLiMoO₄ is observed at the higher heat treatment temperatures (**Figure 4.5.3**), and it is likely that the MoO₄²⁻ stretch can be associated with either of these compounds and their molybdate groups.

As the heating of the calcine progresses, the general microstructure of the particles becomes finer, indicating that more of the material has reacted to give a finer, polycrystalline structure. At 400°C, SEM and elemental mapping (**Figure 4.8.4**) highlights the segregation of Mo, Sr and Cs to the same phase, whilst the Nd segregates to a separate Mo, Zr and Cs containing phase. Ce and Gd appear to be in one phase, and Al and Fe separate to another phase. The rare-earth rich phase is consistent with the fluorite structured crystal phase, whilst the segregation of Zr and Nd to a distinct molybdate phase (apart from the Sr) indicates a decomposition of amorphous nitrates of Zr and Sr consistent with thermal analysis data obtained by Chun (1977), and a segregation of a Zr molybdate containing phase, as often encountered in solids formed from simulated nuclear fuel reprocessing solutions. Rao

(1989), Penneman (1980) and Lloyd (1976) all report the presence of Zr molybdates upon solidification of aqueous HLW, which contains considerable amounts of the Pu present in the waste stream. In this simulant case, it is noted that Nd segregates to the Zr molybdate phase and Nd is often used to represent other fission products and actinides in simulants. The same phase segregation of rare earths to one phase and Sr, Mo and Cs to another is seen in subsequent heat treated samples, and it can be assumed that the phases present are as those discussed earlier identified by XRD (**Figures 4.5.2**). At 700°C however, Nd and Zr segregate to separate phases (**Figures 4.8.5**), coinciding with the formation of the secondary fluorite phase, suggesting that Zr is a constituent of the secondary fluorite-structured phase, as it does not appear in a phase with the rare-earths identified by SEM. ZrO₂ itself has a distorted fluorite structure, and the known industrial process of stabilising zirconia with rare earths (Cotton *et al*, 1999) suggest easy formation of a rare earth containing, cubic zirconia phase.

No evidence of Mo within Nd and Zr containing phases at 1000°C is indicative of the complete formation of CsLiMoO₄ and the possible re-incorporation of Nd and Zr to the fluorite type phase upon decomposition of the molybdate containing phases. Backscattered electron images of the “yellow phase” formed on the surface of sintered and quenched calcine above 1000°C confirm the presence of Cs and Mo in the majority of samples, and also Sr, Te and Cr. The EDX analysis highlights the presence of Mo and Cs in the same phase, and also the presence of minor elements such as Sr, Te and Cr. When examined more closely under the electron microscope, the yellow phase consists of two very different looking microstructures, one of a finer nature than the other. The finer matrix is porous and surrounds grains ranging from ~4 to 10µm in size. The nature of the layer is in line with the density measurement which showed that the density of a major component of yellow phase was approximately 70% that of the calcine (see **section 4.3**), and gives reason for the almost immediate appearance on the melt surface of the yellow phase. The phase evolution, determined by characterisation methods discussed here, is summarised in **Figure 5.1.2**.

TEM of heat treated and as-received samples demonstrated the same propensity for Cs and Mo to combine in one phase, alongside Sr, with rare earths often combining to

form a separate phase and confirms the existence of this amorphous precursor to yellow phase within the simulat calcine.

Hence the phase evolution within the simulat calcine on heating is represented in **Figure 5.1.3** and can be summarised as follows:

- Dehydration of sorbed water (at 230°C and 373°C) Stage I in **Figure 5.1.3**
- Denitration beginning at ~250°C with the decomposition of major crystalline nitrate components. Formation of rare-earth, fluorite-structured oxide phases and assumed to contain R.E's, Zr and Fe (from as-received temperatures and above). Stage II in **Figure 5.1.3**. Actinde surrogates are segregated within this phase.
- Formation of secondary fluorite-structured and molybdates coinciding with the decomposition of amorphous and crystalline nitrates and the formation of CsLiMoO₄ (identified to be major yellow phase constituent) from 700°C to 900°C. Stage III in **Figure 5.1.3**.
- Complete disappearance of all amorphous phases by 1000°C, coinciding with the disappearance of secondary and tertiary fluorite-structured phases and complete crystallisation of the calcine, with a CsLiMoO₄ liquid phase melting and separation. Stage III in **Figure 5.1.3**.

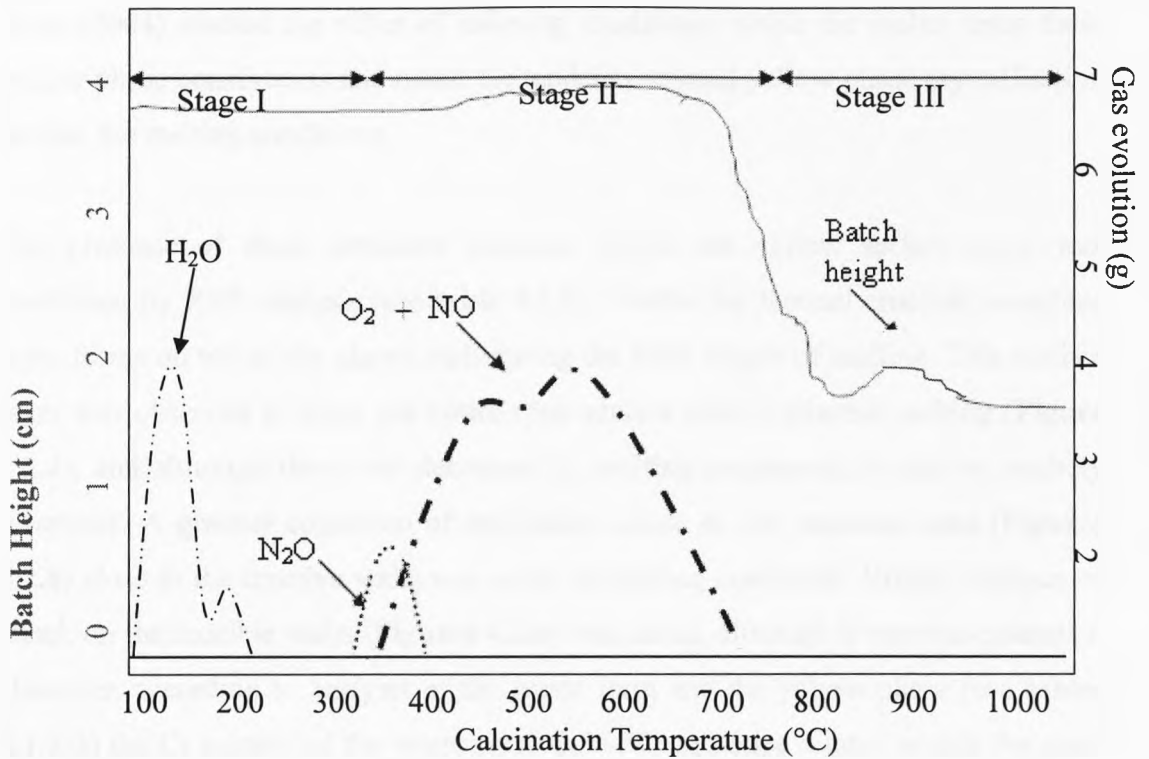


Figure 5.1.3: Off-gas concentration profiles and relative batch height during heat treatment of the calcine.

5.2 Waste Loaded Glasses

5.2.1 Yellow Phase

Samples of “yellow phase” found in V26 glass are consistent with published data for the composition of this yellow phase. Owens (1981) states that the yellow phase is often found to be composed of 70% alkaline earth molybdates and 30% rare earth molybdates. The compositional analysis (**Table 4.1.3**) suggests that the yellow phase analysed from the large scale V26 simulant glass is composed of Sr, Cs, Na, Te, Li and Ba molybdates, as Mo makes around 60wt% of the yellow phase. The formation of the yellow/green low melting point phase, both in the calcine upon heating and in the glass melt, is consistent with the literature discussed in **chapter 2.7**. This surface layer and similar ones having a high percentage of chromates and sulphates were seen in studies by Li, Hrma and Vienna (1992) and are known to accelerate corrosion of

Hrma (1992) also notes that a yellow coloured phase that contains elements that are poorly soluble in borosilicate glass is formed very early on in the melting process. Short (2004) studied the effect of reducing conditions within the melter upon these yellow phase constituents and noted the tendency toward yellow phase crystallisation despite the melting conditions.

The presence of these insoluble elements within the yellow surface layer was confirmed by XRF analysis (see **table 4.1.3**). Within the Inconel crucible, a surface layer forms on top of the glassy melt during the early stages of melting. This surface layer was observed to cover the entire melt surface after 5 minutes melting (**Figure 4.2.4**), and although the cover decreased as melting progressed, it did not entirely disappear. A gradual collection of the yellow phase in the meniscus area (**Figures 4.2.6**) close to the crucible walls was noted as melting continued. Visual evidence of attack on the crucible walls (**Figures 4.2.6**) was noted, although it was not extensive. However, according to analysis of the waste form and the yellow phase (see **tables 4.1.2-3**) the Cr content of the waste was <0.5wt%, and once diluted within the glass matrix, was below the detection limits of the SEM. In all glass samples, Cr was present, and was detected in some yellow phase samples (<4.1wt%). Thus, this shows that the detrimental yellow surface layer segregates before it can be dissolved by the glass- forming melt and begins to corrode the crucible, leaching Cr (and Ni) into the melting process although the extent of this reaction in the current experiment was limited.

Synthesised CsLiMoO₄ was analysed using TA to determine its melting point given the identification of this phase with the use of XRD (see **section 4.5**). The melting point, determined as ~780°C, demonstrates the ability of this phase to form at low temperatures and therefore, as suggested previously, this phase will form and segregate from the body of the melt before it dissolves in the glassy melt.

The segregation of La was also noted within the yellow phase upon examination of the surface of samples 5M25 and 10M25 (**Figures 4.8.9-12**). La could not be detected within the calcine as the Nd, Gd, Ce, and Fe all produced strong signals in the EDX detector, and the R.E elements have very similar L_α and K_α lines. Other rare earths

were all present in increased concentrations of up to 12wt%, in comparison to La (3wt%). Once diluted within the glass, it was not expected that La would be at the detection limits of the microscope when well dispersed, but as it concentrated in one phase, it could be detected upon spot analysis of the yellow phase. The La segregation to the yellow phase is unusual as it would be expected that the rare earths would all behave in a similar manner, and segregate to the same fluorite structured phase observed in the heated calcine (**Figure 4.5.2**). La containing compounds were not detected using XRD, but it is possible that they were present but in insufficient quantities to be detected. The cationic radius of Cs is 1.675Å compared to that of La (1.185 Å), therefore, although La is extremely small compared to Cs, La would substitute for Cs within the cubic CsLiMoO₄ structure, and may not yet be detected by XRD. The difference in charge and ionic radii does not fit well with Goldschmidt (1937), but Goldschmidt's theory has since been proved to be too simplistic. An example is the incorporation of the smaller La³⁺ ions (1.185 Å) in a large site in clinopyroxene, normally occupied by Ca²⁺ ions (1.74Å)*. This substitution requires the presence of a charge compensating cation or anion elsewhere within the lattice (Blundy *et al*, 2003). Other examples of such substitutions are found in geopolymers. Geopolymers are based on aluminosilicates are designated as poly(sialate), which is an abbreviation for poly(silico-oxo-aluminate) or (-Si-O-Al-O-)n (with n being the degree of polymerization) (Davidovits, 1988). Na is present within a geopolymer to act as a charge compensating cation due to the presence of the Al cation. It is believed that Li could act as the charge compensator in a CsLiMoO₄ structure which contains La³⁺ on a Cs⁺ site. It is also possible that a lanthanum molybdate phase was formed, based on the Na₅La(MoO₄)₄ identified in **figure 4.5.6**. The XRD peaks are slightly shifted as higher angles are reached indicating a possible solid solution. There is very little Na present within the simulated waste (0.15wt% **Table 4.1.1**), but Li is added to the waste stream. LiLa(MoO₄)₂ has the same space group (I41/a) as the sodium molybdate indicating that solid solution substitution of some of the Na with Li may have occurred, creating a (Na,Li)La(MoO₄)₄.

Table 4.1.2 gives the yellow phase composition as found in a full-scale, blend glass, in which Cs and Li are thought to form a molybdate phase, and strontium molybdate

* N.B. All ionic radii are taken from Shannon and Prewitt (1974)

is also believed to be a constituent due to the segregation of Sr and Mo to the same phase (**Figure 4.8.2**) and the detection of this phase (**Figures 4.5.2 and 4.5.11**). Li_2O accounts for 20mol% of the yellow phase composition, where Cs_2O accounts for 10mol%, leading to the conclusion that the mixed alkali molybdate which is formed and the Li which is not bound within the CsLiMoO_4 structure is incorporated into another molybdate phase. The presence of Te within the yellow phase suggests a Te compound. BaTeO_4 and MgTeO_4 are isostructural with MgWO_4 (Cotton *et al*, 1999), which has a powellite structure found in yellow phase by Short, (2004). This suggests that these phases may have been formed, or the components associated with one another, within the yellow phase. However, in a reduced state, Te forms complexes of the R_3TeX nature in the IV oxidation state (with its highest, stable oxidation state being VI). This suggests that a reducing atmosphere within the calciner might encourage the formation of a tellurite complex and prevent segregation to a yellow phase.

The difference in behaviour compared to the other rare earth cations could arise due to the large size of the La^{3+} cation in comparison to other lanthanides. Basic nitrates of La are also the most soluble of all the lanthanide nitrates (Krebs, 1968), leading to the conclusion that, in the glass melt the La dissolves from the calcine first and segregates to the yellow phase, which is the soluble low melting phase formed first.

5.2.2 Waste Digestion

Simultaneous TGA/DTA of several fully loaded waste samples (**Figures 4.4.6-9**) illustrates the fact that final incorporation of the waste into the glass does not take place until 1000°C. The endothermic event which begins at 900°C and is complete by the time the material reaches 1000°C is attributed to the final digestion of the waste by the glass melt. This agrees with Owens (1981), who showed that, at temperatures below 1050°C, incorporation of the waste within the glass is incomplete and yellow phase formation is predominant from 850°C to 1050°C. Therefore, it must be assumed that, as the thermal analysis samples are extremely small ($\geq 50\text{mg}$), reaction temperatures have been shifted slightly downwards, and that the incorporation of any

yellow phase formed in these small samples is complete at 1000°C (as opposed to 1050°C) as no more features are observed in the thermal analysis data.

The curve obtained for many of the glass/calcine mixtures using DSC (e.g. **Figure 4.4.16**) has a baseline which is not constant or flat. This is attributed to the fact that the mixtures were already glassy due to the presence of the base glass frit, and so there is no obvious peak for the expected liquid. There is a break in the curve around 520°C (**Figure 4.4.15**) where the T_g should be, and a gradual slope, indicating a slow transition from a solid to a 'free-flowing' liquid. No apparent crystallisation peaks are seen on the DSC curves for the glass and calcine mixtures (**Figures 4.4.14-15**) indicating the formation of the crystalline CsLiMoO_4 may be a low energy reaction and that it may be present in the waste form as a pre-cursor phase. Digestion of the CsLiMoO_4 (into the glassy melt) may also be relatively small in terms of energy expenditure, when compared to the re-melting of the glass.

The relative ΔC_p of the glasses when re-melting and digesting waste decreases as the waste loading increases (**Table 4.4.2**). This suggests that melting increased amounts of glass to achieve a lower waste loading is not energy efficient (**Figures 4.4.16-18**). It would be expected that the increased waste loading would be a contributing factor to increasing the C_p but it appears that at these lower waste loadings the energy needed to re-melt the borosilicate frit ($5.91\text{Jg}^{-1}\text{K}^{-1}$) is dominant. The energy needed to denitrate and recrystallise the calcine is $1.82\text{Jg}^{-1}\text{K}^{-1}$. Therefore the energy expended in re-melting the borosilicate frit is a considerable and notable contribution to overall energy expenditure.

It is upon addition of the heat treated waste stream to the glass, however, that the relative total heat capacity of digestion of the waste in the glass differs notably. Referring to the relative C_p measured for 25wt% oxide waste loadings (**Figure 4.4.19-21 and Table 4.4.3**), it becomes obvious that the development of this yellow phase is not the only problem when melting the waste. The as-received calcine is more difficult to incorporate into the glass in terms of energy than calcine which has previously been heated to 400°C and held. It requires 1.4 times the energy input into the melting system to fully incorporate the as-received sample within the frit. The as-received calcine compares favourably, however, with the sample heated to 700°C,

which is the most difficult to incorporate and requires almost twice the energy of the as-received sample. Surprisingly, the sample heat treated to 1000°C has a lower energy of incorporation within the glass than the as-received waste (**Figure 4.4.22**). The lattice energy of a crystalline phase is defined as the energy liberated when a crystal lattice is formed by the electrostatic binding of its constituent cations and anions from the gaseous state. According to Krebs (1968), the lattice energy can be broadly related to the melting point and solubility of crystal structures, so if the lattice energy is high, the melting point will be correspondingly high. For the simpler compounds detected within the simulant calcine, the lattice energies were found to be as shown in **Table 5.2.1**.

Table 5.2.1: Lattice Energy for simple oxides of crystalline compounds identified within heat treated calcine (* taken from Jenkins, 1998)

Oxide	Lattice Energy* (kJmol ⁻¹)	Melting pt* (°C)
Nd ₂ O ₃	12736	2320
Ce ₂ O ₃	12661	2230
La ₂ O ₃	12452	2305
MgO	3795	2830
SrO	3217	2530
Li ₂ O	878	1570
CsO ₂	668	490

Table 5.2.1 illustrates that oxides of the rare earths, Mg and La all have large lattice energies and correspondingly higher melting points. Li- and Cs- containing phases have lower lattice energies and melting points. Although these simpler oxides are not found within the heated calcine, it can be assumed that the trend observed here means that crystalline phases detected within the calcine at temperatures of 700°C and above (see **Figure 4.5.2**) had increased melting points and were of lower solubility within the glass. This leads to the increase in heat capacity (**Figure 4.4.22**) needed to digest the waste once it has been heat treated.

It is therefore recommended that the waste stream be heated to 400°C before being combined with the glass frit. At 400°C there is still a high (~24wt%) nitrate content suitable for complexing Ru and preventing volatilisation, and from optical observations it can be said that the calcine is not sticky nor contains a high percentage of fines at these temperatures. Both parameters affect the technical operation of the calciner and melter, as an excess of sticky material or fines clogs up the dust scrubbers and the valves which release the calcined material into the glass melter. This is in agreement with Ramshaw (1985) who examined the nature of nitrate content versus particle size. Ramshaw observed that the low nitrate content calcine exhibits slow reactions upon melting, and increasing the nitrate content serves to decrease the reaction times. The calcine also becomes more refractory in nature at low nitrate contents. Thus, the waste, once heated and fully denitrated, the calcine becomes difficult to fully digest in the glassy melt, although the relevant heat capacities would strongly suggest that the subsequent decomposition of such compounds within the calcine at 1000°C makes digestion easier. The formation of the SrMoO₄ phase, as observed in the calcine when heated to temperatures of 750°C and above, confirms this theory.

Scheetz and Freeborn (1982) were particularly instrumental in the development of a 'supercalcine ceramic' for immobilisation of reprocessed commercial nuclear waste, which consisted of a ternary system of molybdate phases of calcia, alumina, strontia and silica. The thermal stability of increased strontia containing phases was good in comparison to other scheelite phases and equilibrium of the ternary systems was easily achieved. The detection of SrMoO₄ within the calcine heat treated to 1000°C (see **Figure 4.5.11**) and lack of detection within the waste loaded glass (**Figure 4.5.13**) means that the dissolution must have been complete (due to convective currents and mixing) and this stable phase no longer had to be digested by the glass melt.

Analysis of waste loaded glasses analysed using XRD became difficult as heat treatment temperatures are increased, due to the presence of the amorphous hump, in the XRD pattern. However, a series of glasses which were analysed after being air quenched (**Figures 4.5.13**) revealed the development of similar phases to those found in the calcine, as discussed in **section 5.2**. The fluorites were in evidence, as was

CsLiMoO₄. McKeown *et al* (2002) studied the environments of Sr within borosilicate glasses with varying Sr content (~2-30wt%) and found in all cases evidence of Sr²⁺ within the structure, regardless of the processing parameters. Evidence of Mo and Sr within the yellow phase from compositional analysis indicates a strong likelihood of SrMoO₄ formation as part of the yellow phase. As discussed previously, SrMoO₄ is a stable phase, and if incorporated into the corrosive, immiscible yellow phase, it is unlikely to easily dissolve within the melt liquid. The MoO₄²⁻ group within the SrMoO₄ component of the yellow phase may, therefore, not be incorporated into the glass structure. According to Calas *et al* (2003) and Short (2004) Mo is present in a tetrahedron coordinated to oxygen in the form of molybdate groups [MoO₄]²⁻. Studies of both simplified borosilicate glass and glasses containing full waste streams (Short, 2004) show that these groups are not directly linked to the borosilicate network but rather located within alkali and alkaline-earth rich domains in the glass. This specific location in the glass network is a route to understanding the low solubility of Mo in glasses melted under oxidizing conditions. It also explains the possible phase separation of yellow phase enriched in alkali molybdates in molten nuclear glasses.

A sample of the surface of a glass revealed the presence of CsLiMoO₄, concurrently with the presence of a yellow phase observed on the glass surface. The low melting point of CsLiMoO₄, and other molybdates (observed in compositional analysis of the yellow phase) strongly suggests that the segregation of the yellow phase to the surface of the melt happens almost immediately upon melting due to the fluid nature of the molybdates. Scheiwer *et al* (1982) confirms that the yellow phase within a large scale, simulant HLW did indeed segregate to the top of the melt, to form a layer almost 3mm thick. The CsLiMoO₄, as the only synthesised component of the yellow phase, was found to be porous in nature (**Figure 4.8.8**) although of a similar density to the calcine, indicating a natural tendency to float on the melt surface.

GC-MS (**Figures 4.7.1-3**) revealed an offgas which consisted mainly of nitrate derived gases, and which corresponded to the temperatures at which the main weight losses took place as determined by TGA. The evolved gas was almost completely composed of NO in both inert and oxidising atmospheres, as expected due to the residual nitrates present in the calcine. The total amount of NO evolved whilst in He-O₂ and in He confirmed a high weight loss of almost 20wt% of the batch due to

denitration. Ramshaw (1985) concluded the effective amount of residual nitrate within the batch was between 15%-34%.

During larger scale melting of a 10g batch in a dynamic He atmosphere, NO, and N₂O were also detected. Scott *et al* (1985) lists three categories of species found in the off-gas of HLW with decreasing volatility (**Table 5.2.1**). N₂O, NO_x and O₂ are all included within the most volatile categorisation.

Table 5.2.1: Types of off-gas species (Scott *et al*, 1985)

Gases (most volatile)	Semi-volatile	Particulate
H ₂ , O ₂ , CO ₂ , N ₂ O, NO _x , SO _x	Compounds of Na, Li, K, Cs, Mo, Ru, Sr, Se, Te, B and halogens	Fe, Al, rare-earth, all other feed components

The evolution of the two NO_x gases took place at different times during the melting process with most of the N₂O evolved in the early stages of the melt, from around 135°C to 335°C, concurrent with the onset of melting of LiNO₃. The NO detected by the GC-MS began to evolve at 280°C, and finished around 695°C. In total, 0.0229 moles of NO were evolved, 0.0053 moles of O₂ and 0.0010 moles of N₂O from a 10g melt conducted under inert conditions. The correlation of the evolution of NO and O₂ may indicate that the evolved gas was actually NO₂, which splits into NO + O₂ at the high temperatures experienced within the crucible:



If the more stable NO₂ was ionising upon contact with the detector, then the number of moles of NO associated with this ionisation would be 0.0106 moles, leaving a total of 0.0123 moles NO and 0.046 moles N₂O. This is equivalent to 0.904g in total of gas evolution. For 1 mole NO₃ in the sample, 3 moles of O⁻ are required, meaning 1.1952g of O. The difference occurs because not all of the oxygen within the sample will be present as NO₃⁻ anions, but some will form oxides as the nitrates decompose. The NO₂ and N₂O gases must be “cleaned” from the offgas system, due to NO_x emission laws which state that a maximum of 21ppb (parts per billion) NO₂ are allowed into the atmosphere annually (DEFRA, 1999). NO_x gases are recovered in the offgas system with a filter membrane immersed in water. The combination of water

and NO_x (whether NO_2 or NO), forms nitric acid which is then re-introduced to the system via the HAL tanks. N_2O however, cannot be “scrubbed” in this way as it does not recombine with water to give nitric acid, presenting a problem if N_2O is an offgas product.

Approximately one third of the waste was lost to gas evolution. The gas evolution begins at around 250°C and continues to 740°C . This corresponds with the melting and decomposition points of LiNO_3 at 264°C , and $\text{Sr}(\text{NO}_3)_2$ at 570°C , the only two identifiable components of the waste. At temperatures below 800°C , Chun (1977) suggests that the decomposition of CsNO_3 proceeds via decomposition of the nitrate to the nitrite, and finally to the oxide, supported by Scott *et al* (1985) who list compounds of Cs as being semi-volatile, and NO_x gases as being extremely volatile. The decomposition of $\text{Sr}(\text{NO}_3)_2$, consistent with published data, occurred rapidly at 600°C . Chun also shows that the decomposition of a zirconia nitrate occurs rapidly from 170°C to 260°C , corresponding with the gas evolved early in the melting process and lack of detection of Zr containing compounds using XRD (**Figure 4.5.13**). Selected rare earth nitrates are decomposed completely in air at $\sim 600\text{-}700^\circ\text{C}$ (see **Figures 4.4.10-13, Table 4.5.3**), which corresponds to the finish of gas evolution at 695°C . The difference in temperature may be accounted for by the fact that the melting and boiling points of products can be influenced by other compounds *in situ*, and as the waste stream is compiled of nearly 40 components, it would be reasonable to suggest that these components have influenced decomposition temperatures.

During GC-MS analysis of a large scale batch (**Figures 4.7.4**), the melt was observed through a silica window inserted in the furnace. The reader is referred to the compact disc included with this work and the results in **section 4.7**. Evolution of brown NO_x gases, visible to the naked eye, is observed in large volumes from 400°C onwards. The fusion of the glass frit, beginning around 800°C , is consistent with reports by Matyas *et al* (2002) who report that the glass forming melt becomes interconnected at around 800°C and so the open porosity stops and digestion of the waste, or corrosion of the particles by the liquid (Lee and Zhang, 1999) becomes easier. This is re-confirmed by the thermal analysis data (**Figures 4.4.6-9**) of fully waste loaded melts.

SEM analysis of the waste loaded glasses melted at a constant T and varying times (**Figures 4.8.9-15**) yielded useful information on the behaviour of the calcine within the glassy matrix. The rare earths and Zr stayed within the calcine particulates and proved more difficult for the glass forming liquid to incorporate. This follows the work of Ewing (2005) and Boccacini *et al* (2003) who studied pyrochlore related phases for possible use in glass matrix composites (GMC's) to immobilise high level wastes. These fluorite-structured phases prove more difficult to dissolve within the melt, thereby proving problematic as the calcine releases other waste stream elements in preference.

When the simulant waste underwent a pre-treatment process and was then added to the glass frit (**section 4.8.1 Figures 4.8.3-6**), the surface of HT400G had a different microstructure to previous samples, and was discernably different to other samples which had been heat treated concurrently. HT400G (**Figure 4.8.4**) appeared to have a surface layer composed of a eutectic phase. Eutectic phases are low melting phases, and the lowest temperature at which two materials will melt, often completely different from the melting temperatures of the separate constituents. The formation of this eutectic phase coincides with the same glass batch having the lowest relative heat capacity, suggesting a strong link between the two. A eutectic is, by definition, a low energy phase. If the solids which form the eutectic are imagined as the vertices of a polyhedron (in compositional space), then reaching the equilibrium point in this composition space where the liquid plot falls inside the polyhedron whose vertices are the solid compositions, the overall energy of digesting the waste is effectively reduced.

Segregation of Cs, Mo, Sr, Te and La (**Figures 4.8.10**) to the surface of the glass melt almost immediately is another problem concerning the melter (see **section 5.2.1**). This is indicative of SrMoO_4 , CsLiMoO_4 and other soluble alkali molybdate formation, and possibly volatile Cs compounds such as caesium pertechnetate forming. This phase would not have been observed in the current work as no technetium was present in the simulant waste stream, although it would be present in the real waste.

Analysis of the NO_x deposits on the quartz crucibles used for GC-MS indicated that a Cs deposition had occurred, as expected due to its volatile nature (Chun, 1977), and

also a Mo deposition in needle like form, accompanied by either Te, Fe or Cr. Te and Cr are key constituents of the yellow phase, and it would suggest that not all of the yellow phase constituents are incorporated into the glass. It is possible that the batch foaming reactions are so vigorous, as noted by Hrma (2002), that elements of the yellow phase were carried with the offgas and plated out on the crucible wall. However, it is more likely that Mo, released due to the relatively rapid dissolution of the HLW in the presence of convective currents at the liquid-solid interface, forms MoO_3 which is above its melting point but not yet at its normal vaporisation temperature, vaporises due to the higher oxygen activity at the melt surface which promotes vaporization of MoO_3 , plating out on a cooler part of the crucible alongside the NO_x residue, along with the Te and Sr. All the constituents of the yellow phase have relatively low vaporisation points, so it is possible that a combination of reactions took place, and that vaporisation of the yellow phase and separate yellow phase components occurred simultaneously. The deposition of Mo, Sr, Fe and Cs on the crucible walls above the melt (**Figures 4.8.23-28**) during GC-MS studies also concurs with the conclusion of Scott *et al* (1985) that compounds of these elements are semi-volatile. Langowski *et al* (1996) conclude that the potential exists for semi-volatiles to leave the melter (as part of an aerosol), and condense as sub-micron particulates in cooler parts of the system. Perry *et al* (2001) also found deposits of Fe, Mo, Cs and Cr, amongst which were identified (using XRD) $\text{Fe}_2\text{Fe}(\text{BO}_3)\text{O}_2$ and $\text{LiAl}(\text{MoO}_4)_2$. Perry *et al* (2001) conclude that some elements found upstream of the melt were volatilised from the melt and others were entrained from the melt surface.

From the offgas studies and the microstructural examination of the heat-treated waste, it can be concluded that, although the waste within the calciner is meant to reach temperatures of $>300^\circ\text{C}$, it is in fact only reaching temperatures of around 200°C . This can be concluded from the presence of crystalline LiNO_3 , and the evolution of NO_x gases (possibly arising from amorphous zirconia nitrate) as soon as the sample reaches 170°C . The presence of sorbed water (**Figure 4.4.2**) is further evidence of the low temperature which the calcine has undergone in the calciner. Evidence in this study suggests that the calcine is more easily digested by the glassy melt if homogeneously heated to 400°C . At this point of the heat treatment some nitrate content remains (**Figures 4.4.4**), but the energy required to digest the waste is approximately 1.4 times less than is currently being used. According to Scott *et al*

(1985) and Cains *et al* (1992), ruthenium volatilisation in any form did not occur below temperatures of 110°C. According to Igarashi *et al* (1993) Ru volatilisation was not significant up to 135°C. However, at temperatures above 135°C, all authors concur that Ru volatilisation is significant, but that with evaporative preparation at 120°C (Cains *et al*, 1992) Ru volatility at 400°C is less (~2%) than that of calcine heated to 200°C (~4%). Igarashi *et al* (1993) showed that at above 300°C some nitrosyl-ruthenium complexes are volatilised, but most of them decompose into RuO₂ and remain in this form in the dry waste. These are significant results when comparing the findings of this work, giving good reason for the calcination process to have an effective temperature of 400°C within the rotary tube calciner.

The melting of glasses under reducing, oxidising and inert atmospheres (**Figures 4.4.6-9**) suggested that the temperatures for complete waste incorporation varied. In a completely oxidising atmosphere, incorporation took place at 965°C, in air at 913°C, in inert atmosphere at 870°C and in a reducing atmosphere at 800°C. This supports the suggestion made by Camara *et al*, (1988) in which a reducing atmosphere is desirable in suppressing yellow phase formation. However, as a reducing atmosphere would lead to an increase in metalloid phase formation (Short, 2004) this is not a viable suggestion. However, the use of an inert atmosphere does not appear to have any detrimental effects upon the melt, and so is suggested as an alternative to the air sparge currently in use.

Based on the microstructural studies discussed here, a phenomenological model (**Figure 5.2.1**) for the early waste digestion in the glass melt is proposed that illustrates the basic mechanisms of dissolution in three stages. These stages of incorporation have been broken down into several parts, based on thermal, diffraction and microscopy analyses.

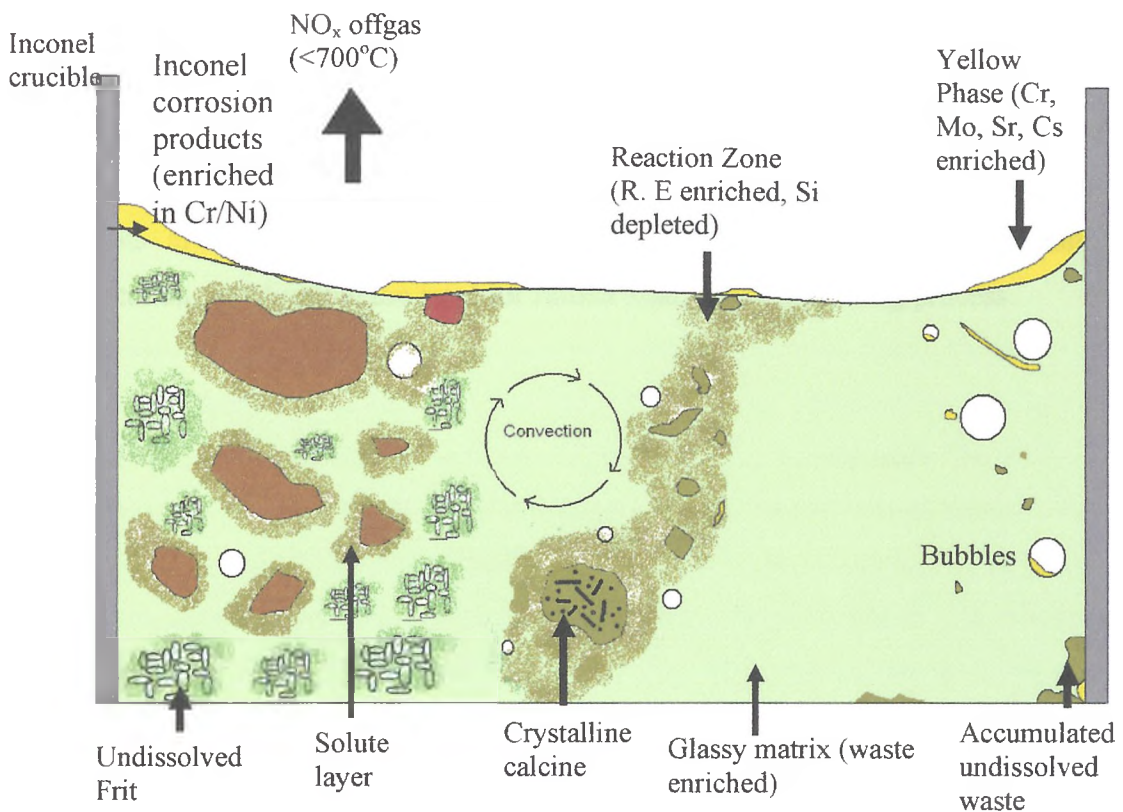


Figure 5.2.1: Proposed phenomenological model for the dissolution of simulant HLW in borosilicate frit (increase t/mins from left to right).

These stages are summarised as follows:

- Dissolution of common yellow phase constituents from HLW, forming yellow phase on melt surface and corroding Inconel crucible. Corrosion products incorporated into the yellow phase. Many gas bubbles arise due to the porous nature of the calcine and the presence of frit. HLW remains enriched in rare-earths.
- Convection and offgas (due to nitrate decomposition) induced dissolution of the waste form occurs. Glass surrounding waste develops solute layer and becomes enriched in rare-earths and depleted in the Si. Internal microstructure of calcine takes on crystalline/needle structure, rich in rare-earths and Zr. Yellow phase begins to mix with the bulk of melt.
- Incorporation of the waste into the glassy melt. The glassy matrix becomes enriched with waste elements. Gas bubbles are still present in glass, often containing the yellow phase. Denser, accumulated, undissolved waste collects and promotes crucible corrosion.

Evidence suggests that the process of incorporating the waste into the glass takes place in several stages, which include partial denitration and crystallisation. The waste loading of the glass is also an influential factor in determining the technical parameters for operation of the vitrification line, and the phases segregation of the calcine suggests amorphous precursors exist within the waste prior to calcination and vitrification, highlighting the need for further studies of the melting process.

Chapter 6: Conclusions and Further Work

6.1: Relevance to Real HLW Glass

It was thought that this simulant waste, having undergone processing on an inactive vitrification line during commissioning, was suitable for characterising the behaviour of the glass melt. The omission of Ru is not believed to be detrimental as yellow phase formation is only increased upon the presence of Ru, so allowing the study to be undertaken with the proviso that there may be more crystal phase present within a Ru-containing waste. The lack of radioactive simulant was not deemed to be a problem due to the nature of the study within the glass melter. The predominant effects within the melter are the heating, corrosion and incorporation of the waste into the glass melt, as opposed to radiation damage effects. Therefore, the simulant was used and added to glass frit (used to vitrify real HLW), in an Inconel 601 crucible at temperatures specified by the industrial process. An air sparge was not used due to technical difficulty of this process and the risk of losing batch in the furnace. In particular an air sparge would destroy all evidence of reactions on the feasible experimental scale. The lack of sparge means the mechanisms proposed for dissolution may be faster in the real process. However, the 5-15M25 melts were conducted in air.

6.2: Waste Characterisation

In summary, it can be said that elemental segregation of the calcine is inevitable, with characteristic segregation of the rare earths and actinide surrogates to a fluorite-structured phase, which may prove detrimental to the final glass product.

Segregation of a yellow phase to the melt surface is indicative of increased melter corrosion, and the corrosion products which are then incorporated into the yellow phase, become incorporated into the glass in immiscible “peanuts”. These “peanuts” are not bound in the glass structure, but rather sit within the solidified glass in an immiscible

form, loosely bonded and highly soluble in aqueous solution, containing heat generating radiotoxic elements from the waste stream.

Yellow phase precursors within the calcine do not appear to be influenced by pre-process heat treatment, but a reducing atmosphere prevents the formation of the phase on the glass surface, although metallic deposits of Mo are then precipitated. This result means that other elements of the waste stream would be reduced in the same way, which would be detrimental to the final glass.

A reducing atmosphere within the calciner increases the rate of denitration and would, according to Lopez *et al*, (2003), increase the actinide solubility within the glass.

6.3: Waste Loaded Glass

Some basic mechanisms for the dissolution of the waste into the glass have been proposed. The formation of a rare-earth enriched solute layer around the waste particles, occurring concurrently with nucleation of yellow phase and segregation to the melt surface, is the first proposed mechanism of dissolution. This solute layer is then removed via mixing of the glass melt.

The yellow phase, once incorporated into the body of the melt via convective mixing and sparging, nucleates around bubbles within the viscous matrix, and remains there in an immiscible, self-contained mass. In de-ionised water, this yellow phase is soluble, and contains crucible corrosion products and molybdates which form readily. Fluorite-structured phases do not undergo dissolution in the glass for quite some time, and are known to contain many rare-earths and actinides. These actinides are highly radiotoxic in the longer term life of the glass, and any unwanted segregation to a phase which may not be completely soluble in glass or an area where crystallisation may occur at elevated canister temperatures is highly undesirable. However, if these actinides can be immobilised in one crystalline fluorite-structured phase which is then incorporated within the glass (e.g. to form a glass matrix composite), a solution may be found.

Further calcination of the waste is required to that which already takes place, for full and effective incorporation within the glass melt. It is recommended that calcination up to 400°C is used, as the simulant waste seems not to have experienced these temperatures but only temperatures of ~200°C. This heat treatment will not remove the problem of the yellow phase, but will increase the efficiency and therefore throughput of the melter, without introducing any detrimental phases such as those after heat treatment to 700°C and above. The formation of the low melting, eutectic phase and the low C_p for the HT400G supports this conclusion. It is therefore recommended that a reducing atmosphere within the calciner is used up to temperatures of 400°C, and an inert sparge in the melter.

A reducing atmosphere within the glass melt leads to waste digestion at a lower temperatures. However, as Short (2004) concluded, a reducing atmosphere has little effect on yellow phase formation and produces metallic deposits within the crucible, which become the most susceptible to leaching (Carter *et al*, 2003) in the longer life of the product. An inert atmosphere produced an incorporation temperature of ~870°C compared to <900°C for oxidising atmospheres, so it is recommended that an Ar or He sparge is used within the Inconel 601 melter as opposed to the current air sparge.

6.3: Suggestions for Further Work

The work done during this study highlights the need for fundamental research into the area of melting during the vitrification of HLW glasses. There are several questions raised which need to be expanded upon.

- Analysis of yellow phase samples to determine fully the composition, and study using thermal analysis methods the nucleation mechanisms of this phase
- Analyses of the effect of calcination atmosphere on yellow phase precursors using SEM and TEM methods.
- Studies of the concentration effects of key oxides on dissolution rates within the glass melt, as a function of time and temperature. This could be done by fabricating rods of the oxides in question and immersing them within a melted

borosilicate glass, as fabricating smaller pellets was not successful. the resulting quenched glass could be analysed using EPMA

- Investigate possible additions to the HAL or borosilicate glass that may suppress the formation of yellow phase.
- Time resolved X-ray diffraction of a yellow phase simulant using a hot stage diffractometer to study in more detail the phase formation and dissolution.
- Fabrication of a LaLiMoO_4 compound and subsequent characterisation (XRD/SEM) to determine if this is a yellow phase precursor/constituent and why La behaves differently to other rare earths.
- A study of the amorphous nitrates present in the calcine.
- MCC-1 and PCT-1 durability studies on the glass and waste stream melted for short periods of time and heat treated to simulate canister cooling. The purpose of this study would be to examine which of the components within an (theoretically) improperly mixed and poured glass would be least durable, with a view to looking at ways to contain these elements.
- Further study of the possibility of forming a composite glass ceramic within the waste form, using the crystallised fluorite phases to form the composite within the glassy matrix.

References

- Bennett, D. G., Higgo, J. J. W., Wickham S. M., *Review of Waste Immobilisation Matrices*, Galson Sciences Ltd for Nirex N/085, (2001) pp 2-20
- Bevilacqua, A. M., Bernasconi, N. B. M., Russo, D., Audero, M. A., Sterba, M. E., Heredia, A. D., *Immobilisation of simulated high level liquid wastes in sintered borosilicate, aluminosilicate and aluminoborosilicate glasses*. *J. Nuc. Mater.* 229 (1996) pp187-193.
- Blundy, J., Wood, B., *Partitioning of trace elements between crystals and melts* *Earth and Planetary Science Letters* 210 (2003) pp383-397
- Boccaccini, A. R., Bernardo, E., Blain, L., Boccaccini, D. N., *Borosilicate and lead silicate glass matrix composites containing pyrochlore phases for nuclear waste encapsulation* *J. Nuc. Mater.* 327, Issues 2-3, (2004), pp 148-158
- Boorse, H. A., Motz, L., Weaver, J. H., *The Atomic Scientists: A Biographical History* J. Wiley and Sons, New York, (1989)
- Bousquet, G., Brahler, G., *A MOX Fuel Plant in Russia: The Engineering Work Has Started* XXII Ann. Int. Symp. Proc The Uranium Institute (1999)
www.uilondon.org/symp/1999
- British Medical Association, *Hazardous Waste and Human Health*, Oxford University Press, Oxford (1991)
- Cains, P. W., Yewer, K. C., Waring, S., *Volatilisation of ruthenium, caesium and technetium from nitrate system in nuclear fuel processing and waste solidification* *Radiochemica Acta.* 56, (1992) pp 99
- Calas, G., Le Grand, M., Galoisy, L., Ghaleb, D., *Structural role of molybdenum in nuclear glasses: and EXAFS study* *J. Nuc. Mats* 322 (2003) pp15-20

Camara, B., Lutze, W., Lux, J., *An investigation on the valency state of molybdenum in glasses with and without fission products* Waste Man. IV (1988) pp 93-102

Carter, M. L., Stewart, M. W. A., Leung, S. H. F., Colella, M., Vance, E. R., *Microstructures of inactive Synroc-C samples produced by different hot-consolidation methods* Ceram.Trans. 71, (1996) pp 491-504

Chandra, R., *The effect of SiO₂ dissolution on the homogeneity of commercial glass melts* PhD Thesis, University of Sheffield, UK, (2002) pp23-116

Chapman, C. C., McElroy, J. L., *Surry-fed ceramic melter- a broadly accepted system to vitrify high level waste* High Level Waste and Spent Fuel Management 2, (1989), pp119-125

Chun, K. S., *Studies on the thermal decomposition of nitrates found in highly active waste and of chemicals used to convert the waste to glass* AERE Report R-8735 HL77/1295, Harwell, (1977) pp 1-14

Clark, D.E., Maurer, C.A., Jurgensen A.R., Urwongse, L., *Effects of Waste Composition and Loading on the Chemical Durability of a Borosilicate Glass Mat.* Res. Soc. Symp. Proc. 4 (1982) pp1-11

Clark, R. J., Hester, R.E., *Spectroscopy of Inorganic-Based Materials* Advances in Spectroscopy 14 Wiley and Sons, London, (1987) pp267-287

Cotton, F. A., Wilkinson, G., Murillo, C. A., Bochmann, M., *Part 2—The chemistry of the main group elements* in *Advanced Inorganic Chemistry (6th Ed.)* Wiley and Sons, New York, (1999), pp 332-336

Davidovits, J., *Geopolymeric reactions in archaeological cements and in modern blended cements*, First European Conference on Soft Mineralogy, Geopolymer 88, (1988), Vol.1, pp 93-105

DEFRA- Department for Environment, Food and Rural Affairs, *Managing Radioactive Waste Safely- Proposals for developing a policy for managing solid radioactive waste in the UK*, (2001), pp14-15

DEFRA- Department for Environment, Food and Rural Affairs, *Chapter 6-Report on the Review of the National Air Quality Strategy Proposals to Amend the Strategy* (1999) pp 6-10

Desvaux, J.L., Pageron, D., Liberge, R., *Industrial Experience of HLW vitrification at La Hague and Marcoule Waste*. *Man IV*, (1998).

Donald, I. W., Metcalfe, B.L., Taylor, R.N.J., *Immobilization of high level radioactive wastes using ceramics and glasses* *J. Mat. Sci.* 32 (1997) pp 5851-5887

Duckworth, H. E., *Mass Spectrometry* Cambridge Univ. Press, London, (1986) pp 1155-1170

Ewing, R. C., *Part I. Non- crystalline waste forms: Silicate Glasses in Radioactive Wasteforms for the Future*. Lutze, W., Ewing, R.C., Oxford, North Holland Publishing (1988) pp 1- 160.

Ewing, R. C., *Nuclear waste forms for actinides*. *Proc. Natl. Acad. Sci* 96 (1999) pp 3432- 3439

Ewing, R. C., *Plutonium and minor actinides: safe sequestration* *Earth and Planetary Science Letters* 229 (2005) pp 165– 181

Fardon, J. B., Clark, K. A., Owens, I. F., *An investigation into calcine and product glass corrosion of Inconel 601* BNFL Research and Development Dept, Sellafield, Series HLWTC/90/P4 (1991) pp 1-28

Fardon, J. B., Owens I. F., *Further Assessments of Calcine and Product Glass Corrosion of Inconel 601 and other alloys* BNFL Research and Development Dept, Sellafield, Series HLWTC/08/P4 (1982) pp 1- 15.

Feng, X., Pegg, I. L., Saad, E., Cucinell, S., Barkatt, A., *Redox effects on the durability and viscosity of nuclear waste glasses* Ceramic Transactions, 9, (1989) pp 165-74

Gobichon, A.E., Auffredic, J.P., Louer, D., *Thermal decomposition of neutral and basic lanthanum nitrates with temperature dependant powder diffraction and thermogravimetric analysis* Solid State Ionics 93 (1996) pp 51-64

Goldschmidt, V. M., *The principles of distribution of chemical elements in minerals and rocks* J. Chem. Soc. Lond., 140 (1937) pp 655-673

Gong, W.L., Lutze, W., Abdelouas A., Ewing, R.C. *Vitrification of radioactive waste by reaction sintering under Pressure* J. Nuc. Mater. 265 (1999) pp 12-21

Goodhew, P. J., *Introduction to Scanning Transmission Electron Microscopy*, Royal Microscopical Society Microscopy Handbooks, (1997), ISBN 1859960669

Gribble, N.R., *Acceptable tolerance on the lithium nitrate addition to HAL* BNFL Commercial No. 10/00772.07.02.01.01 (2002), Sellafield

Hartley, F., *Batch Testing and Homogeneity* Glass Tech. Vol 4, (1963), no. 5, pp 158-161

Heriot, I. D., *Uranium Enrichment by Centrifuge*, Report EUR 11486, Commission of the European Communities, Brussels, (1988)

Hesketh, K. W. *Power Reactors- Chapter 5* in *The Nuclear Fuel Cycle; from Ore to Waste* Ed. Wilson, P. D. Oxford University Press, New York, (1996)

Heyes, S. J., *Lecture 2 - Structures of Simple Inorganic Solids* in *Lectures in the 1st Year Inorganic Chemistry Course* (1999) www.ox.ac.uk

Hofmann, S., *Chapter 1- The Landscape* in *On Beyond Uranium* Ed. Hofmann, S. Taylor and Francis, London (2002)

Hong, K. S., Lee, S. W., Speyer, R. E., *Thermal analysis of reactions in soda-lime silica glass batch containing melting accelerants: II, Multicomponent systems* J Am. Ceram. Soc., (1993) 76, No. 3, pp605-608

Hrma, P., *Advances in the fusion of glass* Ed. Bickford D.F, American Ceramic Society, Westerville, Ohio (1988) pp 10.1-10.18

Hrma, P., Matyas, J., Schweiger, M., *Settling of spinel in a high level waste melter*, Contract Report DE-AC06-76RL01830, Pacific Northwest National Laboratory, Richland, WA, USA (2001) pp 11-41

Igarishi, H., Kato, K., Takahashi, T., *Effect of calcining temperature on volatilisation of ruthenium in batch calcinations of simulated high-level liquid waste* Radiochim. Acta 60 (1993) pp 143

Jantzen, C. M., Brown, K. G., Pickett, J. B., *Impact of phase separation on durability in phosphate containing borosilicate waste glasses: Relevance to vitrification of INEEL high level waste* Ceramic Transactions 119 (2000) pp. 271-280

Jeffrey, P. G., Kipping, P. J., *Gas analysis by gas chromatography* Pergamon Press, London, (1964)

Jenkins, H.D.B., in *CRC Handbook of Chemistry and Physics 1999-2000 : A Ready-Reference Book of Chemical and Physical Data (CRC Handbook of Chemistry and Physics*, D.R. Lide, (ed.), CRC Press, Boca Raton, Florida, USA, 79th edition, (1998)

Jostsons, A., *Synroc - progress and future prospects*, Radwaste Solutions, American Nuclear Society, 9, no. 2, (2002) pp 58

Kawamoto, Y., Clemens, K., Tomozawa, M., *The effect on phase separation of the oxidation state of molybdenum in a $\text{Na}_2\text{O-B}_2\text{O}_3\text{-SiO}_2$ glass* Phys. Chem. Glass, 22, no. 5, (1981) pp 110-114

King, S. J., Putte, D. V., *Identification and Description of UK Radioactive Wastes and Materials Potentially Requiring Long-term Management* Nirex N/085 (2003) pp 5-30

Krebs, H., *Chapter 29 Glasses in Fundamentals of Inorganic Crystal Chemistry* McGraw-Hill, London (1968) pp 342-352

Kutty, G. K. V., Asuvathraman, R., Raja Madhavan, R., Jena, H., *Actinide immobilization in crystalline matrix: a study of uranium incorporation in gadolinium zirconate* J. Phys. Chem. Sol. 66 (2005) 596–601

Langowski, M. H., Hrma, P., Schweiger, M. J., Smith, D. E., *Effect of phosphate on crystallisation, viscosity and chemical durability of simulated Hanford site high-level radioactive waste glasses* Ceramic Transactions 72, (1996) pp 291-298

Larkin, M. J., *Development of highly active waste conditioning at Sellafield* Nucl. Energy 25 no. 6 (1986) pp 343-354

Lee, W. E., Zhang, S., *Melt corrosion of oxide and oxide-carbon refractories* International Materials Reviews 44 no. 3 (1999) pp 77-104.

Li, H., Hrma, P., Langowski, M. H., *Vitrification and chemical durability of simulated high-level nuclear waste glasses with high concentrations of Cr₂O₃ and Al₂O₃* Environ. Issues and Waste. Man. Tech 2 (1996) pp 299-306

Li, H., Strachan, D. M., Li, H., Davis, L. L., Qian, M. *Crystallisation of gadolinium and lanthanum- containing phases from sodium alumino- borosilicate glasses.* J. Non- Cryst. Solids 272 (2000) pp 46-56

Li, H., Hrma, P., Vienna, J. D., *Sulfate retention and segregation in simulated radioactive waste borosilicate glasses* Environ. Issues and Waste. Man. Tech 6 (1997) pp 237- 245

Liu, J. H., Zhang, Y. H., Wang, L. Y., Wei, Z. F., *Drawing out the structural information of the first layer of hydrated ions: ATR-FTIR spectroscopic studies on aqueous NH_4NO_3 , $NaNO_3$ and $Mg(NO_3)_2$ solutions* Spectrochimica Acta Part A: Molecular and Biomolecular Spectroscopy, 61, no. 5, (2005), pp1-17

Lopez, C., Deschanel, X., Bart, J. M., Boubals, J. M., Auwer, C., Simoni, E., *Solubility of actinide surrogates in nuclear glasses* J. Nuc. Mat. 312 (2003) pp76-80

Luo, S., Sheng, J., Tang, B., *A comparison of HLW glass and PWR borate waste glass.* J. Nucl. Mats 298 (2001). pp180-183.

Marples, J.A.C., *Preparation, properties, and disposal of vitrified high level waste from nuclear fuel reprocessing* Glass Technology 29, (1988) pp 230-247,

Matyáš, J., Hrna, P., Kim, D. S., *Melt rate improvement for high level waste glass* Pacific Northwest National Laboratory PNNL-14003, DOE Contract DE-AC06-76RL01830, (2002) National Technical Information Service www.ntis.gov

Matzke, H. J., Vernaz, E., *Thermal and physicochemical properties important for the long term behaviour of nuclear waste glasses* J. Nuc. Mater. 201(1993) 295-309

McCallum N., *Some aspects of the corrosion of refractories* Trans. Br. Ceram. Soc., (1952) 51, pp 523–548

McKeown, D. A., Muller, I. S., Gan, H., Pegg, I. L., Stolte, W. C., *Determination of strontium environments in borosilicate waste glasses using X-ray absorption near edge spectroscopy* Journal of Non-Crystalline Solids 317 (2002) pp 290–300

Mesko, G., *Introduction to nuclear power and radioactive waste* Lecture notes, Spring Semester, Alfred State University of New York (1999) www.alfred.edu

Muller, O., Roy, R., *The major ternary structural families* Springer-Verlag, New York (1974)

Nazri, G. A., and C. Julien *Heat-treatment studies of molybdenum oxide monohydrate* Solid State Ionics, 80, Iss. 3-4, (1995) pp 271-275

Nuclear Regulatory Commission of the United States Factsheet *The accident at Three Mile Island* www.nrc.gov/reading-rm/doc-collections/fact-sheets (2004) pp1-8

Owens, I. F., *An investigation on the kinetics of incorporation of M9, MW and M22 glass composition using Harwell an Marcoule calcines* BNFL Research and Development Dept, Sellafield, Series HLWTC/03/P4 (1981)

Owens, I. F., Leung, T. K., Magrabi, C., *The reaction chemistry of highly active liquor simulates, lithium nitrate and sucrose under calcinations condition* BNFL Research and Development Dept, Sellafield, Series 754/W (1984) pp 1-12

Pacaud, F., Fillet, C., Francillon, N. J., *Effect of platinoids on French LWR reference glass properties*, Mat. Res. Soc. Symp. Proc. 257, (1991) pp 161-167

Park, Y. S., Butt, D. P., Castro, R., Petrovic, J., Johnson, W., *Durability of molybdenum disilicide in molten alkali borosilicate glass* Materials Science and Engineering A261 (1999) pp 278–283

Pegg, I. L., Joseph, I *Chapter 4.2: Vitrification in Hazardous and Radioactive Waste Treatment Technologies Handbook* Ed. By Chang, H. O., CRC Press, London, (2001) pp 4.2.1-26

Penneman, R. A., Eller, P. G., *Stabilization of actinides and lanthanides in high oxidation states* Journal of the Less Common Metals, 127, (1987), pp 19-33

Pennycook, S., *Z-contrast transmission electron microscopy: Direct atomic imaging of materials* Annu. Rev. Mater. Sci. 22 (1992) pp 171-95

Perry, K.J., Kimmitt, R.R., Soelberg, N.R., Tillotson, R.D., Olson, A.N., *Test Results from SBW-FY01-PS-01 Vitrification Demonstration of Sodium Bearing Waste Simulant Using WM-180 Surrogate* Idaho National Engineering and Environmental Laboratory Contract DE-AC07-99ID13727 (2001) pp 43-45

Quang, R. D., Mougard, P., Ladirat, C., Prod'homme, A., *Status and result of the French vitrification program* Environmental Issues and Waste Management Technologies in the Ceramic and Nuclear Industries IX, Cer. Trans (2003), 155 pp 101-110

Ramshaw, C. C., *The effect of nitrate content on the particle size and reactivity of calcine* BNFL Research and Development Dept, Sellafield, Series 4.13.1/B141 (1985) pp 1-14

Ringwood, A. E., *Disposal of high-level nuclear wastes: A geological perspective* Mineral. Mag. 49, no. 2, (1985) pp 159

Roth, G., Weisenburger, S. *Vitrification of high-level liquid waste: Glass chemistry, process chemistry and process technology*. Nuc. Eng. Design 202 (2000) pp 197-207

Scales, C. R., *Vitrification Development for High Active Waste at BNFL Sellafield* BNFL Technology Centre Ref RM 1117 Subject Series HLWTC/90/P40 (1990)

Scheetz, B. E., Freeborn, Pepin, J., W. P., White, W. B., *The system SrMoO₄-BaMoO₄-CaMoO₄: Compatibility relations, the implications for supercalcine ceramics*. Mat. Res. Soc. Symp. 2 (1982)

Schiewer, E. Rabe, H. Weisenburger, Ceram. Trans. 155 (1982) pp 101

Scott, P. A., Goles, R. W., Peters, R. D., *Technology of off-gas treatment for liquid-fed ceramic melters* PNL-5446 UC-70 (1985)

Shannon, R. D., Prewitt, C. T., *Effective ionic radii and crystal chemistry* J. Inorg. Nucl. Chem., 32 (1970) pp 1427-1441.

Shelby, J.E., *Introduction to Glass Science and Technology* RSC Paperbacks, Cambridge, (1997)

Short, R. J., *Incorporation of Molybdenum in Nuclear Waste Glasses* PhD Thesis, (2004) University of Sheffield, UK

Short, R.J., Hand, R.J., Hyatt, N.C., Möbus, G., *Environment and oxidation state of molybdenum in simulated high level nuclear waste glass compositions* Journal of Nuclear Materials 340 (2005) pp179–186

Smith, P. A., Vienna, J. D., Hrma, P., *The effects of melting reactions on laboratory scale waste vitrification*, J. Mat. Res., 10, no. 8, (1995) pp2137-2149

Strydom, C. A., Van Vuuren, C. P. J., *The thermal decomposition of lanthanum(III), praseodymium(III) and europium(III) nitrates* Thermochemica Acta. 124 (1988) pp 277-283

Taylor, R. F., *Chemical Engineering problems of Radioactive Waste Fixation by Vitrification*. Chemical Engineering Science 40 no. 4 (1985) pp 541-569.

Tooley, F. V., Tiede, R. L., *Factors affecting the degree of inhomogeneity of glass* J. Am.Ceram. Soc., 10, no. 2, (1945) pp 54

United States Department of Energy “*End Points for Spent Nuclear Fuel and High-Level Radioactive Waste in Russia and the United States*” published by Committee on End Points for Spent Nuclear Fuel and High-Level Radioactive Waste in Russia and the United States (2003) pp 1-29 www.books.nap.edu/execsumm

Walsh A., *The application of atomic absorption spectra to chemical analysis* Spectrochim. Acta, 7 (1955) pp 108-117

Weast, R. C., *Handbook of Chemistry and Physics- 61st Edition*. Florida, CRC, (1981) pp 15-39

Wiederhorn, S.M., Krause, R.F., Sun, J., *Bull. Am. Ceram. Soc.*, 1988, **67**, 1201-1209

Wilburn, F. W., Thomasson, C. V., *The application of differential thermal analysis and thermogravimetric analysis to study the reactions between major components of a sheet glass batch* *Glass Tech.* (1965) Vol. 6, no. 4, pp107-114

www.nobelprize.org/physics/educational/energy/fission

www.skb.se